

✓

**A THEORETICAL INVESTIGATION OF THE RESOLUTION OF
CHIRAL AMINES VIA CHIRAL MACROCYCLES AND THE
SYNTHESIS OF SOME MACROCYCLIC PRECURSORS**

by

Reshika Ramdhani

BSc (Hons)

Submitted in fulfilment of the academic requirements for the degree of

Master of Science in the

School of Chemistry,

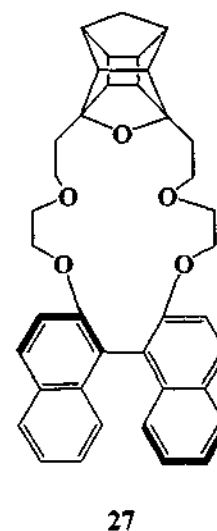
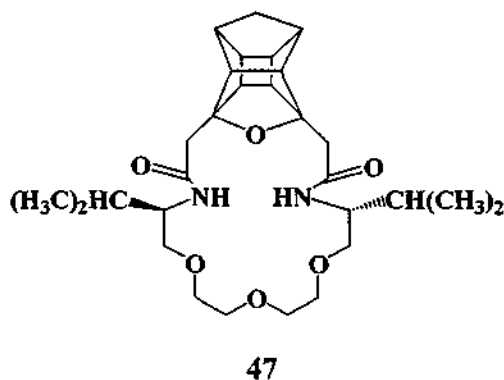
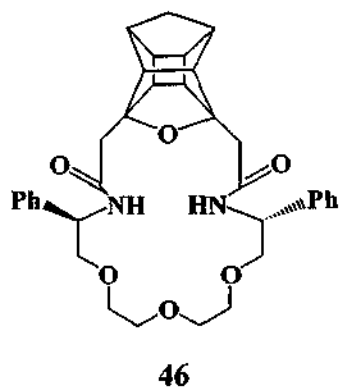
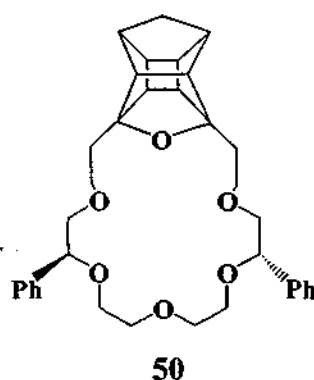
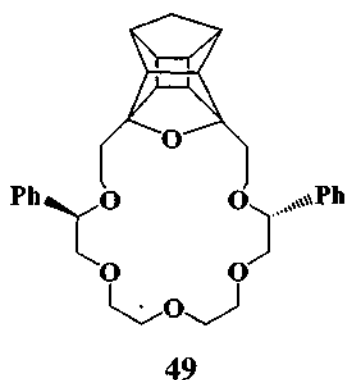
University of KwaZulu-Natal,

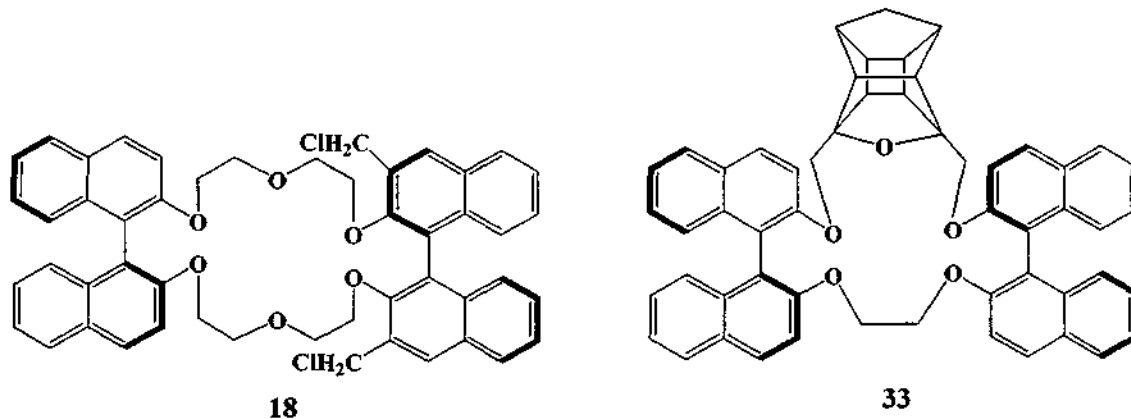
Durban

April 2006

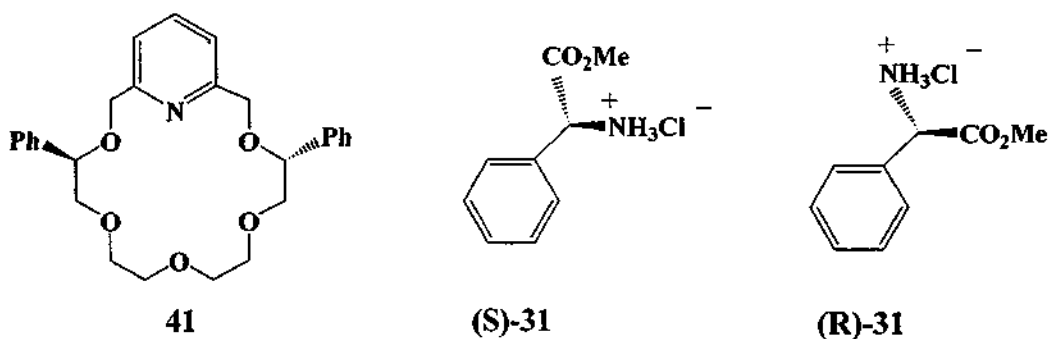
ABSTRACT

The investigation reported in this thesis was carried out in two parts. The first part of the study involved a computational investigation of various host-guest systems. A computational model employing the MM3 force field was used to calculate approximate binding energies and predict the enantiomeric preference of theoretical chiral pentacycloundecane (PCU) cage macrocycles (S,S)-49 and (S,S)-50 towards chiral ammonium ions. The calculations were performed in the "gas phase" using the MM3 force field in Alchemy 2000 and the results were compared with the results obtained previously for host-guest systems studied using the same computational model. Chiral cage annulated macrocycles (S,S)-49 and (S,S)-50 were found to have higher binding energies than cage annulated macrocycles (S,S)-46 and (R)-27. (S,S)-49 was found to have greater chiral recognition than macrocycles (R)-27 and (S,S)-47 reported previously.





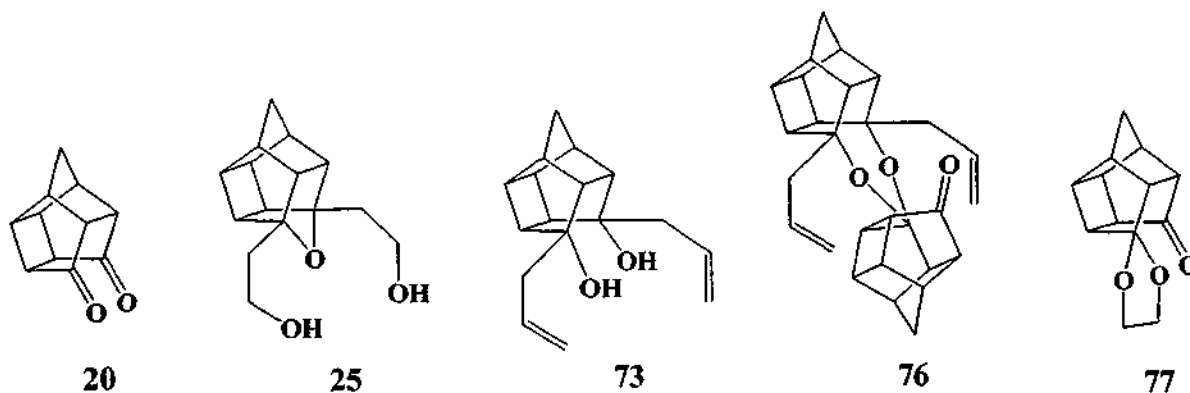
Cram's binaphthyl crown ether (**18**) that was tested previously using the computational model, exhibited the highest calculated enantioselectivity of $1.4 \text{ kcal mol}^{-1}$. This result was set as a benchmark for subsequent computational studies. A theoretical crown ether (*S,S*)-**33** was postulated and its enantiomeric recognition was calculated using the same computational model. (*S,S*)-**33** compared favourably with Cram's binaphthyl crown ether (*R,R*)-**18**, exhibiting a calculated chiral preference of $1.52 \text{ kcal mol}^{-1}$.



The use of solvent in MM3 calculations gives a more realistic representation of binding energy and enantiomeric recognition since experimental work is done in the solvent medium. The computational model was extended to include calculations examining solvent effects (water and chloroform) on the binding energy and enantioselectivity of host-guest complexes. Host-guest complexes (*S,S*)-**41** with (*S*)-**31** and (*S,S*)-**41** with (*R*)-**31** were subjected to MM3 optimizations in MacroModel. Calculations were performed in no solvent (gas phase), water (solvent phase) and chloroform (solvent phase). Calculations performed in the solvent phase (water and chloroform) resulted in an increase in the calculated binding energies to an extent. It was also observed that the polarity of the solvent does have an effect on the enantiomeric recognition. The use of a

polar solvent such as water results in lower enantioselectivity when compared with the use of a less polar solvent such as chloroform. The increase in the binding energies calculated in the solvent medium (water and chloroform) when compared with the binding energies calculated in the gas phase, indicates that a weak host-guest complex is formed in the solvent phase.


The second part of the study involved the multi-step synthesis of precursors for PCU cage annulated macrocycles. During the synthesis of the precursors for the PCU cage annulated macrocycles, four PCU crystal structures were isolated. The X-ray study of the crystal structures of the PCU cage diol (**25**), a novel PCU dimer (**76**) and PCU ketal (**77**) will be reported to our knowledge for the first time. The crystal structure obtained of the PCU dione (**20**) will also be discussed. A complete NMR elucidation of the structure of the PCU dione (**20**), the PCU diol (**25**), PCU endo-endo diol (**73**), a novel PCU derivative (**76**) and the PCU ketal (**77**) are also reported for the first time to our knowledge.



PREFACE

The experimental work described in this thesis was carried out in the School of Chemistry, University of Kwazulu-Natal, Durban, from February 2003 to June 2005, under the supervision of Dr H G Kruger.

These studies represent original work by the author and have not been submitted in any form for any degree or diploma to any tertiary institution. Where use has been made of the work of others it is duly acknowledged in the text.



Reshika Ramdhani

..30.. day of ..April..... 2006

TABLE OF CONTENTS

A THEORETICAL INVESTIGATION OF THE RESOLUTION OF CHIRAL AMINES VIA CHIRAL MACROCYCLES AND THE SYNTHESIS OF SOME MACROCYCLIC PRECURSORS.....	I
ABSTRACT	II
PREFACE.....	V
TABLE OF CONTENTS.....	VI
LIST OF TABLES	X
LIST OF FIGURES	XI
LIST OF SCHEMES.....	XII
LIST OF ABBREVIATIONS.....	XIII
ACKNOWLEDGEMENTS.....	XV
LIST OF CONFERENCE PRESENTATIONS	XVI
LIST OF JOURNAL PUBLICATIONS	XVII
CHAPTER ONE.....	1
HOST-GUEST CHEMISTRY	1
1.1 THE BIOLOGICAL IMPORTANCE OF CHIRALITY.....	1
1.2 THE LOCK-KEY SYSTEM IN ENZYMES.....	4
1.3 HOST-GUEST COMPLEXATION	5
1.4 CROWN ETHERS IN HOST-GUEST INTERACTIONS.....	7
1.5 COMPLEXATION OF AMMONIUM SALTS WITH CHIRAL CROWN ETHERS.....	10
1.6 APPLICATIONS OF CROWN ETHERS.....	11
CHAPTER TWO.....	15
THE DESIGN OF A THEORETICAL CHIRAL MACROCYCLE	15
2.1 PROPERTIES OF A GOOD HOST AND FACTORS REQUIRED FOR GOOD CHIRAL RECOGNITION	15
2.2 CROWN ETHERS WITH BINAPHTHYL CHIRAL GROUPS	16
2.3 APPLICATIONS OF THE PENTACYCLOUNDECANE MOLECULE... 	19
2.4 DESIGN OF A NOVEL THEORETICAL CAGE CROWN ETHER.....	25
CHAPTER THREE	28
COMPUTATIONAL CHEMISTRY.....	28
3.1 INTRODUCTION TO COMPUTATIONAL CHEMISTRY.....	28
3.2 QUANTUM MECHANICS.....	29

3.2.1	AB INITIO	30
3.2.1	DENSITY FUNCTIONAL THEORY (DFT)	30
3.2.3	SEMI-EMPIRICAL METHODS.....	31
3.3	MOLECULAR MECHANICS OR FORCE FIELD METHODS.....	32
3.3.1	THE BASICS OF A MOLECULAR MECHANICS OPTIMIZATION	34
3.4	MOLECULAR DYNAMICS (MD) AND SIMULATED ANNEALING (SA)	36
3.4.1	MOLECULAR DYNAMICS (MD)	37
3.4.2	SIMULATED ANNEALING (SA)	38
3.5	COMPUTATIONAL MODEL	38
	CHAPTER FOUR.....	42
	RESULTS AND DISCUSSION.....	42
4.1	INTRODUCTION	42
4.2	RESULTS AND DISCUSSION.....	49
4.3	THE EFFECT OF SOLVENT ON BINDING ENERGY AND ENANTIOSELECTIVITY	63
	CHAPTER FIVE.....	67
	THE SYNTHESIS OF MACROCYCLIC PRECURSORS	67
5.1	THE RETROSYNTHETIC ROUTE TOWARDS CHIRAL CAGE ANNULATED MACROCYCLES.....	67
5.2	METHODS UNDERTAKEN WHEN SYNTHESIZING MACROCYCLES	70
5.2.1	THE TEMPLATE EFFECT	70
5.2.2	TRIFLUOROMETHANESULPHONATE (TRIFLATE) AS A NEW LEAVING GROUP IN MACROCYCLIC PRECURSORS.....	73
5.2.3	HIGH DILUTION EFFECTS.....	73
5.3	THE MULTI-STEP SYNTHESIS OF PRECURSORS FOR CHIRAL CAGE ANNULATED MACROCYCLES	74
5.3.1	THE MULTI-STEP SYNTHESIS OF THE CAGE DIOL (25).....	74
5.3.2	THE MULTI-STEP SYNTHESIS OF THE (S,S)-ISOPROPYL GLYCOL (56)	76
5.3.3	THE MULTI-STEP SYNTHESIS OF THE (S,S)-MANDELIC GLYCOL (55)	77
5.3.4	THE MULTI-STEP SYNTHESIS OF THE CHIRAL GLYCOL (66)	78
	CHAPTER SIX.....	80

THE NMR ELUCIDATION OF THE PENTACYCLOUNDECANE DIONE STRUCTURE AND ITS DERIVATIVES	80
6.1. THE NMR ELUCIDATION OF THE PCU DIONE (20) STRUCTURE....	81
6.2. THE NMR ELUCIDATION OF THE STRUCTURES OF PCU DERIVATIVES	84
6.2.1 THE NMR ELUCIDATION OF THE PCU KETAL (77) STRUCTURE...85	
6.2.2 THE NMR ELUCIDATION OF THE PCU ENDO-ENDO DIOL (73) STRUCTURE	89
6.2.3 THE NMR ELUCIDATION OF THE PCU NOVEL DIMER (76) STRUCTURE	91
6.2.4 THE NMR ELUCIDATION OF THE PCU DIOL (25) STRUCTURE	98
CHAPTER SEVEN	102
THE X-RAY STRUCTURES OF THE PENTACYCLOUNDECANE DIONE AND DERIVATIVES	102
7.1 THE STRUCTURE OF THE PENTACYCLOUNDECANE DIONE (PCUD) (20)	102
7.2 THE X-RAY STRUCTURE OF THE PCU DIONE (20).....	107
7.3 THE X-RAY STRUCTURE OF THE PCU DIOL (25).....	109
7.4 THE X-RAY STRUCTURE OF THE PCU NOVEL DIMER (76).....	110
7.5 THE X-RAY STRUCTURE OF THE PCU KETAL (77).....	112
CHAPTER EIGHT	114
CONCLUSION.....	114
CHAPTER NINE	116
EXPERIMENTAL	116
9.1 THE MULTI-STEP SYNTHESIS OF THE PCU DITOSYLATE (54).....	116
9.1.1 SYNTHESIS OF 5,8-METHANO-4A,5,8,8A-TETRAHYDRO-1,4- NAPHTHOQUINONE (72).....	116
9.1.2 SYNTHESIS OF PENTACYCLO[5.4.0.0^{2,6}.0^{3,10}.0^{5,9}]UNDECANE-8-11- DIONE (20)	117
9.1.3 SYNTHESIS OF EXO-8-EXO-11- DIALLYLPENTACYCLO[5.4.0.0^{2,6}.0^{3,10}.0^{5,9}]UNDECANE-ENDO-8- ENDO-11-DIOL (73).....	117
9.1.4 SYNTHESIS OF 3,5-DIALLYL-4- OXAHEXACYCLO[5.4.1.0^{2,6}.0^{3,10}.0^{5,9}.0^{8,11}]DODECANE (74).....	118
9.1.5 SYNTHESIS OF 3,5-[BIS (HYDROXYETHYL)]-4-OXAHEXACYCLO [5.4.1.0^{2,6}.0^{3,10}.0^{5,9}.0^{8,11}] DODECANE (25).....	118

9.1.6	SYNTHESIS OF 3,5-[BIS(HYDROXYETHYL)]-4-OXAHEXACYCLO[5.4.1.0^{2,6}.0^{3,10}.0^{5,9}.0^{8,11}]DODECANE DITOSYLATE (54)	119
9.2	THE MULTI-STEP SYNTHESIS OF THE MANDELIC GLYCOL (55)	119
9.2.1	SYNTHESIS OF (S)-(+)-METHYL MANDELATE (61)	120
9.2.2	(S)-(+)-METHYL 2-PHENYL-2-(TETRAHYDROPYRANYLOXY) ACETATE (59)	120
9.2.3	(S)-(+)-2-PHENYL-2-(TETRAHYDROPYRANYLOXY) ETHANOL (57)	120
9.2.4	(S,S)-(+)-1,11-DIPHENYL-3,6,9-TRIOXAUNDECANE-1,11-DIOL (MANDELIC GLYCOL, 55)	121
9.3	THE ATTEMPTED MULTI-STEP SYNTHESIS OF THE (S,S)-(+)-2,10-DIPHENYL-3,6,9-TRIOXAUNDECANE-1,11-DIOL (66)	121
9.3.1	SYNTHESIS OF (S)-(+)-BUTYL MANDELATE (85)	121
9.3.2	(S)-(+)-PHENYL-1,2-ETHANDIOL (68)	122
9.3.3	(S)-(+)-1,4,4,4-TETRA-PHENYL-3-OXA-1-BUTANOL (67)	122
9.3.4	(S,S)-(+)-2,10-DIPHENYL-3,6,9-TRIOXAUNDECANE-1,11-DIOL (66)	122
9.4	THE SYNTHESIS OF (S,S)-(+)-ISOPROPYL GLYCOL (56)	123
9.4.1	SYNTHESIS OF (S)-(+)-HYDROXYISOVALERIC METHYL ESTER (62)	123
9.4.2	(S)-(+)-PROTECTED-HYDROXYISOVALERIC METHYL ESTER (60)	123
9.4.3	(S)-(+)-PROTECTED-HYDROXYISOVALERIC ALCOHOL (58)	123
9.4.4	(S,S)-(+)-ISOPROPYL GLYCOL (56)	124
9.5	THE SYNTHESIS OF THE NOVEL PCU DIMER (76)	124
9.6	THE SYNTHESIS OF THE PENTACYCLO[5.4.0.0^{2,6}.0^{3,10}.0^{5,9}]UNDECANE-8-11-DIONE-MONO-ETHYLENE KETAL (77)	125
	CHAPTER TEN	126
	REFERENCES	126

Supplementary Material: A CD accompanying this thesis includes the following:

- **An electronic copy of this thesis in WORD and PDF format.**
- **PDB files and Cartesian Co-ordinates of optimised structures reported in this thesis.**
- **Appendices**

LIST OF TABLES

Table 1: Binding energies of previously studied host-guest complexes.....	49
Table 2: Binding Energies of E_{complex} host (S,S)-41 with guests (S)-31 and (R)-31 ..	50
Table 3: Binding Energies of E_{complex} host (S,S)-41 with guests (S)-51 and (R)-51 ..	52
Table 4: Binding Energies of E_{complex} host (S,S)-42 with guests (S)-31 and (R)-31 ..	53
Table 5: Binding Energies of E_{complex} host (S,S)-49 with guests (S)-31 and (R)-31..	55
Table 6: Binding Energies of E_{complex} host (S,S)-49 with guests (S)-51 and (R)-51 ..	58
Table 7: Binding Energies of E_{complex} host (S,S)-50 with guests (S)-31 and (R)-31..	60
Table 8: Binding Energies of E_{complex} host (S,S)-33 with guests (S)-31 and (R)-31..	62
Table 9: NMR data for the PCU dione (20).....	83
Table 10: NMR correlations for the PCU dione (20)	83
Table 11: NMR data for the PCU ketal (77)	88
Table 12: NMR correlations for the PCU ketal (77)	89
Table 13: NMR data for the PCU endo-endo diol (73)	91
Table 14: NMR correlations for the PCU endo-endo diol (73).....	91
Table 15: NMR data for the PCU dimer (76).....	97
Table 16: NMR data for the PCU diol (25).....	99
Table 17: NMR correlations for the PCU diol (25).....	101

LIST OF FIGURES

Figure 1: Host-guest complex of host (12) with arbitrary ammonium guest.....	10
Figure 2: 2,2'-disubstituted-1,1'-binaphthyl group (15).....	17
Figure 3: Complexation of host (48) with arbitrary ammonium guest molecule	45
Figure 4: The two faces of the PCU cage annulated macrocycle (22)	45
Figure 5: The template effect of 18-crown-6 (7).....	72
Figure 6: The derivatisation of the PCU dione (20)	84
Figure 7: The conventional numbering and X-ray data numbering of the novel PCU cage dimer (76).....	92
Figure 8: The interatomic distances of selected carbon and oxygen atoms in the PCU dione (20).....	104
Figure 9: Space filling models of the PCU dione (20) showing its near-spherical skeleton	105
Figure 10: C1-C7 and C9-C10 bond lengths of PCU derivatives	106
Figure 11: ORTEP diagrams of the PCU dione (20) drawn at the 50 % probability level	109
Figure 12: ORTEP diagram of the PCU diol (25) drawn at the 50 % probability level	110
Figure 13: ORTEP diagram of the PCU dimer (76) drawn at the 50 % probability level	112
Figure 14: ORTEP diagram of the PCU ketal (77) drawn at the 50 % probability level	113

LIST OF SCHEMES

Scheme 1: Synthetic route to cage annulated macrocycle (22).....	23
Scheme 2: Synthetic route to chiral cage annulated macrocycle (27)	24
Scheme 3a: Proposed retrosynthetic route to chiral cage annulated macrocycles (S,S)-49 and (S,S)-53.....	67
Scheme 4: Proposed retrosynthetic route to chiral macrocycle (S,S)-50.....	69
Scheme 5: Synthetic route for the PCU diol (25).....	74
Scheme 6: Synthesis of the PCU ditosylate (54).....	75
Scheme 7: Synthetic route of the isopropyl glycol (56).....	76
Scheme 8: Synthetic route of the mandelic glycol (55).....	77
Scheme 9: Proposed synthetic route to chiral glycol (66).....	78
Scheme 10: Synthesis of the novel PCU cage dimer (76)	85
Scheme 11: Synthesis of the PCU ketal (77)	86

LIST OF ABBREVIATIONS

AM1	Austin Model 1
Amber	Assisted Model Building and Energy Refinement
BNGER	Bradshaw newglycol (R)-ester guest
BNGES	Bradshaw newglycol (S)-ester guest
BPAR	Bradshaw phenyl (R)-alcohol guest
BPAS	Bradshaw phenyl (S)-alcohol guest
BPER	Bradshaw phenyl (R)-ester guest
BPES	Bradshaw phenyl (S)-ester guest
B3LYP	Becke's 3 parameter functional with the LYP expression (Lee, Yang, Parr)
BSSE	basis set superposition error
CCER	Cage Cram (R)-ester guest
CCES	Cage Cram (S)-ester guest
CNGER	Cage newglycol (R)-ester guest
CNGES	Cage newglycol (S)-ester guest
CPAR	Cage phenyl (R)-alcohol guest
CPAS	Cage phenyl (S)-alcohol guest
CPER	Cage phenyl (R)-ester guest
CPES	Cage phenyl (S)-ester guest
¹³ C NMR	carbon-13 nuclear magnetic resonance
COSY	correlation spectroscopy
CPK	Corey Pauling Koltun Models
DMAP	dimethylamino pyridine
d	doublet
DEPT	distortion enhancement by polarization transfer
DFT	density functional theory
DMAP	4-dimethylaminopyridine
DMF	N, N-dimethylformamide
DFT	Density Functional Theory
ee	enantiomeric excess
FAB	Fast atom bombardment
HMBC	heteronuclear multiple bond correlation
HSQC	hetero single quantum correlation
¹ H NMR	hydrogen-1 nuclear magnetic spectroscopy
HSQC	heteronuclear single quantum coherence
I.R.	Infrared
m	multiplet
M	molarity
MD	Molecular dynamics
MM3	Molecular mechanics
MINDO3	Modified intermediate neglect of differential overlap
mmol	millimole
mol	mole
m.p.	melting point
M.S.	mass spectroscopy

MS-TOF	mass spectroscopy-time of flight
m/z	mass per charge
NMR	nuclear magnetic resonance
NOESY	nuclear Overhauser effect spectroscopy
PM3	Parametric Method Number 3
PPTS	pyridinium <i>p</i> -toluenesulphonate
PCU	pentacyclo[5.4.0.0 ^{2,6} .0 ^{3,10} .0 ^{5,9}]undecane
PCUD	pentacyclo[5.4.0.0 ^{2,6} .0 ^{3,10} .0 ^{5,9}]undecane dione
s	singlet
t	triplet
THF	tetrahydrofuran
THP	tetrahydropyran
Trityl	triphenyl methyl
Tosyl	<i>p</i> -Toluenesulphonyl
Triflate	trifluoromethanesulphonate
U.V.	ultraviolet
ZDO	zero differential overlap

ACKNOWLEDGEMENTS

"I can do all things through God Who strengthens me."

I would like to thank:

Dr H.G. Kruger (my supervisor)

Prof A. Kindness for his encouragement and guidance.

Dr G.E.M. Maguire for helpful discussions of the chemical syntheses.

Prof M. Laing for kindly helping with the proofreading of the final draft.

Dr M.O. Onani for his encouragement and giving up his time to read and comment upon draft copies.

Dr M. Rademeyer for help with the X-ray publications.

Mr J. Magadula and Mr E. Changamu for their help and humour.

Dr N. Koorbanally for helpful comments.

Ryszarda and Andrez Kudlinska for their support and encouragement throughout my MSc.

Kameer Beharry, Mayshree Bejaichand, Jonathan Chetty, Nishlan Govender, Avinash Harilal, Abdul Mahomed, Natasha Misheer, Clandy Naidoo, Tyrone Negus, Amith Singh, Tarryn Toach, and colleagues at the University of KwaZulu-Natal for helping make my research intellectually stimulating and fun. I thank the Technical staff at the University of KwaZulu-Natal. I thank Dr M. Fernandez and Dr D. Levendis from the University of Witwatersrand for the X-ray crystallography data, Dr L. Fourie from University of the North West for the mass spectroscopy data and Mr D. Jagjivan from the University of KwaZulu-Natal, Howard College Campus for processing all the nuclear magnetic resonance data. I thank the NRF and the University of KwaZulu-Natal for the financial support.

"Success is not measured by the position one attains in life but rather the obstacles one overcomes while reaching one's goals."

LIST OF CONFERENCE PRESENTATIONS

- R. Ramdhani and H.G. Kruger, Towards the Rational Design of Pentacycloundecane Host-guest Systems, The Frank Warren Conference, Rhodes University, Grahamstown, RSA, 2003.
- R. Ramdhani and H.G. Kruger, The Design and Synthesis of Chiral Pentacycloundecane Host-guest Systems, The 37th South African Chemical Institute Conference, CSIR International Conference Centre, Pretoria, RSA, 2004.
- R. Ramdhani and H.G. Kruger, The X-Ray Study of Pentacycloundecane Derivatives, The University of KwaZulu-Natal, Howard College, South African Chemical Institute Colloquium, 2005.
- R. Ramdhani and H.G. Kruger, The Structural Investigation of Pentacycloundecane Derivatives, The 2005 Younger European Chemists Conference associated with Masaryk University and the Czech Chemical Society, Brno, Czech Republic, 2005.

LIST OF JOURNAL PUBLICATIONS

- Kruger, H.G. and Ramdhani, R., The NMR elucidation of classic pentacycloundecane derivatives, South African Journal of Chemistry, submitted for publication (October 2005).
- Kruger, H.G.; Rademeyer, M. and Ramdhani, R., 3,5-Bis(2-hydroxyethyl)-4-oxahexacyclo-[5.4.1.0^{2,6}.0^{3,10}.0^{5,9}.0^{8,11}] dodecane, Acta Crystallographica E61, 2005, 3968-3970.
- Kruger, H.G.; Rademeyer, M. and Ramdhani, R., A pentacycloundecane dimer, Acta Crystallographica E62, 2006, 966-968.
- Kruger, H.G.; Rademeyer, M. and Ramdhani, R., Pentacyclo-[5.4.0.0^{2,6}.0^{3,10}.0^{5,9}]undecane-8-11-dione-mono-ethylene ketal, Acta Crystallographica E61, 2006, 268-270.
- Kruger, H.G. and Ramdhani, R., The NMR elucidation of a novel pentacycloundecane dimer, South African Journal of Chemistry, submitted for publication (December 2005).

CHAPTER ONE

HOST-GUEST CHEMISTRY

This thesis focuses on the applications and enantiomeric recognition capabilities of chiral crown ethers, as well as the synthetic routes to some precursors of cage annulated macrocycles. This chapter reviews the significance of chirality in molecular recognition processes, the lock-key system in enzymes and an introduction to host-guest chemistry. A brief discussion on the synthesis and applications of achiral and chiral crown ethers will also be covered.

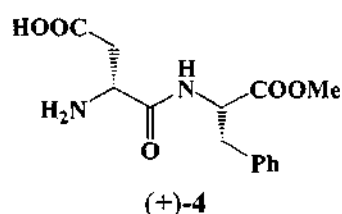
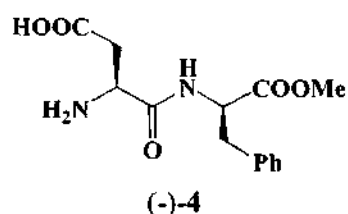
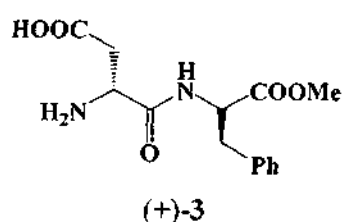
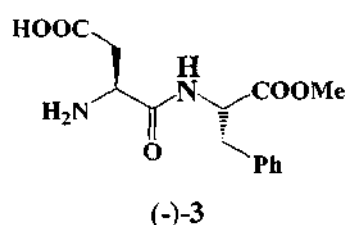
A central feature in Nature is that complexes are characterized by a high degree of mutual structural recognition between host and guest molecules. In enzyme catalysis, transport mechanisms and regulatory systems, complexation occurs which results in the chemical and physical properties of both host and guest being vastly altered.¹ An important objective in current synthetic organic chemistry is the imitation of Nature's selective and highly efficient biological processes.¹ In such processes mutual recognition of a species at a molecular level is essential. With the development of modern and sophisticated synthetic, separation and analytical techniques, chemists are trying to design and synthesize host compounds that will demonstrate some properties of nature's catalysts, carriers and regulators.¹ Chirality and the process of enantiomeric recognition will be explained next, to enable a better understanding of the concept of molecular recognition.

1.1 THE BIOLOGICAL IMPORTANCE OF CHIRALITY

There has been a demand for optically pure chiral compounds and one may ask, "Why is there such a demand for asymmetric synthesis and chiral molecules?"

In order to answer this question, the importance of chirality in the world around us should be considered. The need for chiral synthesis of pharmaceutical drugs will then become apparent. A molecule is said to be chiral if it is not superimposable on its mirror image. In nature the biological macromolecules of most living systems consist of building blocks made up of largely one enantiomeric form only. This is also true for the proteins in our food chain as well as the protein synthesis in our bodies.

Conventional synthesis is only feasible when there is one-stereogenic unit producing two enantiomers [i.e (R)- or (S)-isomer], which can be separated by resolution or other separation techniques. This may still be inefficient as one of the enantiomers could be ineffective with no commercial value. In molecules with multiple stereogenic centres, the desired product with the correct stereochemistry at each centre can in general only be prepared using asymmetric synthesis. This is the case with the artificial sweetener aspartame (-)-(3), in which only one stereoisomer is sweet and the other three stereoisomers (+)-(3), (-)-(4) and (+)-(4) are all slightly bitter and must be avoided in the manufacturing process.²



An expensive asymmetric synthetic procedure may be justified if it produces exclusively the active stereoisomer. Another reason why asymmetric synthesis is becoming increasingly important is due to environmental factors. Inactive stereoisomers in agrochemicals may seem to be inert in the short term but unless they are rapidly and safely biodegraded there is a risk of long-term side effects due to bioaccumulation. It is undesirable for an active pharmaceutical drug to be administered together with several inactive isomers, which could possibly be harmful in the future.²

Although it is desirable to use biologically active compounds as the pure stereoisomer, it is difficult to separate enantiomers and more effective resolution methods are still being developed. At present many synthetic routes to optically pure compounds exist but to produce the pure stereoisomer may prove to be prohibitively expensive in some

cases. As health laws are becoming stricter, laws are being enforced on pharmaceutical companies to manufacture drugs that are in optically pure form.

The purpose of this study is to investigate chiral host-guest interactions of chiral macrocyclic hosts towards chiral ammonium guest ions utilizing a computational model, which could ultimately be used to resolve racemic amino compounds via U-tube or W-tube^{3,4} experiments. To understand host-guest interactions better, the lock-key system in enzymes will be discussed as this represents a host-guest interaction in its simplest form in nature.

1.2 THE LOCK-KEY SYSTEM IN ENZYMES

A host-guest relationship is a subject of great interest to chemists. It is studied for the purpose of designing better host systems, which could lead to a better understanding of wide range of host-guest interactions in nature such as the relationship between enzyme and substrate. In many cases such host systems are macrocyclic in nature, although bidentate or multidendate ligands also serve as host systems.

Receptor sites are usually concave surfaces on the enzyme, onto which substrates with convex surfaces can bind. The receptor site has a strong affinity for the substrate. Upon substrate binding, which involves non-covalent interactions, the enzyme-substrate complex is formed. It is imperative that the substrate molecules have the correct shape or functional groups to fit into the active site and participate in the interactions. This interaction of (chiral) enzymes with (chiral) substrates is called a lock-key system, and depends on structural recognition when binding to the substrate. Complexation of crown ethers with guest molecules functions according to the same principles.⁵

The basis of many biological processes depends on the ability of molecules to recognize each other and form well-defined complexes with receptor sites or bioactive sites.⁶ The binding process is very specific and selective, with one or more compounds of low molar mass binding to a specific region in a high molar mass receptor, most often a protein or a nucleic acid.⁷ Many processes in nature depend on these ideal complexing of substrates to enzymes. Such processes include symport, antiport and uniport transport mechanisms, neurotransmitter receptors in impulse transmission, antibodies

bound to antigens and signal substances bound to receptors and owe their mechanism of action and specificity to the ideal complexing of the host to the guest.⁶

Specificity is a characteristic feature in enzyme-based catalysis. This degree of specificity for a substrate can vary from complete specificity to fairly broad specificity. Enzyme specificity can also extend to selective discrimination between stereoisomers of a substrate molecule. The enzyme (R)-amino acid oxidase is a good example of stereospecificity. (R)-amino acid oxidase exhibits specificity for only (R)-amino acids and will not catalyse the oxidation of (S)-amino acid stereoisomers.⁸ The reason for this specificity stems from a more favourable chiral interaction between the (R)-amino acid (guest) and the enzyme (host), in comparison with complexation between the (S)-amino acid (guest) and the enzyme (host). Enzymes with an absolute specificity require that the particular substrate have a precise shape, whereas enzymes with a broad specificity have more flexible requirements, hence accepting a wider range of substrate molecules.⁸

Structural recognition in complexation is one of the most important means by which receptor sites of genes, enzymes and immune systems operate in the evolutionary biotic world.⁹ High molar mass enzymes (hosts) in reactions normally exhibit a high degree of stereospecificity with respect to low molar mass substrates (guests) in terms of recognition and catalysis. Host-guest studies attempt to mimic or surpass biological host-guest interactions with synthetic hosts. Imitation of these working features has led to the design and the synthesis of synthetic entities, which are capable of complexation. Host-guest chemistry is a term that is conjoined with the field of synthetic molecular complexation chemistry.¹⁰ To obtain a better overview of host-guest interactions, the background of host-guest complexation in general will be presented next, including examples from achiral systems.

1.3 HOST-GUEST COMPLEXATION

The concept of host-guest chemistry describes the chemistry of molecular association. Hosts may be acyclic, macrocyclic or oligomeric, and may possess cavities or clefts into which the guests fit. Hosts are generally large when compared with guests or with the actual portion of the guests that is bound.¹⁰ The term guest is usually used for both

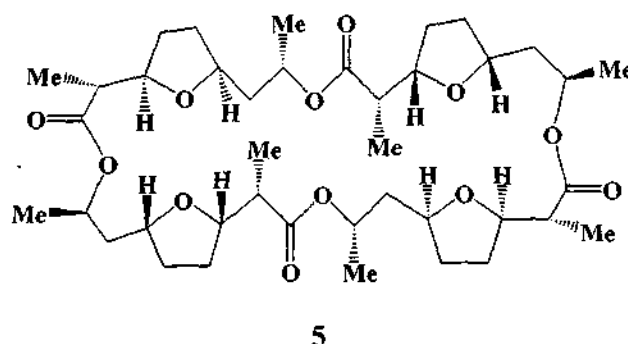
metal ions and organic species and can be described as ionic or neutral molecules, which possess a complementary part to a would-be host either in charge or stereospecificity for effective complexation. Organic guests have more complex steric requirements and offer a greater variety of bonding possibilities than simple ions. Typical guests include ammonium ions, metal ions, and polar neutral species such as hydrogen bonding species, aromatic substrates and salts of organic compounds amongst others.¹⁰

A host-guest complex can be defined as a resultant complex comprising two or more molecules or ions held together by electrostatic forces other than covalent bonds. The molecular complexes are usually held together by hydrogen bonding, ion pairing, π acid to π base interaction, metal to ligand binding, van der Waals interactions, attractive forces due to solvent reorganization, electron donor-acceptor or hydrophobic interactions. Thus in the field of host-guest chemistry, hosts may be referred to as synthetic counterparts of the receptor sites and guests as the counterparts of substrates, inhibitors or co-factors of biological chemistry.⁹

The motivation for research in the field of host-guest chemistry has stemmed from the desire to mimic enzyme behaviour. In many enzyme systems an important property is the ability of the system to differentiate between enantiomeric forms of an organic compound. Since enzymes are chiral, they will interact differently with the two enantiomers of a chiral substrate. Further developments in host-guest chemistry have attempted to synthesize a chiral host that can mimic this enzymatic ability of enantiomeric discrimination, especially since the first step in enzyme catalysis involves the formation of a highly selective molecular complex containing a favourable preorganization of the reactive groups in the system.^{9,11}

The complexing properties of polyethers are not only limited to synthetic ligands, there exists a number of naturally occurring compounds with antibiotic properties, that have the ability to form lipid soluble alkali and alkaline earth ion complexes. Many of these examples contain cyclic ether residues, whilst others are neutral macrocycles with the ring composed of amide and ester linkages (for example valinomycin). The cyclic ether compounds contain macrocyclic neutral molecules and monobasic acids.¹²

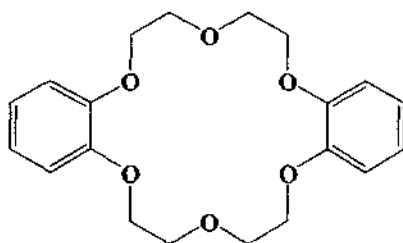
Nonactin (**5**) is a fungal metabolite and is one of the known neutral antibiotics. It contains cyclic ether residues. Its structure consists of this fungal metabolite, which incorporates repeating enantiomeric units. Four units, two of each enantiomeric form, are joined through ester bonds to form a macrocycle. The alternating arrangement of the enantiomeric unit means that the molecule possesses a four-fold alternating axis of symmetry and this is optically inactive. Alkali metal ions can be complexed in this molecule in the sequence $\text{Li}^+ \ll \text{Na}^+ \ll \text{Cs}^+ < \text{Rb}^+ < \text{K}^+$. Nonactin (**5**), in its action with a potassium ion, wraps around it in a conformation resembling the seam of a tennis ball. The potassium ion has a co-ordination sphere of eight oxygen atoms composed of four atoms from the tetrahydrofuran rings and four from the carbonyl groups. Biologically neutral and acidic antibiotics have a marked effect on alkali metal cation transport in respiring cell fragments and on the cation permeability of natural and artificial membranes resulting from their complexation ability to certain cations.¹²



Host-guest chemistry illustrates the 'rules of non-covalency' involved in the recognition and binding of a guest by a synthetic receptor such as crown ethers. A brief introduction to crown ethers and their applications is discussed below.

1.4 CROWN ETHERS IN HOST-GUEST INTERACTIONS

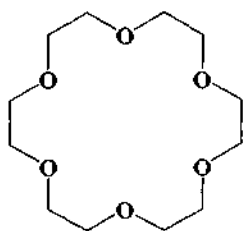
Since the discovery of macrocyclic polyethers (**6**) by Pederson in 1967 and the realization of their ability to form stable selective complexes with alkali and alkaline earth metal cations, there has been an increasing interest in the synthesis and qualitative complexation studies of crown ethers.^{13,14}



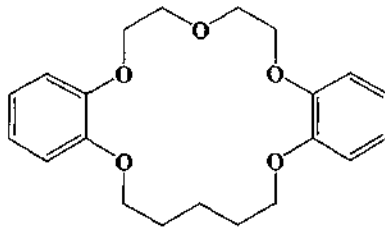
6

The ability to form well-defined complexes with salts and neutral molecules has sparked interest in synthetic macrocyclic ligands. The chemical and physical properties of these complexes have been studied, as well as the factors that determine the ability of the host to recognize the guest so that complexation based on the lock and key mechanism takes place. Crown ethers are capable of high selectivity and structurally specific interactions have been investigated in terms of mimicking the mode of action of enzymes.¹⁵

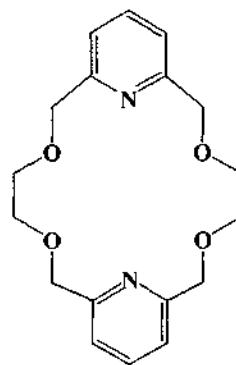
This has resulted in the synthesis of novel molecular hosts, which have become more complex and challenging in design. First generation crown ethers having only oxygen donor atoms (7¹⁴ and 8¹⁴) were soon followed by the synthesis of ligands having additional donor atoms such as nitrogen (9).¹⁶



7

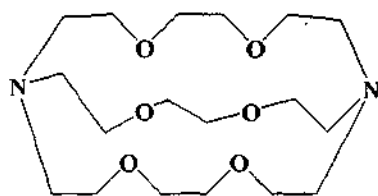


8

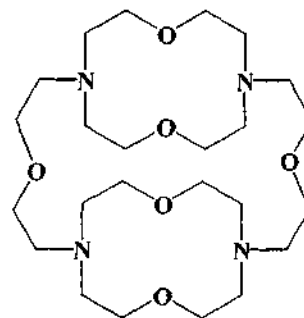


9

Bicyclic (10)¹⁷ and tricyclic (11)¹⁸ compounds such as Lehn's cryptands soon succeeded monocyclic ligands such as (7).

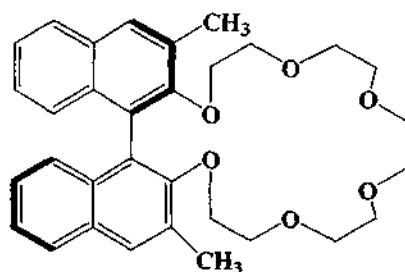


10



11

The next advancement was shape selective ligands (**12**) developed by Cram,¹⁹ which contained additional binding sites or chiral steric barriers at strategic positions near the cavity of the crown ether.^{11,20}



12

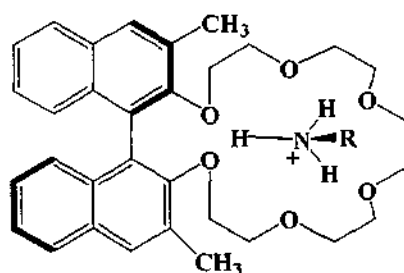
Chiral discrimination can be described as a molecular interaction in which there is a preferred complexation of the chiral host with one enantiomer from a racemic mixture.²¹ Chirality can be induced on a molecular cavity of a crown ether, which is formed by heteroatoms, by incorporating chiral structure elements. There are two different types of chiral elements that can be employed for this purpose.

Type A consists of configurationally stable chiral carbon atoms and type B consists of structural elements that owe their chirality to restricted rotations about a carbon-carbon bond in the molecule.⁷ Crown ethers derived from for example, S-(+) tartaric acid,^{22,23,24} cyclohexane-1,2-diols^{25,26,27} and carbohydrates^{28,29} fall into type A, while Cram's crown ethers incorporating binaphthyl moieties [such as **12**] fall into type B. Recently carbohydrates have been used as a versatile and inexpensive source of chirality

for crown ethers.^{23,30} Sugar units can provide structural constraints to the macrocycles and they are rich in the substituent bismethylenedioxy units and functionalities, which advantageously offer a vast potential for binding molecules with a variety of shapes and sizes.^{31,32,33,34,35} The development of synthetic chiral macrocycles, which exhibit a measure of chiral recognition during complexation, has therefore resulted in much interest. Such chiral macrocycles offer a promise of a tremendous future potential for the separation of enantiomers.

1.5 COMPLEXATION OF AMMONIUM SALTS WITH CHIRAL CROWN ETHERS

Macrocyclic polyethers have the ability to form complexes with primary ammonium ions and this provides a strong motivation to study enantiomeric recognition in compounds containing the $[R-NH_3]^+$ functional group, since amino acids in their zwitterionic and N-protonated forms belong to this class of compounds.¹² Pederson discovered that crown ethers could form complexes with both primary ammonium salts and metal ions. He further explained that these complexes were formed by ion-dipole interactions.^{13,14} Later Cram and co-workers demonstrated the binding interaction between the crown ethers and primary ammonium salts (see Figure 1).



12

Figure 1: Host-guest complex of host (12) with arbitrary ammonium guest

Quantitative data such as the stability constants of these complexes were measured. It was then concluded that complexes of crown ethers with primary ammonium salts were formed by the three hydrogen bonds together with three direct ion-dipole interactions combined alternately (tripod interaction).¹¹ Further experiments by Cram have shown

that it is possible to estimate the relative stability of a host-guest complex formed by a chiral host with a chiral guest by applying CPK (Corey-Pauling-Koltun) molecular models to view the stereochemical relationship between the host and the guest.¹¹

The ability of chiral crown ethers to selectively complex with one enantiomer of an organic ammonium salt can be achieved, provided that the crown ether has effective chiral barriers attached to it. The design and synthesis of optically active crown compounds that were developed by Cram attempted to model the site of substrate binding by enzymes.⁹ Applications such as optical resolution and enzyme models use optically active crown compounds whose functions resemble the substrate binding by enzymes.⁹ This is expected to be useful for asymmetric reactions under the mild conditions of biosynthesis, as well as in research fields of biochemistry and biophysics.³⁶ Further applications of achiral and chiral crown ethers will be discussed below.

1.6 APPLICATIONS OF CROWN ETHERS

Crown ethers are extraordinary molecules, which have played an important role in many biochemical applications. A field, which Cram has named "host-guest chemistry", has become one of the most active and expanding fields of chemical research and interest.^{36,37,38,39,40} Scientists believe that the unique properties of crown compounds hold the potential to break fresh ground in new areas of science such as supramolecular chemistry⁴¹ and biomimetic⁴² chemistry. A variety of modifications to the structure of crown ethers have been achieved during the search for new functions. The applications of achiral crown ethers will be discussed first, followed by chiral crown ethers.

The extraordinary ability of crown ethers to form stable selective complexes with various cations has been used to advance diverse processes ranging from: phase transfer catalysis,^{43,44,45,46} the transport of ions through artificial and natural membranes^{47,48} and for the construction of ion selective electrodes.⁴⁹ Crown ether complexes are often soluble in apolar solvents due to their lipophilic exterior. This property has been successfully exploited in liquid-liquid and solid-liquid phase transfer reactions. Crown ethers have also many other applications including isotope separation. By varying the

type of hosts it is possible to extract radioactive strontium or toxic cadmium and lead ions without affecting the other ions, thereby allowing crown ethers to be used to protect the environment.^{50,51}

Nakatsuji and co-workers⁵² have examined the potential of crown ethers as models for natural ionophores and have succeeded in developing a novel uphill transport system in which two different cations are transported in opposite directions against their concentration gradients through a bulk liquid membrane by using a pH responsive crown ether as the ion carrier.

Applications for chiral crown ethers also exist. One area of interest is the enantiomeric recognition of organic amines by chiral macrocyclic ligands.^{39,53,54} The study and understanding of enantiomeric recognition of amines and protonated amines by chiral macrocyclic ligands is of significance, since such synthetic systems could possibly lead to a better understanding of natural systems.⁵⁵ Other examples of the extensive use of crown compounds in this area are the use of optically active crown compounds for the resolution of amino acids,⁵⁶ applications to enzyme models or enzyme mimics¹⁵ and enantiomeric recognition of chiral organic ammonium salts.^{57,58,59} Synthetic macrocyclic polyethers (crown ethers) have played an important role as substitutes for naturally-occurring molecules in living systems. A possible field of application is in kidney dialysis, since macrocycles are capable of forming complexes with neutral molecules, the possibility of using crown ethers as potential selective complexing agents for urea has been examined.^{60,61}

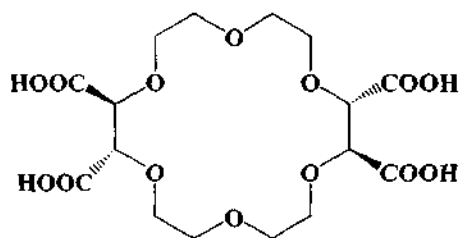
There have been many developments reported in the design and synthesis of chiral and functionalised complexing agents that are capable of enantiomeric recognition of organic primary ammonium cations in the last decade and these are discussed below. The design of receptor molecules for primary ammonium cations requires that an appropriate macrocyclic subunit be selected, which would display efficient binding properties toward primary ammonium cations and provide an anchoring site for the cationic $-\text{NH}_3^+$ head.

Chiral host macrocycles and chiral guests have been studied over the years using a number of different techniques. A high degree of chiral recognition was observed when

Cram and co-workers studied chiral crown ethers incorporated with 1,1'-binaphthyl moieties. The following methods have been used to study enantiomeric recognition of chiral crown ethers: ^1H NMR spectroscopy,^{62,63} enantiomeric separation^{40,64,65,66,67} by silica gel or polystyrene packing material attached to chiral crown molecules (solid-liquid and liquid-liquid chromatography), UV-studies,^{68,69} fluorescence spectroscopy^{70,71,72} and extraction studies using a U-tube and W-tube.^{3,4} Some of the applications will be highlighted and expanded on below.

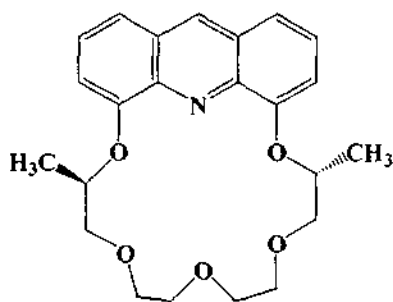
Recently chiral crown ethers have been incorporated into the walls of nanotubes, rendering them useful for enantioselective processes. The ability to incorporate chiral functionalities inside the interlocked nanotubes promises to lead to novel chiral zeolitic materials exploitable for enantioselective separations and catalysis.⁷³ It has been shown that chiral crown ethers derived from (R)-glucose can be used in catalytic asymmetric synthesis to induce enantioselectivity.^{35,74} The chiral nature of the crown ether, the rigidity of its cavity and the quality of the side arms plays an important role as a phase transfer reagent in Michael addition and Darzen's condensation reactions.^{35,75}

Since the 1990's fine chemical industries, which supply drug manufacturers with complex intermediates and active ingredients, have been acquiring, developing and expanding chiral technologies in response to the rising demand for single enantiomers of chiral intermediates.⁷⁶ Optically active (+)-(18-crown-6)-2,3,11,12-tetracarboxylic acid (**13**) has been successfully employed as a chiral selector in enantioseparations of diverse amino acids and chiral primary amines in capillary electrophoresis. Further optimization of these crowns could result in a chiral discrimination tool for optical purity tests of amino acid drugs.⁷⁷



13

Prodi and co-workers⁷⁸ have reported the synthesis of an acridino-18-crown-6 ligand (**14**) that exhibits high enantioselectivities for chiral organic ammonium ions. The interaction between the crown ether and ions causes a pronounced change in the luminescence of the two partners, making the chiral crown ether a suitable fluorescent chemosensor for enantiomeric recognition of organic ammonium salts. The application of photoluminescence spectroscopy is a very sensitive tool for monitoring the chiral recognition of the enantiomerically pure crown ether towards enantiomers of organic ammonium salts and is gaining more interest for practical applications.⁷⁸



14

Fluorescence spectroscopy has been widely used as a new technique for the chiral resolution of enantiomers.^{70,71,72} The study of enantiomeric recognition of chiral amines and their perchlorate salts by crown ethers has also been studied using UV-visible spectroscopy.⁶⁸

It has been shown that crown ethers play a significant role in many fields and are continuously being modified for new applications. The design and modification of chiral crown ethers require that many factors be taken into consideration. Chapter 2 will expand on these factors.

CHAPTER TWO

THE DESIGN OF A THEORETICAL CHIRAL MACROCYCLE

In order to design a theoretical chiral macrocycle for the purpose of complexation with chiral ammonium ions, one must take into account what encompasses a good host and secondly the mechanism of host-guest complexation.

2.1 PROPERTIES OF A GOOD HOST AND FACTORS REQUIRED FOR GOOD CHIRAL RECOGNITION

Cram and co-workers designed host-guest complexes by using and manipulating CPK molecular models. Later his co-workers synthesized these host complexes to test them experimentally. This demonstrated that host-guest complexes could be designed rationally by using molecular modelling and a few physical organic concepts.⁹

Chiral agents, such as (R)- α -ephedrine,⁷⁹ binaphthol³ and amino acid derivatives⁸⁰ have been used to induce chirality in macrocycles.^{69,81,82,83,84,85,86} For a macrocyclic receptor to achieve good chiral recognition there are certain rules and properties that have to be considered. When designing a host system for the purpose of enantiomeric recognition the following rules should be considered:^{40,87}

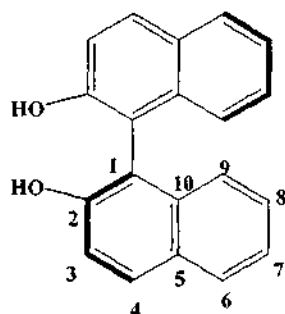
- Good enantiomeric selectivity requires a stable diastereomeric complex between the host and the guest. Enantiomeric discrimination depends on the steric repulsion between the substituents at the chiral portion of the host macrocycle and the guest molecule.⁸⁸
- Both the host and guest compounds should be easy to synthesize. Facile methods to isolate them in a pure form should exist.
- The host and guest compounds should be stable, reusable and recoverable.
- In order to determine the enantioselectivity of the system, the absolute configuration of both the host and guest should be known.
- The systems should be simple and of a low molar mass.

- The incorporation of large chiral barriers in crown ethers result in increased enantiomeric recognition, however if the chiral barrier is too bulky, complexation may be prevented.⁸⁹
- It has been shown by Still *et al.*⁹⁰ that a rigid diastereomeric complex between the host and guest is essential for good enantiomeric discrimination. In flexible complexes, the enantiomers usually orientate themselves so as to avoid the steric hindrance created by the chiral barriers, at the expense of chiral recognition.⁹¹
- Stereochemical complementarity should exist between the chiral macrocyclic compound and guest enantiomers.⁹²
- Higher enantioselectivity for the chiral recognition of α -chiral primary organoammonium ions is shown by macrocyclic ligands possessing C_2 and D_2 symmetry over those with C_1 , C_3 and D_3 symmetry.⁵⁶ These symmetries are preferred so that the host is non-sided and an identical complex is obtained if the guest complexes to either side. It was conclusively reported that chiral recognition in these environments (C_1 , C_3 and D_3 symmetry) may not be feasible.⁴⁰

2.2 CROWN ETHERS WITH BINAPHTHYL CHIRAL GROUPS

Between 1970 and 1974, Cram and co-workers designed and synthesized crown ethers incorporating 1,1'-binaphthyl units or 1,1'-ditetralyl subunits as the chiral elements.^{93,94,95,96,97,98} The principle behind the insertion of the binaphthyl group into an optically active crown ether is that a chiral cavity is produced, therefore making it possible to utilize optical isomerism by restricted rotation (atropisomerism).³⁶

The absolute configuration of the 2,2'-substituted-1,1'-binaphthyl group (**15**) has been determined by Yamada *et al.*⁹⁹ see Figure 2 below.



15

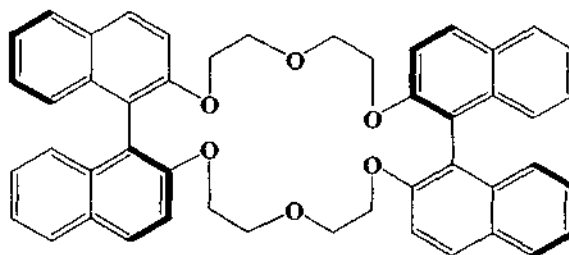
Figure 2: 2,2'-disubstituted-1,1'-binaphthyl group (15)

The advantages of using the 1,1'-binaphthyl unit as a chiral barrier in macrocycles are:⁸⁷

- Firstly the diameter of the cavity is slightly adjustable since the aryl-aryl bond angle is variable and acts as a hinge.
- Moreover the binaphthyl unit can replace an ethylene unit without much change in the spacing of the oxygen atoms attached to the 2,2'-positions of the 1,1'-binaphthyl, retaining the normal crown ether backbone.
- Chains can be attached to the 3,3'-positions to extend the chiral barrier and the substituents are directed along the sides (above and below) of the macrocycle. Cram and co-workers reported that the methyl groups inserted in the 3- and 3'-positions of the 1,1'-binaphthyl groups act as additional steric barriers thereby increasing the chiral recognition ability.¹⁰⁰
- Chains attached to the 6,6'-positions diverge from the binding site and can be used to manipulate solubility properties or attach the hosts onto a solid support for chiral chromatographic separation.⁹⁴

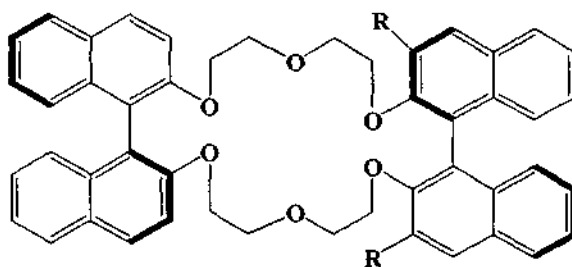
When the 2,2'-bisoxy-1,1'-binaphthyl unit is present in a macrocycle, the unit rigidly extends in three dimensions placing one naphthalene ring above and in a plane tangent to the macrocycle and placing the second naphthalene below and tangent to the macrocycle. The plane of the naphthalene rings is perpendicular to the plane of the macrocycle. The two oxygens are located approximately 75° with respect to one

another. A binaphthyl unit possesses useful symmetry properties. It has a C_2 axis and does not impart the unwanted property of "sidedness" to the hosts. The unit is chiral and the aryl rings are potential chiral barriers that should impart the property of chiral recognition to the central macrocycle and in turn toward suitable guests.⁹⁴



16

The introduction of additional functional groups on the binaphthyl group creates new potential binding sites to achieve stereoselective binding with the guest. It was proposed³⁶ that the introduction of methyl groups on the binaphthyl moiety of the crown ether (16), sterically inhibits electron delocalization into the aromatic rings and act as an extension of the chiral barriers. Furthermore the inductive effect of the methyl groups makes the aryl oxygen more basic, making it a better binder for cations.³⁶



17 R = CH₃
18 R = CH₂Cl

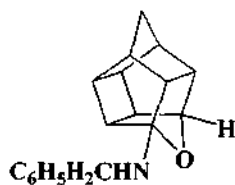
Chiral recognition experiments with binaphthyl crown ethers have been carried out to examine the recognition of a racemic guest by optically pure hosts and have succeeded in the optical resolution of racemic primary ammonium salts and amino acid ester salts.^{1,101} The enhanced chiral recognition that was observed during U-tube extraction studies was associated with hosts bearing -CH₃ (17) and -CH₂Cl (18) groups in the 3,3'-positions of one of the binaphthyl units.¹⁰⁰ Structural refinement of the binaphthyl host

(R,R)-16 has resulted in the highest chiral recognition being exhibited. The results were predicted in advance from the CPK molecular models which indicated that there was a complementarity interaction between the (R,R)-17 host and the (R)-guest and a lack of complementarity between the (R,R)-17 host and the (S)-guest. Secondly it was reported that the -CH₃ (17) and -CH₂Cl (18) groups enforce a conformation on the ArOCH₂ units in which the electron pairs of the oxygen atoms are turned inward and are favourably situated for binding with the -NH₃⁺.³ The experimental results correlated with that predicted by the CPK models and showed that the (R)-enantiomer of the guest was extracted preferentially into the organic layer. Chiral recognition factors between diastereomeric complexes were predicted to be 1.9 kcal mol⁻¹ and 0.42 kcal mol⁻¹ for host (R,R)-17 with the (R)-C₆H₅CH(CO₂CH₃)NH₃⁺PF₆⁻ guest and host (R,R)-17 with the (R)-CH₃CH(CO₂H)NH₃⁺ClO₄⁻ guest respectively.⁹

Another moiety, which was incorporated into crown ethers due to its positive properties, is the pentacycloundecane (PCU) unit. A brief introduction of the PCU unit and its applications is covered in § 2.3. However more focus will be given to the incorporation of the PCU skeleton into macrocycles, and its effect on the structural capabilities of such macrocycles. The full structural NMR elucidation of the PCU dione and its derivatives will be reported in detail in Chapter 6 and the X-ray structures of the PCU derivatives will be reported in Chapter 7.

2.3 APPLICATIONS OF THE PENTACYCLOUNDECANE MOLECULE

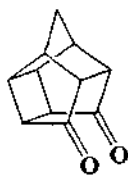
Since 1-aminoadamantane's activity as an anti-viral and anti-Parkinson agent^{102,103,104} has been established, there has been an increased interest in roughly spherical cage amines of similar types.¹⁰⁵ In 1989 a polycyclic amine compound (19, NGP1-01) was reported to have calcium antagonistic activity which is used clinically for the treatment of a variety of cardiovascular disorders.^{106,107,108} Polycyclic cage compounds have a wide scope of pharmaceutical applications ranging from the use as an anti-viral agent against influenza and the immunodeficiency virus (HIV) to the proposed treatment of diseases such as Parkinson's and Alzheimer's disease.¹⁰⁹



19

Since strained polycyclic cage compounds have a high net volumetric heat of combustion associated with them, they have been investigated as a new class of propulsion energetic materials.^{110,111,112,113} The cage structure has a spatially more compact way of arranging the atoms, which is of significance for the potential applications of high-energy organic explosives.^{114,115,116}

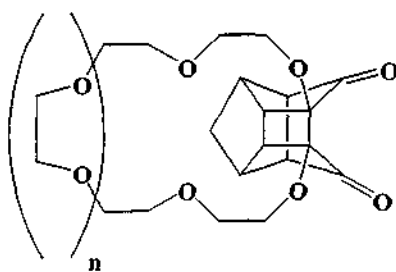
Cage molecules can offer a wealth of information regarding for example, the effects of strain upon molecular stability and chemical reactivity and structure–reactivity relationships in saturated systems.¹¹⁷ Such molecules are sometimes used as intermediates in highly regioselective syntheses of complex organic molecules and of natural products.¹¹⁸ Cage compounds are highly compact and often contain considerable strain energy that results in bond angle and bond length deformations.¹¹⁸ Frequently, the strain energy contained within the cage molecule can express itself through unusual patterns in chemical reactivity.¹¹⁶ Rigid cage molecules have a marked advantage over conformationally mobile molecules since their reaction centres are fixed with regard to the remainder of the molecular skeleton therefore perturbations due to the conformational changes are effectively diminished or removed. This results in the understanding of many chemical transformations being simplified and the analysis of structure-reactivity relationships being permitted. Mechanistic studies as well as organic synthesis have taken advantage of the potential interaction between two reactive centres in conformationally restricted molecules.¹¹⁹



20

Derivatives of pentacyclo[5.4.0.0^{2,6}.0^{3,10}.0^{5,9}]undecane dione (PCUD)^{120,121} (**20**) have been used as valuable substrates in many organic chemical syntheses.¹²² As mentioned above, the pentacycloundecane (PCU) moiety has found various applications. One application that is of great interest is its incorporation into crown ethers and this will be discussed below.

PCUD (**20**) has been incorporated into supramolecular systems with a potential application as new material for nanotechnology applications.¹²³ Crown ethers containing the PCU skeleton have been designed to complex heavy metals for the selective removal of toxic metals from industrial waste disposed in the environment. Their binding abilities have been investigated and evaluated by Electrospray Ionization/Quadrupole Ion Trap Mass Spectrometry.⁵¹ The PCU moiety has also been incorporated into cage functionalized cryptands as hosts for the selective complexation and transport of Li⁺ and Na⁺ picrates.¹²⁴ In 1986 Hayakawa incorporated the first PCU moiety into crown ethers such as (**21**) however their properties as hosts were not examined and the PCU moiety was not used as part of the crown ether backbone.^{125,126,127}



21

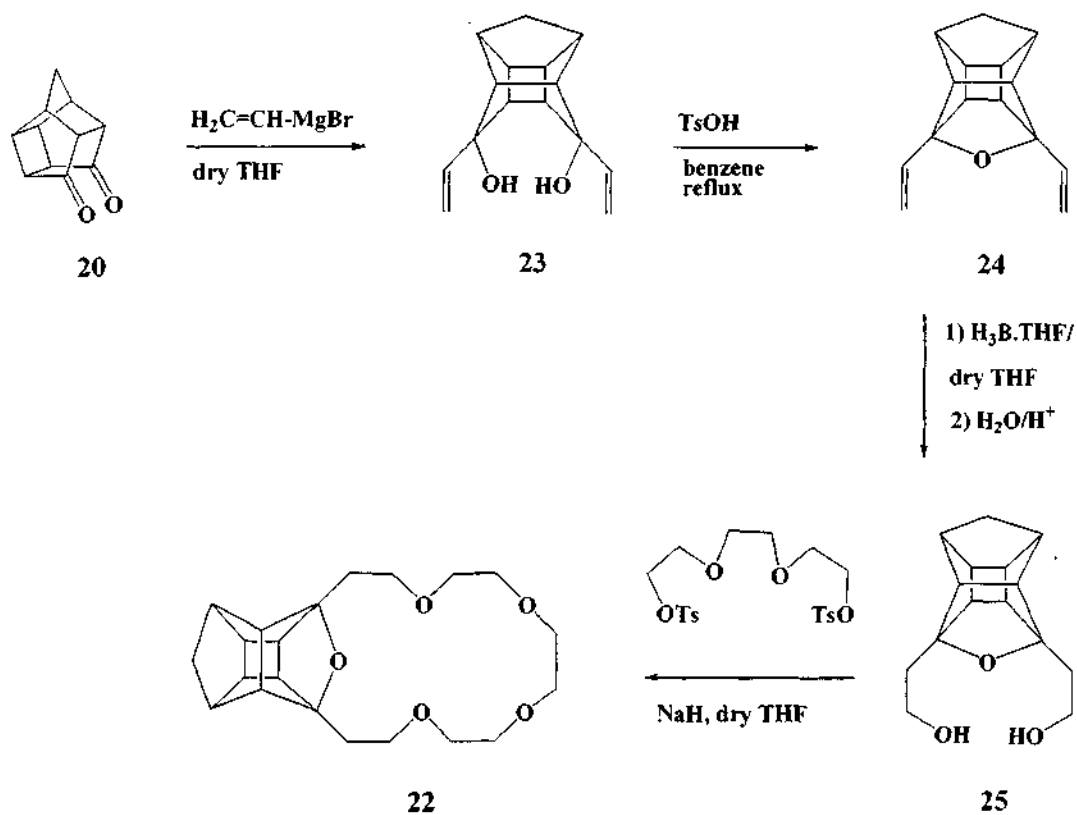
The incorporation of the cage moiety as part of the backbone of the ligand offers the advantage of allowing bridgehead oxygen atoms to participate, together with other donating atoms in the complexation of the guest.¹²⁸ Simple monocyclic crown ethers

lack facial differentiation i.e. there is no distinction between the guest ion approaching toward the top side or bottom side of the approximate plane of the crown ether backbone. Although the PCU (20) unit is a meso compound, when it is attached to chiral ligands it becomes chiral thereby rendering the faces of the crown ether inherently diastereotopically non-equivalent.¹²⁸

According to Cram's initial rules discussed above (see §2.1) this feature is not desirable for chiral discrimination. The reason is that the PCU cage annulated crown ether has C_1 symmetry, which results in two potential complexation "faces" available to the guest molecule (see Figure 4, §3.6). According to literature⁵⁶ C_2 symmetry is preferred for maximum chiral influence since it is non-sided and equivalent (see §2.1). However as will be demonstrated below, the advantages of using the PCU cage seem to outweigh its "disadvantages". Previous studies of cage functionalized crown ethers^{4,128} have demonstrated that the incorporation of the PCU framework into chiral crown ethers leads to the enhanced enantioselectivity by providing:

- A high degree of rigidity in the crown ethers.¹²⁸
- Two potential faces to an approaching guest.¹²⁸
- Increased solubility in non-polar solvents (i.e lipophilicity).¹²⁸
- Higher rates of transport of chiral organic ammonium salts across the U-tube into the organic phase.⁴

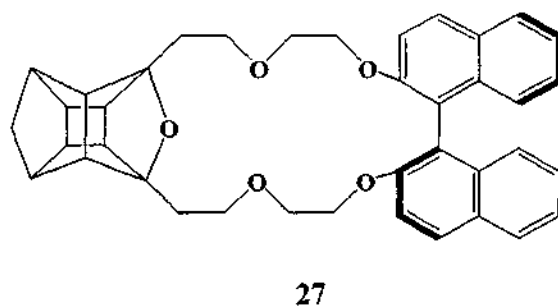
Marchand *et al.* have previously synthesized non-chiral crown ethers containing the cage moiety as part of the "backbone" (22).¹²⁹ The synthetic route of (22) is shown in Scheme 1 below.



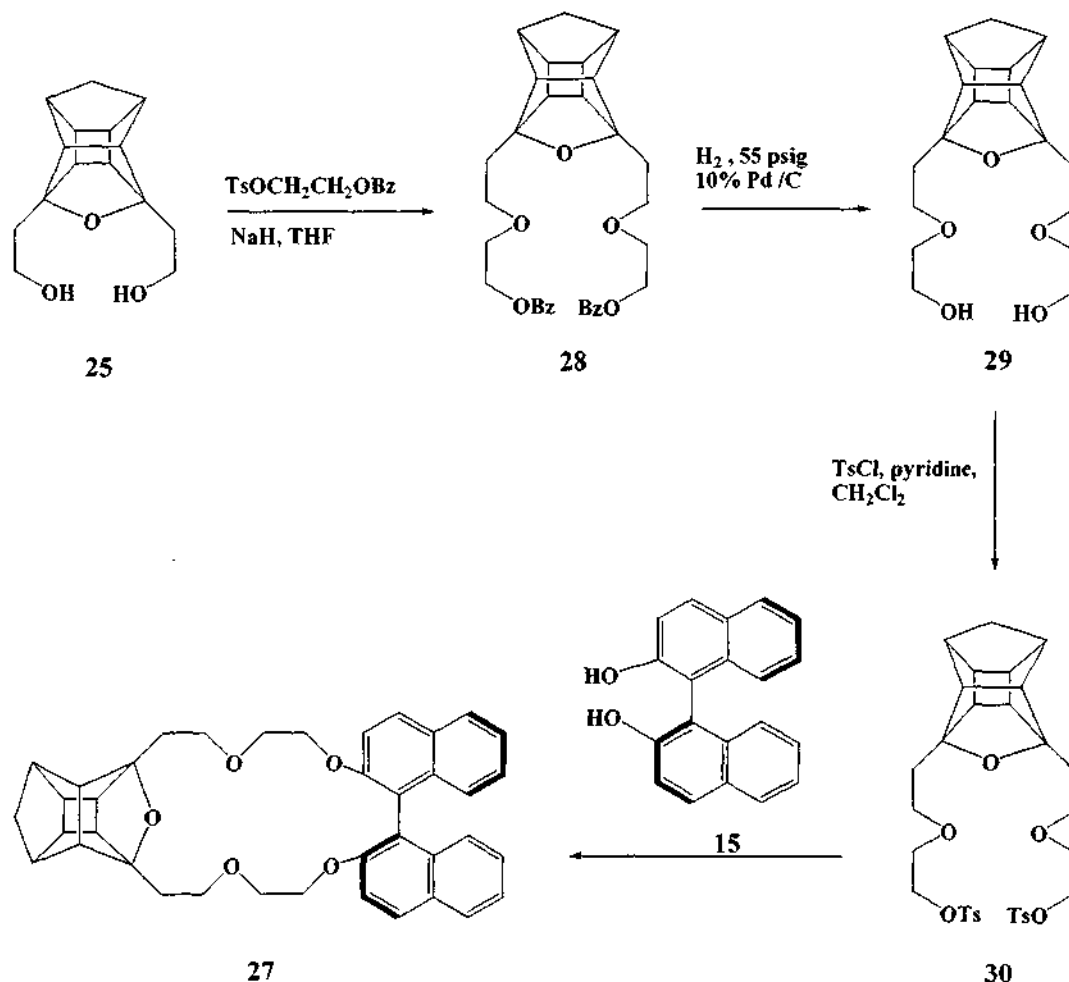
Scheme 1: Synthetic route to cage annulated macrocycle (22)¹²⁹

The synthesis¹²⁹ of this non-chiral crown ether (22) uses the tosylate leaving group on the glycol segment. The cyclisation step is carried out using the cage diol (25) and the triethylene glycol ditosylate.

The first chiral crown ether incorporating the PCU unit (27) was reported in 1999 by Marchand *et al.*⁴ The optically active cage functionalized crown ether incorporates Cram's 1,1'-binaphthyl moiety as a source of chirality.



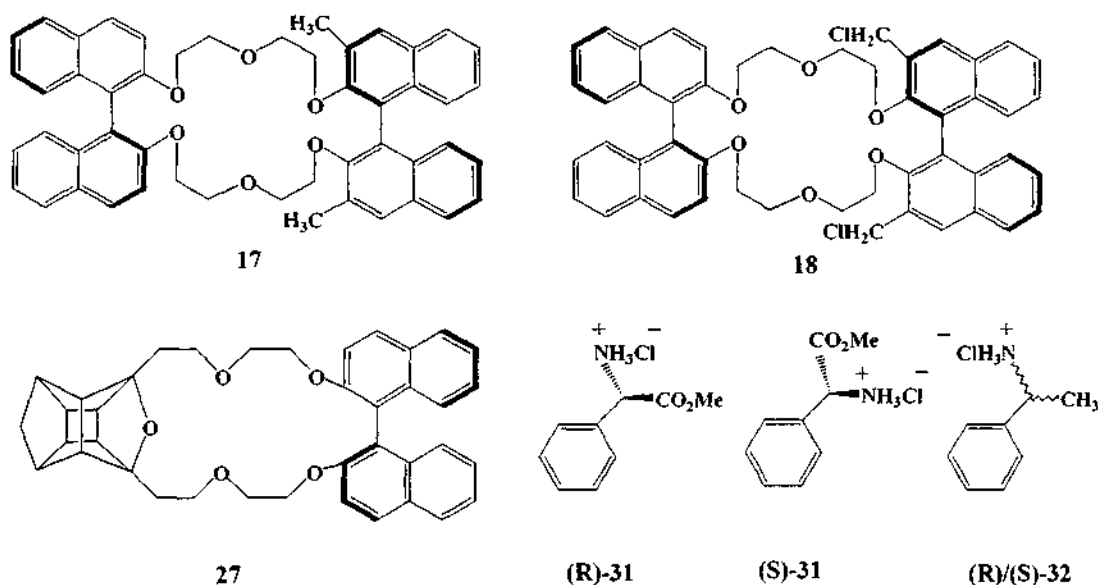
Chiral cage annulated macrocycles such as (27) were synthesized using the following synthetic route. In this synthetic approach (Scheme 2) the tosylate leaving groups are attached to the cage moiety, which is then coupled to the binaphthol (15).



Scheme 2: Synthetic route to chiral cage annulated macrocycle (27)⁴

Crown ethers (R,R)-**17**³, (R,R)-**18**³ and (R)-**27**⁴ have been tested experimentally using a U-tube to determine their chiral recognition capabilities towards chiral organic ammonium salts. Cram's crown ethers (R,R)-**17** and (R,R)-**18** have provided the benchmark for subsequent extraction studies with an experimental enantioselectivity of 78 % and 82 % respectively for (R)-**31** over the (S)-**31** guest molecule (see Chapter 3 for reference to these experimental results being used as benchmark for a computational model).³ Marchand's cage annulated crown ether (R)-**27** exhibited good

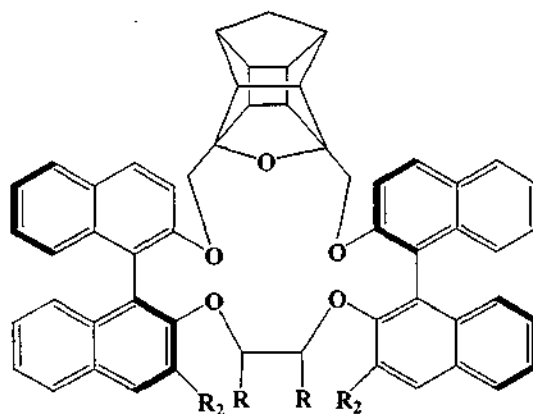
enantioselectivity of 79 % with α -methylbenzylammonium ion (**32**) when tested in extraction/transport studies using a U-tube.⁴



Crown ethers (R,R)-**20**, (R,R)-**32** and (R)-**27** have also been studied previously¹³⁰ using computational methods (see Chapter 3). The computational model also recognises the excellent enantiomeric recognition capabilities of the binaphthyl derived crown ethers. Since cage macrocycles have exhibited promising results as hosts in both experimental extraction studies as well as computational studies,¹³⁰ it was decided to design a theoretical crown ether that incorporated both the binaphthyl and PCU moieties and then examine its enantioselectivity towards chiral ammonium salts utilizing the same computational model.

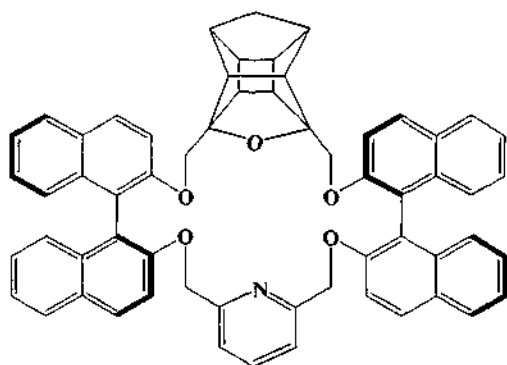
2.4 DESIGN OF A NOVEL THEORETICAL CAGE CROWN ETHER

Based on the above literature it was decided to extend the computational study¹³⁰ by postulating the theoretical crown ether (S,S)-**33** incorporating two 1,1'-binaphthyl subunits as well as the pentacycloundecane cage and examining its enantiomeric recognition capabilities (see Chapter 3).

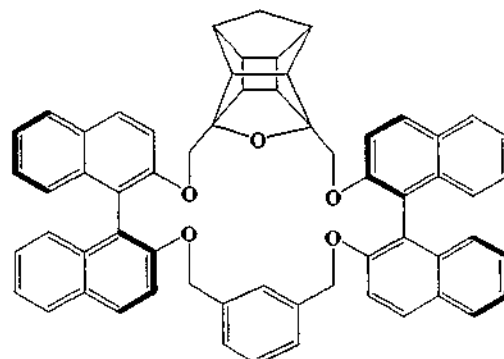


33

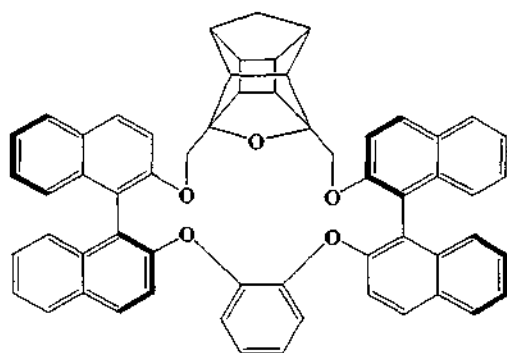
Several crown ether analogues are possible by the substitution of the R-CH-CH-R group in (33). For example a pyridine (34) or benzene (35, 36) moiety can be used for rigidity or an ethylene group (-CH₂-CH₂-, R=H) or diethylene glycol group (37) for flexibility of the crown ether. In addition chains can be attached to the 3,3'-positions (R₂) of the binaphthyl thereby extending the chiral barrier.



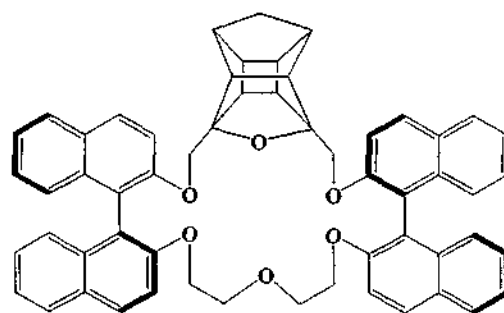
34



35



36



37

Computational models attempt to supply qualitative predictions of the complexing abilities of the crown ether and hence give a “feel” for the expected properties of the new host. Computational studies, which were performed (see Chapter 3) on the novel crown ether (S,S)-**33**, indicated that this system could be a good host capable of excellent enantioselectivity. However it is imperative that the predicted properties of such a system are verified through synthesis and U-tube experiments.

CHAPTER THREE

COMPUTATIONAL CHEMISTRY

This chapter will expand on a computational model¹³⁰ that predicts the enantioselectivity of some new host-guest systems as well as their approximate binding energies. The computational model was developed as a collaborative project in our laboratory. The PhD studies of T Govender¹³⁰ and the results of this investigation formed the basis for the computational model. This study will compare the results obtained using the computational model (MM3 force field “gas phase” calculations in Alchemy 2000¹³¹) with the results obtained previously.¹³⁰ The current study will attempt to improve the computational model by upgrading the MM3 force field “gas phase” calculations in Alchemy 2000¹³¹ to include solvation effects (chloroform and water) using MacroModel.¹³² The effect of solvation (chloroform and water) on the binding energy and enantioselectivity of host-guest complexes will be investigated.

3.1 INTRODUCTION TO COMPUTATIONAL CHEMISTRY

Researchers in host-guest chemistry have found that it is difficult to visualize the resulting host-guest complex without a three-dimensional representation. Designing a new host relies on the aid of molecular models therefore the use of molecular modelling on computer has become necessary.¹⁰

When designing a host, CPK molecular models have been used in established research groups such as that of Cram's to provide invaluable assistance in examining the various molecular possibilities between hosts and guests. Since host-guest binding energies are relatively small, little energy is available to deform bond angles or to compress groups during complexation.¹³³ Space filling scale models have bond angles and distances that are based on X-ray structure data which apply at room temperature and can provide a rough guide for testing whether a host structure will bind to a given organic guest compound. Force field methods¹³⁴ allow for atoms and bonds that are not fixed at one size and length and allow the prediction of relative energies and barriers for the interconversion of different conformations. Computational chemistry or molecular

orbital calculations are at present a better and more advanced option available to organic chemists.

Computational chemistry attempts to supply information about the design of new systems or the interpretation of the properties of existing systems. Computational methods include model building and geometry optimizations.¹³⁵ The geometry calculation is performed by a program using mathematical algorithms to search for a minimum on the potential energy profile of a specific molecule. The use of different software packages allows one to build structures and to perform various molecular orbital calculations on them. Computer programs such as Gaussian,^{136,137} Hyperchem,¹³⁸ and Alchemy¹³¹ are commercially available. Some graphics workstations contain crystallographic databases as well as templates and builders, which allow easy docking operations for the manipulation of the intermolecular positioning.¹⁰ Molecular orbital calculations include *ab initio*,¹³⁹ semi-empirical¹³⁵ and molecular mechanics techniques.^{135,140,141,142,143}

Quantum mechanics and molecular mechanics are the two broad fields within computational chemistry, which deals with the structure and reactivity of molecules. The basic types of calculations performed using quantum mechanics and molecular mechanics include the following amongst others:

- Calculations of the energy of a particular molecular structure or physical arrangement of atoms or nuclei.
- The geometry optimization of the lowest energy molecular structure, which is located in close proximity to the specified start structure.
- The computations of the vibrational frequencies of molecules, which result from interatomic motion within the molecule.

3.2 QUANTUM MECHANICS

Electronic structure methods use the laws of quantum mechanics. Quantum mechanics states that by solving the Schrödinger equation, the energy and other properties of a

molecule may be obtained. The three classes of electronic structure methods are described briefly below.

3.2.1 AB INITIO

Ab initio methods do not use experimental parameters in their calculations and are derived solely from theoretical principles. The laws of quantum mechanics and the input values of a small number of physical constants are used in the computations.¹³⁷ *Ab initio* computations can provide high quality quantitative predictions for a broad range of systems. *Ab initio* methods derive information by solving the Schrödinger equation using a series of mathematical approximations.¹³⁷ The introduction of a basis set (mathematical description of the molecular orbital) is an approximation present in all *ab initio* methods. The type of basis functions used also influences the accuracy. The advantage of using *ab initio* methods is that once the approximations become small, they usually converge to the exact solution. This can be achieved by improving the level of theory (e.g. to include electron correlation) and to increase the size of the basis set (i.e. remove limitations on the size and geometry of the molecular orbitals). The disadvantages of *ab initio* calculations are that they are expensive in terms of the utilization of CPU time, memory and disk space.¹⁴⁴

3.2.1 DENSITY FUNCTIONAL THEORY (DFT)

The Density Functional Theory (DFT) approach approximates the effects of electron correlation via the general functional of the electron density.¹⁴⁵ The DFT method is based on the theory by Hohenberg and Kohn.^{146,147} DFT methods are not as expensive as *ab initio* methods, however they require the same resources. DFT methods perform calculations from first principles and offer the advantage that only the total electron density needs to be considered.¹⁴⁴ Important aspects when using *ab initio* and DFT methods are listed and discussed in the references provided below:

- The Schrödinger equation.¹⁴⁸
- The Born-Oppenheimer approximation of the Schrödinger equation.¹⁴⁹
- The Hartree-Fock approximation.¹⁴⁸

- Linear Combination of Atomic Orbitals (LCAO) approximation.¹³⁷
- Electron correlation.¹⁵⁰
- Roothaan-Hall equations.¹³⁷

The choice of basis set and the density functional determine the accuracy of results obtained by DFT methods. DFT methods may produce energy values that are lower than the true energy. The use of hybrid functionals such as B3LYP^{151,152,153} (Becke's 3 parameter functional where non local correlation is provided by the LYP expression [Lee, Yang, Parr]) has improved DFT methods. B3LYP with a 6-31+G(d) basis set was used to calibrate the molecular mechanics computational model used in this investigation. The model was also calculated with semi-empirical methods since it was reported to produce accurate results for organic molecules and is widely used.¹⁵⁴

3.2.3 SEMI-EMPIRICAL METHODS

Semi-empirical methods reduce the computational effort that is associated with *ab initio* methods, by introducing various approximations.¹⁴⁴ Semi-empirical methods, which include Austin model 1 (AM1), Parametric method number 3 (PM3) and Modified intermediate neglect of differential overlap (MINDO3), solve an approximate form of the Schrödinger equation using parameters derived from experimental or high level *ab initio* results to simplify the calculation. Semi-empirical methods use an assumption, which is the zero differential overlap (ZDO). This approximation neglects all the products of basis functions depending on the same electron co-ordinates when located on different atoms. The remaining integrals are made into parameters and their values are derived from experimental or *ab initio* results as indicated above. Only a minimum basis set is used for the valence electrons. Most semi-empirical methods use only s- and p-functions and the basis functions are taken to be Slater type orbitals i.e exponential functions. The various semi-empirical methods are defined by how many integrals are neglected and how the parameterization is performed.¹³⁴ A variety of data such as heats of formation, dipole moments and ionization potentials can be reproduced by using semi-empirical methods.¹³⁸ Generally semi-empirical methods are faster than *ab initio*,

however the results obtained are highly dependent on the parameterisation set of the model.

3.3 MOLECULAR MECHANICS OR FORCE FIELD METHODS

High quality *ab initio* calculations are more reliable than semi-empirical calculations in model studies.¹⁵⁵ *Ab initio* and semi-empirical calculations are used in host-guest chemistry to determine parameters for subsequent use in other computational methods such as molecular mechanics, which is also referred to as force field methods.¹⁵⁶ *Ab initio* and semi-empirical programs can also be used as the sole calculation technique to study hosts and their complexes, however *ab initio* methods are much more expensive in terms of computational resources and time.¹⁵⁷

A major disadvantage with using both *ab initio* and semi-empirical techniques in host-guest chemistry is that the calculations are heavily dependent on computational resources for such large molecules.¹⁵⁵ Therefore, it is advisable to use molecular mechanics methods, which generally give minimized geometries in a fraction of the time needed for either semi-empirical or *ab initio* calculations. Molecular mechanics calculations make use of quite severe approximations, therefore they are inexpensive in computer resources and time and can be used for large systems with thousands of atoms.¹⁵⁸ Usually host-guest chemistry produces systems that are too large[‡] for the routine handling by *ab initio* methods but can be handled by molecular mechanics.¹⁰ Since molecular mechanics can treat a large number of particles, it is also the only realistic method for performing simulations where solvent effects or crystal packing can be studied.¹³⁴

There are two methods of solvent modelling and these generally follow the approach described below.¹⁵⁹ The first approach involves the use of a solvent box or solvent shell, which consists of several hundred solvent molecules that surround the solute or compound of interest. The solvent box makes use of a continuum in which a solvent molecule will appear on the other side of the box when one is leaving the box due to molecular movement during the optimization. This method is also called a solvent implicit model. Thermodynamic data related to the solvation can be extracted from this

system.¹⁵⁹ Needless to say, currently the size of these calculations excludes this method for quantum mechanical calculations.

An alternative to this simulation method is a solvent explicit model. Instead of implicit solvent molecules, a continuum having an appropriate bulk dielectric constant is used.¹⁵⁹ The calculation also makes use of the volume of the substrate molecule. This simulation method is employed in the MacroModel¹³² software and used in §3.7 to calculate the effects of solvent on the binding energies and enantioselectivity of host-guest complexes. The method is also suitable for quantum mechanical calculations.

There are a number of force fields available which differ in the complexity of the potential energy functions and the parameter sets defined. Force fields such as ECEPP,^{160,161,162} were developed for proteins and have rigid internal geometries for bond lengths and bond angles. MM2¹⁶³ and MM3¹⁴¹ are sophisticated force fields, which can accurately reproduce the experimental structures and vibrational frequencies of organic and bioorganic molecules. Molecular mechanics methods cannot accurately describe bond formation or bond breaking or predict molecular properties, which depend on electronic effects.¹⁵⁸

The potential function and parameter sets for the force fields are more complex, resulting in an increased predictive accuracy. However molecular mechanics methods should be treated with caution, as the specific force field employed by the software may not be calibrated well enough for all chemical systems under investigation. Therefore, no force field can be used generally for all molecular systems. Force fields have parameters, which are specific for a class of molecules. Extensive studies of the 18-crown-6 using the MM2 program, making use of more than a hundred and ninety host starting conformations, led to the conclusion that the host molecule has a potential energy surface with many minima separated by small energy differences.^{60,164} Most molecular mechanics studies use energy minimization algorithms: these include Molecular Dynamics (MD)¹⁶⁵ and Monte Carlo simulations.^{166,167} Current molecular mechanics studies have correctly reproduced many of the properties of both complexed and uncomplexed hosts.¹⁶⁸ Technical information about the basics of molecular mechanics methods is provided below (§3.3.1).

3.3.1 THE BASICS OF A MOLECULAR MECHANICS OPTIMIZATION

The laws of classical physics are used in molecular mechanics simulations to predict the structure and properties of molecules. As discussed earlier, many different molecular mechanics methods exist, each with its own specific force field. The following components¹⁵⁸ are present in a force field:

- A set of equations that demonstrates the variation of the potential energy of a molecule with the location of its component atoms.
- The characteristics of an element within a specific chemical context is defined by a series of atom types. Each atom type has different characteristics and every element has a different behaviour depending upon its environment. An atom type is dependent upon hybridization, charge and types of atoms to which it is bonded.
- Different parameter sets fit the equations and atom types to the experimental data. Force constants are defined by parameter sets and are properties used in equations to relate atomic characteristics to energy components and structural data (eg. bond lengths and angles).

Molecular mechanics calculations are based on interactions among the nuclei rather than electrons in a molecular system. Electronic effects are implicitly included in force fields using parameter sets.¹³⁷ However this only includes crude electronic effects such as dipole-dipole interactions and the calculation of static charges. Polarization and dispersion effects are too subtle to be included in force fields. Molecular mechanics, or force field calculations, calculate energy from simple potential energy functions. Calculations involve the treatment of molecules as a group of atoms governed by bond stretching, angle bending, dihedral angle torsion and inversion and other interactions.¹⁶⁹ The dynamics of the atoms are treated by classical methods e.g. Newton's second law. The force field energy can be written as a sum of terms, which describes the energy required for distorting a molecule in a specific fashion.¹³¹

Potential energy functions describe the features of the molecules and are used to calculate the energy of a molecule. The force field is a combination of the energy

functions used to calculate the overall potential energy of the molecule.¹⁶⁹ The interaction between the atoms of a molecular system and the mechanics of its motion is treated with a classical non-quantized potential energy function by the molecular mechanics programme. The potential energy function of a molecular system is split into a series of additive terms, which describe the different contributions to the overall conformational energy (see Equation 1)

$$V_{\text{total}} = V_{\text{bond stretch}} + V_{\text{angle bend}} + V_{\text{van der Waals}} + V_{\text{hydrogen bond}} + V_{\text{electrostatics}} \quad \text{Eq. 1}$$

These terms may be deviations of the potential energy functions from the ideal bond lengths, bond angles and torsion angles of the interactions energies due to van der Waals forces, hydrogen bonding and electrostatics.¹⁷⁰

Using the molecular mechanics optimization, a single conformation of a molecule can be found by using a mathematical algorithm to find the minimum of the potential energy surface of the wave function as described by the specific software. Optimization can be defined as a mathematical process whereby the structure is obtained by performing a series of calculations, which try to locate the lowest energy molecular structure, which is in close proximity to the starting structure. A geometry optimization is mainly dependent on the gradient of the energy profile of the starting structure. The structure is modified to make it more consistent with the parameter information within the program. An optimization is carried out using potential energy functions, which alter the bond lengths, bond angles and torsion angles thereby altering the geometry of the molecule slightly and generating a more realistic structure with lower energy.¹⁶⁹

Global minimum is the term used to describe the point at which the total energy of the system is at its lowest. There may be many local minima in a given system. A local minimum is a stationary point on the potential energy curve at which the energy of the molecule is lowest within some limited region.¹⁵⁸ Rigid molecules have less conformational freedom and it is in principle much easier to obtain the global minimum of the system. Larger systems such as macrocycles exhibit more conformational flexibility and special care should be taken to ensure a reasonable chance to obtain the global minimum. Most mathematical optimization algorithms are sensitive enough to be trapped in local minima. Fortunately the inclusion of a guest to a host system seems

to impose larger rigidity on the host-guest system, which makes it easier to find conformations closer to the global minimum.

Simulations refer to models involving a statistical component. Note that even sophisticated optimization algorithms such as the Monte Carlo algorithm could be trapped in a global minimum. A Monte Carlo simulation is used to explore the possible states of a system involving large ranges of parameters, by conducting a large number of random trials. At the end of the Monte Carlo simulation, the collection of randomly chosen points provides you with information about the entire range. Basically instead of covering the entire range, results at some random points are calculated.¹⁷¹ The dynamic behaviour and thermodynamic properties of biological macromolecules in solution require the use of molecular simulation techniques such as molecular dynamics (MD) and Monte Carlo sampling. Such techniques are also well established for description of the physical properties of fluids.¹⁷²

In order to overcome potential energy barriers and to find structures closer to the global minimum, various computational solutions are available. One such solution is molecular dynamics (MD). These simulations have been valuable and appear promising in understanding the dynamic structure of proteins, nucleic acids, their complexes, chemical reactivity in condensed media as well as the mechanism of enzyme action. Free energy simulations allow the theoretical evaluation of binding free energies, thus opening up the possibility of predicting the efficacy and safety of potential drug candidates in the future.¹⁷² Molecular dynamics (MD) and simulated annealing (SA) techniques are discussed further below.

3.4 MOLECULAR DYNAMICS (MD) AND SIMULATED ANNEALING (SA)

Molecular dynamics (MD) is a special molecular mechanics program, developed by Allinger and co-workers.^{141,142,143} Molecular dynamics (MD) simulations have become a powerful tool for studying the structure and dynamics of biologically important molecules.^{173,174} A brief overview of molecular dynamics calculations is given below.

3.4.1 MOLECULAR DYNAMICS (MD)

A molecular dynamics calculation uses a mathematical algorithm to “heat” the molecule to higher temperatures to overcome rotational and other conformational energy barriers. This is mathematically achieved by using Newtonian equations of motion, potential energy functions and the associated force field. At the start of the dynamics study the molecule is in a specific conformation. The next step involves the addition of thermal energy in the form of potential energy. This results in the motion of the atoms due to the added forces imposed on it according to Newton’s laws of motion. The acceleration that each atom undergoes can be calculated since at a given time and for each atom, its position, mass and the forces acting on it are known. Thus the current force on each atom as well as the position can be calculated after a short time. The vibrational motion of the molecule as a function of time can also be obtained.¹³¹

It is important to know that it has been reported that the temperature scales of the MD programs do not correlate with reality.¹⁷⁰ A molecular dynamics simulation performed using a cyclohexane molecule in different starting conformations and different simulation temperatures have been used to demonstrate this. At temperatures of 400 K, cyclohexane oscillated between the different twist boat forms, at 600 K the molecule had sufficient kinetic energy allowing it to convert between one of the rigid chair forms and twisted forms. Temperature increases of up to 1000 K yielded both the chair and twisted conformations.

This study¹⁷⁰ has shown that the mathematical scale used during the molecular dynamics does not correlate correctly with the results found in reality, since it is known that cyclohexane interconverts at room temperature (298 K). It is therefore essential that the system be allowed to reach equilibrium at a temperature where all conformations are explored during the MD run. As the MD algorithm is trying to find the lowest energy of the system at the specific temperature the molecule will “occupy” low energy conformations for longer times compared with maxima on the energy surface. Similarly the molecule will theoretically spend more time at the global minimum of the system, especially if the global minimum has a reasonably lower energy in comparison with the various local minima.¹⁷⁰

The displacement of atoms in the molecule is followed over a certain period of time, at a specific temperature and a specific pressure. The motion of the atoms is calculated at separate and small time intervals. Simulations can also be run with varying temperatures so as to obtain different families of conformers. Using higher temperatures makes it feasible to cross more energy barriers hence allowing the structure to convert to more conformers.¹⁷⁰ In practice all the low energy conformations associated with minima on the reaction coordinate of a MD run will be optimized at 0 K and rank ordered by energy. The simulated annealing technique uses a modified approach and the system undergoes cooling as described below.

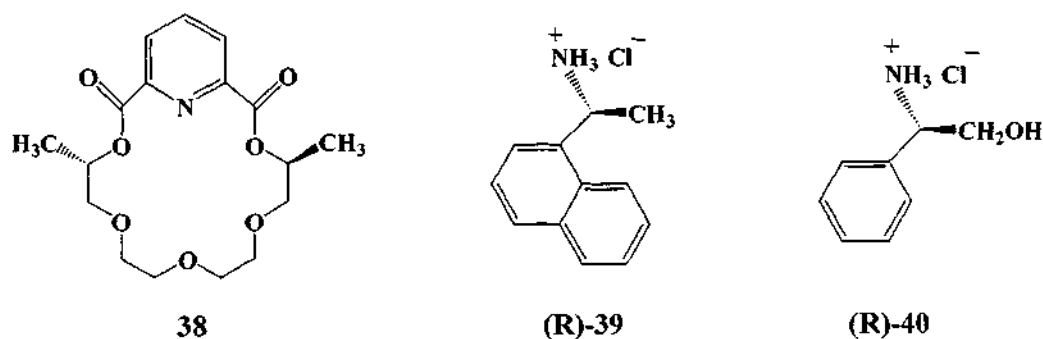
3.4.2 SIMULATED ANNEALING (SA)

Simulated Annealing (SA) examines the equations of state and frozen states of n-body systems.^{175,176} The manner in which liquids freeze or metals crystallize in the process of annealing forms the basis of the concept of simulated annealing. In a typical annealing process a melt, which is initially disordered and at a high temperature, is slowly cooled. As the cooling proceeds the system becomes more ordered and approaches a “frozen” ground state at $T = 0$ K.¹⁷⁵ To describe the principle of the simulated annealing technique, the molecule is first “heated” using a typical MD algorithm and then cooled at regular time intervals. The simulation temperature is decreased stepwise, so that the conformation changes due to slow cooling lead to the location of the local minimum. At the end of this annealing cycle, the geometry that is trapped in the nearest local minimum is saved and is used as a starting geometry in further simulations at higher temperatures. The simulated annealing is repeated until several low energy conformations are obtained which are possible global minima.¹⁷⁰ In the case of flexible molecules, statistical analysis is required^{177,178} to ensure that a slight chance exists to obtain structures with lower energy.

3.5 COMPUTATIONAL MODEL

Quality assessment is an absolute requirement in computational chemistry. When choosing a method, a basic understanding of the theory behind the method is needed as well as the knowledge of the performance of that method for similar or other systems. When using a computational method, it is necessary to develop a way of calibrating the

results that are obtained.¹³⁴ It has already been illustrated by Hay and co-workers that the MM3 force field is a worthy option for the optimization of crown ethers with alkali metal guests.^{179,180} Previous work carried out in our laboratory,¹³⁰ on the advice of Hay¹⁸⁰ and with the initial assistance¹⁸¹ of Allinger^{141,142,143} has examined optimized host-guest complexes using co-ordinates from two X-ray structures of host complex (R,R)-38 with organic ammonium salts (R)-39 and (R)-40 respectively using MM3, AM1, PM3 and DFT calculations. The DFT calculations were performed using B3LYP^{151,152,153} (a hybrid functional) with the 6-31+G(d) basis set.



It was found that the MM3 results compared well with the DFT optimized complexes, in terms of root mean square (RMS) overlay and relative binding energies. The RMS overlay for complexes [(R,R)-38-(R)-39] and [(R,R)-38-(R)-40] optimized with MM3 differed by 0.035 Å and 0.082 Å respectively from the same complexes optimized with B3LYP/6-31+G(d). Similarly the binding energies calculated by MM3 were calculated to be -45.3 kcal mol⁻¹ and -41.5 kcal mol⁻¹ for complex [(R,R)-38-(R)-39] and complex [(R,R)-38-(R)-40] respectively and -53 kcal mol⁻¹ for the complexes when calculated by DFT methods. The MM3 results were considerably better than those obtained for the PM3 calculations.

The proposed model,¹³⁰ is a qualitative method used to predict the enantioselectivity of chiral macrocycles towards chiral ammonium ions. Although the MM3 force field was developed for amino acids, including the zwitterions of amino acids¹⁸² the force fields have to be adjusted to suit specific systems. On this basis a collaborating project was started using MM3 to examine the optimization of macrocycles with chiral organic

ammonium salts. All MM3 calculations reported before¹³⁰ as well in the initial stage of this study were performed in the 'gas phase' or '*in vacuo*'.

The calculations performed using Alchemy 2000 are for two isolated molecules excluding all solvent effects. This corresponds to a physical situation, which occurs under low pressure (vacuum) or in the gas phase. Experimentally, most chemical reactions occur in solution. Reactions occurring in the gas and solution phase are both qualitatively and quantitatively different, especially when it involves ions or polar species.¹⁷² Molecular properties are also dependent on the type of environment. Experimental transport studies are performed in solution (e.g. water or chloroform). Therefore the effects of the solvents on the computational model have to be taken into account. Due to the importance of solvent effects in these studies, suitable software (MacroModel)¹³² was purchased and the effects of solvent on the binding energy and enantioselectivity were examined (see § 3.7)

Alchemy 2000 was used to calculate the heats of formation for the complexed and uncomplexed hosts.¹³¹ It is important to realize that the counter ion plays an important role in the stabilization of host-guest complexes and this was demonstrated by Marchand *et al.*¹⁸³ The gas phase interaction between the 20-crown-6 macrocyclic host-potassium ion guest and the picrate counterion was calculated to be $-64.9 \text{ kcal mol}^{-1}$ and the basis set superposition error (BSSE) was used to demonstrate that the picrate counterion participated as an additional bidentate ligand.¹⁸³

The approximated interaction energy between a macrocyclic host and a sodium ion was calculated using DFT calculations B3LYP with the 6-31+G(d) basis set recently.⁷⁵ An approximate contribution of one donor atom towards the stabilization of the complex was reported to be approximately 6 kcal mol^{-1} .

However in order to simplify the computational model, the contributions of the counter ion to the binding energy were neglected. Since the approximate binding energy (see Equation 2 below) was calculated as the energy difference between the energy of the host-guest complex and the sum of the energies of the free host and free guest, the error is supposed to cancel out.

The Molecular dynamics algorithm in Alchemy 2000¹³¹ makes use of

- A leapfrog algorithm.¹⁸⁴
- Coupling dynamic simulations to an external temperature bath.¹³¹
- SHAKE algorithm, which constrains certain bond lengths during dynamics simulations.¹³¹

The binding energy was calculated for each system using Equation 2 and is reported as an approximate thermodynamic quantity.

$$\text{Binding Energy} = E_{\text{complex}} - (E_{\text{host}} + E_{\text{guest}}) \quad \text{Eq. 2}$$

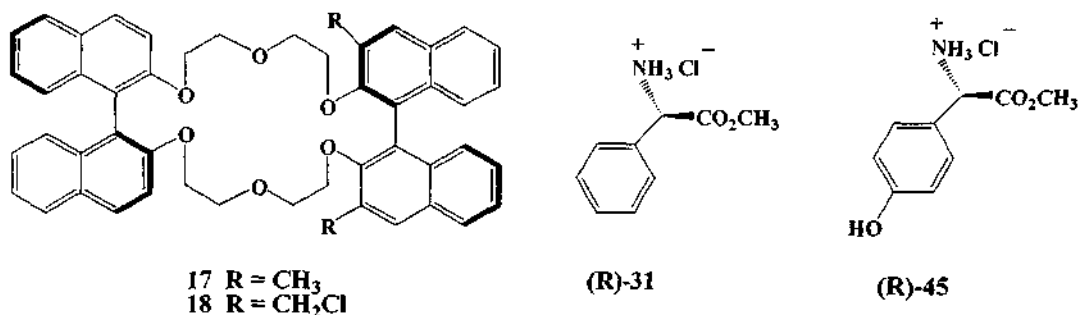
The computational model used to calculate the enantioselectivity and approximate binding energies is described in Appendix 2.

CHAPTER FOUR

RESULTS AND DISCUSSION

4.1 INTRODUCTION

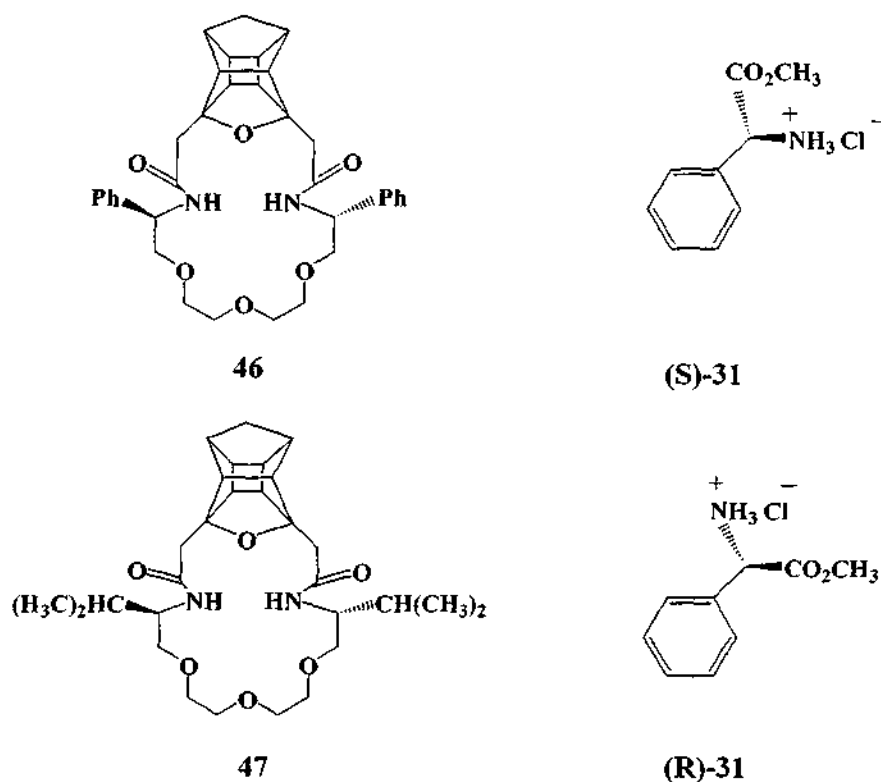
Previous work done on various macrocycles attempted to correlate the results obtained experimentally with that obtained computationally.¹³⁰ Previously the MM3 computational method was applied on temperature-dependent ¹H NMR spectroscopy, UV spectroscopy studies and extraction studies.



Cram *et al.* conducted experimental transport studies³ with crown ethers (R,R)-17 and (R,R)-18 using a U-tube. The hosts (R,R)-17 and (R,R)-18 had their chiral barriers extended with -CH₃ and -CH₂Cl substituents respectively, and gave the greatest chiral recognition ever reported in transport studies. Crown ether (R,R)-17 preferred the (R)-31 guest by 78 % and the (R)-45 guest by 74 % and the (R,R)-18 host preferred the (R)-31 guest by 82 %.³

It was previously reported¹³⁰ that the computed results obtained using the MM3 computational model compared favourably with the results from the experimental transport studies. This indicates that the model is able to correctly predict the enantiomeric preference of the chiral hosts towards the chiral ammonium guests. If the experimental results obtained by Cram *et al.* are taken as a benchmark for enantioselectivity, one could determine the calculated degree of chiral preference of the crown ethers towards chiral amino ester guests such as C₆H₅CH(CO₂CH₃)NH₃Cl (R/S)-(31) and *p*-HOC₆H₄(CO₂CH₃)NH₃Cl (R/S)-(45).

As mentioned above the experimental result by Cram *et al.* reported an enantiomeric excess (*ee*) of 82 % for host (R,R)-18 with guest (R)-31. According to the computational model¹³⁰ an experimental enantiomeric excess (*ee*) of 82 % correlates with a calculated enantiomeric preference of about 1.4 kcal mol⁻¹ of the (R,R)-18 host for the (R)-31 guest. Thus it can be assumed that any system with a calculated chiral preference higher than 1.4 kcal mol⁻¹ should exhibit an exceptional chiral separation experimentally during transport studies using a U-tube.

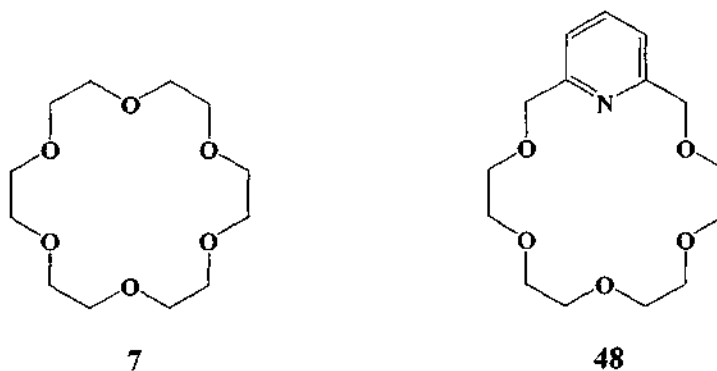


Chiral cage annulated macrocycles (46) and (47) exhibited a weak (29 %) to moderate (68 %) enantioselectivity for the (R)-31 guest over the (S)-31 guest during experimental U-tube extraction studies.¹⁸⁵ The calculated enantiomeric preference was 0.13 kcal mol⁻¹ for host (46) with the (R)-31 guest and 0.72 kcal mol⁻¹ for host (47) with the (R)-31 guest and these results were in agreement with the experimental results obtained.¹³⁰

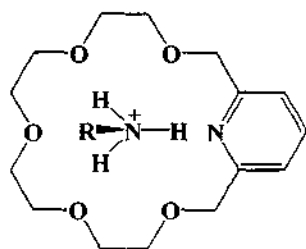
This computational study had three aims: firstly, to determine the binding energy and enantiomeric preference of the host systems 33, 41, 42, 49 and 50 for guest molecules (S)-31 and (R)-31 and to compare the computed results with those previously

reported¹³⁰ for host systems 17, 18, 27, 46 and 47. Secondly, to examine whether the position of the chiral barriers (phenyl groups) are significant in the design of a chiral cage annulated macrocycle and play a role in chiral discrimination according to the computational model. The third aim was to investigate the effects of solvent (water and chloroform) on the binding energy and enantioselectivity.

This computational investigation will concentrate on the results obtained for temperature-dependent ¹H NMR spectroscopy and extraction studies. Incorporation of a pyridine ring into a crown ether provides a Lewis base centre (the pyridine's nitrogen) in an aromatic ring. The pyridine ring lends rigidity and a degree of lipophilicity to the resulting crown ether with the consequence that such systems can form complexes with a variety of both ionic and neutral guest molecules.¹⁸⁶ The use of the pyridine nitrogen as a macrocyclic donor atom is desirable since Cram and co-workers have shown that crown ligands (such as 48) which incorporate a pyridine sub-cyclic unit, form complexes with alkylammonium cations which are thermodynamically more stable than the corresponding complexes formed by 18-crown-6 crown ligands.¹⁶

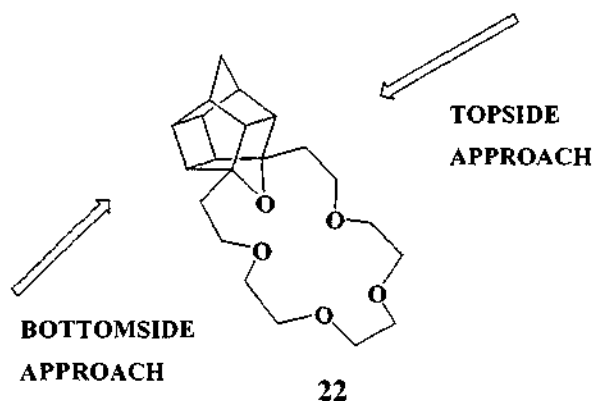


Since the ammonium ion binds to 18-crown-6 ligands by hydrogen bonding to alternate donor atoms,¹⁸⁷ it was postulated¹⁸⁸ that the pyridine nitrogen of (48) forms a stronger hydrogen bond with the ammonium hydrogen (see Figure 3) than the corresponding 18-crown-6 analogue which has an ether oxygen (7). Such macrocyclic ammonium ion complexes have been studied as models for enzyme substrate binding.^{189,190}



48

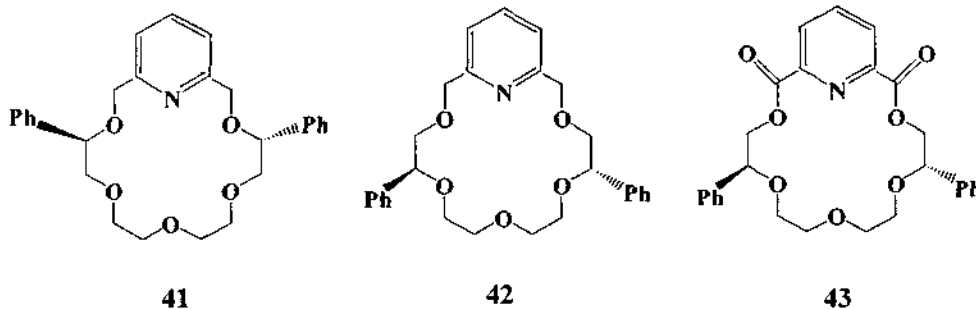
Figure 3: Complexation of host (48) with arbitrary ammonium guest molecule



22

Figure 4: The two faces of the PCU cage annulated macrocycle (22)

The pyridine-based crown ethers are non-sided whereas PCU annulated host systems have two diastereotopically non-equivalent sides to which the approaching guest can complex (see Figure 4). Complexation can occur on the topside or the bottomside of the cage annulated macrocycle.



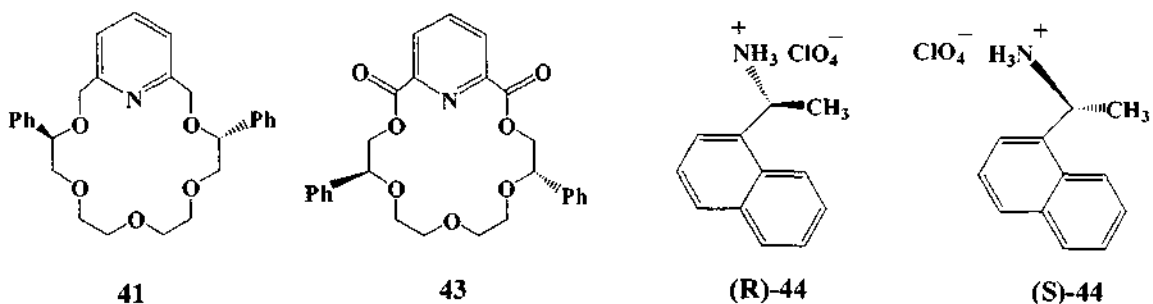
41

42

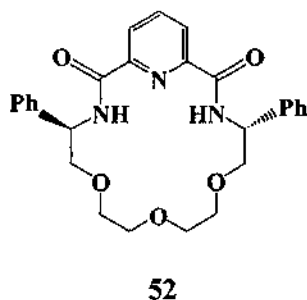
43

The pyridine derived crown ethers (41) and (43) have been studied experimentally by Bradshaw *et al.* using temperature-dependent ^1H NMR spectroscopy.^{57,89} The

experimental ^1H NMR spectroscopy study reports kinetic data therefore the thermodynamic data obtained from the MM3 computational model cannot be compared with them. It is hoped that comparison of the computed enantiomeric preference obtained from this computational study and the experimental enantiomeric preference obtained from the systems used in experimental transport studies can be compared. This could enable one to predict if hosts (**41** and **42**) have the potential to be used in transport studies and hence lead to a better understanding of host-guest interactions.

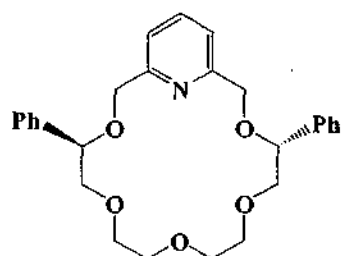


During the experimental temperature-dependent ^1H NMR spectroscopy studies, crown ether **(R,R)-41** was reported to have a preference for **(R)-[α -(1-naphthyl) ethyl] ammonium perchlorate ion [**(R)-44**, **(R)-NapEt**] over the **(S)-[α -(1-naphthyl) ethyl] ammonium perchlorate ion [**(S)-44**, **(S)-NapEt**],⁸⁹ while crown **(43)** was reported to have poor enantiomeric recognition capabilities.⁵⁷****

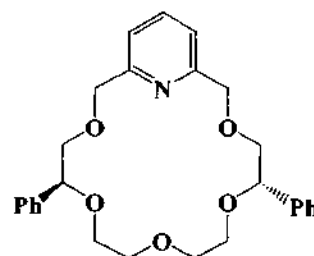


Pyridine host systems such as **(52)**¹⁹¹ were tested experimentally¹⁸⁵ using extraction studies. It was found that the host could not be used in extraction/transport studies due to its low lipophilicity.¹⁸⁵ Since it has been postulated¹⁸⁸ that the pyridine nitrogen forms a stronger hydrogen bond with the ammonium guest, pyridine nitrogen donor

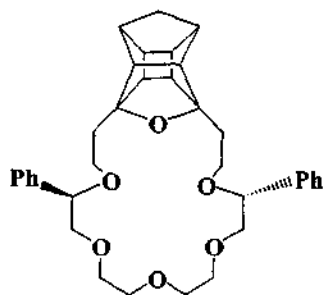
atoms have been used in crown ethers to increase the binding energies with ammonium guests. Bradshaw *et al.* examined macrocycle (R,R)-**41** using temperature-dependent ^1H NMR techniques. (R,R)-**41** was found to form kinetically stronger complexes with one enantiomer of [α -(1-naphthyl) ethyl] ammonium perchlorate guest (NapEt) over the other. The (R)-**44** guest was preferred to the (S)-**44** guest by $2.8 \text{ kcal mol}^{-1}$.⁸⁹ As pointed out above it should be noted that the calculated MM3 thermodynamic data will not coincide with the experimental kinetic data ($\Delta\Delta G_c^\ddagger$) of the host-guest systems and cannot therefore be directly compared.



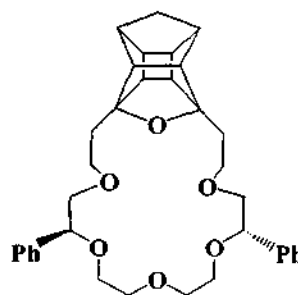
41



42

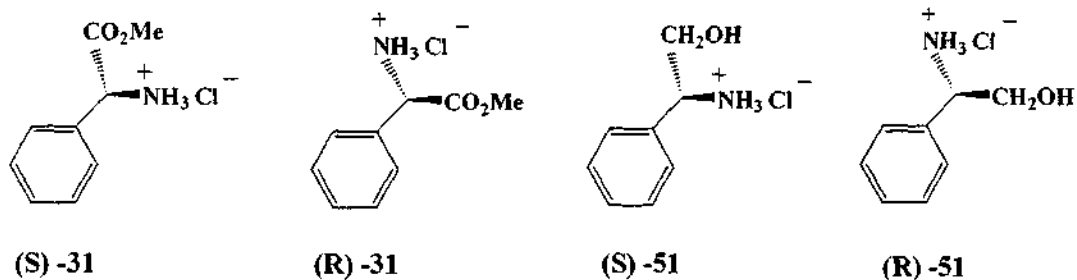


49

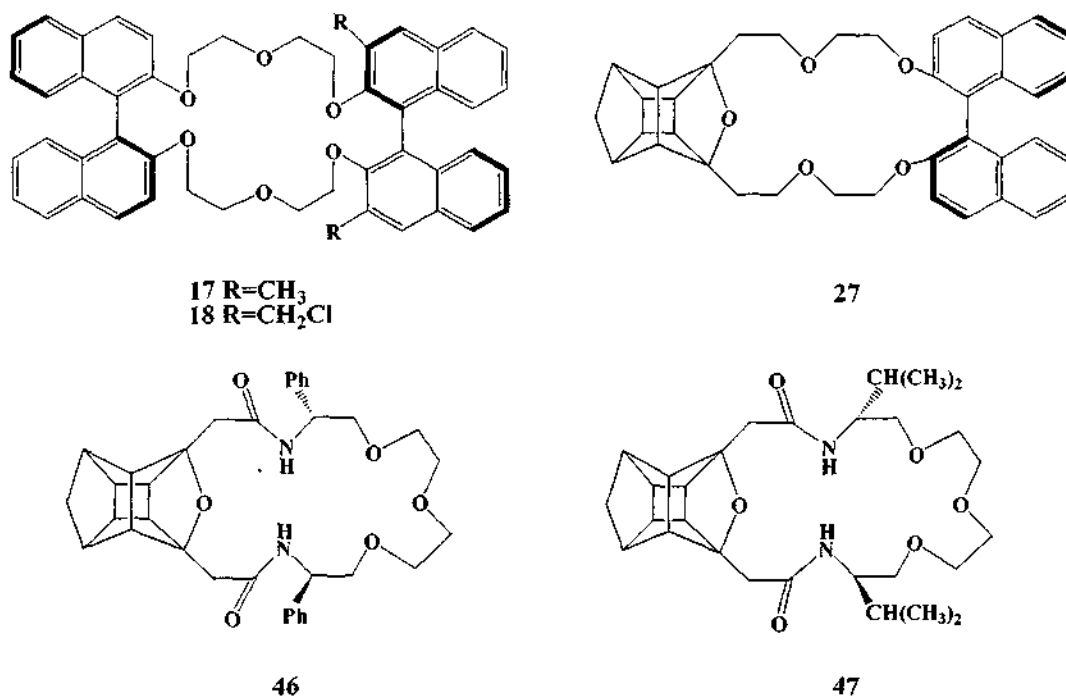


50

The theoretical chiral cage annulated host systems (**49**) and (**50**) were proposed as hosts after studying the literature on pyridine-containing macrocycles that were synthesized by Bradshaw *et al.*^{57,59,89}



As mentioned earlier guest molecules (S)-31 and (R)-31 that were used previously¹³⁰ when studying host-guest systems (17, 18, 27, 46, 47) computationally and experimentally in U-tube studies (see Table I), will be used in this study for comparison with results previously obtained.¹³⁰ The results obtained for guest molecules (S)-51 and (R)-51 with host systems (S,S)-41 and (S,S)-49 will also be reported.



The results of the calculated and experimental preferences of host-guest systems previously studied are tabulated in Table 1.

Table 1: Binding energies of previously studied host-guest complexes¹³⁰

Host-guest Complex	Binding energy ¹ / kcal mol ⁻¹	Calculated enantiomeric preference ² /kcal mol ⁻¹	Experimental enantiomeric excess (<i>ee</i>)
(<i>R,R</i>)-17 and (<i>S</i>)-31	-38.53		
(<i>R,R</i>)-17 and (<i>R</i>)-31	-39.63	1.1	78 ³
(<i>R,R</i>)-18 and (<i>S</i>)-31	-36.93		
(<i>R,R</i>)-18 and (<i>R</i>)-31	-37.33	1.4	82 ³
(<i>R</i>)-27 and (<i>S</i>)-31	-41.68		
(<i>R</i>)-27 and (<i>R</i>)-31	-41.79	0.11	15 ⁴
(<i>S,S</i>)-46 and (<i>S</i>)-31	-49.08		
(<i>S,S</i>)-46 and (<i>R</i>)-31	-49.21	0.13	29 ⁵
(<i>S,S</i>)-47 and (<i>S</i>)-31	-44.03		
(<i>S,S</i>)-47 and (<i>R</i>)-31	-44.75	0.72	68 ⁵

¹ See equation: Binding energy = $E_{\text{complex}} - (E_{\text{host}} + E_{\text{guest}})$

² Relative energy (*R*)-complex vs (*S*)-complex

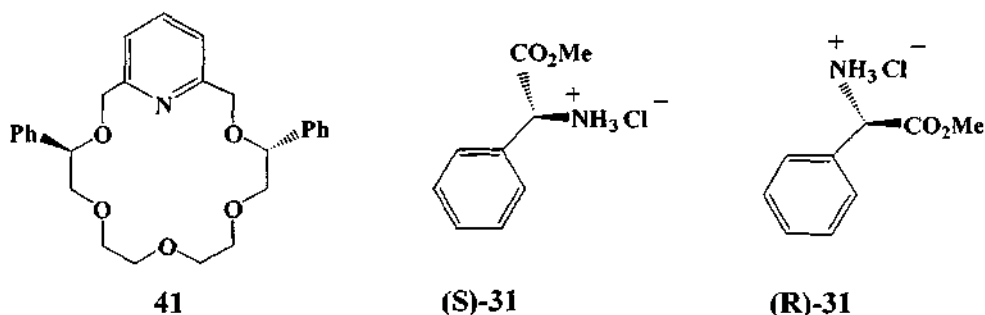
³ See reference 64, experimental data

⁴ See reference 4, experimental data

⁵ See reference 185, experimental data

To get a better understanding of chiral recognition capabilities and for comparison purposes, host systems (**17**, **18**, **27**, **46**, **47**) with guest molecules (*S*)-**31** and (*R*)-**31** will be referred to in this computational study. The systems to be examined in this computational study consist of pyridine based crown ethers (*S,S*)-**41** and (*S,S*)-**42** and cage annulated macrocycles (*S,S*)-**33**, (*S,S*)-**49** and (*S,S*)-**50**. The results obtained will be compared with the results obtained for the experimental U-tube extraction studies, experimental temperature dependent ¹H NMR studies and the calculated enantiomeric preferences of previously studied macrocycles that are reported in Table 1.

4.2 RESULTS AND DISCUSSION



The pyridine annulated macrocycle (S,S)-**41** was the first host that was studied with guests (S)-**31**, (R)-**31**, (S)-**51** and (R)-**51**. The calculated results for (S,S)-**41** with guests (**31**), are tabulated in Table 2. Table 2: Binding Energies of E_{complex} host (S,S)-**41** with guests (S)-**31** and (R)-**31**

Host-guest complex ¹	Binding energy ² / kcal mol ⁻¹	Calculated enantiomeric preference ³ / kcal mol ⁻¹
(S,S)- 41 and (S)- 31 BPESa	-39.18	
(S,S)- 41 and (S)- 31 BPESb	-40.43	0.56
(S,S)- 41 and (S)- 31 BPESc	-40.42	
(S,S)- 41 and (S)- 31 BPESd	-39.94	
(S,S)- 41 and (R)- 31 BPERa	-39.46	
(S,S)- 41 and (R)- 31 BPERb	-39.66	
(S,S)- 41 and (R)- 31 BPERC	-39.87	
(S,S)- 41 and (R)- 31 BPERd	-39.75	

¹3D structure and Cartesian co-ordinates of all optimised conformations are available as supplementary material on the CD attached to the thesis. BPES (Bradshaw phenyl (S)-ester guest) and BPER (Bradshaw phenyl (R)-ester guest) refer to the name of the PDB file and Cartesian co-ordinates on the CD attached and in Appendix 2.

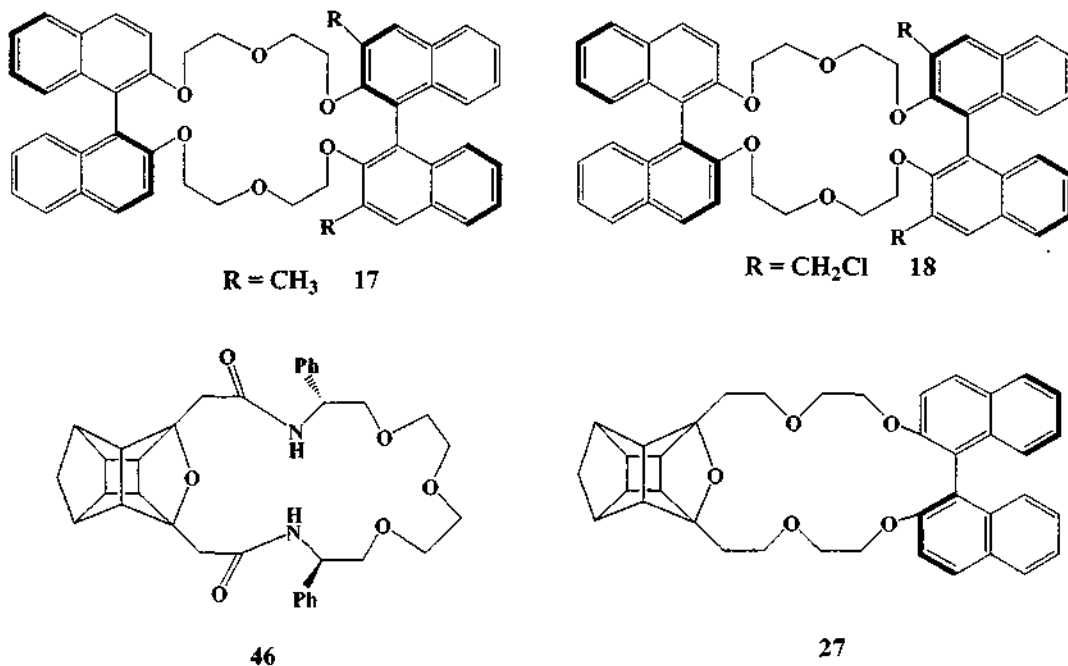
²See equation: Binding energy = $E_{\text{complex}} - (E_{\text{host}} + E_{\text{guest}})$.

³Relative energy lowest (S,S)-**41**-(S)-**31** complex vs lowest (S,S)-**41**-(R)-**31** complex.

Host (S,S)-**41** which has bulky chiral groups close to the pyridine group, preferred the (S)-**31** guest to the (R)-**31** by 0.56 kcal mol⁻¹. An interesting observation made was that the calculated thermodynamic enantioselectivity of host (S,S)-**41** toward the (S)-**31** guest produced a thermodynamic result that agreed with the experimental kinetic enantioselectivity. Bradshaw *et al.*⁸⁹ mentioned that the kinetic result obtained for host (**41**) was a surprise since it was the first time that a (R,R)-**41** host had formed a kinetically more stable complex with a guest [(R)-**44**] of the same configuration. This preference indicates that (S,S)-**41** exhibits recognition for the enantiomers of (**31**).

The calculated binding energy of -40.43 kcal mol⁻¹ for host (S,S)-**41** with the (S)-**31** guest was lower than the calculated binding energies of host-guest complexes previously reported.¹³⁰ This result indicated that a more stable complex is formed

between host (S,S)-41 with guest (S)-31 than host (R,R)-17 with guest (R)-31 (-39.63 kcal mol⁻¹) and host (R,R)-18 with guest (R)-31 (-37.33 kcal mol⁻¹). The calculated enantioselectivity of host (S,S)-41 with guest (S)-31 (0.56 kcal mol⁻¹) was higher than the calculated enantioselectivity reported¹³⁰ for host (R,R)-27 with guest (R)-31 (0.11 kcal mol⁻¹) and host (S,S)-46 with guest (R)-31 (0.13 kcal mol⁻¹).



Host (S,S)-41 was tested with guests (S)-51 and (R)-51 and the results obtained are tabulated in Table 3 below.

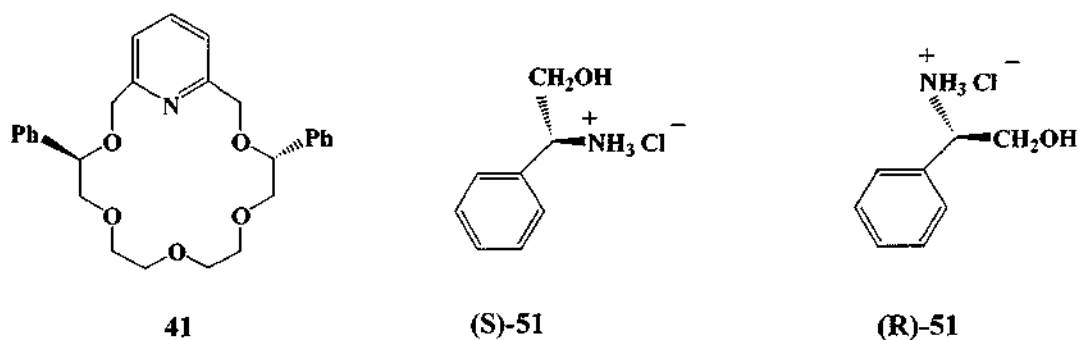


Table 3: Binding Energies of E_{complex} host (S,S)-41 with guests (S)-51 and (R)-51

Host-guest complex ¹	Binding energy ² /kcal mol ⁻¹	Calculated enantiomeric preference ³ /kcal mol ⁻¹
(S,S)-41 and (S)-51 BPASa	-31.71	0.32
(S,S)-41 and (S)-51 BPASb	-31.71	
(S,S)-41 and (S)-51 BPASc	-31.71	
(S,S)-41 and (S)-51 BPASd	-31.71	
(S,S)-41 and (R)-51 BPARa	-30.97	
(S,S)-41 and (R)-51 BPARb	-31.01	
(S,S)-41 and (R)-51 BPARc	-30.96	
(S,S)-41 and (R)-51 BPARD	-31.39	

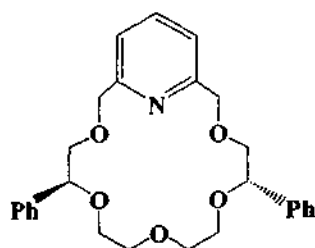
¹3D structure of all optimised conformations are available as supplementary material on the CD attached to the thesis. BPAS (Bradshaw phenyl (S)-alcohol guest) and BPAR (Bradshaw phenyl (R)-alcohol guest) refer to the name of the PDB file and Cartesian co-ordinates on the CD attached and in Appendix 2.

²See equation: Binding energy = E_{complex} - (E_{host} + E_{guest})

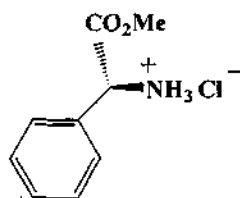
³Relative energy lowest (S,S)-41-(S)-51 complex vs lowest (S,S)-41-(R)-51 complex.

The calculated chiral preference of host (S,S)-41 for guest (S)-51 over (R)-51 is 0.32 kcal mol⁻¹. The binding energy calculated for host (S,S)-41 with guest (S)-51 is -31.71 kcal mol⁻¹ which is higher than the binding energy calculated for host (S,S)-41 with guest (S)-31 (-40.43 kcal mol⁻¹). This indicates that a weaker complex is formed between host (S,S)-41 with guest (S)-51.

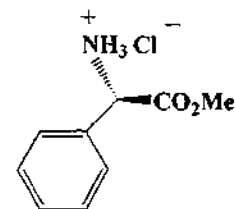
The pyridine-containing crown ether (S,S)-42 which is analogous to crown ether (43), previously studied experimentally by Bradshaw *et al.*,^{57,59} was also studied computationally using guests (31). The results obtained are tabulated in Table 4 below.



42



(S)-31



(R)-31

Table 4: Binding Energies of E_{complex} host (S,S)-42 with guests (S)-31 and (R)-31

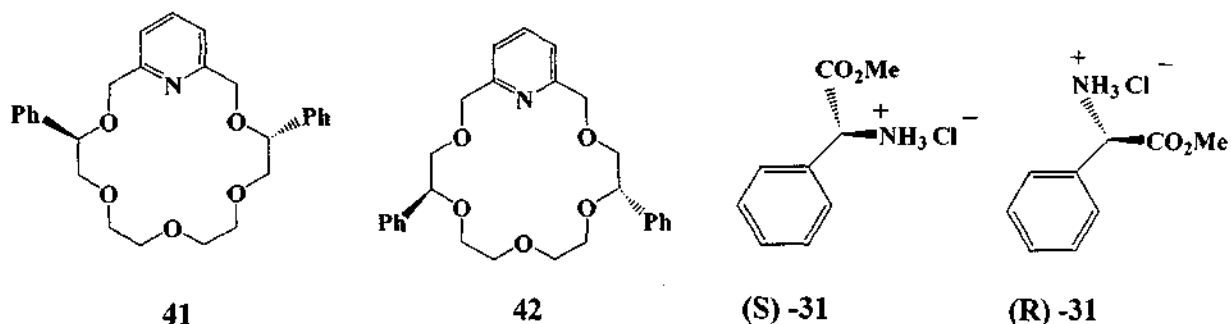
Host-guest complex ¹	Binding energy ² /kcal mol ⁻¹	Calculated enantiomeric preference ³ /kcal mol ⁻¹
(S,S)-42 and (S)-31 BNGESd	-43.64	
(S,S)-42 and (S)-31 BNGESa	-42.46	
(S,S)-42 and (S)-31 BNGESc	-41.91	
(S,S)-42 and (S)-31 BNGESb	-40.83	
(S,S)-42 and (R)-31 BNGERb	-43.91	0.27
(S,S)-42 and (R)-31 BNGERc	-43.91	
(S,S)-42 and (R)-31 BNGERa	-41.92	
(S,S)-42 and (R)-31 BNGERe	-41.91	

¹3D structure of all optimised conformations are available as supplementary material on the CD attached to the thesis. BNGERS (Bradshaw newglycol (S)-ester guest) and BNGER (Bradshaw newglycol (R)-ester guest) refer to the name of the PDB file and Cartesian co-ordinates on the CD attached and in Appendix 2.

²See equation: Binding energy = $E_{\text{complex}} - (E_{\text{host}} + E_{\text{guest}})$.

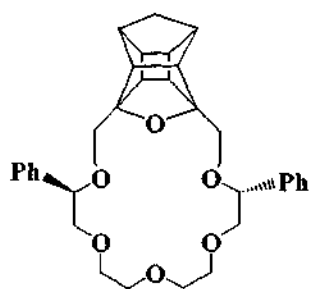
³Relative energy lowest (S,S)-42-(R)-31 complex vs lowest (S,S)-42-(S)-31 complex.

A low binding energy of $-43.91 \text{ kcal mol}^{-1}$ is calculated for host (S,S)-42 with guest (R)-31 which indicates a stable, strong complex is formed. Host (S,S)-42 preferred the (R)-31 guest to the (S)-31 guest by $0.27 \text{ kcal mol}^{-1}$. The chiral pyridine-based macrocycle (S,S)-42 has phenyl groups positioned at the lower end of the crown ether. A decreased enantiomeric recognition is observed probably since the chiral barriers farther away from the rigid pyridine moiety and cannot provide sufficient steric interaction with the chiral guest.

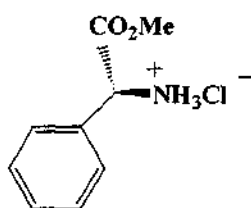


Host (S,S)-**41** which has chiral barriers close to the pyridine moiety, had a chiral preference of $0.56 \text{ kcal mol}^{-1}$ for the (S)-**31** guest (see Table 2), while host (S,S)-**42** with guest (S)-**31** had a chiral preference of $0.27 \text{ kcal mol}^{-1}$. Hua *et al.*⁵⁵ suggested that the hydrogen bonding of the host with the guest leads to the formation of the complex while steric interaction with the chiral substituents contributes to enantiomeric recognition.

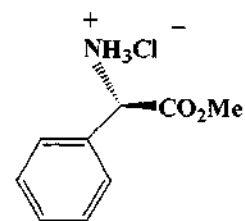
The computational results for cage annulated macrocycle (S,S)-**49** and guests (**31**) are tabulated below in Table 5.



49



(S)-**31**



(R)-**31**

Table 5: Binding Energies of E_{complex} host (S,S)-49 with guests (S)-31 and (R)-31

Host-guest complex ¹	Topside ² Binding energy ³ /kcal mol ⁻¹	Bottomside ² Binding energy ³ /kcal mol ⁻¹	Calculated enantiomeric preference ⁴ /kcal mol ⁻¹
(S,S)-49 and (S)-31 CPESa top	-48.34		
(S,S)-49 and (S)-31 CPESb top	-48.73		
(S,S)-49 and (S)-31 CPESc top	-48.74		
(S,S)-49 and (S)-31 CPESd top	-47.28		
(S,S)-49 and (S)-31 CPESa bot		39.60	
(S,S)-49 and (S)-31 CPESb bot		48.82	
(S,S)-49 and (S)-31 CPESc bot		46.72	
(S,S)-49 and (S)-31 CPESd bot		-48.14	
(S,S)-49 and (R)-31 CPERc top	-49.38		0.56
(S,S)-49 and (R)-31 CPERd top	-48.84		
(S,S)-49 and (R)-31 CPERb top	-48.04		
(S,S)-49 and (R)-31 CPERa top	-38.69		
(S,S)-49 and (R)-31 CPERa bot		-49.18	
(S,S)-49 and (R)-31 CPERd bot		-48.79	
(S,S)-49 and (R)-31 CPERb bot		-47.93	
(S,S)-49 and (R)-31 CPERc bot		41.60	

¹3D structure of all optimised conformations are available as supplementary material on the CD attached to the thesis. CPES bot/top (Cage phenyl (S)-ester guest bottom/ top) and CPER (Cage phenyl (R)-ester guest bottom/ top) refer to the name of the PDB file and Cartesian co-ordinates on the CD attached and in Appendix 2.

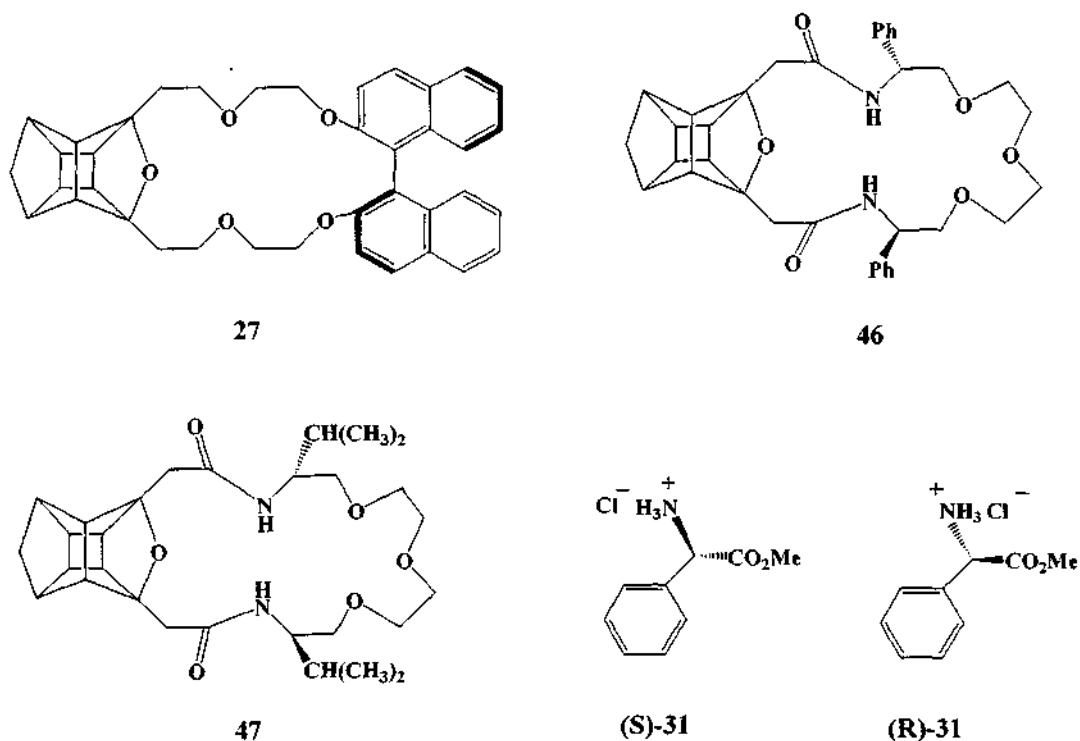
²Four complex structures for each the bottom side and the topside of the complex were obtained according to the computational model described in Appendix 4.

³See equation: Binding energy = E_{complex} - (E_{host} + E_{guest}).

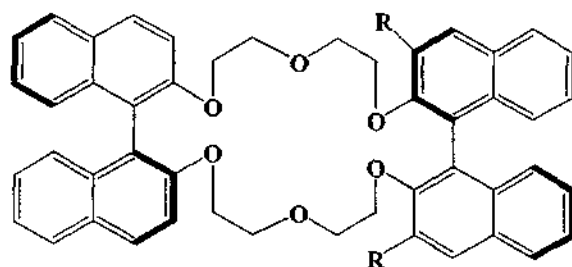
⁴Relative energy lowest (S,S)-49-(R)-31 complex vs lowest (S,S)-49-(S)-31 complex.

The (S,S)-49 host preferred the (R)-31 guest to the (S)-31 guest by 0.56 kcal mol⁻¹. The binding energies calculated for host (S,S)-49 with guests (S)-31 and (R)-31 are lower (-49.38 kcal mol⁻¹) than the binding energies that were reported for the cage annulated hosts (S,S)-46 (-44.75 kcal mol⁻¹), (S,S)-47 (-49.21 kcal mol⁻¹) and (R)-27 (-41.79 kcal mol⁻¹) with the same guests (31) (see Table1). This indicates that a more stable complex is formed between host (S,S)-49 with the guests (31) than hosts (S,S)-46, (S,S)-47 and (R)-27 with guests (31).

The calculated enantioselectivity of host (S,S)-49 with guest (R)-31 (0.56 kcal mol⁻¹) was higher than the calculated enantioselectivity of cage annulated hosts (R)-27 with (R)-31 (0.11 kcal mol⁻¹) and (S,S)-46 with (R)-31 (0.13 kcal mol⁻¹). This indicates that host system (S,S)-49 exhibits better chiral preference than cage annulated hosts (R)-27 and (S,S)-46 as well as stronger binding interactions than host systems (R)-27, (S,S)-46 and (S,S)-47.

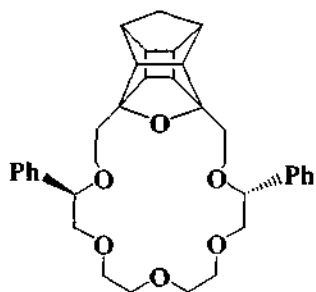


However since host (S,S)-**49** has a calculated enantioselectivity of $0.56 \text{ kcal mol}^{-1}$, it is not a good enough host system to warrant synthesis as a theoretical enantioselectivity of about $1.4 \text{ kcal mol}^{-1}$ is required to compete with Cram's host system (**18**) in U-tube studies.

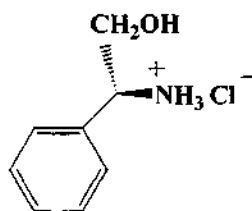


18 R = CH₂Cl

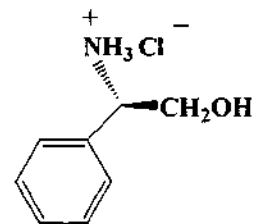
Cage annulated macrocycle (S,S)-**49** was next tested with guests (**51**). The results obtained are tabulated in Table 6 below.



49



(S)-**51**



(R)-**51**

Table 6: Binding Energies of E_{complex} host (S,S)-49 with guests (S)-51 and (R)-51

Host-guest complex ¹	Topside ² Binding energy ³ /kcal mol ⁻¹	Bottomside ² Binding energy ³ /kcal mol ⁻¹	Calculated enantiomeric preference ⁴ /kcal mol ⁻¹
(S,S)-49 and (S)-51 CPASc top	-38.43		
(S,S)-49 and (S)-51 CPASa top	-37.97		
(S,S)-49 and (S)-51 CPASd top	-37.96		
(S,S)-49 and (S)-51 CPASb top	-36.93		
(S,S)-49 and (S)-51 CPASb bot		-42.49	
(S,S)-49 and (S)-51 CPASa bot		-41.50	
(S,S)-49 and (S)-51 CPASd bot		-35.60	
(S,S)-49 and (S)-51 CPASc bot		-34.34	
(S,S)-49 and (R)-51 CPARa top	-41.40		
(S,S)-49 and (R)-51 CPARb top	-41.39		
(S,S)-49 and (R)-51 CPARc top	-41.39		
(S,S)-49 and (R)-51 CPARd top	-36.10		
(S,S)-49 and (R)-51 CPARc bot		-43.40	0.91
(S,S)-49 and (R)-51 CPARa bot		-40.20	
(S,S)-49 and (R)-51 CPARd bot		-40.07	
(S,S)-49 and (R)-51 CPARb bot		-39.07	

¹3D structure of all optimised conformations are available as supplementary material on the CD attached to the thesis. CPAS bot/top (Cage phenyl alcohol S guest bottom/ top) and CPAR (Cage phenyl alcohol R guest bottom/ top) refer to the name of the PDB file and Cartesian co-ordinates on the CD attached and in Appendix 2.

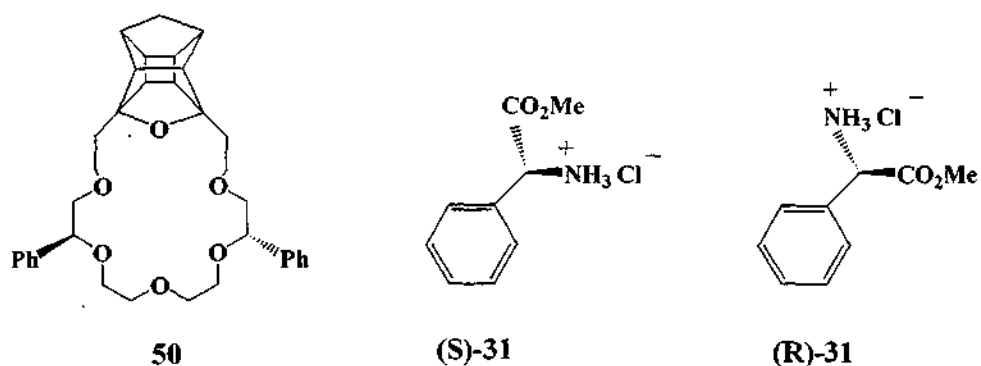
²Four complex structures for each the bottom side and the topside of the complex were obtained according to the computational model described in Appendix 4.

³See equation: Binding energy = $E_{\text{complex}} - (E_{\text{host}} + E_{\text{guest}})$.

⁴Relative energy lowest (S,S)-49-(R)-51 complex vs lowest (S,S)-49-(S)-51 complex.

As shown in Table 5, host (S,S)-**49** demonstrated good chiral recognition for guest (R)-**31** (0.56 kcal mol⁻¹). Host (S,S)-**49** prefers the (R)-**51** to the (S)-**51** by 0.91 kcal mol⁻¹. The host (S,S)-**49** demonstrated greater calculated enantiomeric preference with guest (R)-**51** than with guest (R)-**31**. It is possible that the alkyl groups on the chiral carbon of the host and guest can be responsible for the steric interaction that contributes to the enhanced enantiomeric recognition of the (R)-guest molecules over the (S)-guest molecules, in both cases.

Host (S,S)-**50** with the phenyl moieties placed farther away from the cage, was examined next, to investigate the effect of changing the position of the chiral barriers on the cage annulated macrocycle.



The results obtained for host (S,S)-**50** with guests (**31**) are tabulated in Table 7.

Table 7: Binding Energies of E_{complex} host (S,S)-50 with guests (S)-31 and (R)-31

Host-guest complex ¹	Topside ² Binding energy ³ /kcal mol ⁻¹	Bottomside ² Binding energy ³ /kcal mol ⁻¹	Calculated enantiomeric preference ⁴ /kcal mol ⁻¹
(S,S)-50 and (S)-31 CNGESd top	-48.61		
(S,S)-50 and (S)-31 CNGESa top	-46.39		
(S,S)-50 and (S)-31 CNGESb top	-42.95		
(S,S)-50 and (S)-31 CNGESc top	-48.61		
(S,S)-50 and (S)-31 CNGESc bot		-42.76	
(S,S)-50 and (S)-31 CNGESa bot		-42.14	
(S,S)-50 and (S)-31 CNGESb bot		-42.14	
(S,S)-50 and (S)-31 CNGESd bot		-42.14	
(S,S)-50 and (R)-31 CNGERa top	-48.64		0.03
(S,S)-50 and (R)-31 CNGERd top	-47.95		
(S,S)-50 and (R)-31 CNGERb top	-48.64		
(S,S)-50 and (R)-31 CNGERc top	-47.94		
(S,S)-50 and (R)-31 CNGERa bot		-44.82	
(S,S)-50 and (R)-31 CNGERd bot		-42.56	
(S,S)-50 and (R)-31 CNGERbbot		-44.82	
(S,S)-50 and (R)-31 CNGERc bot		-42.52	

¹3D structure of all optimised conformations are available as supplementary material on the CD attached to the thesis. CNGES bot/top (Cage newglycol (S)-ester guest bottom/ top) and CNGER (Cage newglycol (R)-ester guest bottom/ top) refer to the name of the PDB file and Cartesian co-ordinates on the CD attached and in Appendix 2.

²Four complex structures for each the bottom side and the topside of the complex were obtained according to the computational model described in Appendix 4.

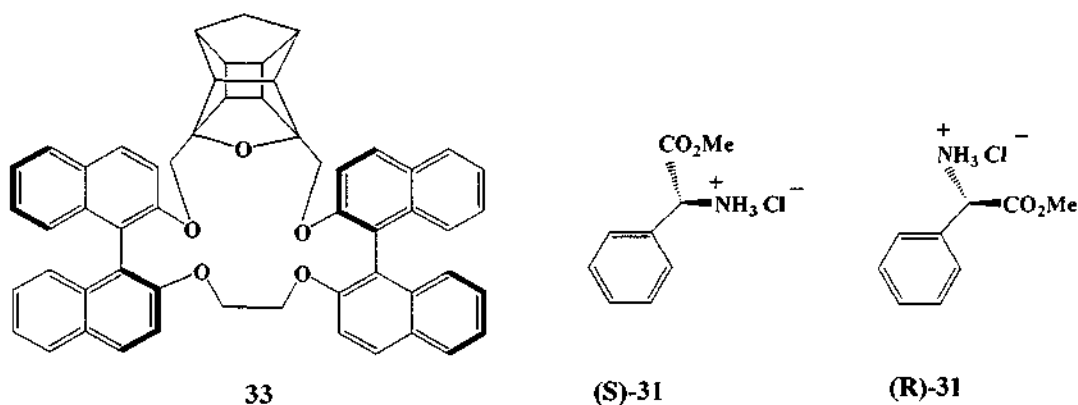
³See equation: Binding energy = E_{complex} - (E_{host} + E_{guest})

⁴Relative energy lowest (S,S)-50-(R)-31 complex vs lowest (S,S)-50-(S)-31 complex. Host (S,S)-50 preferred the (R)-31 guest to the (S)-31 guest by 0.03 kcal mol⁻¹. The effect of moving the chiral phenyl barriers farther away from the rigid PCU moiety of the cage annulated macrocycle resulted in poor chiral recognition being observed when compared with the cage annulated macrocycle (S,S)-49. (S,S)-49 has chiral barriers placed closer to the PCU moiety of the cage macrocycle and had a calculated enantiomeric preference of 0.56 kcal mol⁻¹ for the (R)-31 guest.

The bulky phenyl substituents are situated in the less rigid portion of the (S,S)-50 macrocycle, i.e away from the rigid PCU cage moiety, and it appears that the chiral barriers are not effective when placed in the less rigid portion of the cage annulated macrocycle resulting in reduced enantioselectivity. Poor enantiomeric recognition is probably the result of the chiral barriers being unable to provide effective chiral interference due to less rigidity at the lower end of the macrocycle.

Macrocycle (S,S)-33 which was discussed earlier in Chapter 2, was examined for its enantioselectivity towards guest molecules (S)-31 and (R)-31. Host (S,S)-33 has the advantage of having both the PCU cage moiety as well as chiral binaphthyl groups incorporated into the macrocycle. The design of novel crown (S,S)-33 was inspired by the superior results obtained by the binaphthyl crown ethers (R,R)-17 (calculated enantiomeric preference of 1.1 kcal mol⁻¹) and (R,R)-18 (calculated enantiomeric preference of 1.4 kcal mol⁻¹) designed by Cram.

The synthesis of this crown ether could be very challenging. Nevertheless, in the light of the incorporation of the PCU moiety, (S,S)-33 may be an improvement on the chiral cage annulated macrocycle (R)-27 synthesized by Marchand *et al.*⁴, which resulted in a calculated chiral preference of 0.11 kcal mol⁻¹ (see Table 1). It has been shown that the PCU cage provides rigidity⁴ to the macrocycle and also enhances its lipophilicity, thereby increasing its extraction ability in U-tube studies.



The results of (S,S)-33 with guests (31) are tabulated in Table 8.

Table 8: Binding Energies of E_{complex} host (S,S)-33 with guests (S)-31 and (R)-31

Host-guest complex ¹	Topside ² Binding energy ³ /kcal mol ⁻¹	Bottomside ² Binding energy ³ /kcal mol ⁻¹	Calculated enantiomeric preference ⁴ /kcal mol ⁻¹
(S,S)-33 and (S)-31 CCESa top	-39.99		1.52
(S,S)-33 and (S)-31 CCESb top	-40.03		
(S,S)-33 and (S)-31 CCESc top	-38.70		
(S,S)-33 and (S)-31 CCESd top	-34.11		
(S,S)-33 and (S)-31 CCESa bot		-26.8	
(S,S)-33 and (S)-31 CCESb bot		-37.81	
(S,S)-33 and (S)-31 CCESc bot		-36.46	
(S,S)-33 and (S)-31 CCESd bot		-36.5	
(S,S)-33 and (R)-31 CCERa top	-36.78		
(S,S)-33 and (R)-31 CCERb top	-37.76		
(S,S)-33 and (R)-31 CCERc top	-38.35		
(S,S)-33 and (R)-31 CCERd top	-38.51		
(S,S)-33 and (R)-31 CCERa bot		-31.88	
(S,S)-33 and (R)-31 CCERb bot		-36.37	
(S,S)-33 and (R)-31 CCERc bot		-36.30	
(S,S)-33 and (R)-31 CCERd bot		-36.49	

¹3D structures of all optimised conformations are available as supplementary material on the CD attached to the thesis. CCES bot/top (Cage Cram (S)-ester guest bottom/ top) and CCER (Cage Cram (R)-ester guest bottom/ top) refer to the name of the PDB file and Cartesian co-ordinates on the CD attached and in Appendix 2.

²Four complex structures for each the bottom side and the topside of the complex were obtained according to the computational model described in Appendix 4.

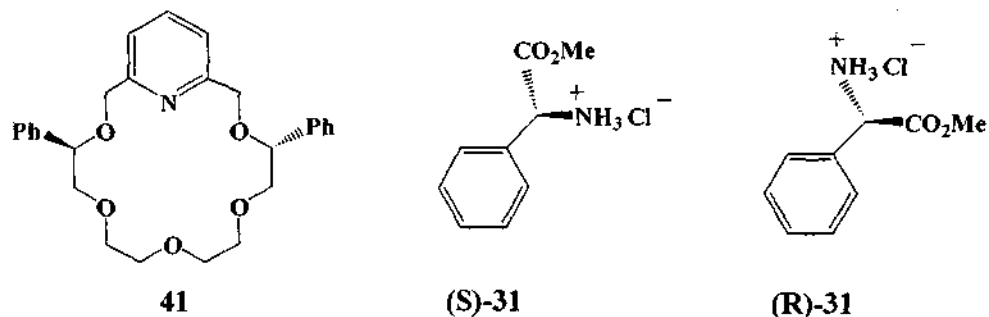
³See equation: Binding energy = $E_{\text{complex}} - (E_{\text{host}} + E_{\text{guest}})$.

⁴Relative energy lowest (S,S)-33-(S)-31 complex vs lowest (S,S)-33-(R)-31 complex.

A calculated enantiomeric preference of 1.52 kcal mol⁻¹ was observed for host (S,S)-33 with guest (S)-31 which indicates that this host system has excellent potential. The calculated enantiomeric preference is better than that of Cram's binaphthyl crown (R,R)-18, which had a calculated enantiomeric preference of 1.4 kcal mol⁻¹ with guest (R)-31 (see Table 1). It would be interesting and challenging to find a synthetic route to theoretical host (S,S)-33. The calculated enantioselectivity could then be verified experimentally via U-tube transport studies.

4.3 THE EFFECT OF SOLVENT ON BINDING ENERGY AND ENANTIOSELECTIVITY

It has been shown by Bradshaw *et al.*¹⁹² that solvation has a notable hindering effect on the experimentally observed binding energies in host-guest recognition experiments that were performed in solvent (methanol) and in gas phase. Bradshaw *et al.*¹⁹² compared the experimental results obtained using titration calorimetry with molecular mechanics calculations performed on these systems. The experimental results using methanol as a solvent suggested that solvation decreased the binding energy when compared with the experimental gas phase values. As both host and guest molecules had benzene ring substituents, recognition was found to be dependent on π -stacking interaction to a certain extent, which would certainly be different and probably weaker in a polar solvent than in the gas phase. It was proposed¹⁹² that solvation of the chiral host and guest by a polar solvent such as methanol would lead to a decrease in the strength of the interactions between the two chiral species thus resulting in a decrease in the binding energy in a solvation medium when compared with the gas phase. It was concluded that molecular mechanics calculations yields a reasonable qualitative and quantitative estimate of the degree of chiral recognition and that experimental titration calorimetry conducted in a polar solvent medium has a negative effect on the extent of chiral recognition.¹⁹²



Since it is clear that solvent does play a significant role in host-guest interactions, calculations were performed to examine the effects of solvent using MacroModel software¹³² which allows the use of solvent (water and chloroform) in calculations. Host-guest complexes (S,S)-**41** with (S)-**31** and (S,S)-**41** with (R)-**31** were chosen for this study since these complexes were studied previously using gas phase calculations in Alchemy 2000¹³¹.

The free host, free guests and the host-guest complexes were subjected to the docking procedure as described in Appendix 3. The lowest free host, free guest and the host-guest complex were subjected to MM3 optimization using MacroModel¹³² software. Calculations were performed in the absence of solvent, using water as a solvent and using chloroform as a solvent using MacroModel¹³² software and compared with a MM3 optimization result performed in the gas phase using Alchemy 2000¹³¹ software. The binding energy as described in Equation 2 was calculated for each host-guest complex.

Table 9: Binding Energies of E_{complex} host (S,S)-41 with guests (S)-31 and (R)-31

Host-guest complex ¹	Gas/Solvent Phase	Binding energy ² / kcal mol ⁻¹	Calculated enantiomeric preference ³ / kcal mol ⁻¹
(S,S)-41 and (S)-31	Gas Phase MM3 (MacroModel)	-50.98	0.56
(S,S)-41 and (S)-31	Water MM3 (MacroModel)	-6.34	0.34
(S,S)-41 and (S)-31	Chloroform MM3 (MacroModel)	-27.13	0.67
(S,S)-41 and (S)-31	Gas Phase MM3 (Alchemy 2000)	-40.43	0.56
(S,S)-41 and (R)-31	Gas Phase MM3 (MacroModel)	-50.42	
(S,S)-41 and (R)-31	Water MM3 (MacroModel)	-6.00	
(S,S)-41 and (R)-31	Chloroform MM3 (MacroModel)	-26.46	
(S,S)-41 and (R)-31	Gas Phase MM3 (Alchemy 2000)	-39.94	

¹3D structure of all optimised conformations are available as supplementary material on the CD attached to the thesis. PDB files and Cartesian co-ordinates labelled MacroModel: BradshawSShostSguest or BradshawSShostRguest are on the CD attached and in Appendix 2.

²See equation: Binding energy = $E_{\text{complex}} - (E_{\text{host}} + E_{\text{guest}})$.

³Relative energy lowest (S,S)-41-(S)-31 complex vs lowest (S,S)-41-(R)-31 complex.

The above results indicate that solvent does play a role in enantiomeric recognition. It can be observed that binding energies calculated when using solvent (water and chloroform) are higher than those obtained in the “gas phase” (Alchemy 2000)¹³¹ or in the absence of solvent (gas phase) (MacroModel).¹³² Lower binding energies indicate a stable complex and a strong binding interaction between the host and guest. Using water as a solvent increases the binding energies while the effect of chloroform does so to a lesser extent. The MM3 optimization with Alchemy 2000 in the gas phase produces comparable binding energies when compared with that of MacroModel with no solvent (gas phase). This study indicates that solvent does have a negative effect on the binding of ammonium ions by crown ethers in the solvent medium.

The enantiomeric preference calculated in the gas phase using MacroModel and Alchemy 2000 software between host-guest complexes (S,S)-41 and (S)-31 and (S,S)-41 and (R)-31 produces the same result of 0.56 kcal mol⁻¹ which is higher than the calculated enantioselectivity observed in water (0.34 kcal mol⁻¹). The calculated

enantioselectivity is decreased in water ($0.34 \text{ kcal mol}^{-1}$) and increased in chloroform ($0.67 \text{ kcal mol}^{-1}$). Solvation with a polar solvent decreases the binding energy when compared with a less polar solvent. Since both host and guest molecules have benzene ring substituents and are lipophilic to a certain extent, chiral recognition will be enhanced in a non-polar solvent and would certainly be different and probably weaker in a polar solvent such as water.

It has been suggested¹⁹³ that it is possible to improve chiral recognition by making small adjustments to the design of the host structure. Variation of the guest structure will also affect the extent of recognition that is displayed by a given ligand and the stability of the complex formed between the host and the guest. Chiral guests that differ by a single methylene group can be differentiated by well-designed hosts, as can the (R)- and (S)- forms of the enantiomer. Such precision in molecular recognition can play a significant role in the rapid analysis of racemic chiral amines, thus providing vital information as to the basis of the structural and enantiomeric recognition process. Keeping this in mind, this study can be extended to calculate the chiral recognition of various guest molecules, by developing and modifying host systems.¹⁹³

A computational method can be advantageous to researchers in host-guest chemistry, since it provides predictions about the effectiveness of the systems under investigation, saving time, labour and costs in the laboratory. The MM3 computational model calculates crude relative binding energies, which correspond in most cases to a reasonable extent with the magnitude of the reported experimental chiral preferences.¹³⁰ Consequently new theoretical host systems with promising predicted enantioselectivity can then be synthesized and their enantioselectivity can then be tested experimentally using transport studies.

The calculated chiral preference has been determined for the theoretical host systems, cage annulated macrocycles (S,S)-**49** and (S,S)-**50**. In Chapter 5, the synthesis of precursors to chiral macrocycles such as (S,S)-**49** and (S,S)-**50** will be reported.

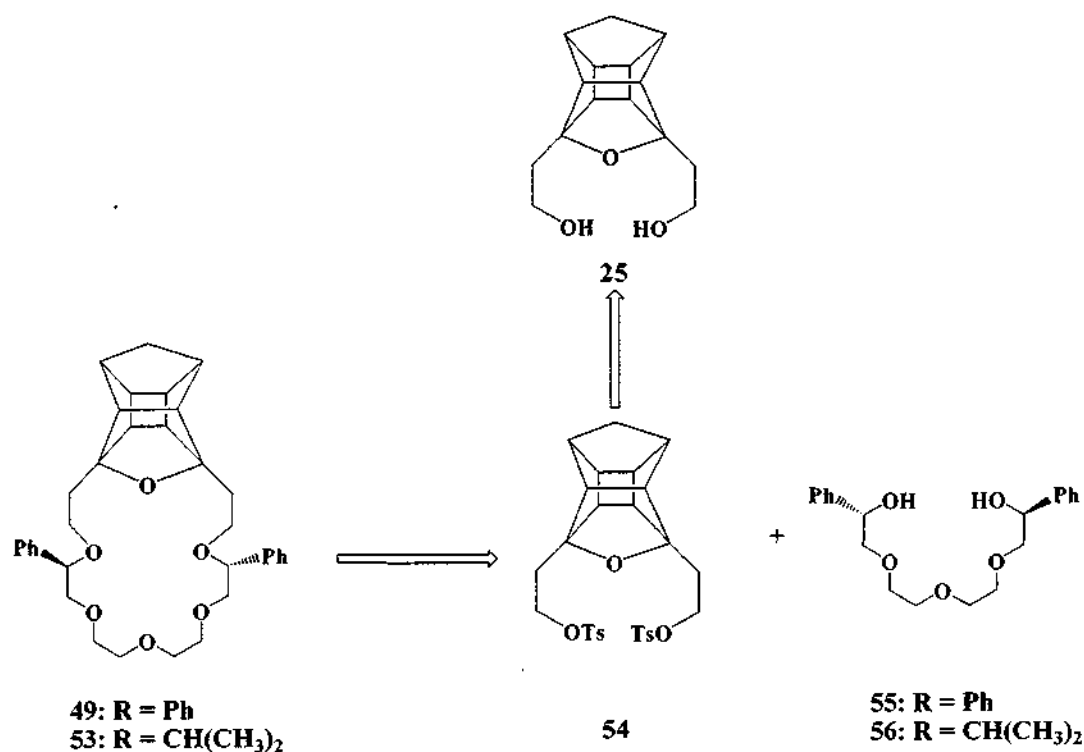
CHAPTER FIVE

THE SYNTHESIS OF MACROCYCLIC PRECURSORS

In the previous chapters theoretical chiral cage annulated macrocycles (S,S)-49 and (S,S)-50 were postulated as possible host systems for the separation of chiral ammonium ions. Various synthetic routes that have been used previously will be discussed as well as the synthetic routes used to synthesize macrocyclic precursors for the chiral cage annulated macrocycles (S,S)-49, (S,S)-50 and (S,S)-53.

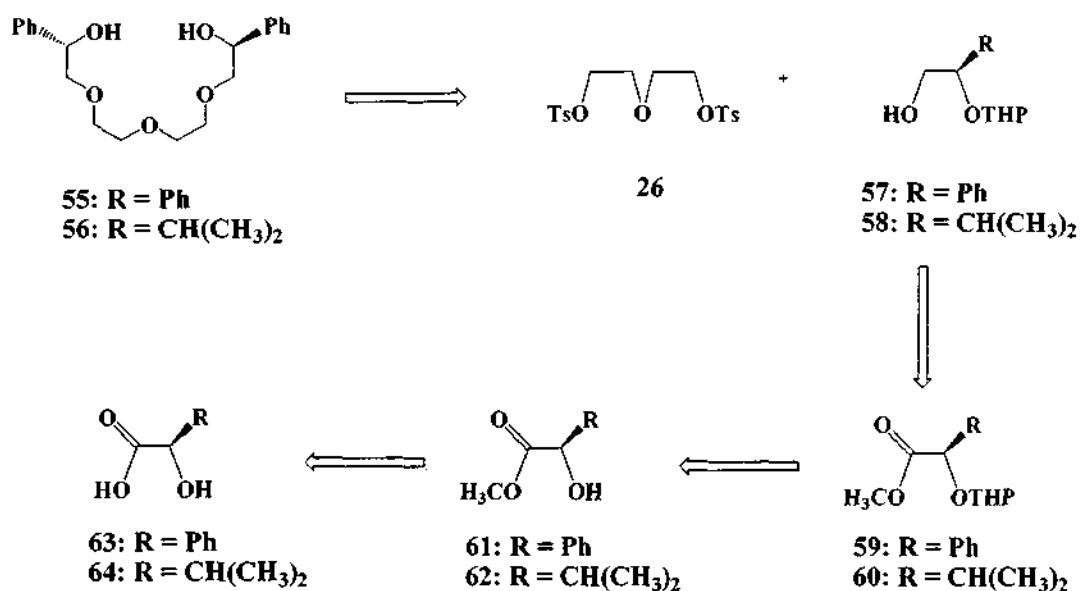
5.1 THE RETROSYNTHETIC ROUTE TOWARDS CHIRAL CAGE ANNULATED MACROCYCLES

Scheme 3a illustrates a possible retrosynthetic route to chiral cage annulated macrocycles (S,S)-49 and (S,S)-53 using macrocyclic precursors such as the cage diol (25), the cage ditosylate (54) and the chiral glycols (55) and (56) respectively.



Scheme 3a: Proposed retrosynthetic route to chiral cage annulated macrocycles (S,S)-49 and (S,S)-53

The retrosynthetic route to the chiral glycols (**55**) and (**56**) is illustrated below.

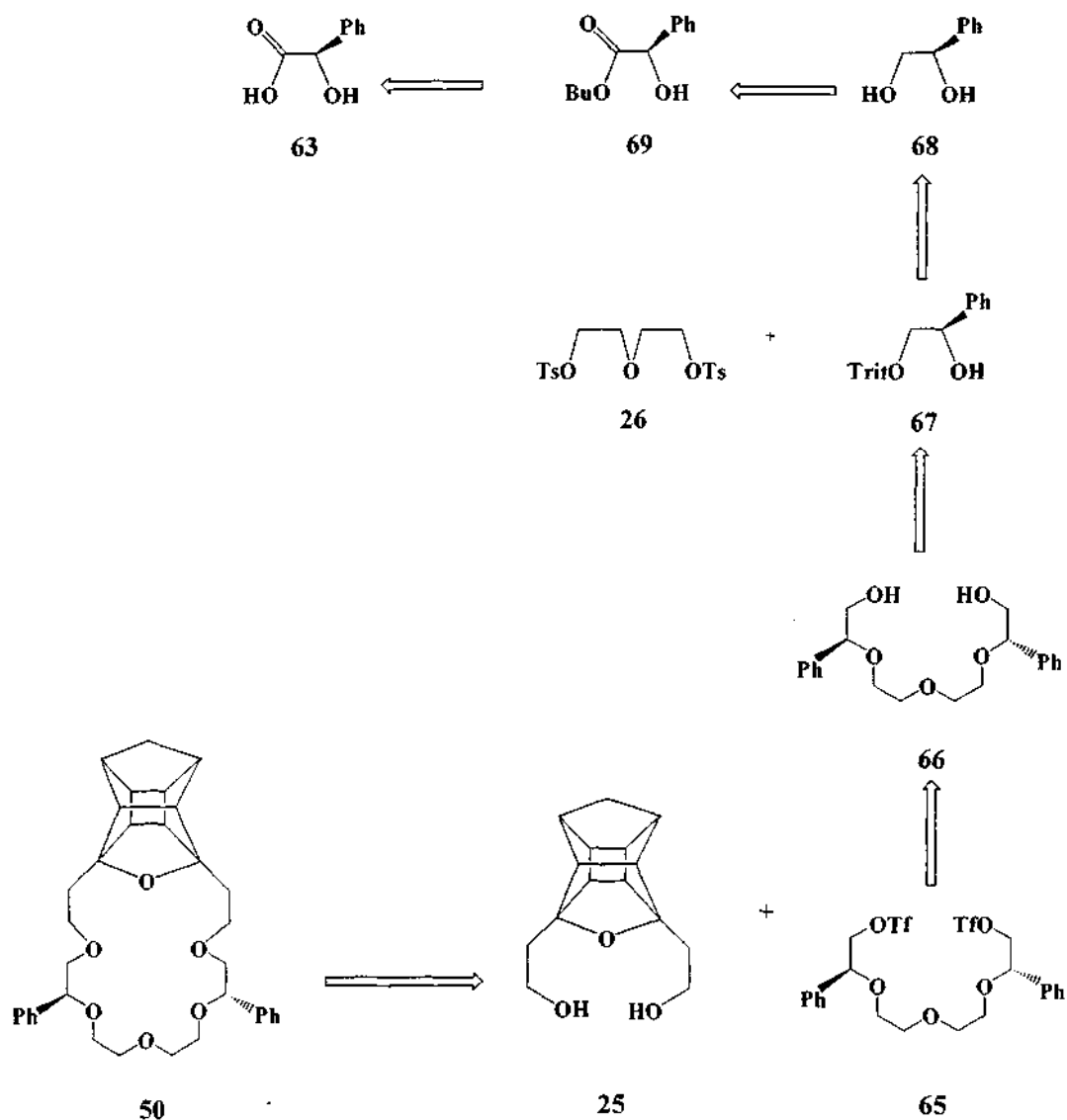


Scheme 3b : Proposed retrosynthetic route to chiral glycols (S,S)-55 and (S,S)-56

The flaw in the proposed synthesis in Scheme 3b is the fact that the incoming nucleophiles (**55** and **56**) are sterically hindered due to the close proximity of the R-groups. If such a synthesis is successful, the yield of the cage annulated macrocycle is expected to be very low.

The macrocyclic precursors, namely the cage diol (**25**) and the cage ditosylate (**54**) were synthesized via multi-step synthesis beginning with the synthesis of a cage dione (**20**) as shown in Scheme 5 and Scheme 6 (§5.3.1) respectively. The synthesis of the chiral glycols (**55**) and (**56**) are illustrated in Schemes 8 (§5.3.3) and Scheme 7 (§5.3.2) respectively. The syntheses of the macrocyclic precursors will be discussed in detail in §5.3.

Scheme 4 illustrates a possible retrosynthetic route for the chiral cage annulated macrocycle (S,S)-**50** using macrocyclic precursors such as the cage diol (**25**) and a chiral glycol (**65**) which is protected with a triflate group instead of a tosylate group.



Scheme 4: Proposed retrosynthetic route to chiral macrocycle (S,S)-50

The chiral glycol (**66**) has phenyl substituents attached to the β carbon atoms. The preparation of this glycol was reported by Bradshaw *et al.* to be the most challenging part of synthesizing the crown ethers and the yield was not reported.¹⁹⁴ Nevertheless the synthesis of a chiral glycol (**66**) with the phenyl substituents attached to the β carbon atoms was attempted. Since the bulky phenyl groups are farther away than in chiral glycol **55**, it was proposed that ring closure of (S,S)-**50** would be more favoured than in the case of (S,S)-**49**.

The proposed synthetic route for the chiral glycol (66) is illustrated below in Scheme 9 (§5.3.4). A brief overview on the synthesis of macrocycles will be covered in §5.2.

5.2 METHODS UNDERTAKEN WHEN SYNTHESIZING MACROCYCLES

Although several synthetic routes for the crown ethers have been developed during the last decade, most methods are tedious and the target compound is obtained in very low yields. The synthesis of large macrocycles usually involves condensation reactions of two bifunctional molecules (precursors). A major problem is that such molecules tend to polymerize thereby decreasing the yield of the product. The template effect and high dilution methods are techniques that help prevent the unwanted side reaction of polymerization. A general procedure used to avoid polymerization in coupling reactions between bifunctional molecules (precursors), is the use of protecting groups.

Two methodologies, which have resulted in the increased yield of macrocycles, will be discussed farther. It has been proposed that the use of cesium carbonate induces a kinetic template effect that plays a role in the cyclisation step in the formation of crown ethers. In addition, trifluoromethanesulfonate as an improved leaving group on the glycol, in comparison with the tosylate leaving group, will be briefly discussed.

5.2.1 THE TEMPLATE EFFECT

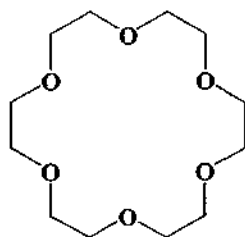
Some early studies into the preparation of many multi-ring systems involve a base-induced cyclisation under the conditions of high dilution. Such systems include mono- ω -haloalkyl ethers of hydroquinone, resorcinol and other related dihydric phenols. The surprisingly high yields sometimes obtained in the synthesis of macrocyclic compounds in base-catalysed Williamson type reactions between diols and dihalides or ditosylates suggest that the complexation and encirclement of the metal cation present may act as a template facilitating cyclization.¹²

The template effect can be defined as a reaction in which reactive groups are preorganised in a favourable orientation by a complexed metal ion, thereby allowing a selective reaction to occur.¹⁹⁵ A two-fold benefit is derived from using the template effect, which is:

- The suppression of polymerization reactions since the local concentration of reactants around the metal ion is very high.
- Multi-step reactions can be achieved since the metal holds the reactants together.

The use of the metal ion in the kinetic template effect depends on the size of cavity of the crown ether to be synthesized, as there is a close link between the cation diameter and the size of the cavity of the crown ether. The optimum ring size is 15-18 Å for Na⁺, 18 Å for K⁺ and 18-21 Å for Cs⁺.¹² Therefore the cyclisation step of a 15-crown-5 or a 16-crown-5 may be achieved with a sodium ion whereas a 18-crown-6 may require a potassium ion. The relatively high yields obtained in the cyclisations of the crown ethers can be attributed to the operation of a possible template effect resulting from coordination of the reactants around the potassium ions, although it is likely that complexation is important only in the final ring closure.

There are various factors that may affect the yield of the final product such as the effect of solvent or base used. For example the reaction of triethylene glycol with di-*p*-toluenesulphonate in dimethylsulphoxide in the presence of potassium *t*-butyl alcoholate, was reported to give 1,4,7,10,13,16-hexaoxacyclo-octadecane (18-crown-6) (7) in a yield of 93 %. However when the same reaction was conducted in tetrahydrofuran, yields of 30-60 % were obtained.¹²



7

Using *t*-butylammonium hydroxide as a base in tetrahydrofuran (a co-ordinating solvent), produced 18- and 21-membered cyclic ethers in decreased yields as most of the starting materials polymerized.¹²

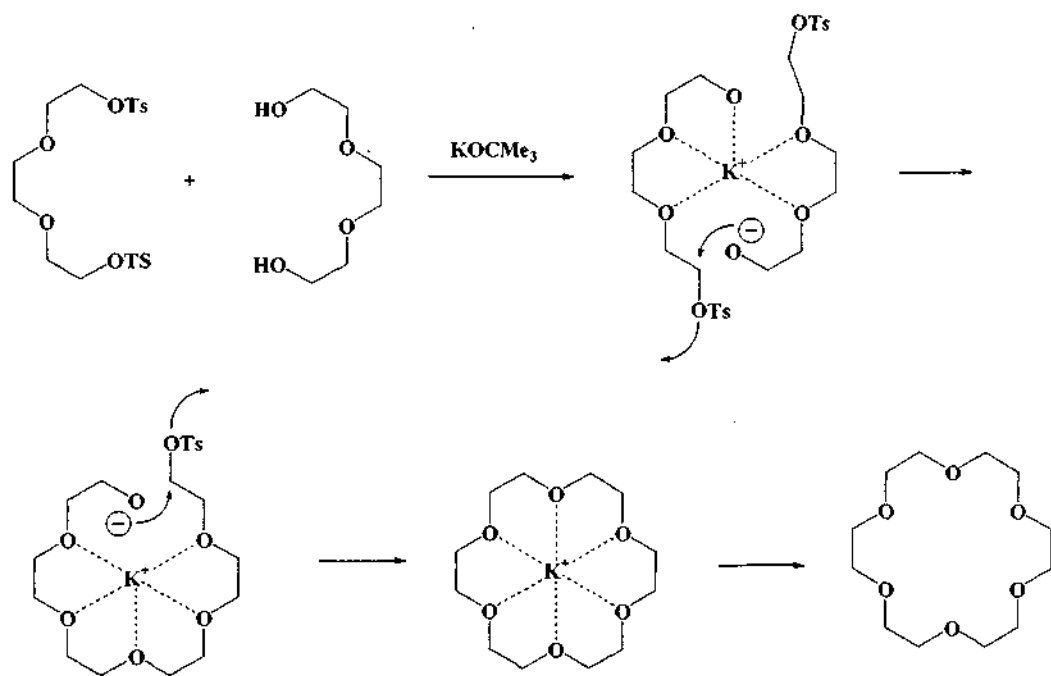


Figure 5: The template effect of 18-crown-6 (7)¹⁹⁵

The cyclization step is a S_N2 reaction involving a nucleophilic displacement of a halide or tosylate or other leaving group by alkoxide ions. An alkoxide anion brings the two ends of the linear bifunctional precursor into close proximity resulting in a cyclic structure, which promotes the formation of the crown ether. Although there is a rate enhancement due to the proximity effect, there is also a rate retardation factor since the alkoxide ion interacts with the metal ion resulting in a reduced nucleophilicity of the alkoxide ion. Many cyclisation reactions involving the use of metal ions have resulted in increased yields of crown ethers, however the mechanistic nature of the improvement remains unclear.¹⁹⁶ The precise role of metal co-ordination in the formation of cyclic ethers is still not understood.¹⁹⁷

The cesium salt method, which was first developed for peptide chemistry,¹⁹⁸ has been applied to the synthesis of crown ethers and has helped in the crucial ring closure reaction.^{199,200,201} It is believed that the Cs⁺ ion can play an irreplaceable role compared with Na⁺ or K⁺ during the formation of some macrocycles such as (21-crown-7) since it probably complexes more weakly than for example potassium. It has been suggested that cesium helps with the template effect in the early stages of ring closure

thereby binding the ends of the glycol and bringing it closer together for the coupling step.²⁰⁰

5.2.2 TRIFLUOROMETHANESULPHONATE (TRIFLATE) AS A NEW LEAVING GROUP IN MACROCYCLIC PRECURSORS

The conversion of an alcohol to the corresponding ether is a widely used functional transformation in organic synthesis. There are several methods available to accomplish this reaction under a variety of conditions.²⁰² Triflate is a leaving group, which is far more reactive than the analogous bromides.²⁰³ The use of the triflate in crown ether synthesis, due to its excellent leaving group properties has been demonstrated in many cases.^{204,205,206}

It has also been reported that treatment of diols with triflic anhydride yields the desired ditriflates without affecting the stereochemistry at the carbon. The stereochemistry of the glycolization is thus transferred to the ditriflate.²⁰⁷ It has been shown that alkylation of diols with ditriflate using sodium hydride as a base without high dilution conditions produced macrocycles in yields of 35 %. A similar procedure based upon the use of ditosylate instead of ditriflate was found to be ineffective as a major proportion of the starting materials was recovered.²⁰⁸ A note of caution should be highlighted, if the leaving group is very reactive, an elimination reaction can occur as an unwanted side reaction.

5.2.3 HIGH DILUTION EFFECTS

High dilution techniques help to increase the yield in the synthesis of crown ethers. This technique requires the slow mixture of reagents, over approximately 8-24 hours or using a very large volume of solvent and a concentration approximately 100 mmol.dm⁻³.¹⁹⁵ A reaction procedure carried out in a highly diluted solution results in a lower probability of intermolecular collisions and hence a depression of chain extension (polymers). It also encourages ring closure, which is an intramolecular reaction. In practice, the reactants are held in separate dropping funnels and over a long period of time (usually 8-24 hours), are added drop by drop to a large amount of a solvent containing a condensing agent.

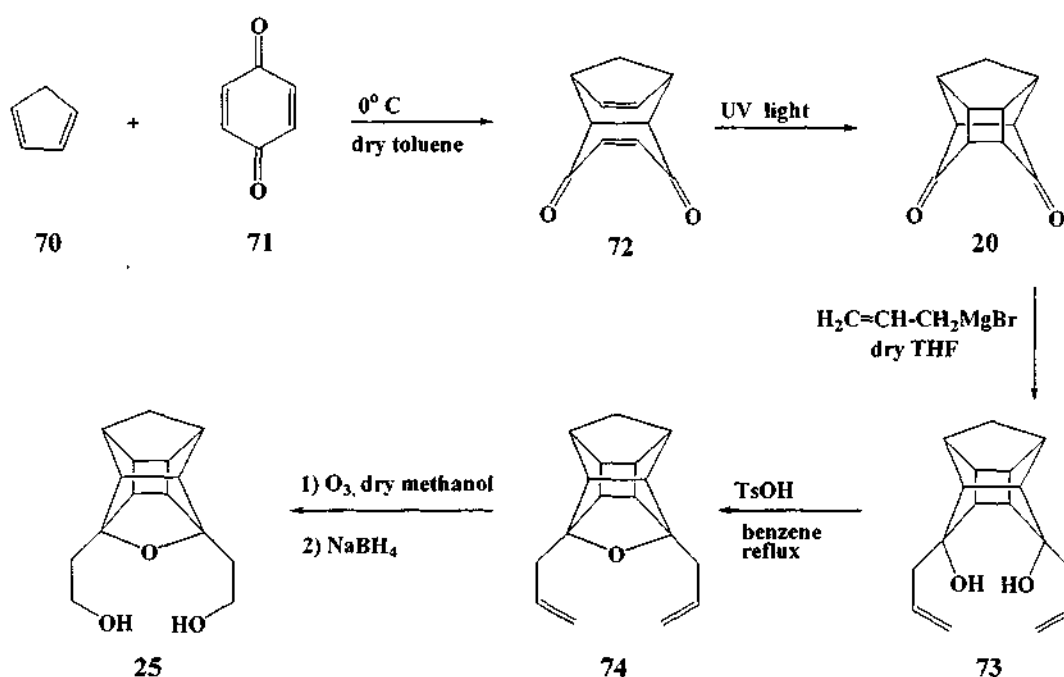
Similar synthetic routes were used by Marchand *et al*^{4,129} (see Chapter 2, Scheme 1 and Scheme 2) for the synthesis of cage annulated crown ethers. The multi step synthesis of precursors for chiral macrocycles (S,S)-49, (S,S)-50 and (S,S)-53 will be illustrated in §4.3.

5.3 THE MULTI-STEP SYNTHESIS OF PRECURSORS FOR CHIRAL CAGE ANNULATED MACROCYCLES

The schemes below show the synthetic routes of precursors for chiral cage annulated macrocycles.

5.3.1 THE MULTI-STEP SYNTHESIS OF THE CAGE DIOL (25)

Scheme 5 illustrates the synthesis of the cage diol (25) beginning with the synthesis of the cage dione (20).



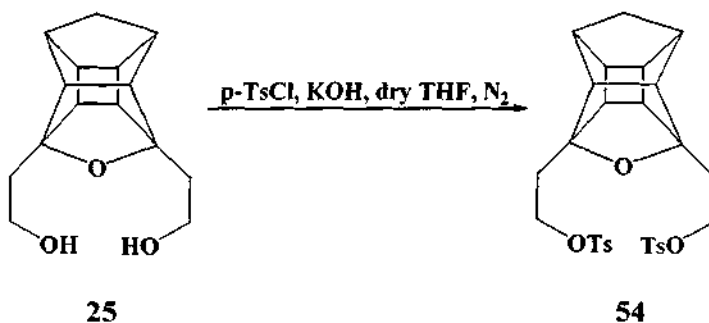
Scheme 5: Synthetic route for the PCU diol (25)⁷⁵

If two double bonds are within reach of one another in the same molecule, especially if one of them is conjugated, a photochemical addition can occur. The adducts of cyclopentadiene (70) and of *p*-benzoquinone (71) have structures that are ideal to meet those requirements.^{120,121} The synthetic route involves the Diels–Alder cycloaddition

of freshly cracked cyclopentadiene (70) to *p*-benzoquinone (71) followed by the intramolecular [2+2] photocyclization of the resulting endo-cycloaddition. The adduct (72) is subjected to ultraviolet (UV) light producing the pentacyclo[5.4.0.0^{2,6}.0^{3,10}.0^{5,9}]-undecane-8,11-dione (PCUD) (20).^{120,121} The complete NMR elucidation of the PCUD (20) structure will be reported Chapter 6 and its X-ray data will be reported in Chapter 7.

Formation of the PCU dione (20) is followed by the allyl Grignard addition to the dione (20) resulting in the PCU endo-endo diol (73) being produced.²⁰⁹ The complete NMR elucidation of the endo-endo diol will be reported in Chapter 6. The endo-endo pentacyclic diol (73) was converted to the PCU diene (74) by removing water azeotropically using the Dean-Stark method.¹²⁹

The next step was the ozonolysis of the pentacycloundecane PCU diene (74), which is followed by a reduction with NaBH₄ to form the pentacycloundecane PCU diol (25).⁷⁵ The procedure used was slightly modified from that of Marchand,¹²⁹ using NaBH₄ instead of H₃B-THF to produce the diol (25). The full NMR elucidation of the PCU diol (25) as well as the X-Ray data are reported in Chapters 6 and 7 respectively.



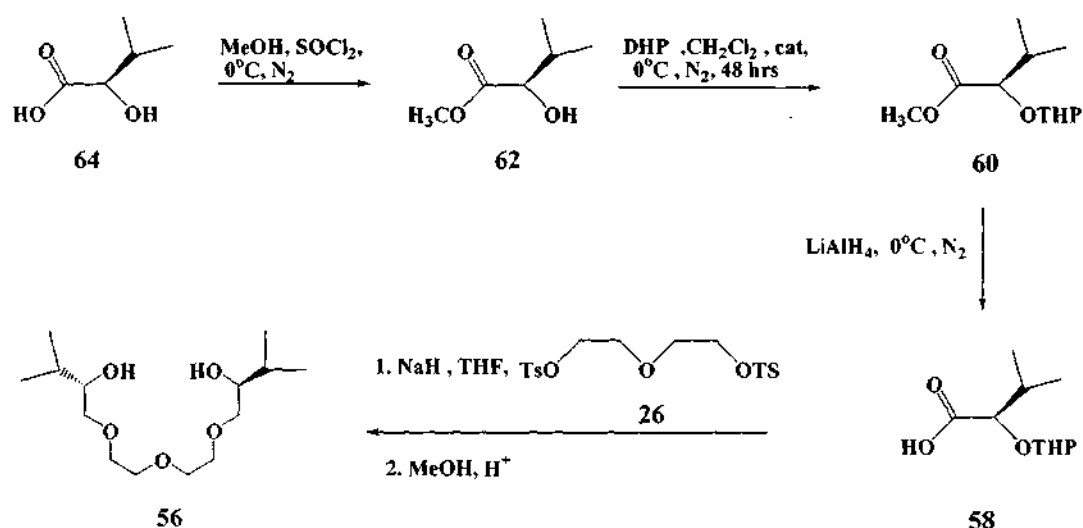
Scheme 6: Synthesis of the PCU ditosylate (54)

The PCU diol (25) was reacted with toluenesulphonyl chloride and KOH to produce the PCU ditosylate (54) (see Scheme 6). Again a different method was followed from that reported by Marchand.^{210,211} The PCU diol (25) was added to KOH (5 equivalents) and *p*-toluenesulphonyl chloride (10 equivalents) in dry THF producing the PCU ditosylate

(54) in 75 % yield. In the next section the multi-step synthesis of chiral precursors for the potential use in macrocycle synthesis will be discussed (refer to Schemes 7 and 8).

5.3.2 THE MULTI-STEP SYNTHESIS OF THE (S,S)-ISOPROPYL GLYCOL (56)

The isopropyl glycol was synthesised by Bradshaw *et al.*⁵³, however the chemicals used in the synthesis were expensive and therefore it was not viable to use the synthetic route proposed. It was decided to use the chemicals available and a different synthetic route was carried out.⁸⁹



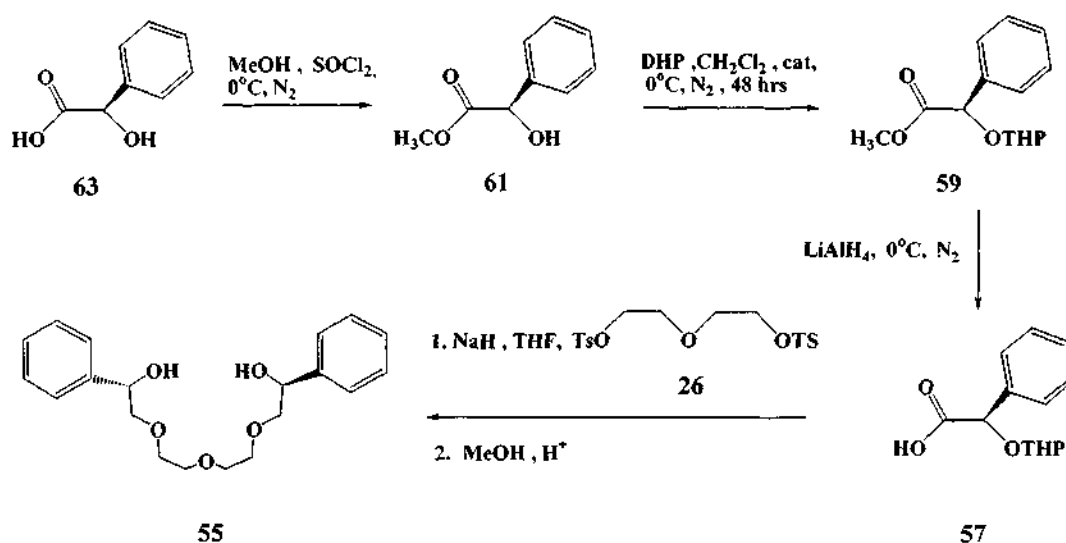
Scheme 7: Synthetic route of the isopropyl glycol (56)⁸⁹

Isohydroxy valeric acid (64) was converted to an ester (62) using methanol and thionyl chloride. This was followed by protection of the alcohol moiety to produce (60). Reduction of the protected ester (60) produced the protected alcohol (58). In order to synthesize the chiral glycol (56), 2 equivalents of the alcohol (58) were reacted with 1 equivalent of diethylene glycol ditosylate (26), followed by deprotection. The final step produced the desired chiral glycol (56) in low yields (20 %) and it was decided that it was not viable to continue with the present synthetic route.

The synthetic procedure was modified to synthesize a chiral glycol with phenyl groups on the α -carbon of the glycol. Scheme 8 below illustrates the synthetic route to a chiral glycol (55).

5.3.3 THE MULTI-STEP SYNTHESIS OF THE (S,S)-MANDELIC GLYCOL (55)^{89,212}

The mandelic glycol (55) was synthesised in 1991 by Bradshaw *et al.*⁸⁹ with a yield of 75 %. In 1992 Naemura *et al.*²¹² reported a different synthetic route with a yield of 76 %.

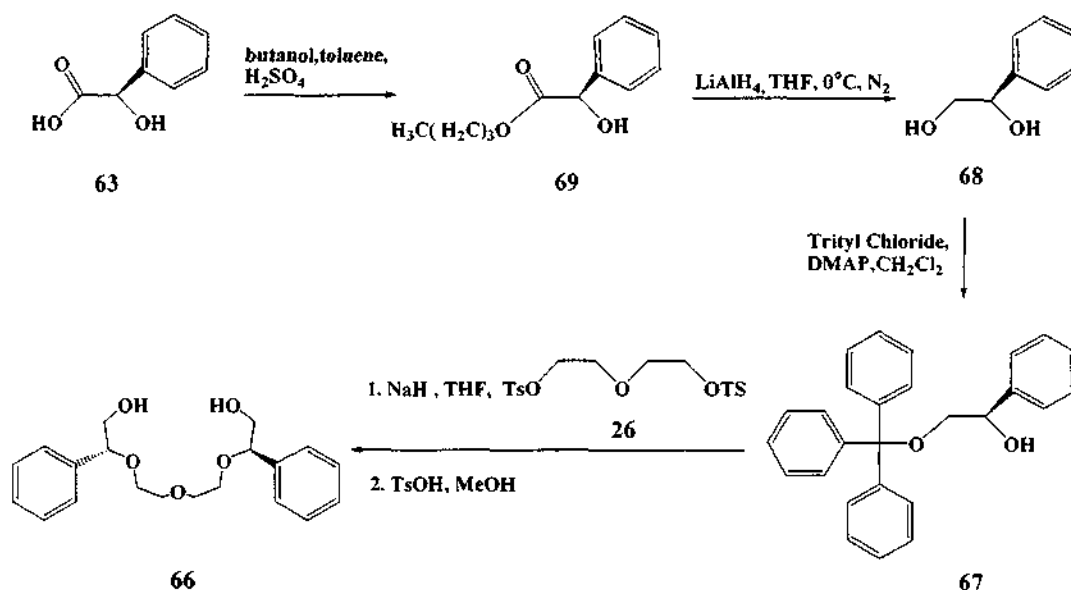


Scheme 8: Synthetic route of the mandelic glycol (55)^{89,212}

Formation of the chiral glycol (55), began with the conversion of the (S)-mandelic acid (63). The (S)-mandelic acid (63) was converted to an ester (61) using thionyl chloride and methanol. The ester (59) was then reacted with dihydropyran to protect the alcohol group. This was followed by a reduction of the protected ester (59) with LiAlH₄ in THF to produce (57). The mandelic glycol (55) was prepared by reacting 2.2 equivalents of the tetrahydropyran (THP) protected alcohol (57) with 1 equivalent of diethylene glycol ditosylate (26) in the presence of NaH in THF. This is a S_N2 reaction with the alkoxide of the alcohol being formed acting as a nucleophile. This was followed by column purification after deprotection with HCl and MeOH producing the chiral glycol (55) in 60 % yield.

5.3.4 THE MULTI-STEP SYNTHESIS OF THE CHIRAL GLYCOL (66)¹⁹⁴

Chiral glycol (66) was synthesised by Bradshaw *et al.*¹⁹⁴ in 1980 however no yield was reported for the final step. This synthetic route¹⁹⁴ was modified to increase the yield of the intermediate steps and this will be discussed below.



Scheme 9: Proposed synthetic route to chiral glycol (66)

The chiral glycol (66) was synthesized via a multi-step synthesis beginning with the conversion of (S)-(+)-mandelic acid (63) to the butyl ester (69). The original procedure¹⁹⁴ involved the reduction of mandelic acid to an alcohol (68) before protection. However better yields were obtained by converting the mandelic acid to the ester (69) before reduction to the alcohol.

The limiting factor in this case is the presence of two hydroxyl functional groups of comparable reactivity in the molecule, which have to be transformed. This difficulty was overcome by protecting one of the hydroxyl functional groups thus allowing the manipulation of the desired group. On a practical level there are many difficulties involved in selectively protecting and regenerating specific hydroxyl functional groups. A method was needed in which only the primary alcohol was protected. This was achieved using triphenylmethyl chloride as the protecting group.²¹³

The bulky triphenylmethyl group was used to selectively protect the primary hydroxyl functional groups in carbohydrates.²¹⁴ The original method for the preparation of trityl ethers involved the reaction of the primary alcohol substrate with triphenylmethyl chloride using pyridine as a solvent, at temperatures ranging from 25°C to 100°C. Chaudhary *et al.*²¹⁵ have reported a successful method using trityl chloride, N,N-dimethylformamide (DMF) solution overnight at room temperature in the presence of triethylamine and 4-dimethylaminopyridine (DMAP). DMAP acts as a group transfer agent in the triphenylmethylation of alcohols. This procedure produced yields up to 88 % of the triphenylmethyl-protected alcohol.²¹⁶

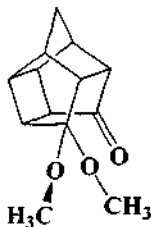
This combination of reagents is also effective in solvents other than DMF. For example yields up to 90 % were reported in dichloromethane solution at room temperature.¹¹⁹ This method offers the advantages of increased selectivity, wide choice of solvents, milder reaction conditions and simplified workup operations. There are many difficulties involved with using pyridine as a solvent, namely the formation of addition complexes of the product with pyridine and other trityl ethers which are contaminants and which are difficult to remove by simple crystallization.

Then 2 equivalents of the protected alcohol (**67**) are reacted with 1 equivalent of diethylene glycol ditosylate (**26**) to produce the protected glycol. This is followed by removal of the protecting groups to produce the glycol (**66**). A negligible yield of the chiral glycol (**66**) was obtained and the majority of the starting materials were recovered instead.

CHAPTER SIX

THE NMR ELUCIDATION OF THE PENTACYCLOUNDECANE DIONE STRUCTURE AND ITS DERIVATIVES

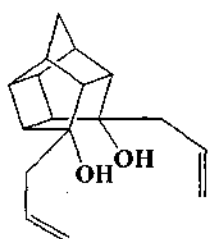
The difficulty of assigning the NMR spectrum of pentacyclo-[5.4.0.0^{2,6}.0^{3,10}.0^{5,9}]undecane-8,11-dione (**20**) and its derivatives had been commented on by many researchers.^{118,217,218,219,220,221} The complete correlation between the spectra and the structures of the compounds has so far proved difficult to achieve and in many cases it has been necessary to resort where available to single crystal X-ray crystallography to elucidate the structures. In 1993 Cadd *et al.*²²² published the NMR assignment of the PCU dione (**20**) by analogy after studying a PCU derivative (**75**). However the full NMR elucidation of the structure of the dione (**20**) has not been reported.



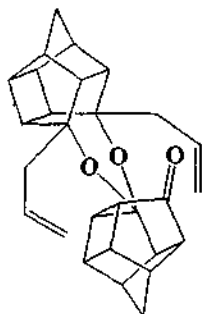
75

The complete NMR elucidation of the structure of the PCU dione (**20**) will be reported in this chapter as well as the structural elucidation of a novel PCU dimer (**76**) that was obtained serendipitously during the synthesis of the macrocyclic precursors.

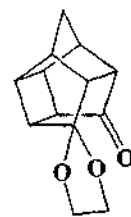
The NMR elucidation of the structures of PCU derivatives (**25**) and (**77**) was performed since it was hoped that the structural similarities present in these PCU derivatives would help with the structural elucidation of the novel PCU dimer (**76**). The complete NMR elucidation of the structures of the PCU dione (**20**) and its derivatives (**25**), (**73**), (**76**) and (**77**) will be reported.



73



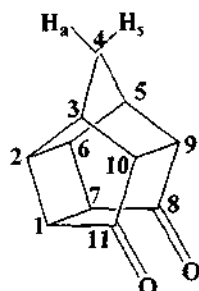
76



77

The first PCU structure to be elucidated was the PCU dione (**20**).

6.1. THE NMR ELUCIDATION OF THE PCU DIONE (**20**) STRUCTURE



20

The pentacycloundecane dione (**20**, PCUD) is a meso compound with a plane of symmetry, which simplifies the NMR spectra, as each atom except C4 is in duplicate. In the ^1H NMR spectrum (spectrum 1) the methylene protons (H_{4a} and H_{4s}) are registered as an AB spin system at 1.89 and 2.03 ppm. A relatively complex pattern between 2.68 and 3.15 ppm, which integrates to eight protons, represents the methine protons. The four broad signals at (2.68, 2.79, 2.91 and 3.15 ppm) are due to the long-range proton-proton interactions in the high field regions.²²³

It was previously observed and reported from the proton NMR of pentacycloundecane derivatives that the geminal coupling constants of the PCU bridgehead methylene protons (H_4) are in the order of 10 Hz.^{224,225,226,227} Therefore it can be concluded that the high field chemical shifts of the doublets at 1.89 ppm (H_{4a}) and 2.03 ppm (H_{4s}) with $J=11.3$ Hz are associated with the methylene protons on C4. It was previously shown that for PCU derivatives the H_{4a} resonates at a higher field than the H_{4s} .^{225,226}

The ^{13}C NMR spectrum (spectrum 2) of the dione exhibits a total of six resonance signals. Since the PCU dione is symmetrical it exhibits one carbonyl resonance at 212.1 ppm, one methylene carbon resonance at 40.5 ppm and four pairs of methine carbon resonances at 38.7, 43.8, 44.6 and 54.7 ppm. The electronegative oxygen atoms present in the molecule help to draw electrons away from the carbonyl carbons making them highly deshielded such that their resonances appear low field region at 212.1 ppm.

It is evident from the HSQC (Hetero Single Quantum Correlation) spectrum (spectrum 5) that H_a (1.89 ppm) and H_s (2.03 ppm) are connected to C4 (40.5 ppm). The most convenient tool to elucidate the structure of the dione is the NOESY spectrum (spectrum 4). From the NOESY spectrum (spectrum 4), long-range connectivities are observed between the doublets H_{4a} and H_{4s} , which interact with the methine carbon resonances H_3/H_5 (2.91 ppm). First it is clear that H_3/H_5 (2.91 ppm) interacts with two other protons (2.68 and 3.15 ppm), which should be H_2/H_6 and/or H_9/H_{10} . Both these sets of protons should interact with H_3/H_5 , possibly with $\text{H}_{4a}/\text{H}_{4s}$ and only H_2/H_6 should interact with one more set of protons, namely H_1/H_7 . Through elimination it is clear that H_2/H_6 should register at 3.15 ppm and H_1/H_7 at 2.79 ppm. H_9/H_{10} is therefore registered at 2.68 ppm.

The positions of H_{4a} and H_{4s} can also be verified from the NOESY spectrum (spectrum 4). H_{4s} (2.03 ppm) interacts with H_9/H_{10} (2.68 ppm) and H_{4a} (1.89 ppm) interacts with H_2/H_6 (3.15 ppm). The rest of the signals can easily be verified utilizing the HSQC (heteronuclear single quantum correlation) (spectrum 5), COSY (proton–proton chemical shift correlation) (spectrum 3), NOESY (nuclear Overhauser effect spectroscopy) (spectrum 4) and HMBC (heteronuclear multiple bond correlation) (spectrum 6) spectra. The NMR data for (20) are tabulated in Table 9 below.

Table 9: NMR data^{a,b} for the PCU dione (20)

Carbon/Proton	¹ H NMR (ppm)	¹³ C NMR (ppm)
1/7	2.79 (m, 1H)	43.8
2/6	3.15 (td, 1H, J=2.9, 6.2 Hz)	38.7
3/5	2.91 (m, 1H)	44.6
4 _a	1.89 (d, J=11.3 Hz)	40.5
4 _s	2.03 (d, J=11.3 Hz)	
8/11	-	212.1
9/10	2.68 (broad s, 1H)	54.7

^a400 MHz for ¹H NMR and 100 MHz ¹³C NMR, Solvent CDCl₃

^bAll NMR data were processed using Mestrec 4.5.91 (NMR data Processing made easy), Copyright 1996-2005, www.mestrec.com

The assignments for the dione (20) from HETCOR, COSY, HMBC and NOESY are presented in Table 10. These assignments correspond well with the NMR elucidation obtained by analogy for (20) through comparison with a related PCU compound (75) by Cadd *et al.*²²²

Table 10: NMR correlations^a for the PCU dione (20)

Proton	COSY correlations	NOESY correlations	HMBC correlations
1/7	H2/H6, H9/H10	H2/H6	C2/C6, C3/C5, C9/C10
2/6	H1/H7, H3/H5	H1/H7, H3/H5	C1/C7, C3/C5, C4
3/5	H2/H6, H9/H10, H4 _{a/s}	H9/H10, H2/H6, H4 _{a/s}	C1/C7, C2/C6, C4
4 _a	H4 _s , H3/H5	H4 _s , H2/H6	C2/C6, C9/C10, C3/C5
4 _s	H4 _a	H4 _a , H9/H10	
8/11	-	-	-
9/10	H1/H7, H3/H5	H3/H5	C1/C7, C3/C5, C4

^a400 MHz for COSY, NOESY, HSQC, HMBC spectra, Solvent CDCl₃

The dione (20) was used as starting material for the syntheses of the four PCU derivatives (25, 73, 76 and 77) and the conversions are shown below.

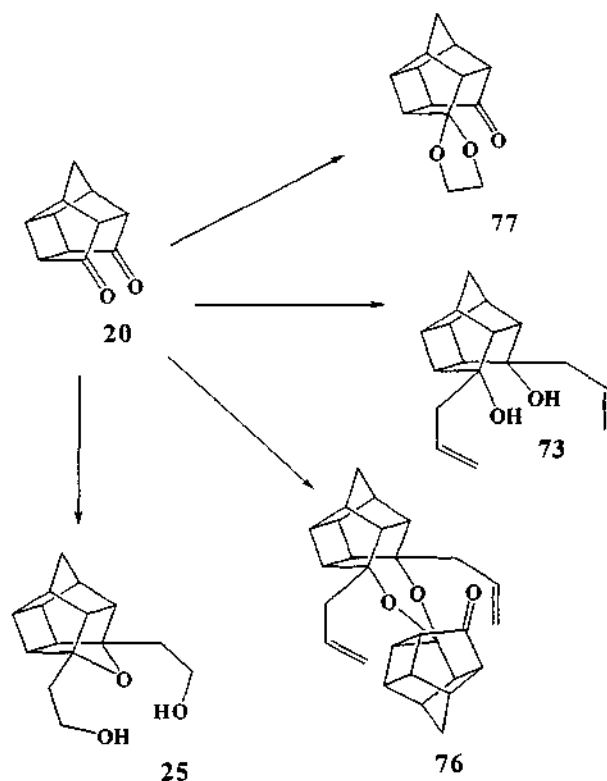
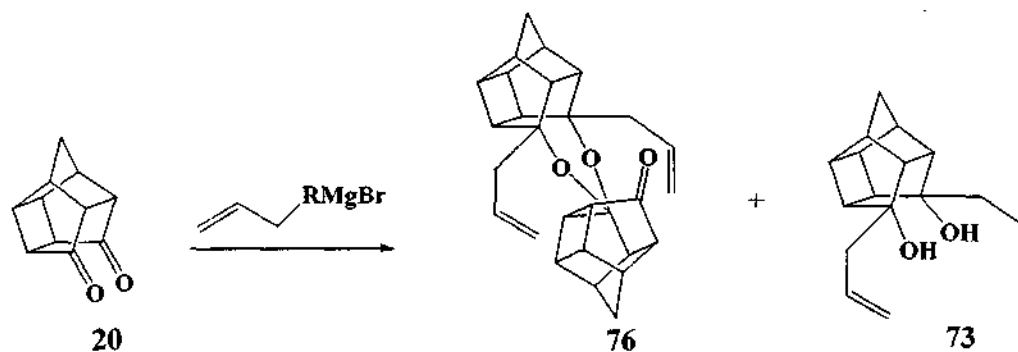


Figure 6: The derivatisation of the PCU dione (20)

The NMR elucidation of the structure of the novel cage dimer (76), the cage endo-endo diol (73) and the cage ketal (77) will be discussed next.

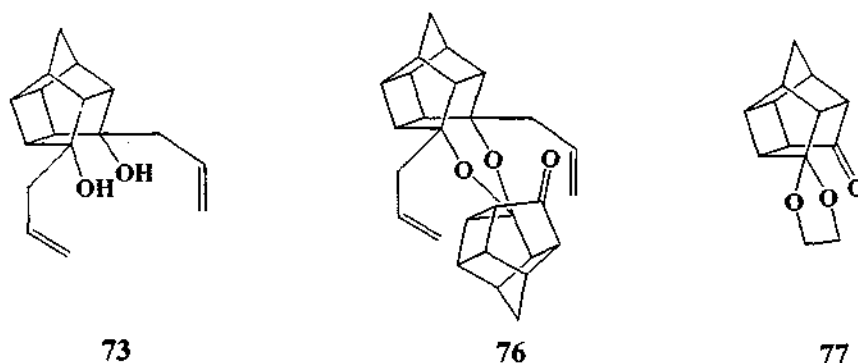
6.2. THE NMR ELUCIDATION OF THE STRUCTURES OF PCU DERIVATIVES

During the multi-step synthesis of the precursors of PCU macrocycles, a novel PCU dimer (76) was serendipitously synthesized and isolated as a by-product (Scheme 10). The NMR elucidation of the structure of (76) was performed. The X-ray data (Chapter 7) of (76) will be reported.



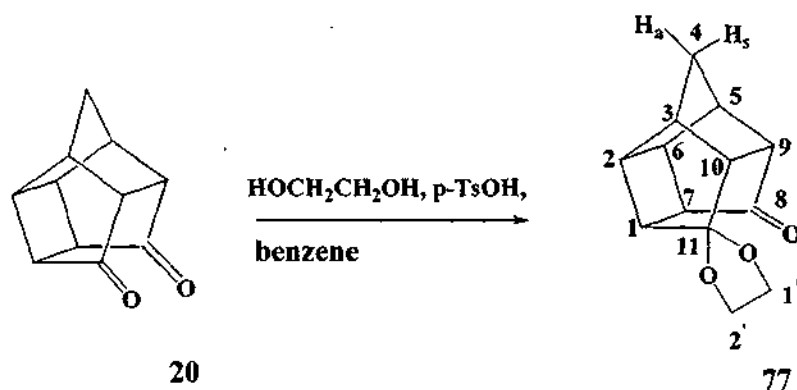
Scheme 10: Synthesis of the novel PCU cage dimer (76)

The complete NMR elucidation of the structure of the novel cage dimer (76) is very difficult due to the overlapping of both proton and carbon peaks in the spectra. It was suggested that the NMR elucidation of the structure of the endo-endo diol (73) as well as the structure of the PCU ketal (77) would be useful in solving the NMR elucidation of structure (76), as the structural similarities present in (76) are obvious.



6.2.1 THE NMR ELUCIDATION OF THE PCU KETAL (77) STRUCTURE

The ketal (77)²²³ was synthesised from the dione (20) and ethylene glycol in the presence of a catalytic amount of *p*-toluenesulphonic acid by refluxing in a Dean-Stark apparatus using an azeotropic solvent such as benzene as shown in Scheme 11.



Scheme 11: Synthesis of the PCU ketal (77)²²³

The usual numbering system for the unsymmetrical cage skeleton is followed. The 400 MHz ¹H NMR spectrum (spectrum 49) of the ketal shows an AB spin system (1.56 and 1.86 ppm) for the methylene protons (H_{4a} and H_{4s}) and four broad signals due to long-range proton-proton interactions in the high field region (2.41-2.48 ppm, 2.53-2.62 ppm, 2.77-2.80 ppm and 2.94 ppm).²²³ The peaks at 1.56 ppm (H_{4a}) and 1.86 ppm (H_{4s}) which integrate to one proton each, are attached to C4 whereas the peaks at 3.83-3.90 ppm integrate to the two protons on C2' and C1'. The complex pattern at 2.41-2.94 ppm integrates to the eight methine protons on the cage (H1, H2, H3, H5, H6, H7, H9 and H10).

The successful synthesis of the ketal (77) is evident from the appearance of one carbonyl, one quaternary carbon, three methylene carbons and eight methine carbon resonance signals present in the ¹³C spectrum (spectrum 50). The ¹³C spectrum (spectrum 50) of the PCU ketal exhibits signals that can be associated with thirteen different carbons atoms since it is an unsymmetrical compound. The carbonyl carbon resonance of C8 is registered at 215.2 ppm. A quaternary carbon resonance is present at 113.9 ppm and is associated with carbon C11 that is attached to two oxygen atoms. The other signals present in the ¹³C spectrum consist of three methylene (C4, C1' and C2') and eight methine carbon signals (C1, C2, C3, C5, C6, C7, C9 and C10).

The C2' and C1' were assigned to low field signals at 64.5 and 65.7 ppm due to their direct attachment to the oxygen atoms, this assignment was confirmed by the correlations in the HSQC experiment (H1' and H2' at 3.83-3.90 ppm correlates with C1' and C2') (spectrum 53). At this stage it is not yet possible to distinguish between these

two methylene groups. C4 was assigned to the signal at 38.7 ppm and this was confirmed by the HSQC correlation with the AB spin system at 1.56 and 1.85 ppm with a coupling constant $J=11.0$ Hz.

The NOESY spectrum (spectrum 52) of the ketal shows correlations between the two methylene groups (3.83 and 3.90 ppm) and two methine protons on the cage (2.62 and 2.48 ppm) respectively. This proves to be a valuable handle when solving the NMR spectrum of the ketal (77). The ketal (77) was optimised using density functional theory (DFT) at the B3LYP level of theory, using a 6-31+G(d) basis set. A high level DFT optimization [B3LYP/6-31+G(d)] of (77) indicates two possible conformations for the ketal group. The ketal group is twisted with either C1' up or C2' down (conformation 1), or C1' down and C2' up (conformation 2). The Cartesian coordinates of the optimised conformations are provided on a CD attached to the back of this thesis (Appendix 2 §2.9). Both conformations were optimised and it turned out that conformation 1 is $0.1 \text{ kcal mol}^{-1}$ lower in energy than conformation 2. Although this energy difference is small, a larger fraction of conformation 1 should exist in solution. Closer inspection of the DFT optimised structure of conformation 1 indicates that proton H2' (3.83 ppm) is in close proximity to H1 (2.89 Å) and H1' (3.90 ppm) to H10 (3.16 Å). The strongest NOESY interaction (largest spot at 2.62 ppm) should therefore correspond to H1 (2.62 ppm) and the weaker interaction to H10 (2.48 ppm).

Another convenient approach to solving the NMR elucidation of the structure of the ketal (77) is the NOESY correlations between H4_a and H3/H5 as well as H2 (2.94 ppm) and between H4_s and H9/H10 (2.41 and 2.48 ppm) as well as H3/H5. Protons H3/H5 (2.80 and 2.55 ppm) are the common factor and the positions of H2 (2.94 ppm) and H9/H10 (2.41 and 2.48 ppm) are therefore apparent through elimination. At this stage distinction between H3 and H5 as well as between H9 and H10 is still required.

The position of H3 (2.80 ppm) can also be determined from the NOESY interaction with H2 (2.94 ppm) and H10 (2.48 ppm). H9 (2.41 ppm) has a NOESY interaction with H10 (spectrum 52). H5 can then be assigned to (2.55 ppm) through elimination since H-3 (2.80 ppm) is now known. The position of H5 is confirmed through COSY correlation with H9 (2.41 ppm) (spectrum 51). The position of the corresponding carbon signals is obtained from the HSQC spectrum (spectrum 53).

The next convenient tool to be used in the elucidation of the structure of the ketal is the HMBC spectrum (spectra 54 and 55). H2 (2.94 ppm) correlates with C10 (53.0 ppm). Both H3 (2.80 ppm) and H6 (2.77 ppm) correlate with C9 (50.7 ppm). H3 correlates with C1 (42.3 ppm) and C6 (36.3 ppm). H6 (2.77 ppm) correlates with C1 (42.3 ppm). The evading proton H7 (2.53 ppm) is also found through interaction with C9 (50.7 pm).

Table 11: NMR data^{a,b} for the PCU ketal (77)

Carbon/Proton	¹ H NMR (ppm)	¹³ C NMR (ppm)
1	2.62 (m, 1H)	42.3
2	2.94 (td, 1H, J=5.5 Hz, J=6.6 Hz)	41.4
3	2.80 (m, 1H)	45.8
4 _a	1.56 (d, 1H, J=11.0 Hz)	38.7
4 _s	1.85 (d, 1H, J=11.0 Hz)	
5	2.55 (m, 1H)	42.9
6	2.77 (m, 1H)	36.3
7	2.53 (dd, 1H, J=1.1 Hz, J=2.3 Hz)	41.3
8		215.2
9	2.41 (m, 1H)	50.7
10	2.48 (m, 1H)	53.0
11		113.9
1	3.90 (m, 2H)	65.7
2	3.83 (dt, 2H, J=6.1 Hz, J=10.0 Hz)	64.5

^a400 MHz for ¹H NMR and 100 MHz ¹³C NMR, Solvent CDCl₃

^bAll NMR data was processed using Mestrec 4.5.91 (NMR data Processing made easy), Copyright 1996-2005, www.mestrec.com

The COSY (spectrum 51), NOESY (spectrum 52) and HMBC (spectra 54 and 55) correlations for the ketal (77) are tabulated in Table 12.

Table 12: NMR correlations^a for the PCU ketal (77)

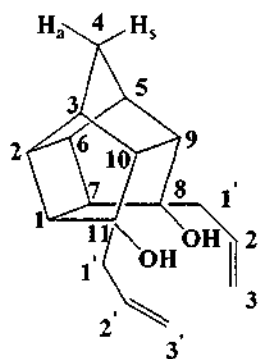
Proton	COSY correlations	NOESY correlations	HMBC correlations
1	H2	H1, H2, H7	C3, C6, C10
2	H1, H3	H1, H3	C4, C9
3	H2, H10	H2, H10	C1, C6
4 _a	H5, H4 _s , H9	H2, H4 _s , H3, H5	
4 _s	H4 _a	H4 _a , H3, H5, H9, H10	
5	H6		C3, C4, C6, C7
6	H5		C1, C2, C3, C4, C6
7		H1	C2, C5, C9
8			-
9	H5	H4 _s , H10	C3, C4, C6, C7
10		H1	C1, C2, C4, C5
11			-
1			C2
2		H1	C1

^a400 MHz for COSY, NOESY, HSQC, HMBC spectra, Solvent CDCl₃

The NMR elucidation of the structure of the endo-endo diol (**73**) is discussed next.

6.2.2 THE NMR ELUCIDATION OF THE PCU ENDO-ENDO DIOL (**73**) STRUCTURE

The synthesis of the endo-endo diol (**73**) was achieved through the Grignard addition of allylbromide to the dione (**20**). The endo-endo diol (**73**) is a meso compound, which makes the elucidation of the NMR spectra less complicated since one set of duplicate resonance signals is observed.



73

The complex pattern of resonances in the ¹H spectrum (spectrum 21) between 2.36 ppm and 2.71 ppm integrates for six protons (H1/H7, H2/H6, H3/H5 and H9/H10). The

integration value of the ^1H spectrum can be used to assign: H4_a (1.07 ppm) and H4_s (1.51 ppm); $\text{H3}'$ (5.07 ppm); $\text{H2}'$ (5.91 ppm) and OH (5.30 ppm exchange with D_2O). Some of the cage methine protons (2.18 ppm) partially overlap with $\text{H-1}'$ (1.97-2.24 ppm). The resonance pattern between 2.18-2.36 ppm integrates to six hydrogens, which belong to the methylene carbon $\text{C1}'$ and C9/C10 , (four of the hydrogens belong to $\text{C1}'$ and the other two hydrogens still need to be assigned to C9/C10 at this stage. The ^1H NMR spectrum of the endo-endo diol shows an AB spin system for the methylene protons H4_a (1.07 ppm) and H4_s (1.51 ppm), which integrate to one proton each.

The ^{13}C spectrum (spectrum 22) consists of nine resonance signals. The endo-endo diol is symmetrical, exhibiting one set of duplicate signals except for the bridgehead methylene. According to the DEPT spectrum (spectrum 31) there are five methine signals (39.9, 42.7, 44.0, 49.1 and 133.7 ppm), three methylene signals (33.8, 43.9 and 117.8 ppm) and one quaternary carbon at 77.2 ppm.

Carbon C4 was assigned 33.8 ppm due to correlations in the HSQC (spectra 27 and 28) with the AB spin system at 1.07 (H4_a) and 1.51 ppm (H4_s) ($J=10.8$ Hz). The same approach of using NOESY correlations to elucidate the structure of the ketal (77) was also used in the elucidation of the structure of the endo-endo diol (73). H4_a (1.51 ppm) shows NOESY correlations (spectra 25 and 26) with H3/H5 and H2/H6 and H4_s (1.07 ppm) shows correlations with H3/H5 and H9/H10 . H3/H5 (2.36 ppm) is the common factor and the positions for H2/H6 (2.45 ppm) and H9/H10 (2.15 ppm) are apparent through elimination. NOESY correlation between OH (5.30 ppm) and H1/H7 (2.44 ppm) as well as H9/H10 (2.18 ppm) confirms these assignments.

Interestingly, $\text{H2}'$ (5.91 ppm) shows NOESY correlation with H9/H10 (strongest at 2.18 ppm), $\text{H1}'$ (1.97-2.24 ppm), H1/H7 (2.44 ppm) and H3/H5 (2.36 ppm). The positions of the carbon signals were obtained from the HSQC spectra (spectra 27 and 28). Note that the $\text{C1}'$ peak overlaps with C3/C5 peak. Assignment of the C4 methylene carbon allowed the $\text{C1}'$ methylene group to be assigned to 43.9 ppm. Carbon C8/11 of the cage was assigned to 77.2 ppm, this was confirmed by the absence of a signal in the HSQC spectrum and the visible correlations in the HMBC spectrum (spectra 29 and 30) with C1/7 (2.44 ppm), C9/10 (2.18 ppm) of the cage and $\text{C1}'$ (43.9 ppm) of the allylic arm. The NMR data of (73) are tabulated in Table 13 below.

Table 13: NMR data^{a,b} for the PCU endo-endo diol (73)

Carbon/Proton	¹ H NMR (ppm)	¹³ C NMR (ppm)
1/7	2.44 (m, 1H)	42.7
2/6	2.52 (dd, 1H, J=2.6 Hz, J=4.6 Hz)	39.9
3/5	2.36 (dd, 1H, J=1.7 Hz, J=3.1 Hz)	44.0
4 _a	1.07 (d, 1H, J=10.8 Hz)	33.8
4 _s	1.51 (d, 1H, J=10.8 Hz)	
8/11		77.2
9/10	2.18 (td, 1H, J=1.3 Hz, J=6.5 Hz)	49.1
1	1.97-2.24 [*]	43.9
2	5.91 (m, 1H)	133.7
3	5.07 (t, 2H, J=13.7 Hz)	117.9

^a400 MHz for ¹H NMR and 100 MHz ¹³C NMR, Solvent CDCl₃

^bAll NMR data was processed using Mestrec 4.5.91 (NMR data Processing made easy), Copyright 1996-2005, www.mestrec.com

^{*} Some of the cage methine protons H9/10 (2.18 ppm) partially overlap with H1' (1.97-2.24 ppm).

The details of all the NMR correlations for (73) are provided in Table 14 below.

Table 14: NMR correlations^a for the PCU endo-endo diol (73)

Proton	COSY correlations	NOESY correlations	HMBC correlations
1/7		H1, H9/H10	C1, C2/C6, C9/C10
2/6		H1, H3/H5, H9/H10	C1/C7, C3/C5, C4, C9/C10
3/5		H4 _{a/s} , H2/H6, H9/H10	C1/C7, C4
4 _a	H4 _s , H3/H5, H9/H10	H4 _s , H2/H6, H3/H5	
4 _s	4 _a , 2/6, 3/5	H4 _a , H3/H5, H9/H10	
8/11			C9/C10, C1/C7, C1
9/10		H1/H7, H2/H6, H3/H5, H4 _{a/s}	C1/C7, C2/C6, C4
1		H1/H7, H2/H6, H3/H5	C8/C11
2	H1, H3, H1/H7, H9/H10	H1, H3, H1/H7, H3/H5, H9/H10	C1, C3, C1/C7, C9/C10
3	H1, H2, H1/H7, H3/H5, H9/H10	H1, H2, H3/H5, H9/H10	C1, C1/C7, C9/C10

^a400 MHz for COSY, NOESY, HSQC, HMBC spectra, Solvent CDCl₃

The NMR elucidation of the structure of the PCU novel dimer (76) was attempted next.

6.2.3 THE NMR ELUCIDATION OF THE PCU NOVEL DIMER (76) STRUCTURE

Conventional mass spectrometric ionisation techniques lead to molecular decomposition of the cage skeleton and produce un-interpretable mass spectra. Molecular ions are seldom observed in electron impact (EI) spectra, however the fast atom bombardment

mass spectrometry (FAB-MS) is a convenient tool for the analysis of cage compounds and derivatives.²²⁸ The appearance of the expected molecular ion peak of m/z 415 $[M+H]^+$ in the mass spectrum (spectrum 47) confirmed the formation of novel compound (76). The presence of one carbonyl absorption band in the IR spectrum (spectrum 48) at 1748 cm^{-1} confirmed the structure of the cage dimer (76).

Taking into consideration the techniques learnt while elucidating the ketal (77) and endo-endo diol (73), the same approach was used when trying to elucidate the PCU cage dimer (76). The PCU cage dimer (76) is not numbered the conventional way but according to the numbering in the X-ray data (see Chapter 7).

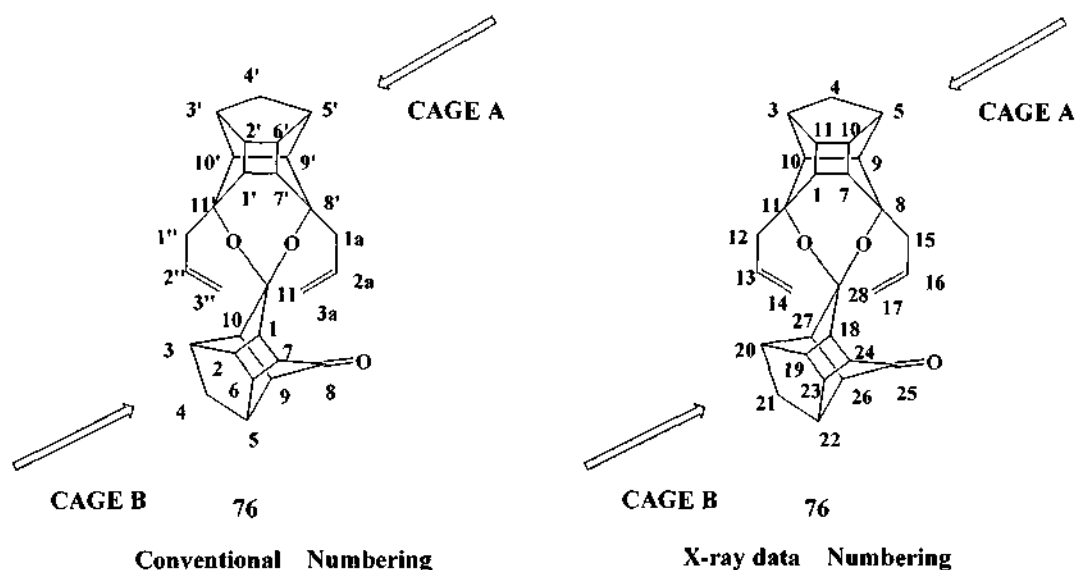


Figure 7: The conventional numbering and X-ray data numbering of the novel PCU cage dimer (76)

Confirmatory evidence for the correctness of the allocated structure of the PCU cage dimer (76) was obtained from the ^1H NMR and ^{13}C NMR study and MS spectrum. The ^1H NMR spectrum shows two cage AB spin systems, which appear at high field region and are associated with the two different bridgehead methylene groups of (76). There are three quaternary carbons (C8, C11 and C28), one carbonyl carbon (C25), six methylene carbons and eighteen methine carbons present in this molecule. This data is supportive of the structure of the novel cage dimer (76).

Since there is major overlap between peaks in the spectra, the structural elucidation is complex and certain assumptions have to be made when assigning the exact positions on the novel PCU cage dimer (76) by using the same approach as when elucidating the structure of the endo-endo diol (73) and ketal (77). In order to elucidate this structure systematically the molecule was divided into two parts namely cage A and cage B. Cage A consists of the PCU moiety with the two allylic arms (“endo-endo diol part”) while Cage B consists of the cage with the carbonyl group and ketal linkage (“ketal part”).

There are five methylene carbon signals present in the DEPT spectrum: (35.1, 38.0, 42.3, 43.2 and 116.9 ppm, which needs to be assigned to the six methylene carbons of which C14/C17 are overlapping. The bridgehead methylene carbons C4 and C21 need to be assigned to either cage A or cage B. From the ¹H spectrum of the PCU ketal (77) and the PCU endo-endo diol (73), it can be observed that the protons of the methylene group appear further downfield for the PCU ketal (77) when compared with PCU endo-endo diol (73). Furthermore the coupling constants for the PCU ketal (77) (J=11.0 Hz) are larger than that observed for the PCU endo-endo diol (73) (J=10.8 Hz). Therefore it can be assumed that the protons at 1.15 and 1.57 ppm (J=10.7 Hz – H4 a/s) belong to C4 (35.1 ppm) on cage A (the “endo-endo diol part”) and those at 1.47 and 1.77 ppm (J=10.9 Hz, H21a/s) belong to C21 (38.0 ppm) on cage B (the “ketal part”).

The peak at 214.0 ppm in the ¹³C NMR is assigned to the carbonyl at carbon C25 (Cage B). The next assumption to be made from the structural elucidation of the PCU endo-endo diol (73) and PCU ketal (77) is the assignment of the quaternary carbons. The quaternary carbon at 105.0 ppm was assigned to carbon C28 of cage B, while signals 84.0 and 84.3 ppm still need to be assigned to either carbon C8 or carbon C11 of cage A.

The structure of cage A (“endo-endo diol part”) will be elucidated first. The positions of C12/C15 (42.3 and 43.2 ppm), C13/C16 (134.5 and 134.1 ppm) and C14/C17 (116.9 ppm) can be determined from the DEPT spectrum. The exact positions of these carbons still need to be determined.

In order to determine which side of cage A is left and which side is right, the chemical shifts of H12/H15 were used. For the endo-endo diol (73), the corresponding protons

(H1') experience a chemical non-equivalence shift of about 1 ppm. For the dimer (76), the one set of protons experience a shift of about 1 ppm (1.88 ppm and 2.04 ppm, H12) while the other set of protons is split by about 2.4 ppm (1.82 ppm and 2.16 ppm, H15). It seems obvious that the set of protons closer to O25 will experience a larger through space shielding and deshielding effect, with result that H15 will experience much larger chemical shifts, when compared with H12.

The positions of C8 (84.3 ppm) and C11 (84.0 ppm) can then be assigned using HMBC correlations with H12 and H15 respectively. This enables us to assign H14 (4.85 ppm), H17 (5.05 ppm), H13 (5.55 ppm) and H16 (5.75 ppm) using the HSQC and NOESY spectra. Knowing the position of H13 and H16 enables us to distinguish between C13 (134.5 ppm) and C16 (134.1 ppm) using the HSQC spectrum.

The HMBC spectrum can also be used to determine the position of C9/C10. For the ketal (77), the proton corresponding to H4 of the dimer showed HMBC correlation with carbons corresponding to C9/C10 (51.1 ppm and 49.5 ppm) of the dimer. At this stage it is not yet possible to distinguish between the two carbons. The HMBC spectrum can also be used for this distinction as the interaction of C9 (49.5 ppm) and C10 (51.1 ppm) with H15 and H12 is observed. The corresponding proton signals, H9 (2.31 ppm) and H10 (2.21 ppm) were assigned using the HSQC spectrum. Lastly the positions of C1 (40.4 ppm) and C7 (41.5 ppm) are also determined through HMBC interaction with H12 and H15 respectively. The corresponding protons are H1 (2.53 ppm) and H7 (2.33 ppm).

NOESY interactions between H4a and H2/H6 (2.52 ppm) and H3/H5 (2.27 ppm) are observed. The positions of H3/H5 can be confirmed using the COSY spectrum. H4a/s interacts with H3/H5, which overlap at 2.27 ppm. The positions of H3/H5 and H9/H10 are also confirmed through NOESY interaction with H4s.

Most of the positions of the corresponding carbon and proton signals can be obtained from the HSQC spectrum. The positions of C2 and C6 (39.2 and 39.6 ppm) are difficult to distinguish from the overlapping proton signals. Possible discrimination can be made by a rather uncertain HMBC interaction between H9 and C6 (39.2 ppm). The position of C2 (39.6 ppm) is then assigned through elimination.

The carbon signals for C3 and C5 are overlapping with C12 and are difficult to distinguish. The three carbons peaks register at 42.2, 42.28 and 42.34 ppm. C15 also registers at ~42 ppm. Note that there is an overlap of five carbon signals at ~42 ppm – see the HSQC spectrum.

All the protons and carbons have been assigned in Cage A and the structure of Cage B can now be elucidated. It was observed from the structural elucidation of the ketal (77) and the diol (73) that C10 of (77) is the most downfield methine carbon. Therefore the carbon in the most downfield position at 56.8 ppm of the dimer (76) is assigned to the corresponding carbon C27 (C10 of the ketal (77) corresponds to C27 of the dimer (76). The proton H27 (2.54 ppm) is determined from the HSQC spectrum and is later verified using the COSY spectrum (interaction with H26). The position of H21a (1.47 ppm) is known by analogue of the corresponding ketal (77) proton and shows HMBC correlations with some carbons in the “ketal part” namely C27 (56.8 ppm) and C26 (50.5 ppm). This allows for assignment of proton H26 to 2.34 ppm using the HSQC spectrum. The positions of H26 and H27 should be confirmed later.

Another important observation made from the NMR data of (77), is that the most downfield proton in the PCU ketal (77) was H2 (2.94 ppm). The position of this proton corresponds to H19 of the dimer (76). There are two downfield proton signals at 2.81 and 2.83 ppm for the dimer (76). One proton signal (H18, 2.81 ppm) shows weak HMBC correlations with C28 (105.0 ppm). The second downfield proton signal at 2.81 ppm also belongs to cage B, but it is still unclear which proton shifted so far downfield.

Based on the NOESY data of the ketal (77), interaction of H21a with H19 (2.83 ppm), H20 (2.72 ppm) and H22 (2.51 ppm) is determined. It appears as if H21a is also interacting with a proton which is overlapping with H20. The positions of H20 and H22 are confirmed using the COSY spectrum. H21a/s interacts with H20 and H22. The position of H20 is also confirmed through COSY correlations with H19. The distinction between H20 and H22 also coincide with the assumption that H20 will be shifted more downfield compared with H22 as observed for the structural elucidation of (77). The position of H20 is confirmed via NOESY interaction with H19. A clear NOESY interaction between H20 and H27 is also observed.

One particular NOESY interaction is posing lots of difficulties and confusion with the elucidation of the NMR data. The interaction is observed between a proton at 2.81 ppm and a proton at 2.32 ppm (H7). The only conclusion is that this is due to a NOESY interaction between cage A and cage B; say H7 with H18 or H9 with H27. At this point is it not possible to confirm that.

The position of C23 is obtained through HMBC interaction of H21a/s with C23 (35.8 ppm). H23 is registered at 2.68 ppm (HSQC). H23 also exhibits weak HMBC interaction with C19 (overlap at 42 ppm). H23 shows COSY interaction with H19, H22 and H24 (2.4 ppm). H23 shows NOESY interaction with H19, H22 and H24.

Knowing the position of H23 and H24 is helpful with the assignment of H18. H24 should have two COSY interactions, one with H23 and one with H18 (2.81 ppm). The position of H18 is verified using NOESY interaction with H24. The position of H26 should still be confirmed. There appears to be a COSY interaction between H26 and H27, although there are major overlaps at 2.54 ppm.

The only remaining mystery is the NOESY interaction between a proton at 2.81 ppm and a proton at 2.32 ppm, mentioned above. According to the X-ray structure close interactions between H1 and H18 (2.23Å) and H7 and H18 (2.4Å) are present. Both these NOESY interactions are observed in the NOESY spectrum and the specific one is between H7 and H18. Note that distance between H18 and H19 is about 2.5Å and one observes a NOESY interaction between them.

Again the positions of some of the carbon signals (C19, C22, and C24) are not clear from the HSQC spectrum. C19 is overlapping at about 42 ppm with several other carbons. C22 appears to be at 42.6 ppm and C24 is overlapping with C7 at 41.5 ppm.

Some additional information should be pointed out. There is a NOESY interaction between H13 (5.55 ppm) and H20 (2.72 ppm). There are five proton signals overlapping at 2.49-2.58 ppm: H1, H2/H6, H22 and H27. Five corresponding carbon peaks are visible in the HSQC spectrum.

The NMR data for (76) are tabulated in Table 15 below.

Table 15: NMR data^{a,b} for the PCU dimer (76)

Carbon/Proton	¹ H (ppm)	¹³ C (ppm)
1	2.53	40.4
2	2.52	39.6
3	2.27	42.3
4	a= 1.15, (d, J=10.7 Hz, 1H) s= 1.57, (d, J=10.7 Hz, 1H)	35.1
5	2.27	42.3
6	2.52	39.2
7	2.33	41.5
8		84.3
9	2.31	49.5
10	2.21	51.1
11	2.56	84.0
12	α= 2.04 β= 1.88	43.2
13	5.55	134.5
14	4.85	116.9
15	α= 2.16, (dd, J=7.4, 14.0 Hz, 1H) β= 1.82, (dd, J=7.3, 14.0 Hz, 1H)	42.2
16	5.75	134.1
17	5.05	116.9
18	2.81	44.1
19	2.83	42.0
20	2.72	38.0
21	a= 1.47, (d, J=10.9 Hz, 1H) s= 1.77, (d, J=10.9 Hz, 1H)	214.0
22	2.51	42.6
23	2.68	35.8
24	2.4	214.0
25		50.5
26	2.34	56.8
27	2.54	105.0
28		

^a 400 MHz for ¹H NMR and 100 MHz ¹³C NMR, Solvent CDCl₃

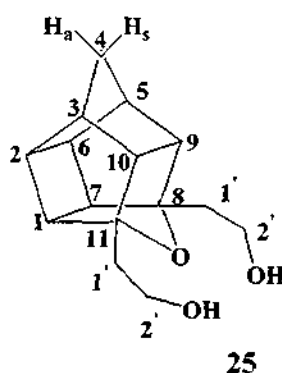
^b All NMR data was processed using Mestrec 4.5.91 (NMR data Processing made easy), Copyright 1996-2005, www.mestrec.com

^c 400 MHz for COSY, NOESY, HSQC, HMBC spectra, Solvent CDCl₃

The fifth and last PCU derivative to be elucidated is the PCU diol.

6.2.4 THE NMR ELUCIDATION OF THE PCU DIOL (25) STRUCTURE

The endo-endo diol (73) is an intermediate for the diol (25), which is used in the synthesis of various crown ethers and ligands. The same methodology that was used to elucidate the structures of the other PCU derivatives was used to solve the NMR elucidation of the structure of the diol (25). The PCU diol (25) has a plane of symmetry running through the molecule and hence one set of duplicate resonance signals are observed except for the methylene bridgehead group.



The typical AB spin system in the ¹H NMR spectrum (spectrum 8) is due to the methylene protons on C4. The AB spin system at 1.52 ppm (H_{4a}) and 1.88 ppm (H_{4s}) integrates for one proton each. The complex pattern between 2.40 ppm and 2.61 ppm integrated to eight cage methine protons (H1/H7, H2/H6, H3/H5 and H9/H10). The methylene groups on the arm of the diol present at 3.75 ppm and 2.00 ppm integrate to two protons each (H1' and H2').

The ¹³C NMR spectrum (spectrum 9) enables a quick overview of the PCU diol (25) with the presence of one quaternary carbon C8/C11 at 96.4 ppm, three methylene carbons at 60.0, 43.4 and 34.2 ppm and four methine carbons at 58.1, 47.6, 44.0 and 41.3 ppm. The methylene carbons on the arm of the diol were assigned first. C1' was assigned at 34.2 ppm and C2' was assigned to the low field signal 60.0 ppm due to its attachment to the electronegative hydroxyl groups. The assignment of C1' and C2' methylene carbons enabled the assignment of the bridgehead carbon C4. The bridgehead C4 carbon was assigned to 43.4 ppm due to correlations in the HSQC with the AB spin system of which the coupling constants were J= 10.5 Hz.

The HMBC spectrum (spectrum 13) is useful to determine the interaction between H1' and C1/C7 as well as with C9/C10. Distinction between C1/C7 and C9/C10 is possible through HMBC correlation between H4_a and C9/C10, which is not possible with C1/C7.

Through elimination of NOESY interactions between H4_a and H4_s with H3/H5, H2/H6 and H9/H10 the positions of these proton signals are assigned (spectrum 11). H4_a should exhibit NOESY correlations with C3/C5 and C2/C6 and H4_s should exhibit NOESY correlations with C3/C5 and C9/C10. Once again C3/C5 is common to both. Therefore C3/C5 was assigned to 41.3 ppm, which is confirmed by COSY correlations with H4 (spectrum 10). However C2/C6 and C9/C10 still needed to be distinguished from each other. The C9/C10 was assigned the downfield signals 58.1 ppm due to its direct attachment to the deshielded C8/C11 carbons, which is part of the ether linkage of the cage. Furthermore NOESY correlations (spectrum 11) of H9/H10 with H2', H4, and H1' confirmed the assignment. This allowed C2/C6 to be assigned to 44.0 ppm due to HMBC correlations of H2/H6 with C4, C3/C5 and C9/C10. C1/C7 was assigned through elimination to 47.6 ppm, which was confirmed by HMBC correlations with C9/C10, C4 and C1'. The quaternary carbons of the cage C8/C11 were assigned to 96.4 ppm due to their absence in the HSQC spectrum (spectrum 12). The HMBC correlation of C8/C11 with H1' and H2' of the allylic arm was also confirmed (spectrum 13). The HMBC correlations of H1/H7 with C9/C10, C4 and C1' confirmed the assignment at 2.58 ppm. The NMR data for (25) are tabulated in Table 17 below.

Table 16: NMR data^{a,b} for the PCU diol (25)

Carbon/Proton	¹ H NMR (ppm)	¹³ C NMR (ppm)
1/7	2.58 (m, 1H)	47.6
2/6	2.57 (m, 1H)	41.3
3/5	2.40 (br s, 1H)	44.1
4 _a	1.52 (d, J=10.5 Hz)	43.5
4 _s	1.88 (d, 1H, J=10.5 Hz)	
8/11		96.4
9/10	2.61 (dd, 1H, J=4.8 Hz, J=6.8 Hz)	58.1
1	2.00 (m, 2H)	34.2
2	3.75 (m, 2H)	60.0

^a400 MHz for ¹H NMR and 100 MHz ¹³C NMR, Solvent CDCl₃

^bAll NMR data was processed using Mestrec 4.5.91 (NMR data Processing made easy), Copyright 1996-2005, www.mestrec.com

Two-dimensional NMR techniques were essential for the full elucidation of the structure of the PCU diol (**25**) and the assignments are tabulated in Table 17 below.

Table 17: NMR correlations^a for the PCU diol (25**)**

Proton	COSY correlations	NOESY correlations	HMBC correlations
1/7		H2, H4, H1	C9/C10, C4, C1
2/6		H1	C3/C5, C9/C10, C4
3/5	H4 _s	H1/H7, H9/H10, H2/H6, H4	C1/C7, C9/C10, C4
4 _a 4 _s	H4 _s , H3/H5 H4 _a	H2/H6, H3/H5 H9/H10, H3/H5	
8/11			C1, C2
9/10		H2, H4, H1	C1/C7, C4, C1
1	H2	H1/H7, H9/H10, H2/H6, H3/H5	C1/C7, C9/C10, C4
2	H1	H1/H7, H9/H10	C1

^a400 MHz for COSY, NOESY, HSQC, HMBC spectra, Solvent CDCl₃

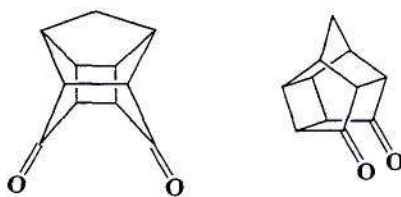
CHAPTER SEVEN

THE X-RAY STRUCTURES OF THE PENTACYCLOUNDECANE DIONE AND DERIVATIVES

The pentacycloundecane dione (PCUD, **20**) was first synthesised by Cookson *et al.*¹²¹ in 1964, but evaded scrutiny by X-ray crystallographic analysis. This is possibly as a result of the difficulty to obtain suitable crystals for X-ray analysis, as the PCUD (**20**) resembles almost a perfect sphere, with the result that the level of disorder in most crystals would be too large for effective X-ray analysis. The structure of the PCUD (**20**) will be discussed in further detail in this chapter and the X-ray crystallographic data of the PCUD (**20**) are reported in Appendix 3. The crystal structure of the pentacycloundecane diol (**25**), novel pentacycloundecane cage dimer (**76**), and the pentacycloundecane ketal (**77**) will also be briefly discussed in this chapter and X-ray crystallographic data will be reported in Appendix 3.

7.1 THE STRUCTURE OF THE PENTACYCLOUNDECANE DIONE (PCUD) (**20**)

Strained polycyclic “cage compounds” such as (PCUD, **20**) have special structural and chemical features that render them unique among complex organic compounds, especially the deformation of the ideal carbon-carbon-carbon bond angle, the inherent ring strain, their unique, distinctive structure and their synthetic challenge.²²⁹



20

Cage compounds have a rigid carbocyclic ring structure which results in a relatively fixed molecular geometry. The intramolecular photochemical [$\pi^2 + \pi^2$] cycloaddition reaction has been used as a powerful and convenient tool for the synthesis of highly



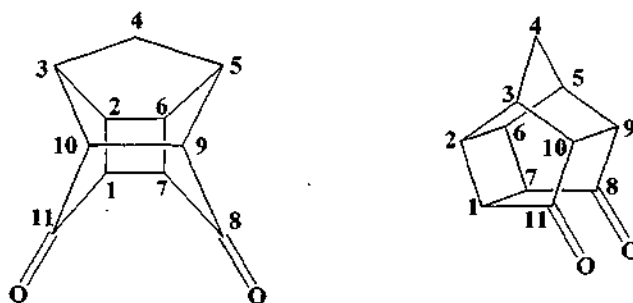
strained polycyclic ring systems.²²⁹ The considerable amount of strain energy in most saturated cage molecules is evident by the fact that they:¹¹⁸

- Contain unusually long carbon-carbon σ -bonds.
- Contain unusual C-C-C bond angles that deviate significantly from 109.5° .

Since their structures are highly compact, steric constraints are imposed upon the carbon-carbon bond lengths as well as bond angles hence causing great deviations from the values that are normally associated with a sp^3 -hybridized carbon in a strain-free system. Together with structural compactness and steric strain, cage systems also possess properties such as:¹¹⁸

- Increased positive heat of formation when compared with non-strained systems.
- Increased negative heat of combustion.
- Increased densities relative to corresponding unstrained systems.

The PCUD (20) has a rigid and strained open-ended structure composed of four fused five-membered rings in envelope conformations and a planar four membered ring. The molecule contains two exocyclic ketone moieties.²³⁰ The lengthening of the C1-C7 and the C9-C10 bonds accommodates much of the strain inherent in this ring system.²³⁰ The corresponding carbon-carbon bonds in a closely related polycyclic system studied by Mehta and co-workers²³¹ have an average length of 1.590\AA .



20

The PCUD (**20**) has a mirror plane passing through and bisecting the C9–C10, C2–C6 and C1–C7 bonds.¹¹⁵ The two five-membered rings that contain C4 form almost an ideal envelope conformation.¹¹⁵ In 1974 Sasaki and co-workers²³² studied Dreiding stereo models to examine the molecular geometry of the PCUD (**20**). It was reported that there was a presence of increased strain in the molecular geometry. The C-C bonds adjacent to the C-O groups i.e. (C1-C11), (C10-C11), (C7-C8) and (C9-C8) were extremely stretched as shown in Figure 8. The stereo models were further inspected to analyse the transannular distances in the PCUD (**20**). An interesting observation was made, namely that the carbonyl groups in the PCUD (**20**) are not parallel. The estimated transannular distance between the carbonyl carbon atoms, at positions 8 and 11, was estimated by Dreiding stereo models to be 2.44 Å.²³²

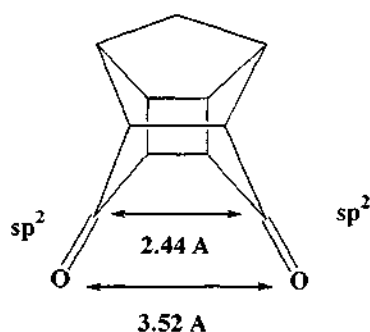
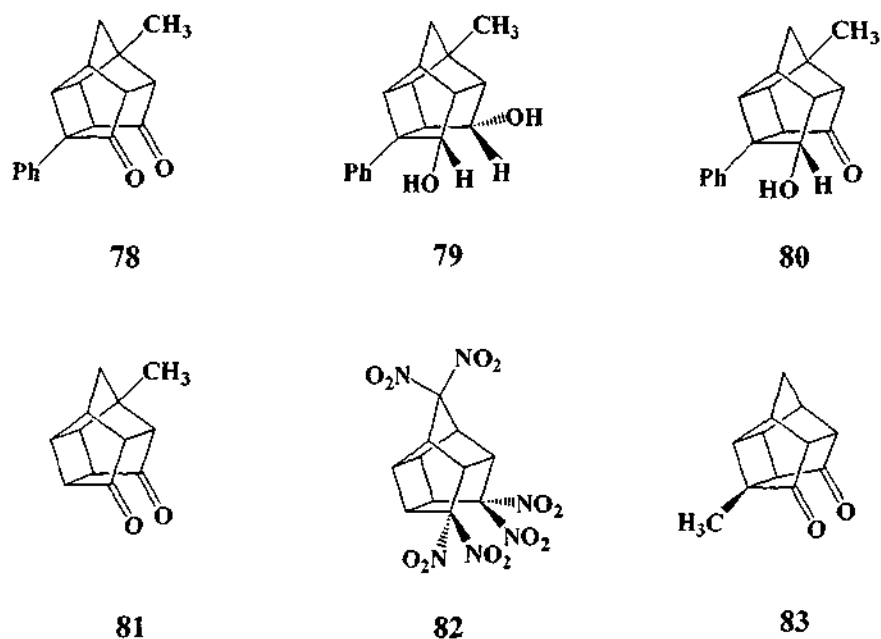


Figure 8: The interatomic distances of selected carbon and oxygen atoms in the PCU dione (20**)**

The 8,11-ketone groups in the PCUD (**20**) can be transformed into a variety of substituted exocyclic moieties. The PCUD (**20**) has been used as a convenient starting material for the synthesis of several additional PCU derivatives.^{233,234} Although several results of single crystal X-ray structural analyses of some PCU derivatives (78,²³⁵ 79,²³⁵ 80,²³⁵ 81,²³⁶ 82,¹¹¹ 83¹²²) have been published, the X-ray structure of the title compound, the PCUD (**20**), has not been reported until recently.²³⁷



It is clear from the structures above that substituents on the cage skeleton disturb the almost perfect sphere that the unsubstituted PCUD (20) represents. Figure 9 illustrates the space filling models of the unsubstituted PCUD (20) and its near-symmetrical skeleton.

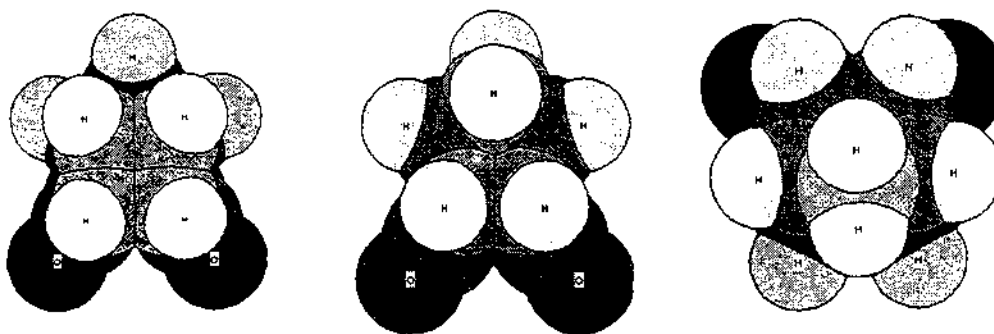


Figure 9: Space filling models of the PCU dione (20) showing its near-spherical skeleton

The PCUD (20) and its derivatives (78,²³⁵ 79,²³⁵ 80,²³⁵ 81,²³⁶ 82,¹¹¹ 83¹²²) are known to react with nucleophiles, thereby affording products that give rise to transannular reactions across the 8,11-position¹¹⁸ and further insight is needed, regarding the structural features of the PCUD derivatives that account for the ease with which they

regarding the structural features of the PCUD derivatives that account for the ease with which they undergo transannular reactions. The following significant geometric factors should be studied further:¹¹⁸

- The through-space interatomic distance that separates C-8 and C-11 in these PCUD derivatives.
- The relative orientation of the 8,11 carbonyl groups in the derivatives of the PCUD (20).

As mentioned earlier a number of X-ray crystal studies have been carried out on PCU derivatives and some of the bond lengths are reported below (see Figure 10).

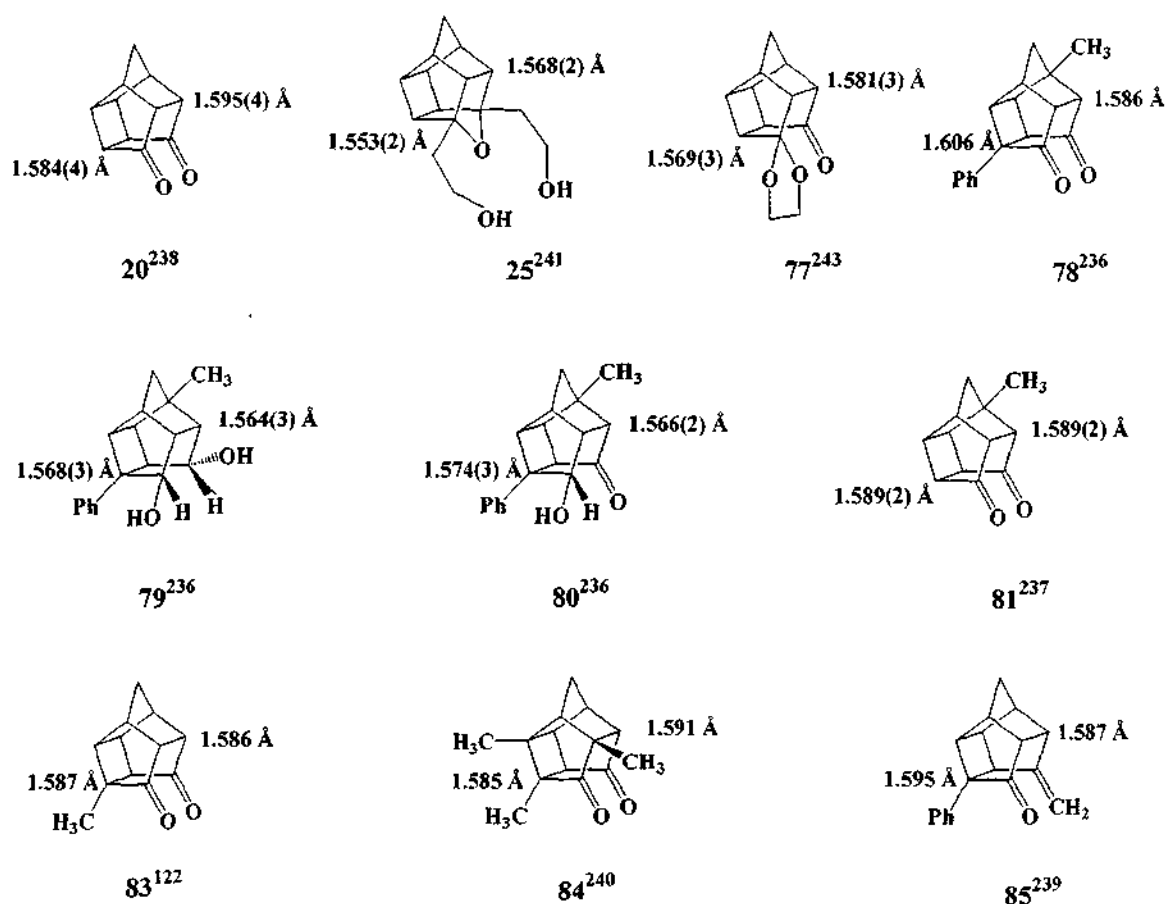


Figure 10: C1-C7 and C9-C10 bond lengths of PCU derivatives

The C1-C7 and C9-C10 bond lengths for substituted PCU derivatives (79) and (80) are 1.568(3) Å and 1.564(3) Å, and 1.574(3) Å and 1.566(2) Å respectively, which is not indicative of any significant additional strain.²³⁵ It was reported²³⁸ that substituting the carbonyl oxygen atoms of the dione with methylene groups leads to a small change in the overall structural framework. The C7-C8 and C1-C11 and the C8-C9 and C10-C11 bond distances decrease by 0.02 Å when compared with that of the PCUD (20).²³⁸ Watson *et al.*²³⁵ reported the C1-C7 bond length in the PCU derivative (78) to be 1.606 Å and the C9-C10 bond length to be 1.586 Å, which is unusually longer than that found in substituted PCU derivatives (see Figure 10). The distance between the oxygens in the substituted dione (84) was reported to be 3.84 Å.²³⁹ Varying substitution patterns at the highly strained ring junctions make comparisons difficult in some cases.

The crystals of the PCU compounds (20), (25), (76) and (77) were obtained by the slow evaporation of solvent over several days at room temperature. The crystallographic details for these compounds (20), (25), (76) and (77) are given in Appendix 3 and in the compact disc attached to this thesis. The cage geometry of the PCU derivatives obtained is generally consistent with observations made in Figure 10, such as the bond length of the C1-C7 bond and the bond length of the C9-C10 bond in particular. The carbon-carbon bond lengths of normal sp³ carbons are in the order of ~1.54Å.

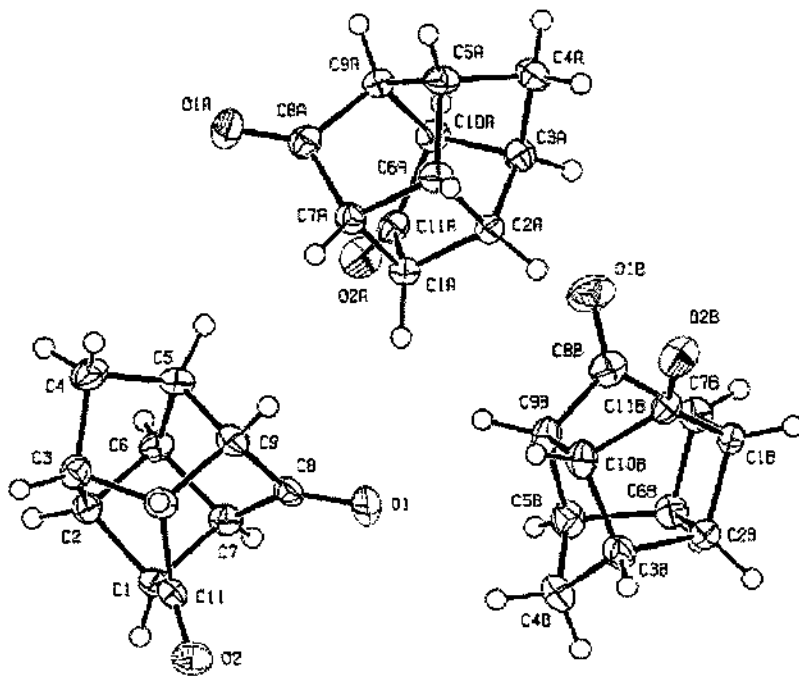
7.2 THE X-RAY STRUCTURE OF THE PCU DIONE (20)

A single crystal of compound (20) was subjected to X-ray diffraction analysis in 2003. The bond lengths differed from one dione in the unit cell to the next. Initially it was thought that the space group (P3₁ or R3) was incorrect and Professor Demi Levendis from the University of the Witwatersrand was consulted. After studying the X-ray data, he discovered what the problem was. The automatic system, used by the X-ray operator, assigned the slightly different values. For dimensions *a* and *b* of the unit cell (*a* = 18.0810, *b* = 18.1180 and *c* = 6.4370). For the space group P3₁ which is a trigonal cell, the dimensions of *a* = *b*. This must be set manually when the data are collected. When a new sample was sent to the University of Witwatersrand in 2005, the crystal structure was correctly solved and at the time the X-ray structure of the PCUD (20) appeared in literature.²³⁷ Nevertheless the crystal structure of (20) is reported *vide*

infra. (See Appendix 3 for X-ray crystallography data). The numbering used in the discussion below is according to Figure 11 below.

Linden et al reported ²³⁷ that the two bonds across from the ketone moieties in the PCUD (**20**) are elongated to 1.584 (4) Å (C1-C7 bond length) and 1.595 (4) Å (C9-C10 bond length). This is in agreement with the bond lengths 1.587 (3) Å (C1-C7 bond length) and 1.595 (3) Å (C9-C10 bond length) obtained for the PCU dione (**20**) that was synthesized at the University of KwaZulu-Natal.

The C9-C10 bond in the PCU dione (**20**), which lies across from the cyclobutane ring and is parallel to and immediately adjacent to the C8-C11 axis, is elongated (1.59 Å). The long bond length is probably a consequence of the stretching strain introduced by the open mouth of the cage, which is formed by the adjacent atoms at C8 and C11. The C1-C7 bond, which is also immediately parallel to the C8-C11 axis, is elongated as well 1.587 (3) Å.



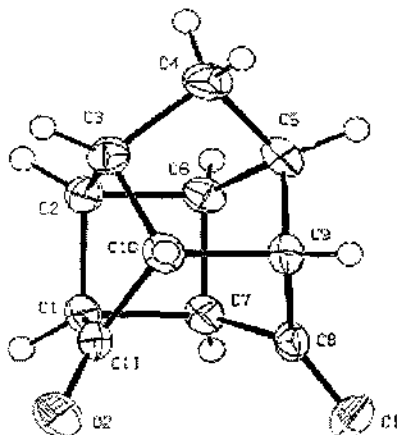


Figure 11: ORTEP diagrams of the PCU dione (20) drawn at the 50 % probability level

The PCU diol (25) is the next crystal structure to be discussed. (See Appendix 3 for X-ray crystallography data). The numbering used in the discussion below is according to Figure 12.

7.3 THE X-RAY STRUCTURE OF THE PCU DIOL (25)²⁴⁰

The PCU diol has been used in the synthesis of various macrocycles as discussed in Chapter 3. As mentioned earlier certain bonds in PCU cage derivatives tend to be longer or shorter than the value of 1.54 Å, which is expected for a C-C bond. The C1-C7 bond length is 1.553(2) Å and the C9-C10 bond length 1.568(2) Å for the PCU diol. It can be seen that they are shorter than those of the dione (20) which is 1.587(3) for the C1-C7 bond length and 1.595(3) Å for the C9-C10 bond length. The C9-C10 bond is significantly shorter, this can be attributed to the lessened stretching strain since there is an oxo bridge linking C8 and C11.

The bonds involving the C4 atom are shorter than normal, C4-C3 [1.532(2) Å] and C4-C5 [1.531(2) Å]. The bonds, which form part of the cyclobutyl group, are also long with values of C2-C6 [1.567(2) Å] and C1-C7 [1.553(2)] respectively. The bonds involving atoms C4, C12 and C14 are shorter than expected: C4-C5 [1.531(2) Å], C4-C3 [1.532(2) Å], C11-C13 [1.5090(19) Å, C8-C12 [1.5104(19) Å], C15-C13 [1.513(2) Å] and C12-C14 [1.519(2) Å]. The ethyl alcohol chains are in the energetically favourable all-trans conformation with atoms O3, C15, C14, C8, O1, C11, C12 and C13

co-planar. Both the alcohol functional groups on the diol participate in hydrogen bonding, each alcohol group acting as both hydrogen-bond donor and acceptor. The oxo atom does not interact with any of the hydrogen-bond donors. An interesting observation is that the C12-C14 [1.519(2) Å] and C13-C15 [1.513(2) Å] bonds are also short, despite not forming part of the cage.

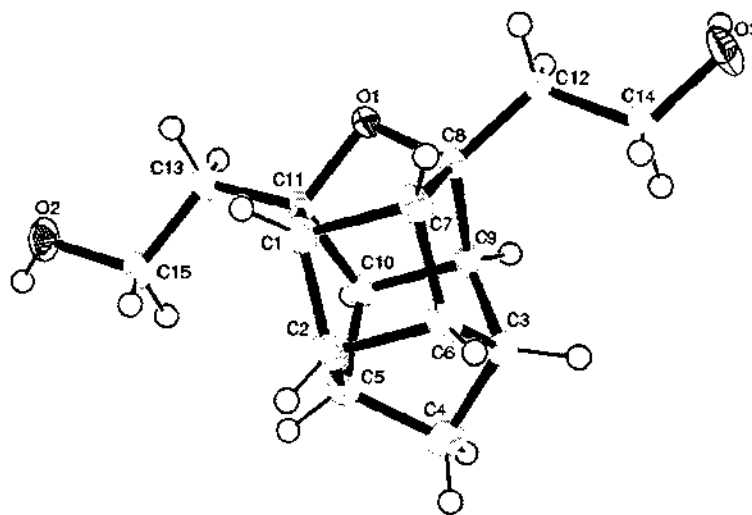


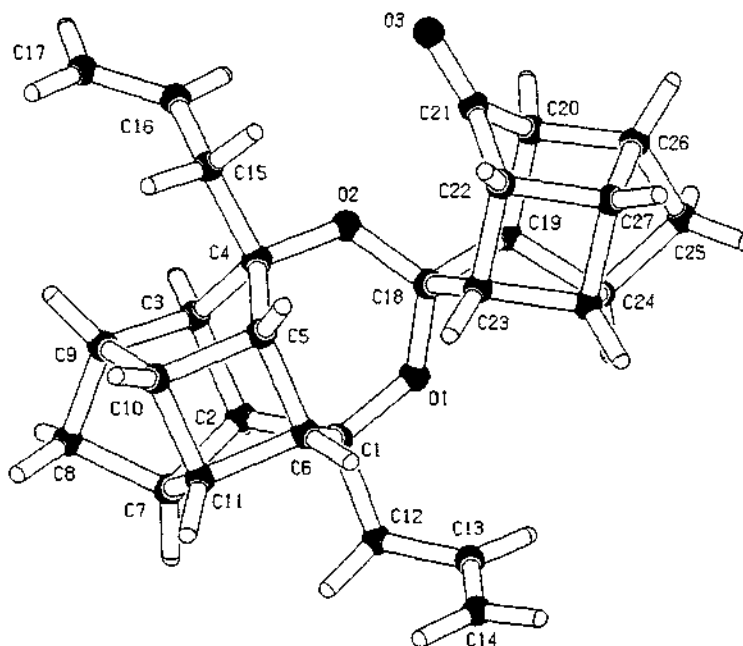
Figure 12: ORTEP diagram of the PCU diol (25) drawn at the 50 % probability level

The next crystal structure to be discussed is the novel PCU dimer (76) (see Appendix 3 for X-ray crystallography data). The numbering used is according to Figure 13.

7.4 THE X-RAY STRUCTURE OF THE PCU NOVEL DIMER (76)²⁴¹

The dimer is chiral and forms a racemate. The asymmetric unit comprises one molecule with both enantiomers in the unit cell. Since there is no such similar structure to that of the novel compound (76) in the literature, the structure will be discussed by looking at the two cage moieties independently and comparing them with reported cage derivatives from literature, which are in Figure 10. In this compound (76) the two PCU cage derivatives are connected via a double ether bridge. If the compound (76) has to be

divided into two parts, cage A has two allylic arms (similar to the endo-endo diol) while cage B has a carbonyl group (similar to the ketal).



In cage A the C5-C6 bond length is 1.557(17) Å and the C2-C3 bond length is 1.586(17) Å and in the cage B the C22-C23 bond length is 1.571(18) Å and the C19-C20 bond length is 1.580(18) Å, these bonds correspond to the C1-C7 position in PCU derivatives (see Figure 7). It can be seen that these bond lengths are shorter than those obtained for the dione (**20**) which are 1.587(3) Å for the C1-C7 bond length and 1.595(3) Å for the C9-C10 bond length, however these bond lengths are still longer than the expected C-C bond length of 1.54 Å.

The unsymmetrical substitution at the mouth of cage B appears to affect bond lengths in this cage. The bonds involving atom C21 that contains the ketone substituent are shorter than normal C21-C20 [1.514(2) Å] and C21-C22 [1.518(18) Å]. The corresponding bonds on the opposite side of cage B are not affected as severely with C18-C23 [1.541(17) Å] falling within the expected range and C18-C19 slightly shorter than normal at [1.529(17) Å].

The C12-C13 and C15-C16 bonds on the allylic arms of cage A are shorter than expected at 1.504(2) Å and 1.496(18) Å respectively.

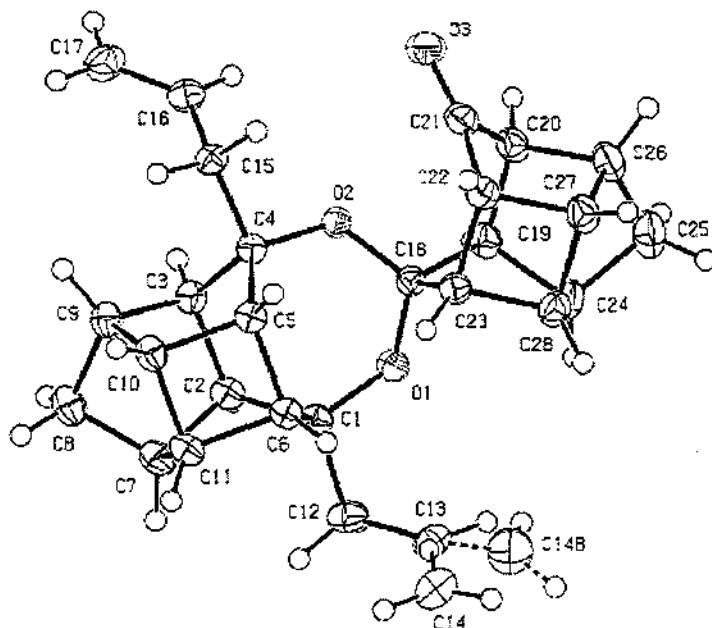


Figure 13: ORTEP diagram of the PCU dimer (76) drawn at the 50 % probability level

The C14 group on the allyl arm is disordered over two positions since there are no repulsions from carbons C23, C24 and C28. However the C17 group on the other allyl arm is ordered due to the steric hindrance from the carbonyl group on C21, which prevents it from being disordered over two positions.

The final crystal structure to be briefly discussed is the ketal (77) (see Appendix 3 for X-ray crystallography data). The numbering used in the discussion below is according to Figure 14.

7.5 THE X-RAY STRUCTURE OF THE PCU KETAL (77)²⁴²

The PCU ketal is unsymmetrically substituted at the mouth of the cage with a ketone substituent at atom C7 and a ketal substituent at atom C11. The asymmetric unit comprises one chiral molecule, with eight molecules (four of each enantiomer) in the

unit cell. The longest C-C single bond is the C2-C6 bond at 1.581(3) Å, with the C3-C2, C9-C8, C5-C6, C10-C9, C5-C9 and C8-C11 bonds also exceeding the expected value of 1.54 Å. The length of the C8-C11 bond is 1.569(3) Å and the C2-C6 bond is 1.581(3) Å in the ketal, these bonds correspond to the C1-C7 position in PCUD (20). These bonds are shorter than that of the PCUD (20) which is 1.587(3) Å for the C1-C7 bond length and 1.595(3) Å for the C9-C10 bond length.

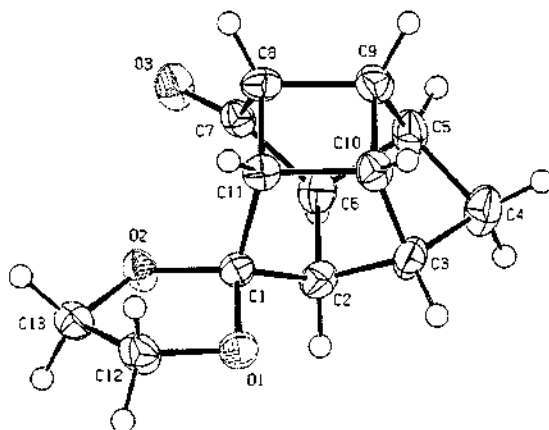


Figure 14: ORTEP diagram of the PCU ketal (77) drawn at the 50 % probability level

Bonds involving the bridgehead atom C4 are shorter than expected with C3-C4 and C4-C5 exhibiting values of 1.525(3) Å and 1.521(3) Å respectively. The shortest bond is the C7-C8 bond with a value of 1.509(3) Å with the C1-C2, C6-C7 and C12-C13 bonds also exhibiting short C-C single bond lengths. The unsymmetrical substitution at the mouth of the cage results in corresponding bonds in the molecule displaying different bond lengths. The C7-C8 bond, which is parallel to the carbonyl group, is shorter (1.509 Å) than the C1-C11 bond, which is protected with the ketal group (1.536 Å).

CHAPTER EIGHT

CONCLUSION

Various new synthetic routes were tested to synthesize precursors (**54**), (**55**) and (**56**) to theoretical pentacycloundecane (PCU) cage annulated macrocycles. The use of different solvents, bases and reaction conditions were investigated during the synthesis of precursors to PCU cage annulated macrocycles. The multi-step synthesis of the cage ditosylate (**54**) was successful with a yield of 75 %. The multi-step synthesis of the mandelic glycol (**55**) was successful and (**55**) was obtained in a 60 % yield. A new synthetic route for the synthesis of isopropyl glycol (**56**) was developed which produced (**56**) in low yield (20 %).

The X-ray structures of a novel PCU dimer (**76**), the PCU ketal (**77**) and the PCU diol (**25**), have been reported for the first time and compared with the X-ray structure obtained independently for the PCUD (**20**). The bond lengths of the PCUD (**20**) and PCU derivatives (**25**), (**76**) and (**77**) are generally in good agreement with similar bond lengths found in the substituted PCU derivatives listed in Figure 10. The X-ray study has indicated that PCU derivatives display C-C bonds that deviate from the expected value of 1.54 Å. It was found that carbon C-C bonds involving atoms C4, C8 and C11 are shorter than normal and that the C1-C7 and the C9-C10 bond lengths are longer than expected. The complete NMR elucidation of PCU derivatives (**20**), (**25**), (**73**), (**76**) and (**77**) have been reported for the first time.

A computational model employing the MM3 force field in Alchemy 2000 was used to calculate the binding energies and enantioselectivity of various host-guest complexes. Calculations were performed in the gas phase and results indicated that the cage moiety does play a role in the enantiomeric process by rigidifying the macrocycle. However for optimum enantiomeric recognition to take place, the positions of the chiral barriers have to be strategically placed when designing the chiral macrocycles. The theoretical cage annulated macrocycle that was postulated exhibited a computed enantioselectivity of 1.52 kcal mol⁻¹, which is better than that reported for Cram's crown ether (**18**) (1.4 kcal mol⁻¹).

A computational investigation using MacroModel software was carried out to investigate the effects of solvent on the binding energy and enantioselectivity. Calculations were performed in no solvent (gas phase), water (solvent phase) and chloroform (solvent phase). Results indicated that solvent does play a significant role in both the enantioselectivity and binding energy of macrocycles. A polar solvent such as water results in lower enantioselectivity when compared with a less polar solvent such as chloroform. The binding energies calculated in the solvent medium (water and chloroform) are higher than those obtained in gas phase calculations indicating that a weak host-guest complex is formed in the solvent phase.

CHAPTER NINE

EXPERIMENTAL

Melting points were recorded with a Bombay 400 013 instrument from Shital Scientific Industries. All melting points are uncorrected. The infrared spectra were recorded on a Nicolet Impact 410 FTIR spectrometer. The one-dimensional NMR spectrum was recorded on a Varian Gemini 300 MHz spectrometer, while the two-dimensional NMR spectra were recorded on a Varian Unity Inova 400 MHz spectrometer. All one-dimensional and two-dimensional NMR spectra used for the structural elucidation of the PCU derivatives were recorded on a Varian Unity Inova 400 MHz spectrometer. All NMR data were processed using Mestrec 4.5.91 (NMR data Processing made easy), Copyright 1996-2005, www.mestrec.com. The fast atom bombardment (FAB) mass spectra were obtained from a Micromass VG70-70E mass spectrometer, equipped with an Intech FAB gun. The samples were bombarded with xenon atoms (1 mA at 8 keV), with *m*-nitrobenzyl alcohol as the matrix. Electron impact (EI) mass spectra (70 eV) were obtained from a Micromass Autospec-TOF mass spectrometer. Elemental analyses were obtained from a Leco CHNS 932 instrument. Analytical grade solvents were used and were freshly distilled before use.

9.1 THE MULTI-STEP SYNTHESIS OF THE PCU DITOSYLATE (54)

The cage ditosylate (54) was synthesized via multi-step synthesis beginning with the cage dione (20).

9.1.1 SYNTHESIS OF 5,8-METHANO-4A,5,8,8A-TETRAHYDRO-1,4-NAPHTHOQUINONE (72)^{120,121}

p-Benzoquinone (71) (200 g, 0.54 mol) was dissolved in dry toluene (4.00 l) and placed in an ice/salt bath within a dark fumehood. Cold, freshly cracked cyclopentadiene (70) (132.00 ml, 1.96 mol) was added over two hours *via* a dropping funnel. The slow addition and cool temperatures ensured a successful Diels-Alder reaction without polymerisation of the cyclopentadiene (70). The reaction mixture was left to stir overnight. The solution was removed from the ice/salt bath, covered in tin foil and left in the dark in the fumehood to allow the complete evaporation of the toluene leaving

behind yellow crystals of adduct (**72**) (230 g, 74 %). m.p. 77°C, IR (KBr): ν_{\max} 3308, 1672 (vs, C=O), 1598, 1296, 1281, 1055 cm^{-1} , ^{13}C NMR [CDCl_3 , 75 MHz]: δ_{C} 48.4 (d), 48.7 (t), 48.8 (d), 135.3 (d), 142.1 (d), 199.5 (s). Elemental analysis. Calculated $\text{C}_{11}\text{H}_{10}\text{O}_2$: C, 75.84, H, 5.79 %. Experimental: C, 75.22, H, 6.22 %. M.S. was identical to an authentic sample.

9.1.2 SYNTHESIS OF PENTACYCLO[5.4.0.0^{2,6}.0^{3,10}.0^{5,9}]UNDECANE-8-11-DIONE (**20**)^{120,121}

The synthesised adduct (**72**) (200 g, 1.149 mol) was added to a volumetric flask (5.00 l) and dissolved in 10 % (v/v) acetone in hexane solution (5.00 l). The volumetric flask was exposed to direct sunlight until a colourless solution was obtained. The solution was evaporated *in vacuo* to give a white microcrystalline solid (**20**) (190.10 g, 95 %). The crystals of (**20**) were obtained by the slow evaporation of solvent over several days at room temperature. m.p. 240°C. IR (KBr): ν_{\max} 3052, 2981, 1755 cm^{-1} (vs, C=O). ^1H NMR [CDCl_3 , 400MHz]: δ_{H} 1.89 ($\text{H}_{4\text{a}}$, $J_{\text{AB}} = 11.3$ Hz), 2.03 ($\text{H}_{4\text{b}}$, $J_{\text{AB}} = 11.3$ Hz) (AB quartet, 2H, methylene bridge protons), 2.68 (H_9/H_{10}), 2.79 (H_1/H_7), 2.91 (H_3/H_5), 3.15 (H_2/H_6) (broad absorption, 8H, methine protons). ^{13}C NMR [CDCl_3 , 100 MHz]: δ_{C} 38.7 (d, C2/C6), 40.5 (t, C4), 43.8 (d, C1/C7), 44.6 (d, C3/C5), 54.7 (d, C9/C10), 212.1 (s, C8/C11). Elemental analysis. Calculated $\text{C}_{11}\text{H}_{10}\text{O}_2$: C, 75.84, H, 5.79 %, Experimental: C, 74.44, H, 5.87 %. M.S. and m.p were identical to an authentic sample.

9.1.3 SYNTHESIS OF EXO-8-EXO-11-DIALLYLPENTACYCLO[5.4.0.0^{2,6}.0^{3,10}.0^{5,9}]UNDECANE-ENDO-8-ENDO-11-DIOL (**73**)²⁰⁹

To a mechanically stirred solution of activated Mg (30.3 g, 1.246 mol) in dry ether (300 ml) under nitrogen in an ice/salt bath was added dropwise a solution of freshly distilled allyl bromide (60 ml, 690 mmol) in ether (800 ml) over 8 hours. The resulting mixture was stirred at ambient temperature for 17 hours and then refluxed for 1.5 hours. The ether phase was then transferred to a dry flask and 800 ml of dry THF was added. A solution of (**20**) (25 g, 143 mmol) in dry THF (300 ml) was added dropwise to the above allylmagnesiumbromide-THF complex at 0°C and the resulting mixture was stirred mechanically at ambient temperature for 20 hours. It was recooled to 0°C and a

saturated NH₄Cl solution (400 ml) added dropwise. The two layers were separated, the aqueous phase was extracted with ethyl acetate (6 x 200 ml). Combined organic extracts were added to the upper layer and dried with anhydrous MgSO₄. Evaporation of the solvent gave a brown residue, which was recrystallized from hexane to give a colourless crystalline solid (**73**) (33 g, 90 %). m.p. 83°C. IR (KBr): ν_{\max} 3072, 2959, 1639 cm⁻¹. ¹H NMR [CDCl₃, 400 MHz]: δ_{H} 1.07 (H_{4a}, J_{AB} = 10.8 Hz), 1.51 (H_{4s}, J_{AB} = 10.8 Hz), 1.97-2.24 (H1', H9/H10, m, 6H), 2.18 (H9/H10), 2.36 (H3/H5), 2.44 (H1/H7), 2.52 (H2/H6), 5.07 (H3'), 5.30 (OH), 5.91 (H2', m); ¹³C NMR [CDCl₃, 100 MHz]: δ_{C} 33.8 (t, C4), 39.9 (d, C2/C6), 42.7 (d, C1/C7), 44.0 (t, C1', C3/C5), 49.1 (d, C9/C10), 77.2 (s, C8/C11), 117.9 (t, C3'), 133.7 (d, C2').

9.1.4 SYNTHESIS OF 3,5-DIALLYL-4-

OXAHEXACYCLO[5.4.1.0^{2,6}.0^{3,10}.0^{5,9}.0^{8,11}]DODECANE (**74**)¹²⁹

A solution of the endo-endo diol (**73**) (30.5 g, 0.118 mol) and TsOH (0.75 g, 0.395 mmol, catalytic amount) in benzene (600 ml) was refluxed in a Dean-Stark apparatus and the resulting water was removed azeotropically. After every 12 hours additional *p*-TsOH (500 mg) was added. When the TLC indicated an absence of the starting material (7 days) the reaction mixture was allowed to cool gradually to ambient temperature and washed sequentially with 10 % NaHCO₃ (100 ml) and water (100 ml) and brine (100 ml). The organic layer was dried with anhydrous MgSO₄ and filtered and the filtrate was concentrated *in vacuo*. The residue was purified *via* column chromatography on silica gel by eluting with 5 % EtOAc/Hexane. Pure diene (**74**) (23.8 g, 84 %) was obtained as a colourless oil. IR (KBr): ν_{\max} 3077, 2959, 1634, 998, 913 cm⁻¹. ¹³C NMR [CDCl₃, 75 MHz]: δ_{C} 37.6 (t), 41.8 (d), 43.4 (t), 44.6 (d), 47.9 (d), 58.6 (d) 111.2 (s), 117.1 (t), 134.5 (d).

9.1.5 SYNTHESIS OF 3,5-[BIS (HYDROXYETHYL)]-4-OXAHEXACYCLO

[5.4.1.0^{2,6}.0^{3,10}.0^{5,9}.0^{8,11}] DODECANE (**25**)¹²⁹

A stirred solution of the diene (**74**) (5.56 g, 23.30 mmol) dry methanol was cooled to -78°C and a slow stream of ozone was bubbled through the solution until a blue-purple colour persisted which indicated the presence of excess ozone and the completion of the reaction. Passing oxygen through the solution until it turned clear flushed out excess

ozone. Sodium borohydride (2.23 g) was added carefully to the solution and the reaction mixture stirred for 12 hours until it reached room temperature. The solution was then diluted with water (15 ml) and partially concentrated to remove most of the methanol. Brine (25 ml) was added and the mixture was extracted with CH₂Cl₂ (3 x 40 ml). The combined organic extracts were dried with anhydrous MgSO₄ and concentrated to give the diol as a white solid (**25**) (4.23 g, 73 %). The crystals of the PCU diol (**25**) were obtained by the slow evaporation of solvent over several days at room temperature. m.p. 153°C. IR (KBr): ν_{\max} 3053, 2964, 1269, 742 cm⁻¹. ¹H NMR [CDCl₃, 400 MHz]: δ_{H} 1.52 (H_{4a}, J_{AB} = 10.5 Hz), 1.88 (H_{4s}, J_{AB} = 10.5 Hz), 2.00 (H1', m), 2.40 (H3/H5), 2.58 (H1/H7), 2.61 (H9/H10), 3.75 (H2', m) 12.15 (OH), ¹³C NMR [CDCl₃, 100 MHz]: δ_{C} 34.2 (C1'), 41.3 (C2/C6), 43.5 (C4), 44.1 (C3/C5), 47.6 (C1/C7), 58.1 (C9/C10), 60.0 (C2'), 96.4 (C8/C11). Elemental analysis. Calculated: C₁₅H₂₀O₃ C, 72.55, H, 8.12 %, Experimental: C, 71.38, H, 8.39 %.

9.1.6 SYNTHESIS OF 3,5-[BIS(HYDROXYETHYL)]-4-

OXAHYDROXYCYCLO[5.4.1.0^{2,6}.0^{3,10}.0^{5,9}.0^{8,11}]DODECANE DITOSYLATE (**54**)^{210,211}

To (0.0162 mol, 3.98 g) of the diol (**25**) in 200 ml of THF was added (8.28 g, 0.1458 mol) of powdered potassium hydroxide in 50 ml of deionised water at ambient temperature under a nitrogen atmosphere. *p*-Toluene sulphonyl chloride (12.27 g) was added over four hours. The solution was left to stir overnight. The solution was diluted with 80 ml of water and extracted with ethyl acetate (3 x 100 ml). The organic phases were combined and dried over anhydrous MgSO₄, filtered and concentrated. Column chromatography produced (6.81 g, 75 %) of the product (**54**). ¹³C NMR [CDCl₃, 75 MHz]: δ_{C} 32.0 (t), 41.9 (d), 42.9 (t), 44.0 (d), 48.0 (d), 59.2 (d), 66.9 (t), 93.9 (s), 128.0 (d), 128.0 (d), 130.0 (d), 144.3 (s).

9.2 THE MULTI-STEP SYNTHESIS OF THE MANDELIC GLYCOL (**55**)

The multi-step synthesis of the mandelic glycol (**55**) began with the conversion of mandelic acid to an ester.

9.2.1 SYNTHESIS OF (S)-(+)-METHYL MANDELATE (61)^{89,212}

To a stirred solution (3.00 g, 0.02 mol) of (S)-(+)-mandelic acid (63) in 150 ml of pure, dry methanol was slowly added (1.6 ml, 0.02 mol) of thionyl chloride at -10°C under nitrogen. The mixture was stirred at -10°C for 20 min and then at room temperature overnight. After evaporation of the solvent, the residue was dissolved in a mixture of 15 g of ice, 15 ml of water and 50 ml of diethyl ether. The mixture was shaken and separated. The organic phase was washed with saturated brine, dried with anhydrous MgSO_4 and filtered and the solvent was removed under reduced pressure to give (3.24 g, 97 %) of (61). Spectral data were identical to those of the authentic sample.

9.2.2 (S)-(+)-METHYL 2-PHENYL-2-(TETRAHYDROPYRANYLOXY) ACETATE (59)^{89,212}

To a mixture of (61) (3.74 g, 0.023 mol) and of dihydropyran (3.086 g, 0.0345 mol) in 150 ml of pure, dry CH_2Cl_2 at 0°C and under N_2 was added 0.8 g of pyridinium *p*-toluenesulphonate (PPTS) catalyst. The reaction mixture was stirred at 0°C for 10 min and then at room temperature overnight. The mixture was washed three times with 50 ml portions of ice-cold water and once with 50 ml NaHCO_3 , dried with anhydrous MgSO_4 and filtered. The solvent was evaporated under reduced pressure. The residue (5.31 g, 89 %), a colourless oil (59), was used in the next step without further purification. Spectral data were identical to those of the authentic sample.

9.2.3 (S)-(+)-2-PHENYL-2-(TETRAHYDROPYRANYLOXY) ETHANOL (57)^{89,212}

A solution of (59) (5.31 g, 0.02 mol) was added drop wise to a stirred suspension of (1.63 g, 0.042 mol) of LiAlH_4 in 150 ml of dry THF at 0°C under nitrogen over 20 min. The reaction mixture was stirred at 0°C for one hour and at room temperature overnight and then it was heated at 60°C for 4 hours. The reaction mixture was diluted with diethyl ether and then quenched with Na_2SO_4 . The white precipitate was filtered and washed with ether. The filtrate and washings were combined, dried with anhydrous MgSO_4 and then filtered and the solvent was evaporated under reduced pressure to produce (57) (4.23 g, 95 %). Spectral data were identical to those of the authentic sample.

9.2.4 (S,S)-(+)-1,11-DIPHENYL-3,6,9-TRIOXAUNDECANE-1,11-DIOL (MANDELIC GLYCOL, 55)^{89,212}

To a stirred suspension of NaH (0.55 g, 0.0123 mol) (60 % dispersion in mineral oil) was added dropwise under nitrogen at 0°C of (57) (1.5 g, 0.00675 mol). The reaction mixture was stirred at 0°C for 20 min and at room temperature for 72 hours. After evaporation of the solvent under reduced pressure, the residue was dissolved in 80 ml of ice and extracted with 50 ml portions of CH₂Cl₂. The organic phases were combined and dried with MgSO₄ and the solvent was evaporated under reduced pressure. The residue was dissolved in 170 ml of pure, dry MeOH and 1.5 g of *p*-TsOH acid and stirred overnight. The solvent was then evaporated under reduced pressure and the residue washed once with NaHCO₃ and extracted with ethyl acetate (3 x 50 ml), the organic phases were dried over anhydrous MgSO₄ and concentrated to produce (55) (1.75 g, 75 %). IR (KBr): ν_{\max} 3031, 2873, 1641, 1459, 1356, 1249, 1202, 1103, 905, 775, 750 cm⁻¹. ¹³C NMR [CDCl₃, 75 MHz]: δ_c 70.3 (t), 70.5 (t), 72.5 (t), 76.6 (d), 126.1 (t), 127.5 (t), 128.3 (t), 140.2 (s).

9.3 THE ATTEMPTED MULTI-STEP SYNTHESIS OF THE (S,S)-(+)-2,10-DIPHENYL-3,6,9-TRIOXADECANE-1,11-DIOL (66)¹⁹⁴

The attempted multi-step synthesis of the diphenyl glycol (66) began with the conversion of mandelic acid (63) to an ester (69). A new synthetic route was used to increase the yield of the intermediate steps.

9.3.1 SYNTHESIS OF (S)-(+)-BUTYL MANDELATE (85)

A solution of (S)-(+)-mandelic acid (63) (5 g, 0.0335 mol), butanol (4.2 ml, 0.0470 mol) and 0.5 ml of concentrated sulphuric acid (a catalytic amount) in toluene (600 ml) was refluxed in a Dean-Stark apparatus for 6 days and the resulting water was removed azeotropically. The reaction mixture was allowed to cool gradually to ambient temperature and washed sequentially with 10 % NaHCO₃ (100 ml) and water (100 ml) and brine (100 ml). The organic layer was dried with anhydrous MgSO₄ and filtered and the filtrate was concentrated *in vacuo*. The NMR spectra indicated pure product (69) (5.76 g, 82 %) and was used in the next step without any purification. Spectral data were identical to those of the authentic sample.

9.3.2 (S)-(+)-PHENYL-1,2-ETHANDIOL (68)²⁴³

The ester (69) (4.89 g, 0.0235 mol) was treated with (1.78 g, 0.0470 mol) of lithium aluminium hydride in THF at 0°C under a nitrogen atmosphere. The reaction mixture was stirred at 0°C for one hour and at room temperature overnight. The reaction mixture was diluted with diethyl ether and then quenched with Na₂SO₄. The white precipitate was filtered and washed with ether. The filtrate and washings were combined, dried with anhydrous MgSO₄ and then filtered and the solvent was concentrated under reduced pressure to produce (68) (2.45 g, 75 %). Spectral data were identical to those of the authentic sample.

9.3.3 (S)-(+)-1,4,4,4-TETRA-PHENYL-3-OXA-1-BUTANOL (67)²¹⁵

Compound (68) (10 g, 0.0725 mol) was stirred with 12.9 ml triethylamine triphenylmethyl chloride (8.07 g, 0.0797 mol) and 4-dimethylaminopyridine (DMAP) (0.58 g, 0.003 mol) in dry dichloromethane at 0°C under nitrogen. The reaction mixture was allowed to warm up to room temperature and was left stirring overnight. The crude product was poured into ice and washed with saturated ammonium chloride, water and dried with anhydrous MgSO₄ and concentrated under reduced pressure. The resulting (S)-(+)-1,4,4,4-tetraphenyl-3-oxa-1-butanol (67) (17 g, 61 %) could not be further purified. Spectral data were identical to those of the authentic sample.

9.3.4 (S,S)-(+)-2,10-DIPHENYL-3,6,9-TRIOXAUNDECANE-1,11-DIOL (66)^{59,57,194}

Compound (67) (1.04 g, 0.00273 mol) was added to (0.198 g, 0.00496 mol) of NaH in THF at 0°C under a nitrogen atmosphere. Diethylene glycol ditosylate (0.514 g, 0.00152 mol) was added to the reaction mixture and stirred overnight. The resulting mixture was cooled and concentrated under reduced pressure and poured into ice. The reaction mixture was extracted with dichloromethane and dried over anhydrous MgSO₄ and concentrated under reduced pressure. The crude (S,S)-(+)-1,1,1,4,12,15,15-octaphenyl-2,5,8,11,14-pentaoxapentadecane was used in the next step without further purification. Deprotection of the trityl groups involved the use of *p*-TsOH acid in methanol at room temperature overnight. This was followed by column chromatography, which resulted in the starting materials being recovered.

9.4 THE SYNTHESIS OF (S,S)-(+)-ISOPROPYL GLYCOL (56)⁸⁹

A modified synthetic route was followed for the synthesis of the isopropyl glycol⁵³ (56), beginning with the conversion of α -hydroxyisovaleric acid (64) to an ester (62).

9.4.1 SYNTHESIS OF (S)-(+)-HYDROXYISOVALERIC METHYL ESTER (62)⁸⁹

To a stirred solution of 3 g (0.02 mol) of (S)-(+)- α -hydroxyisovaleric acid (64) in 150 ml of pure, dry methanol was slowly added 1.6 ml (0.002 mol) of thionyl chloride at -10°C under nitrogen. The mixture was stirred at -10°C for 20 min and then at room temperature overnight. After evaporation of the solvent, the residue was dissolved in a mixture of 15 g of ice, 15 ml of water and 50 ml of diethyl ether. The mixture was shaken and separated. The organic phases were washed with saturated brine, dried with anhydrous MgSO_4 and filtered and the solvent was removed under reduced pressure to give (1.14 g, 43 %) of (62). Spectral data were identical to the authentic sample.

9.4.2 (S)-(+)-PROTECTED-HYDROXYISOVALERIC METHYL ESTER (60)⁸⁹

To a mixture of (62) (3.74 g, 0.023 mol) and (3.086 g, 0.0345 mol) of dihydropyran in 150 ml of pure, dry CH_2Cl_2 at 0°C and under N_2 was added (0.8 g) of pyridinium *p*-toluenesulphonate (PPTS) catalyst. The reaction mixture was stirred at 0°C for 10 min and then at room temperature overnight. The mixture was washed three times with 50 ml portions of ice-cold water and once with 50 ml NaHCO_3 , dried with anhydrous MgSO_4 and filtered and the solvent was evaporated under reduced pressure. The residue (2.31 g, 46 %) colourless oil (60) was used in the following step without further purification. Spectral data were identical to the authentic sample.

9.4.3 (S)-(+)-PROTECTED-HYDROXYISOVALERIC ALCOHOL (58)⁸⁹

A solution of (60) (2.00 g, 0.009 mol) was added dropwise to a stirred suspension of (5.80 g) LiAlH_4 in 150 ml of dry THF at 0°C under nitrogen over 20 min. The reaction mixture was stirred at 0°C for one hour and at 40 - 50°C overnight and then it was heated at 60°C for 2 hours. The reaction mixture was diluted with diethyl ether and then quenched with Na_2SO_4 . A white precipitate was filtered and washed with ether. The

filtrate and washings were combined, dried with anhydrous MgSO₄ and then filtered and the solvent was evaporated under reduced pressure to produce (58) (0.86 g, 47 %). Spectral data were identical to the authentic sample.

9.4.4 (S,S)-(+)-ISOPROPYL GLYCOL (56)⁸⁹

To a stirred suspension of (0.55 g, 0.0123 mol) NaH (60 % dispersion in mineral oil) was added dropwise under nitrogen at 0°C of (0.80 g, 0.004 mol) (58). The reaction mixture was stirred at 0°C for 20 min and at room temperature for 72 hours. After evaporation of the solvent under reduced pressure, the residue was dissolved in 80 ml of ice and extracted with 50 ml portions of CH₂Cl₂. The organic phases were combined and dried with MgSO₄ and the solvent was evaporated under reduced pressure. The residue was dissolved in 170 ml of pure, dry MeOH and (1.5 g) of *p*-TsOH acid and stirred overnight. The solvent was then evaporated under reduced pressure and the residue was washed once with NaHCO₃ and extracted with ethyl acetate (3 x 50 ml). The organic phases were dried over anhydrous MgSO₄ and concentrated under reduced pressure to produce (56) (0.23 g, 20 %). ¹³C NMR [CDCl₃, 75 MHz]: δ_c 4.98 (d), 74.2 (t), 70.4 (t), 70.3 (t), 30.8 (d), 18.7 (q), 18.3 (q).

9.5 THE SYNTHESIS OF THE NOVEL PCU DIMER (76)

To a mechanically stirred solution of activated Mg (30.3 g, 1.246 mol) in dry ether (300 ml) under nitrogen in an ice/salt bath was added a dropwise a solution of freshly distilled allyl bromide (60 ml, 690 mmol) in ether (800 ml) over 8 hours. The resulting mixture was stirred at ambient temperature for 17 hours and then refluxed for 1.5 hours. The ether phase was then transferred to a dry flask and 800 ml of dry THF was added. A solution of (20) (25 g, 143 mmol) in dry THF (300 ml) was added dropwise to the above allylmagnesiumbromide–THF complex at 0°C and the resulting mixture was stirred mechanically at ambient temperature for 20 hours. It was recooled to 0°C and a saturated NH₄Cl solution (400 ml) was added dropwise. The resulting layers were separated, the aqueous phase was extracted with ethyl acetate (6 x 200 ml). Combined organic extracts were added to the upper layer and dried with anhydrous MgSO₄. Evaporation of the solvent gave a brown residue, which was cleaned by column chromatography (60 % ethyl acetate, 40 % hexane) to produce novel compound (76) (12.06 g). The crystals of the novel PCU dimer (76) were obtained by the slow

evaporation of solvent over several days at room temperature. m.p. 122° C. Elemental analysis. Calculated: C₂₈ H₃₀ O₃: C, 81.54, H, 7.95%, Experimental: C, 79.77, H, 7.49%. M.S [M+H]⁺ 415 m/z. IR (KBr) ν_{\max} 3068, 2972, 1748 cm⁻¹. See Table 15.

**9.6 THE SYNTHESIS OF THE
PENTACYCLO[5.4.0.0^{2,6}.0^{3,10}.0^{5,9}]UNDECANE-8-11-DIONE-MONO-
ETHYLENE KETAL (77)²²³**

A mixture of (20) (183.00 g, 1.05 mol), ethylene glycol (81.20 ml, 1.45 mol), *p*-TsOH acid (6.11 g, 3.21 x 10⁻² mol) and A4 molecular sieves (2 g) in dry benzene (700 ml) was refluxed with stirring in a Dean-Stark apparatus for four days. The reaction mixture was left to cool and poured slowly into ice cold 10 % (v/v) aqueous sodium carbonate (1.00 l). This was extracted with dichloromethane (3 x 500 ml). The mixture was filtered and the solvent evaporated *in vacuo*. The resulting brown residue was recrystallised from hexane to give the mono-ketal as white crystals (170.05 g, 74 %). The crystals of the PCU ketal (77) were obtained by the slow evaporation of solvent over several days at room temperature. m.p. 73°C. ¹H NMR [CDCl₃, 400 MHz]: δ_{H} 1.56-1.85 ppm (2H, bridgehead protons), 2.41-2.94 ppm (8H, methine protons) and 3.83-3.90 ppm (4H, ketal protons). ¹³C NMR [CDCl₃, 100 MHz]: δ_{C} 36.3 (m), 38.7 (dd), 41.4 (td) 41.3 (dd), 42.3 (m), 42.9 (m), 45.8 (m), 50.7 (m), 53.0 (m), 64.5 (dt), 65.7(m), 113.9 (s), 215.2 (s)

CHAPTER TEN

REFERENCES

1. Cram, D.J.; Helgeson, R.C.; Sousa, L.R.; Timko, J.M.; Newcomb, M.; Moreau, P.; De Jong, F.; Gokel, G.W.; Hoffman, D.H.; Domeier, L.A.; Peacock, S.C.; Madan, M.; Kaplan, L., *Pure Appl. Chem.*, **1975**, 43, 327.
2. Aitken, R.A.; Kilényi, S.N., *Asymmetric Synthesis*, Blackie Academic and Professional, London, **1992**, pp 2-5.
3. Newcomb, M.; Toner, J.L.; Helgeson, R.C.; Cram, D.J., *J. Am. Chem. Soc.*, **1979**, 101, 4941.
4. Marchand, A.P.; Chong, H.-S.; Ganguly, B., *Tetrahedron Asymmetry*, **1999**, 10, 4695.
5. Morrison, R.T.; Boyd, R.N., *Organic Chemistry*, Prentice Hall International, Inc., New Jersey, **1992**, pp 478-481.
6. Frangmyr, T.; Forsen, S., *Nobel Lectures in Chemistry 1971-1980*, World Scientific, Singapore, **1993**.
7. de Jong, F.; Reinhoudt, D.N., *Stability and reactivity of crown ether complexes*, Academic Press, London, **1981**.
8. Bickerstaff, G.F., *Enzymes in Industry and Medicine*, Edward Arnold Publishers, London, **1987**, pp 2-6.
9. Cram, D.J., *From Design to Discovery*, American Chemical Society, Washington DC, **1990**.
10. Weber, E.; Toner, J.L.; Goldberg, I.; Vogtle, F.; Laidler, D.A.; Stoddart, J.F.; Bartsch, R.A.; Liotta, C.L., *Crown ethers and analogs*, Patai, S. Ed., John Wiley and Sons, New York, **1989**.
11. Cram, D.J.; Cram, J.M., *Science*, **1974**, 183, 803.
12. Stoddart J.F., *Comprehensive Organic Chemistry: The synthesis and reactions of Organic compounds*, Vol.1, Pergamon Press, New York, **1987**.
13. Pederson, C.J., *J. Am. Chem. Soc.*, **1967**, 89, 2495.
14. Pederson, C.J., *J. Am. Chem. Soc.*, **1967**, 89, 7017.
15. Chao, Y.; Cram, D.J., *J. Am. Chem. Soc.*, **1976**, 98, 1015.
16. Newcomb, M.; Timko, J.M.; Walba, D.M.; Cram, D.J., *J. Am. Chem. Soc.*, **1977**, 99:19, 6392.
17. Lehn, J.-M., *Structure and Bonding*, **1973**, 16, 141.
18. Lehn, J.-M., *Accounts Chem. Res.*, **1978**, 11, 49.
19. Cram, D.J.; Helgeson, R.C.; Koga, K.; Kyba, E.P.; Madan, K.; Sousa, L.R.; Siegel, M.G.; Moreau, P.; Gokel, G.W.; Timko, J.M.; Sogah, G.D.Y., *J. Org. Chem.*, **1978**, 43, 2758.
20. Cram, D.J.; Cram, J.M., *Acc. Chem. Res.*, **1978**, 11, 8.
21. Kim, S.-G.; Kim, K.-H.; Jung, J.; Shin, S.K.; Ahn, K.H., *J. Am. Chem. Soc.*, **2002**, 124, 591.
22. Girondeau, J.-M.; Lehn, J.-M.; Sauvage, J.-P., *Angew. Chem.*, **1975**, 87, 813.

23. Curtis, W.D.; Laidler, D.A.; Stoddart, J.F.; Jones, G.H., *J. Chem. Soc. Chem. Comm.*, **1975**, 833.
24. Curtis, W.D.; Laidler, D.A.; Stoddart, J.F.; Jones, G.H., *J. Chem. Soc. Chem. Comm.*, **1975**, 835.
25. Hayward, R.C.; Overton, C.H.; Whitham, G.H., *J. Chem. Soc. Perkin Trans. I*, **1976**, 2413.
26. Stoddart, J.F.; Wheatley, C.M., *J. Chem. Soc. Chem. Comm.*, **1974**, 390.
27. Burden, I.J.; Coxon, A.C.; Stoddart, J.F.; Wheatley, C.M., *J. Chem. Soc. Perkin Trans. I*, **1977**, 220.
28. Laidler, D.A.; Stoddart, J.F., *Carbohydr. Res.*, **1977**, 55, C1.
29. Hain, W.; Lehnert, R.; Röttele, H.; Schröder, G., *Tetrahedron Lett.*, **1978**, 625.
30. Marchand, A.P.; Takhi, M.; Kumar, V.S.; Krishnudu, K.; Ganguly, B., *Arkivoc*, **2001**, 3, 13.
31. Kanakamma, P.P.; Mani, N.S.; Maitra, U.; Nair, V., *J. Chem. Soc. Perkin Trans. I*, **1995**, 2339.
32. Seebach, D.; Pichota, A.; Beck, A.K.; Pinkerton, A.B.; Litz, T.; Karjalainen, J.; Gramich, V., *Organic Lett.*, **1999**, 1, 55.
33. Rathjens, A.; Thiem, J., *Polish Journal of Chemistry*, **2005**, 79, 2, 211.
34. Töke, L.; Bakó, P.; Keglevich, G.; Bako, T., *Kemija u Industriji*, **2004**, 53, 349.
35. Bakó, P.; Vizvárdi, K.; Toppet, S.; van der Eycken, E.; Hoornaert, G.J.; Töke, L., *Tetrahedron*, **1998**, 54, 14975.
36. Hiraoka, M., *Crown compounds: Their characteristics and applications*, Kodansha Ltd, Tokyo, **1982**.
37. Stoddart, J.F., *Chem. Soc. Rev.*, **1979**, 8, 85.
38. Behr, J.-P.; Girodeau, J.-M.; Hayward, R.C.; Lehn, J.-M.; Sauvage, J.-P., *Helv. Chim. Acta.*, **1980**, 63, 2096.
39. Behr, J.-P.; Lehn, J.-M.; Vierling, P., *Helv. Chim. Acta*, **1982**, 65, 1853.
40. Zhang, X.X.; Bradshaw, J.S.; Izatt, R.M., *Chem. Rev.*, **1997**, 97, 3313.
41. Steed, J.W.; Atwood, J.L., *Supramolecular Chemistry*, John Wiley and Sons, New York, **2000**.
42. Hossain, A.; Schneider, H.-J., *J. Am. Chem. Soc.*, **1998**, 120, 11208.
43. Gokel, G.W.; Du Pont, H.D., *Synthesis*, **1976**, 168.
44. Liotta, C.L., *Synthetic Multidentate Macrocyclic Compounds*, Academic Press, New York, **1978**, p 111.
45. Weber, W.P.; Gokel, G.W., *Phase Transfer Catalysis in Organic Synthesis*, Springer Verlag, Berlin, **1977**.
46. Starks, C.M.; Liotta, C., *Phase Transfer Catalysis*, Academic Press, New York, **1978**.
47. Moriarty, R.M.; Rao, M.S.C.; Tuladhar, S.M.; D' Silva, C.; Williams, G.; Gilardi, R., *J. Am. Chem. Soc.*, **1993**, 115, 1194.
48. Mlinarić-Majerski, K.; Kragol, G., *Tetrahedron*, **2001**, 57, 449.
49. Ryba, O.; Petranek, J., *Electroanal. Chem. Interf. Electrochem.*, **1973**, 44, 423.
50. Jepson, B.E.; De Witt, R., *J. Inorg. Nucl. Chem.*, **1976**, 38, 1175.
51. Blair, S.M.; Brodbelt, J.S.; Marchand, A.P.; Kumar, K.A.; Chong, H.-S., *Anal. Chem.*, **2000**, 72, 2433.
52. Nakatsuji, Y.; Kita, K.; Inoue, H.; Zhang, W.; Kida, T.; Ikeda, I., *J. Am. Chem. Soc.*, **2000**, 122, 6307.

53. Bradshaw, J.S.; Huszthy, P.; McDaniel, C.W.; Zhu, C.Y.; Dalley, N.K.; Lifson, S., *J. Org. Chem.*, **1990**, 55, 3129.
54. Bradshaw, J.S.; Colter, M.L.; Nakatsuji, Y.; Spencer, N.O.; Brown, M.F.; Izatt, R.M.; Arena, G.; Tse, P.-K.; Wilson, B.E.; Lamb, J.D.; Dalley, N.K.; Morin, F.G.; Grant, D.M., *J. Am. Chem. Soc.*, **1985**, 107, 4865.
55. Zhao, H.; Hua, W., *J. Org. Chem.*, **2000**, 65, 2933.
56. Helgeson, R.C.; Koga, K.; Timko, J.M.; Cram, D.J., *J. Am. Chem. Soc.*, **1973**, 95, 3021.
57. Davidson, R.B.; Bradshaw, J.S.; Jones, B.A.; Dalley, N.K.; Morin, F.G.; Grant, D.M., *J. Org. Chem.*, **1984**, 49, 353.
58. Bradshaw, J.S.; Jolley, S.T.; Brown, P.R.; Christensen, J.J.; Izatt, R.M., *J. Org. Chem.*, **1983**, 48, 2635.
59. Bradshaw, J.S.; Thompson, P.K.; Izatt, R.M.; Morin, F.G.; Grant, D.M., *Heterocyclic Chem.*, **1984**, 21, 897.
60. Uiterwijk, J.W.H.M.; Harkema, S.; Feil, D., *J. Chem. Soc. Perkin Trans. II*, **1987**, 721.
61. Uiterwijk, J.W.H.M.; van Staveren, C.J.; Reinhoudt, D.N.; den Hertog, H.J., Jr.; Kruse, L.; Harkema, S., *J. Org. Chem.*, **1986**, 51, 1575.
62. Kyba, E.B.; Koga, K.; Sousa, L.R.; Siegel, M.G.; Cram, D.J., *J. Am. Chem. Soc.*, **1973**, 95, 2692.
63. Peacock, S.C.; Domeier, L.A.; Gaeta, F.C.A.; Helgeson, R.C.; Timko, J.M.; Cram, D.J., *J. Am. Chem. Soc.*, **1978**, 100, 26.
64. Sogah, G.D.Y.; Cram, D.J., *J. Am. Chem. Soc.*, **1979**, 101, 3035.
65. Sousa, L.R.; Sogah, G.D.Y.; Hoffman, D.H.; Cram, D.J., *J. Am. Chem. Soc.*, **1978**, 100, 4569.
66. Helgeson, R.C.; Timko, J.M.; Cram, D.J., *J. Am. Chem. Soc.*, **1973**, 95, 3023.
67. Helgeson, R.C.; Koga, K.; Timko, J.M.; Cram, D.J., *J. Am. Chem. Soc.*, **1973**, 95, 3021.
68. Turgut, Y.; Hoşgören, H., *Tetrahedron Asymmetry*, **2003**, 14, 3815.
69. Togrul, M.; Askin, M.; Hoşgören, H., *Tetrahedron Asymmetry*, **2005**, 16, 2771.
70. Diamond, D., *Anal. Commun.*, **1998**, 35, 123.
71. Zhao, H.; Hua, W., *J. Org. Chem.*, **2000**, 65, 2933.
72. Jennings, K.; Diamond, D., *Analyst*, **2001**, 126, 1063.
73. Cui, Y.; Lee, S.J.; Lin, W., *J. Am. Chem. Soc.*, **2003**, 125, 6014.
74. Stoddart, J.F., *Chem. Soc. Rev.*, **1979**, 8, 85.
75. Boyle, G.A.; Govender, T.; Kruger, H.G.; Maguire, G.E.M., *Tetrahedron Asymmetry*, **2004**, 15, 3775.
76. *Chemistry & Engineering*, **2002**, 43, [Http:// pubs.acs.org/ CEN](http://pubs.acs.org/CEN).
77. Lee, W.; La, S.; Choi, Y.; Kim, K.-R., *Bull. Korean Chem. Soc.*, **2003**, 24, 1232.
78. Prodi, L.; Bolletta, F.; Montalti, M.; Zaccheroni, N.; Huszthy, P.; Samu, E.; Vermes, B., *New J. Chem.*, **2000**, 24, 781.
79. Wudl, F.; Gaetea, F., *J. Chem. Soc. Chem. Commun.*, **1972**, 107.
80. De Vries, J.G.; Kellog, R.M., *J. Am. Chem. Soc.*, **1979**, 101, 2759.
81. Karakaplan, M.; Aral, T., *Tetrahedron Asymmetry*, **2005**, 16, 2119.
82. Perkins, C.; Marchand, A.P.; Sivappa, R.; Polla, B., Abstracts, 59th Southwest Regional Meeting of the American Chemical Society, Oklahoma City, U.S.A, October 2003.

83. Naemura, K.; Tobe, Y.; Kaneda, T., *Coord. Chem. Rev.*, **1996**, 148, 199.
84. Webb, T.H.; Wilcox, C.S., *Chem. Soc. Rev.*, **1993**, 22, 383.
85. Yokota, K.; Haba, O.; Satoh, T., *Macromol. Chem. Phys.*, **1995**, 196, 2383.
86. Still, W.C., *Acc. Chem. Res.*, **1996**, 29, 155.
87. Cram, D.; Cram, J., *Container Molecules and their Guests*, Monographs in Supramolecular Chemistry, Royal Society Of Chemistry, Cambridge, **1994**
88. Pirkle, W.H.; Pochapsky, T.C., *Chem. Rev.*, **1989**, 89, 347.
89. Huszthy, P.; Bradshaw, J.S.; Zhu, C.Y.; Izatt, R.M.; Lifson, S., *J. Org. Chem.*, **1991**, 56, 3330.
90. Still, W.C.; Kilburn, J.D.; Sanderson, P.E.J.; Lui, R.; Wiley, M.R.; Hollinger, F.P.; Hawley, R.C.; Nakajima, M.; Bernadi, A.; Hong, J.I.; Namgoong, S.K., *Isr. J. Chem.*, **1992**, 32, 41.
91. Yamamoto, K.; Isoue, K.; Sakato, Y.; Kaneda, T., *J. Chem. Soc. Chem. Commun.*, **1992**, 791.
92. Namemura, K.; Matsumura, T.; Komatsu, M.; Hirose, Y.; Chikamatsu, H., *Bull. Chem. Soc. Jpn.*, **1989**, 62, 3523.
93. Kyba, E.P.; Siegel, M.G.; Sousa, L.R.; Sogah, G.D.Y.; Cram, D.J., *J. Am. Chem. Soc.*, **1973**, 95, 2691.
94. Kyba, E.P.; Gokel, G.W.; de Jong, F.; Koga, K.; Sousa, L.R.; Siegel, M.G.; Kaplan, L.; Sogah, G.D.Y.; Cram, D.J., *J. Org. Chem.*, **1977**, 42, 4173.
95. Cram, D.J.; Helgeson, R.C.; Koga, K.; Kyba, E.P.; Madan, K.; Sousa, L.R.; Siegel, M.G.; Moreau, P.; Gokel, G.W.; Timko, J.M.; Sogah, G.D.Y., *J. Org. Chem.*, **1978**, 43, 2758.
96. Kyba, E.P.; Koga, K.; Sousa, L.R.; Siegel, M.G.; Cram, D.J., *J. Am. Chem. Soc.*, **1973**, 95, 2692.
97. Helgeson, R.C.; Timko, J.M.; Cram, D.J., *J. Am. Chem. Soc.*, **1973**, 95, 3023.
98. Gokel, G.W.; Cram, D.J., *J. Chem. Soc. Chem. Commun.*, **1973**, 52, 481.
99. Akimoto, H.; Shioiri, T.; Iitaka, Y.; Yamada, S., *Tetrahedron Lett.*, **1968**, 97.
100. Peacock, S.S.; Walba, D.M.; Gaeta, F.C.A.; Helgeson, R.C.; Cram, D.J., *J. Am. Chem. Soc.*, **1980**, 102, 2043.
101. de Jong, F.; Siegel, G.M.; Cram, D.J., *J. Chem. Soc. Chem. Commun.*, **1975**, 551.
102. Oliver, D.W.; Dekker, T.G.; Snyckers, F.O., *Eur. J. Med. Chem.*, **1991**, 26, 375.
103. Schwab, R.S.; England, A.C.; Poskanzer, D.C.; Young, R.R., *JAMA*, **1969**, 208, 7, 1168.
104. Bailey, E.V.; Stone, T.W., *Arch. Int. Pharmacodyn.*, **1975**, 216, 246.
105. Dekker, T.B.; Oliver, D.W., S African Patent ZA8202, 158 (to Noristan Ltd) 24 Dec 1984, pp 52, Chem Abstr 1986, 104, p 148375.
106. van der Schyf, C.J.; Squier, G.J.; Coetzee, W.A., *Pharmacol. Res. Commun.*, **1986**, 18, 407.
107. van der Walt, J.J.; van der Schyf, C.J.; van Rooyen, J.M.; de Jager, J.; van Aarde, M.N., *S. Afri. J. Sci.*, **1988**, 84, 448.
108. van der Schyf, C.J.; Liebenberg, W.; Bornman, R.; Dekker, T.G.; van Rooyen, P.H.; Fourie, T.G.; Matthee, E.; Snyckers, F.O., *S. Afri. Tydskr. Chem.*, **1989**, 42, 46.
109. Geldenhuys, W.J.; Malan, S. F.; Bloomquist, J.R.; Marchand, A.P.; van der Schyf, C.J., *Medicinal Research Reviews*, **2005**, 25, 21.

-
110. Marchand, A.P., *Tetrahedron*, **1988**, 44, 2377.
111. Marchand, A.P.; Dave, P.R.; Rajapaksa, D.; Arney, B.E., Jr.; Flippen-Anderson, J.L.; Gilardi, R.; George, C., *J. Org. Chem.*, **1989**, 54, 1769.
112. Marchand, A.P.; Reddy, D.S., *J. Org. Chem.*, **1984**, 49, 4078.
113. Marchand, A.P.; Kruger, H.G.; Power, T.D.; Segal, C., *Kem. Ind.*, **2002**, 51, 51.
114. Watson, W.H.; Nagl, A.; Kashyap, R.P.; Marchand, A.P.; Zhao, D., *Acta Cryst. C*, **1989**, 45, 1342.
115. Marchand, A.P.; Suri, S.C.; Earlywine, A.D.; Powell, D.R.; van der Helm, D., *J. Org. Chem.*, **1984**, 49, 670.
116. Marchand, A.P., *Chem. Rev.*, **1989**, 89, 1011.
117. Jiménez, P.; Roux, M.V.; Dávalos, J.Z.; Abboud, J.-L.; Molina, M.T., *J. Chem. Thermodynamics*, **1999**, 31, 263.
118. Marchand, A.P., *Advances in Theoretically Interesting Molecules*, **1989**, Thummel, R.P., Ed.; JAI Press, Greenwich, CT, U.S.A, Vol 1, pp 357-399.
119. Barborak, J.C.; Khoury, D.; Maier, W.F.; Schleyer, P.V.R.; Smith, E.C.; Smith, W.F., Jr.; Wyrick, C., *J. Org. Chem.*, **1979**, 44, 26.
120. Marchand, A.P.; Allen, R.W., *J. Org. Chem.*, **1974**, 39, 1596.
121. Cookson, R.C.; Crundwell, E.; Hill, R.R.; Hudec, J., *J. Chem. Soc.*, **1964**, 3062.
122. Bott, S.G.; Marchand, A.P.; Alihodžić, S.; Kumar, K.A., *J. Chem. Cryst*, **1998**, 28, 4.
123. Macias, A.T.; Kumar, K.A.; Marchand, A.P.; Evanseck, J.D., *J. Org. Chem.*, **2000**, 65, 2083.
124. Marchand, A.P.; Hariprakash, H.K.; Chong, H.-S.; Takhi, M., *Heterocycles*, **2001**, 54, 151.
125. Hayakawa, K.; Kido, K.; Kanematsu, K., *J. Chem. Soc. Chem. Commun.*, **1986**, 268.
126. Hayakawa, K.; Kido, K.; Kanematsu, K., *J. Chem. Soc. Perkin. Trans. I*, **1988**, 511.
127. Hayakawa, K.; Naito, R.; Kanematsu, K., *Heterocycles*, **1988**, 27, 2293.
128. Marchand, A.P.; Kumar, K.A.; Mlinarić-Majerski, K.; Kragol, G., *Tetrahedron*, **1997**, 55, 3467.
129. Marchand, A.P.; Kumar, K.A.; McKim, A.S.; Mlinarić-Majerski, K.; Kragol, G., *Tetrahedron*, **1997**, 53, 3467.
130. Govender, T., PhD Thesis, **2005**, School of Chemistry, Faculty of Science, University of KwaZulu-Natal, Howard College Campus, Durban, 4041.
131. Alchemy is a registered product of Tripos. Alchemy 32, Version 2.05, Tripos, Inc., St. Louis, MO, U.S.A.
132. MacroModel is a registered trademark of Schrödinger, LLC, U.S.A, **2004**
133. Kyba, E.P.; Helgeson, R.C.; Madan, K.; Gokel, G.W.; Tarnowski, T.L.; Moore, S.S.; Cram, D.J., *J. Am. Chem. Soc.*, **1977**, 99, 2564.
134. Jensen, F., *Introduction To Computational Chemistry*, John Wiley and Sons, Chichester, **1999**.
135. Clark, T., *A Handbook of Computational Chemistry: A practical Guide to chemical structure and energy calculations*, Wiley, New York, **1985**.
136. Gaussian 98, Revision A.9, Frisch M.J.; Trucks, G.W.; Schlegel, H.B.; Scuseria, G.E.; Robb, M.A.; Cheeseman, J.R.; Zakrzewski, V.G.; Montgomery, J.A., Jr; Stratmann, R.E.; Burant, J.C.; Dapprich, S.; Millam, J.M.; Daniels, A.D.; Kudin,

- K.N.; Strain, M.C.; Farkas, O.; Tomasi, J.; Barone, V.; Cossi, M.; Cammi, R.; Mennucci, B.; Pomelli, C.; Adamo, C.; Clifford, S.; Ochterski, J.; Petersson, G.A.; Ayala, P.Y.; Cui, Q.; Morokuma, K.; Malick, D.K.; Rabuck, A.D.; Raghavachari, K.; Foresman, J.B.; Cioslowski, J.; Ortiz, J.V.; Baboul, A.G.; Stefanov, B.B.; Lui, G.; Liashenko, A.; Piskorz, P.; Komaromi, I.; Gomperts, R.; Martin, R.L.; Fox, D.J.; Keith, T.; Al-Laham, M.A.; Peng, C.Y.; Nanayakkara, A.; Challacombe, M.; Gill, P.M.W.; Johnson, B.; Chen, W.; Wong, M.W.; Andres, J.L.; Gonzalez, C.; Head-Gordon, M.; Replogle, E.S.; Pople, J.A., Gaussian, Inc., Pittsburgh PA, U.S.A., 1998.
137. Foresman, J.B.; Frisch, A.E., *Exploring Chemistry with Electronic Structure Methods: A Guide to Using Gaussian*, 2nd Edition, Gaussian, Inc., Pittsburgh, PA, U.S.A., 1996, p 39.
 138. Hyperchem, Computational Chemistry, Hypercube, Inc., U.S.A., 1996.
 139. Hehre, W.J.; Radom, L.; Schleyer, P.; Pople, J., *Ab Initio Molecular Orbital Theory*, Wiley, New York, 1986.
 140. Burkett, U.; Allinger, N.L. (Eds), *Molecular Mechanics*, ACS Monograph No. 177, American Chemical Society, Washington DC, 1982.
 141. Allinger, N.L.; Yuh, Y.H.; Lii, J.-H., *J. Am. Chem. Soc.*, 1989, 111, 8551.
 142. Lii, J.-H.; Allinger, N.L., *J. Am. Chem. Soc.*, 1989, 111, 8566.
 143. Lii, J.-H.; Allinger, N.L., *J. Am. Chem. Soc.*, 1989, 111, 8576.
 144. Raasch, T., MSc Thesis, 2004, School of Chemistry, Faculty of Science, University of KwaZulu-Natal, Howard College Campus, Durban, 4041.
 145. Seminario, J.M.; Politzer, P. (Eds), *Modern Density Functional Theory: A Tool for Chemistry*, Elsevier Science, Amsterdam, 1998, p 11.
 146. Hohenberg, P.; Kohn, W., *Phys. Rev.*, 1964, 136B, 864.
 147. Kohn, W.; Sham, L.J., *Phys. Rev.*, 1965, A140, 1133.
 148. Hehre, W.J., *A guide to Molecular Mechanics and Quantum Chemical Calculations*, Wavefunction, Inc., Irvine, New York, 2003, p 458.
 149. Hehre, W.J.; Yu, J.; Klunzinger, P.E.; Lou, L., *A Brief Guide to Molecular Mechanics and Quantum Chemical Calculations*, Wavefunction, Inc., New York, 1998.
 150. Leach, R., *Molecular Modelling: Principles and Applications*, Addison Wesley. Longman Ltd., Oxford, England, 1996.
 151. Becke, A.D., *J. Chem. Phys.*, 1993, 98, 5648.
 152. Lee, C.; Yang, W.; Parr, R.G., *Phys. Rev.*, 1988, B37, 785.
 153. Mielich, B.; Savin, A.; Stoll, H.; Peus, H., *Chem. Phys. Lett.*, 1989, 157, 200.
 154. Young, D., *Computational Chemistry: A Practical Guide for Applying Techniques to Real World Problems*, John Wiley and Sons, Inc., New York, 2001.
 155. Badertscher, M.; Welti, M.; Portmann, P.; Pretsch, E., *Top Curr. Chem.*, 1986, 136, 17.
 156. Wipff, G.; Weiner, P.; Kollman, P., *J. Am. Chem. Soc.*, 1982, 104, 3249.
 157. Lao, K.; Tian, A.; Yan, G.; Liu, H., *J. Mol. Sci. (Int. Ed)*, 1986, 4, 333.
 158. Venayamoorthy, M., PhD Thesis, 2002, School of Chemistry, Faculty of Science, University of Natal, Durban, 4041.
 159. <http://www.chemistry.umece.maine.edu/modelling>

-
160. Momany, F.A.; McGuire, R.F.; Burgess, A.W.; Sheraga, H.A., *J. Phys. Chem.*, **1975**, 79, 2361.
 161. Nemethy, G.; Pottle, M.S.; Sheraga, H.A., *J. Phys. Chem.*, **1983**, 87, 1883.
 162. Sippl, M.J.; Nemethy, G.; Scheraga, H.A., *J. Phys. Chem.*, **1984**, 88, 6231.
 163. Allinger, N.L., *J. Am. Chem. Soc.*, **1977**, 99, 8127.
 164. Uiterwijk, J.W.H.M.; Harkema, S.; van de Waal, B.; Göbel, F.; Nibbeling, H.T.M., *J. Chem. Soc. Perkin Trans. II*, **1983**, 1843.
 165. McCammon, J.A.; Karplus, M., *Acc. Chem. Res.*, **1983**, 16, 187.
 166. Jorgensen, W.; Chandrasekar, J.; Madera, J.; Impey, R.; Klein, M., *J. Chem. Phys.*, **1983**, 926, 79.
 167. Alagona, G.; Ghio, C.; Kollman, P., *J. Am. Chem. Soc.*, **1985**, 107, 2229.
 168. Jorgensen, W.H., *J. Phys. Chem.*, **1983**, 87, 5304.
 169. <http://www.chem.swin.edu.au>.
 170. Bisetty, K., **2002**, PhD Thesis, School of Chemistry, Faculty of Science, University of Natal, Durban, 4041.
 171. <http://www.members.aol.com/btluke/smcsim.htm>.
 172. http://www.chem.ucsb.edu/~kalju/comp_tools.html.
 173. van Gunsteren, W.F.; Mark, A.E.; *J. Biochem.*, **1992**, 204, 947.
 174. Karplus, M.; Petsko, G.A., *Nature*, **1990**, 347, 631.
 175. Metropolis, N.; Rosenbluth, A.; Rosenbluth, M.; Teller, E.; Teller, E., *J. Chem. Phys.*, **1953**, 21, 1087.
 176. Kirkpatrick, S.; Gelatt, C.D.; Vecchi, M.P., *Science*, **1983**, 220, 675.
 177. Filizola, M.; Centeno, N.B.; Farina, M.C.; Perez, J.J., *J. Biomolecular Struct. and Dynamics*, **1998**, 15, 639.
 178. Corcho, F.J.; Filizola, M.; Perez, J.J., *J. Biomolecular Struct. and Dynamics*, **1999**, 5, 1043.
 179. Paulsen, M.D.; Hay, B.P., *Journal of Molecular Structure (Theochem)*, **1998**, 429, 49.
 180. Hay, B.P.; Yang, L.; Lii, J.-H.; Allinger, N.L., *Journal of Molecular Structure (Theochem)*, **1998**, 428, 203.
 181. Prof Allinger kindly assisted with the MM3 calculations required for the validation of the MM3 model. Thereafter a copy of Alchemy 2000 was purchased and used for the remainder of the calculations.
 182. Private communication with Prof. Allinger. The MM3 force field was optimised for amino acids (including the zwitterionic form) and would therefore most likely produce reasonable results for the interaction between ammonium ions and macrocycles.
 183. Marchand, A.P.; Hazlewood, A.; Huang, Z.; Vladakonda, S.K.; Rocha, J.-D.R.; Power, T.D.; Mlinaric-Majerski, K.; Klaić, L.; Kragol, G.; Bryan, J.C., *Struct. Chem.*, **2004**, 14, 279.
 184. Hockney, R.W.; Eastwood, J.W., *Computer Simulation Using Particles*, McGraw-Hill, New York, **1981**.
 185. Govender, T.; Hariprakash, H.K.; Kruger, H.G.; Marchand, A.P., *Tetrahedron Asymmetry*, **2003**, 14, 1553.
 186. Marchand, A.P.; Chong, H.-S.; Alihodžić, S.; Watson, W.H.; Bodige, S.G., *Tetrahedron*, **1999**, 55, 9687.
 187. Negano, O.; Kobayashi, A.; Sasaki, Y., *Bull. Chem. Soc. Jpn.*, **1978**, 51, 790

-
188. Bradshaw, J.S.; Maas, G.E.; Lamb, J.D.; Izatt, R.M.; Christensen, J.J., *J. Am. Chem. Soc.*, **1980**, 102, 467.
 189. Laidler, D.A.; Stoddart, J.F., *Tetrahedron Lett.*, **1979**, 453.
 190. Beckford, H.F.; King, R.M.; Stoddart, J.F.; Newton, R.F., *Tetrahedron Lett.*, **1978**, 171.
 191. Huszthy, P.; Oue, M.; Bradshaw, J.S.; Zhu, C.Y.; Wang, T.; Dalley, N.K.; Curtis, J.C.; Izatt, R.M., *J. Org. Chem.*, **1992**, 57, 5383.
 192. Chu, I.H.; Dearden, D.V.; Bradshaw, J.S.; Huszthy, P.; Izatt, R.M., *J. Am. Chem. Soc.*, **1993**, 115, 4318
 193. <http://www.ncsr.ie/htm>.
 194. Bradshaw, J.S.; Jolley, S.T.; Izatt, R.M., *J. Org. Chem.*, **1982**, 47, 1229.
 195. Fuhrhop, J.; Penzlin, G., *Organic Synthesis: Concepts, Methods, Starting materials*, Verlag Chemie, Weinheim, **1984**.
 196. Anelli, P.L.; Montanari, F.; Quici, S., *J. Org. Chem.*, **1988**, 53, 5292.
 197. Stoddart, J.F., *Comprehensive Organic Chemistry: The synthesis, reactions, preparations and applications of co-ordination compounds*, Vol 1, Pergamon Press, New York, **1987**.
 198. Wang, S.-S.; Gisin, B.F.; Winter, D.P.; Makofske, R.; Kulesha, I.D.; Tzougraki, C.; Meienhofer, J., *J. Org. Chem.*, **1977**, 42, 1286.
 199. de Vries, J.G.; Kellog, R.M., *J. Am. Chem. Soc.*, **1979**, 101, 2759.
 200. Piepers, O.; Kellog, R.M., *J. Chem. Soc. Chem. Commun.*, **1978**, 383.
 201. Coterón, J.M.; Vicent, C.; Bosso, C.; Penadés, S., *J. Am. Chem. Soc.*, **1993**, 115, 10066.
 202. Nishiyama, T.; Kameyama, H.; Maekawa, H.; Watanki, K., *Can. J. Chem.*, **1999**, 77, 258.
 203. Vedejs, E.; Engler, D.A.; Mullins, M.J., *J. Org. Chem.*, **1977**, 42, 19, 3109.
 204. Stang, P.J.; Hanack, M.; Subramanian, L.R., *Synthesis*, **1982**, 85.
 205. Penadés, S.; Coterón, J.M., *J. Chem. Soc. Chem. Commun.*, **1992**, 683.
 206. Flores-Santos, L.; Martin, E.; Diéguez, M.; Masdeu-Bultó, A.M.; Claver, C., *Tetrahedron Asymmetry*, **2001**, 12, 3029.
 207. Hembre, R.T.; Scott, C.P.; Norton, J.R., *J. Org. Chem.*, **1987**, 52, 3650.
 208. Cassel, S.; Debaig, C.; Benvegnu, T.; Chaimbault, P.; Lafosse, M.; Plusquellec, D.; Rollin, P., *Eur. J. Org. Chem.*, **2001**, 875.
 209. Marchand, A.P.; Huang, Z.; Chen, Z.; Hariprakash, H.K.; Namboothiri, I.N.N.; Brodbelt, J.S.; Reyzer, M.L., *J. Heterocycl. Chem.*, **2001**, 38, 1361.
 210. Marchand, A.P.; Alihodžić, S.; McKim, A.S.; Kumar, K.A.; Mlinarić-Majerski, K.; Šumanovac, T., *Tetrahedron Lett.*, **1998**, 39, 1861.
 211. Marchand, A.P.; Cal, D.; Mlinarić-Majerski, K.; Ejsmont, K.; Watson, W.H., *J. Chem. Cryst.*, **2002**, 11, 447.
 212. Naemura, K.; Nishikawa, Y.; Fuji, J.; Hirose, K.; Tobe, Y., *Tetrahedron Asymmetry*, **1997**, 8, 6.
 213. Ichihara, A.; Ubukata, M.; Sakamura, S., *Tetrahedron Lett.*, **1977**, 39, 3473.
 214. Greene, T.W., *Protective Groups in Organic Synthesis*, John Wiley & Sons, New York, **1981**, p34
 215. Chaudhary, S.K.; Hernandez, O., *Tetrahedron Lett.*, **1979**, 2, 99.
 216. Chaudhary, S.K.; Hernandez, O., *Tetrahedron Lett.*, **1979**, 2, 95.

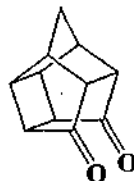
-
217. Fourie, L.; Govender, T.; Hariprakash, H.K.; Kruger, H.G.; Raasch, T., *Magn. Reson. Chem.*, **2004**, 42, 617.
218. Govender, T.; Kruger, H.G.; Raasch, T., *Struct. Chem.*, **2005**, 16, 129.
219. Marchand, A.P.; Arney, B.E., Jr.; Dave, P.R.; Satyanarayana, N.; Watson, W.H.; Nagl, A., *J. Org. Chem.*, **1988**, 53, 2644.
220. Craze, G.A.; Watt, I., *J. Chem. Soc., Perkin Trans. I*, **1981**, 2175.
221. Martins, F.J.C.; Coetzee, G.H.; Fourie, L.; Venter, H.J.; Viljoen, A.M.; Wessels, P.L., *Magn. Reson. Chem.*, **1993**, 31, 578.
222. Cadd, D.H.; Feast, W.J.; Kenwright, A.M.; Say, J.M., *Magn. Reson. Chem.*, **1993**, 31, 801.
223. Kruger, H.G., PhD Thesis, **1996**, Department of Chemistry, Potchefstroom University for Christian Higher Education, Potchefstroom.
224. Martins, F.J.C.; Viljoen, A.M.; Coetzee, M.; Fourie, L.; Wessels, P.L., *Tetrahedron*, **1991**, 47, 9215.
225. Martins, F.J.C.; Viljoen, A.M.; Kruger, H.G.; Joubert, J.A., *Tetrahedron*, **1993**, 49, 9573.
226. Martins, F.J.C.; Viljoen, A.M.; Kruger, H.G.; Wessels, P.L., *Tetrahedron*, **1993**, 49, 6527.
227. Martins, F.J.C.; Viljoen, A.M.; Kruger, H.G.; Joubert, J.; Wessels, P.L., *Tetrahedron*, **1994**, 50, 10783.
228. Fourie, L.; Martins, F.J.C.; Viljoen, A.M.; Kruger, H.G., *Amino Acids*, **1993**, 5, 137.
229. Klunder, A.J.H.; Zwanenburg, B., *Chem. Rev.*, **1989**, 89, 1035.
230. Marchand, A.P.; Reddy, G.M.; Watson, W.H.; Kashyap, R.P.; Nagl, A., *J. Org. Chem.*, **1991**, 56, 277.
231. Mehta, G.; Singh, V.; Srikrishna, A.; Cameron, T.S.; Chan, C., *Tetrahedron Lett.*, **1979**, 4595.
232. Sasaki, T.; Eguchi, S.; Kiriya, T.; Hiroaki, O., *Tetrahedron*, **1974**, 30, 2707.
233. Bott, S.G.; Marchand, A.P.; Alihodzic, S.; Kumar, K.A.; *J. Chem. Cryst.*, **1998**, 28, 251.
234. Kruger, H.G.; Martins, F.J.C.; Viljoen, A.M.; Boeyens, J.C.A.; Cook, L.M.; Levendis, D.C., *Acta Cryst.*, **1996**, B52, 838.
235. Watson, W.H.; Kashyap, R.P.; Krawiec, M.; Marchand, A.P.; Tsay, F.-R., *Struct. Chem.*, **1994**, 5, 1.
236. Marchand, A.P.; Keith, J.M.; Alihodžić, S.; Ganguly, B.; Somers, A.W.; Hariprakash, H.K.; Power, T.D.; Watson, W.H.; Bodige, S.G., *Struct. Chem.*, **2001**, 12, 313.
237. Linden, A.; Romanski, J.; Mlostoń, G.; Heimgartner, H., *Acta Cryst.*, **2005**, C61, 221.
238. Watson, W.H.; Kashyap, R.; Marchand, A.P.; Vidyasagar, V., *Acta Cryst.*, **1990**, C46, 928.
239. Watson, W.H.; Nagl, A.; Kashyap, R.P.; Marchand, A.P.; Zhao, D., *Acta Cryst.*, **1989**, C45, 1346.
240. Kruger, H.G.; Rademeyer, M.; Ramdhani, R., *Acta Cryst.*, **2005**, E61, 3968.
241. Kruger, H.G.; Rademeyer, M.; Ramdhani, R., *Acta Cryst.*, **2006**, E62, 966.
242. Kruger, H.G.; Rademeyer, M.; Ramdhani, R., *Acta Cryst.*, **2006**, E61, 268.

243. Dale, J.A.; Mosher, H.S., *J. Org. Chem.*, **1970**, 35, 4002.

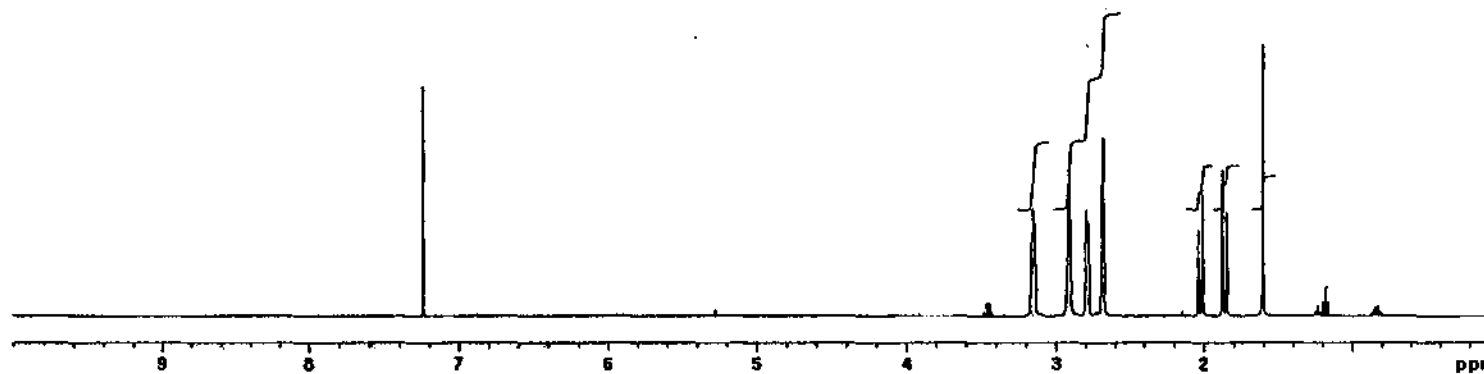
APPENDIX ONE

SPECTRA

hdione.dione in cdcl3
probe=5mmASW
Pulse Sequence: s2pul



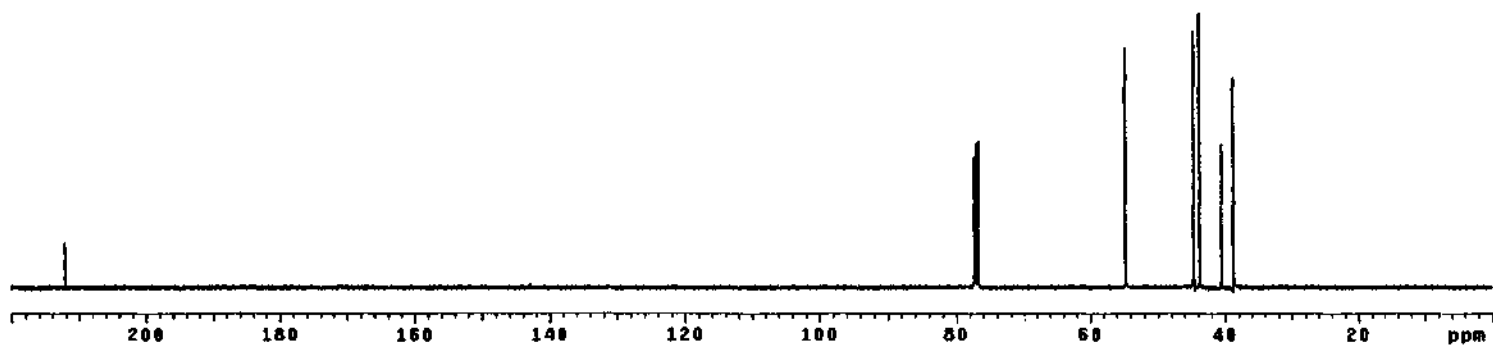
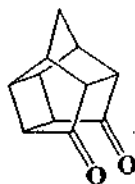
INDEX	FREQUENCY	PPM	HEIGHT
1	2895.544	7.240	42.4
2	1263.485	3.159	15.7
3	1262.030	3.158	15.8
4	1260.198	3.151	20.1
5	1258.367	3.146	17.0
6	1256.902	3.143	17.0
7	1253.972	3.135	9.8
8	1176.099	2.928	11.1
9	1167.718	2.920	20.5
10	1165.887	2.915	27.4
11	1164.971	2.913	19.8
12	1164.055	2.911	28.4
13	1162.224	2.906	20.0
14	1160.678	2.902	9.4
15	1159.843	2.900	11.5
16	1120.654	2.802	13.9
17	1113.855	2.799	17.8
18	1118.456	2.797	20.0
19	1110.080	2.796	19.8
20	1116.075	2.791	17.5
21	1114.610	2.787	15.7
22	1119.878	2.785	17.6
23	1113.329	2.784	17.8
24	1112.413	2.781	17.5
25	1111.131	2.778	14.6
26	1073.408	2.684	33.2
27	815.560	2.039	16.1
28	804.206	2.011	22.9
29	752.381	1.881	14.0
30	750.915	1.878	27.1
31	749.450	1.874	14.9
32	741.027	1.853	10.2
33	739.581	1.848	19.5
34	738.896	1.846	10.6
35	642.197	1.606	80.0



SPECTRUM 1: ¹H NMR spectrum of dione (20) in CDCl₃

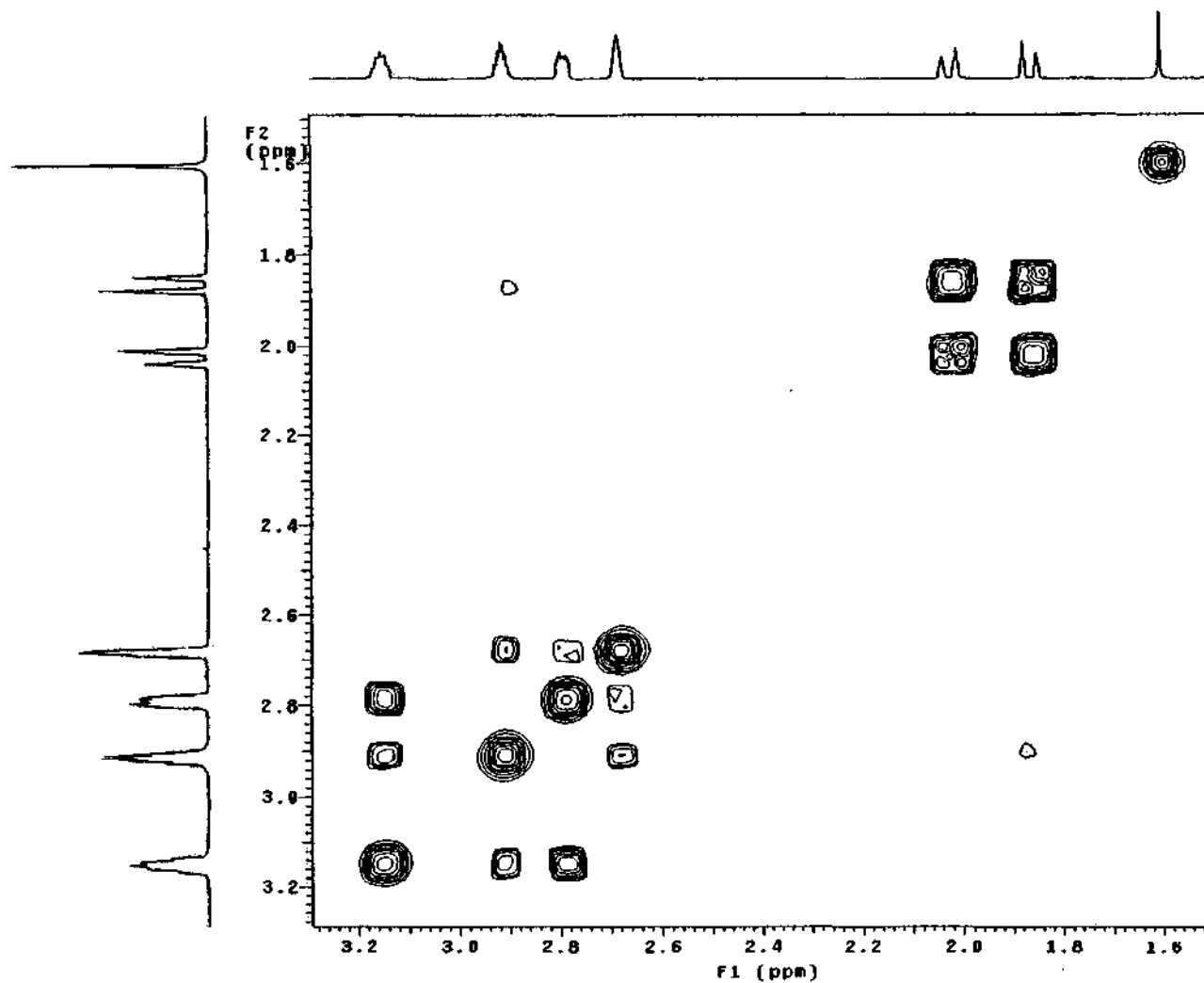
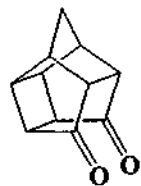
cdione.dione in cdc
probe=5mmA3W
Pulse Sequence: s2pu1

INDEX	FREQUENCY	PPM	HEIGHT
1	21328.588	212.058	8.5
2	7775.581	77.320	24.3
3	7743.445	77.000	26.7
4	7711.310	76.680	27.0
5	5488.722	54.688	43.3
6	4488.215	44.610	46.8
7	4408.520	43.758	50.0
8	4068.452	40.456	26.4
9	3692.443	36.711	38.2



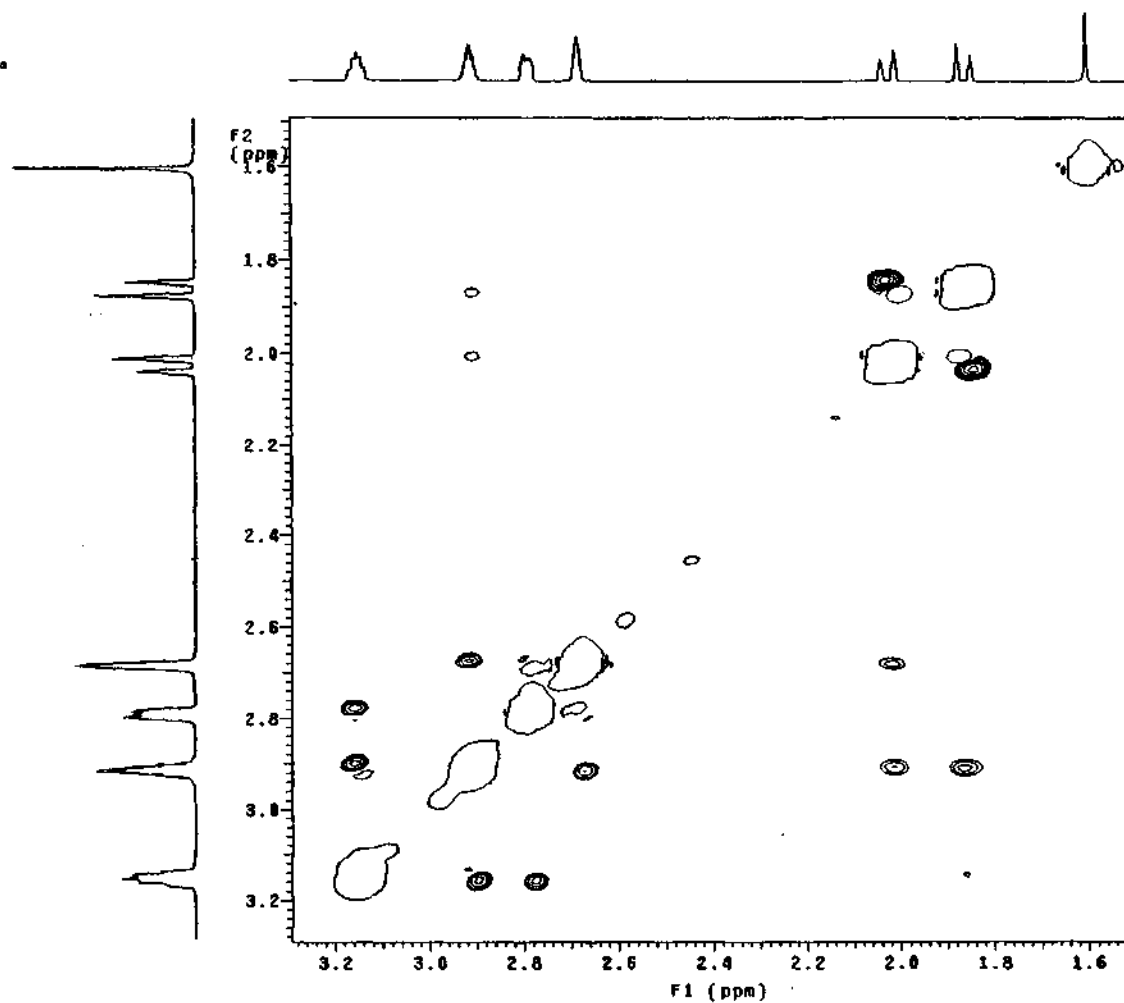
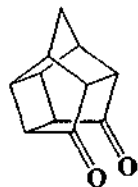
SPECTRUM 2: ^{13}C NMR spectrum of dione (20) in CDCl_3

cydione.dione in cdcl3
1H Cosy-90
probe-SmASV
Pulse Sequence: relayh



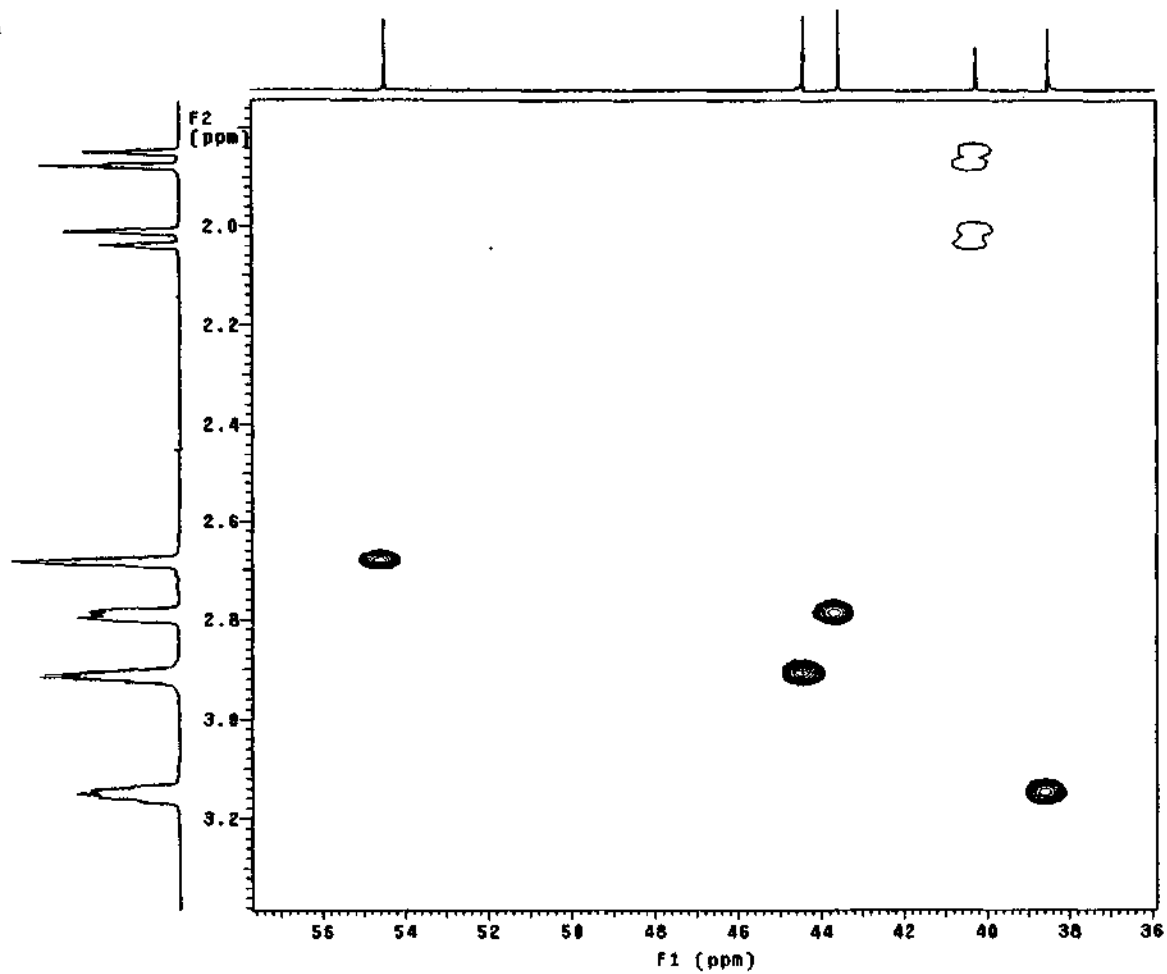
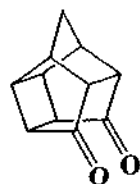
SPECTRUM 3: COSY spectrum of dione (20) in CDCl₃

NOESY.dione in cdcl3
NOESY expt.
mix=1sec
probe=5mmASV
Pulse Sequence: noesy_da



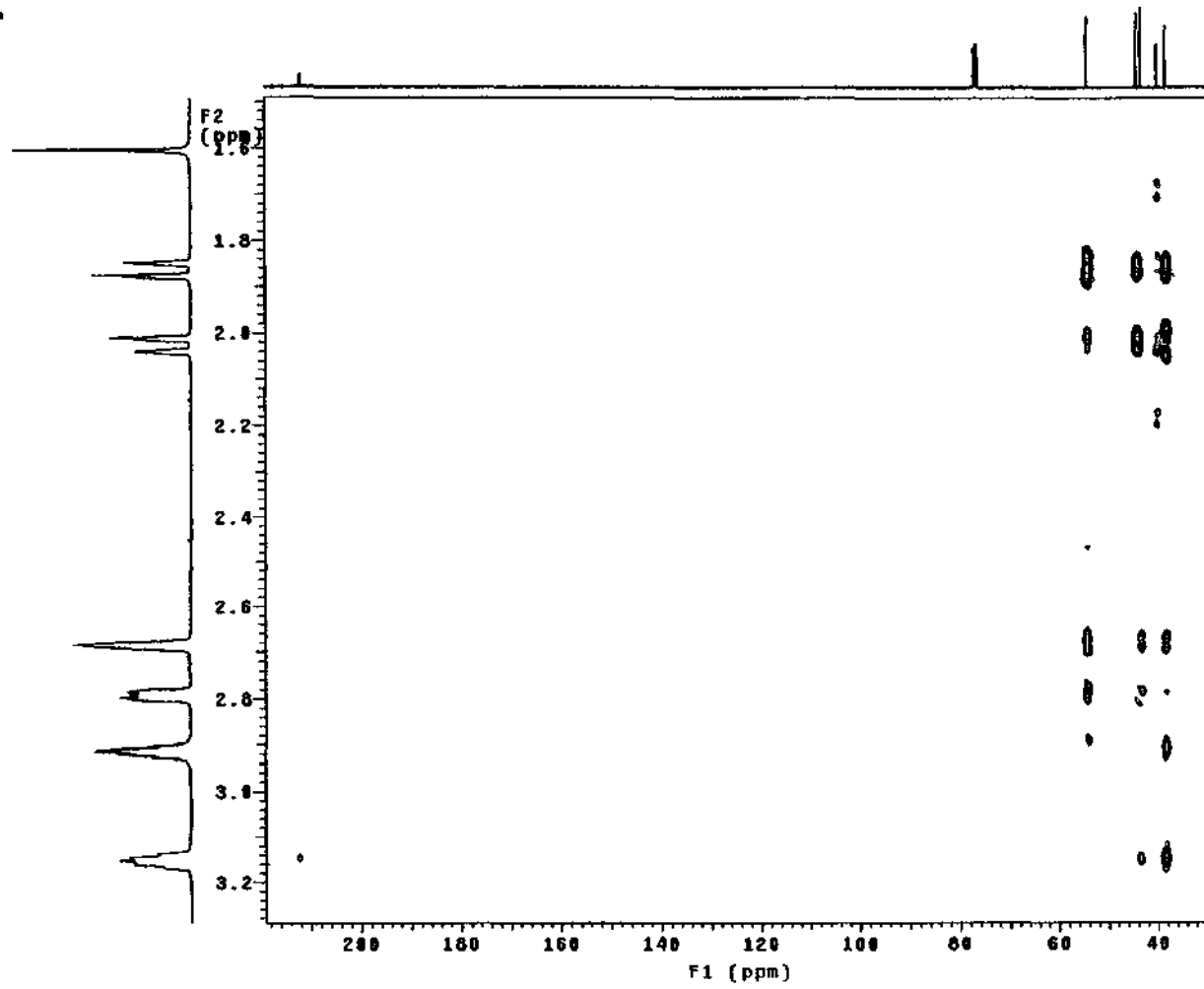
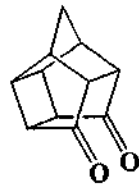
SPECTRUM 4: NOESY spectrum of dione (20) in CDCl₃

HDione.dione in cdcl3
Gradient HSQC expt.
with mult.editing
probe=5mmASV
Pulse Sequence: ghsqc_dg

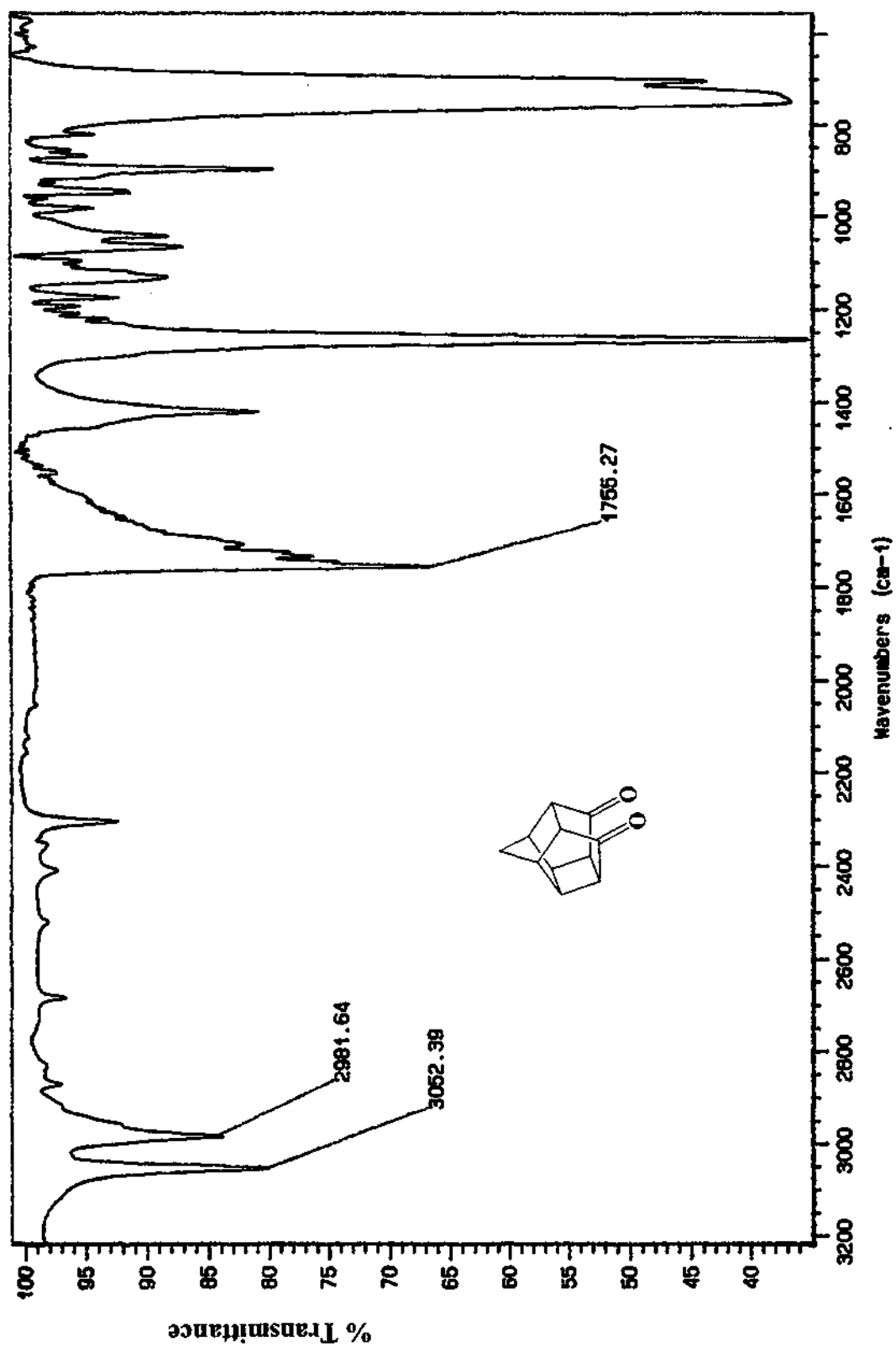


SPECTRUM 5: HSQC spectrum of dione (20) in CDCl₃

nmr001.d1000 01-14-13
Gradient HMQC expt.
probe=5mmASV
Pulse Sequence: ghmqc_da

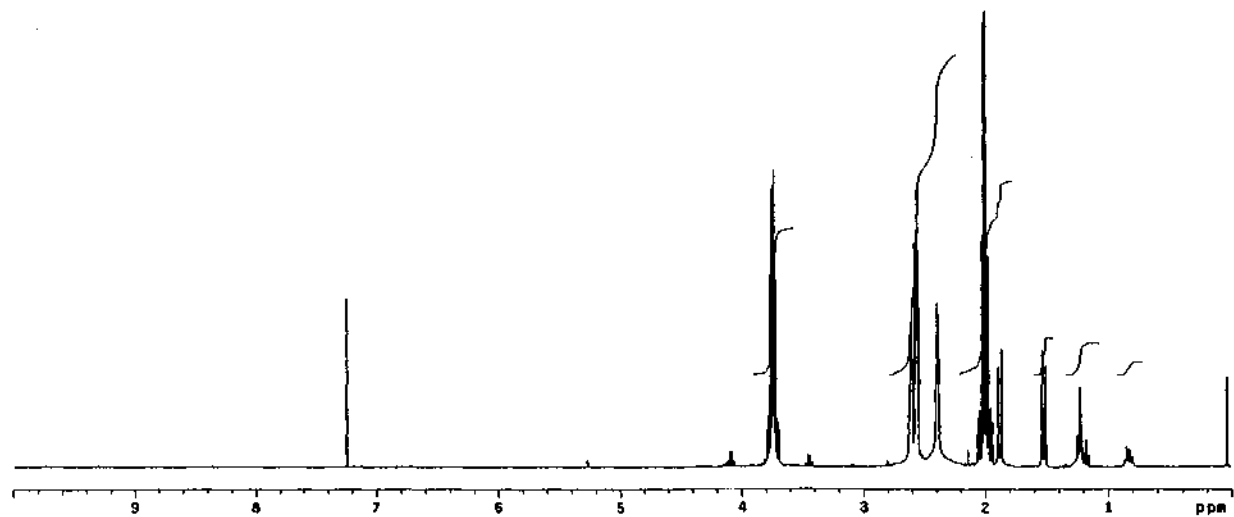
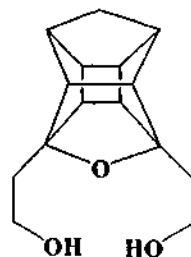


SPECTRUM 6: HMBC spectrum of dione (20) in CDCl_3



SPECTRUM 7: Infrared spectrum (NaCl) of dione (20)

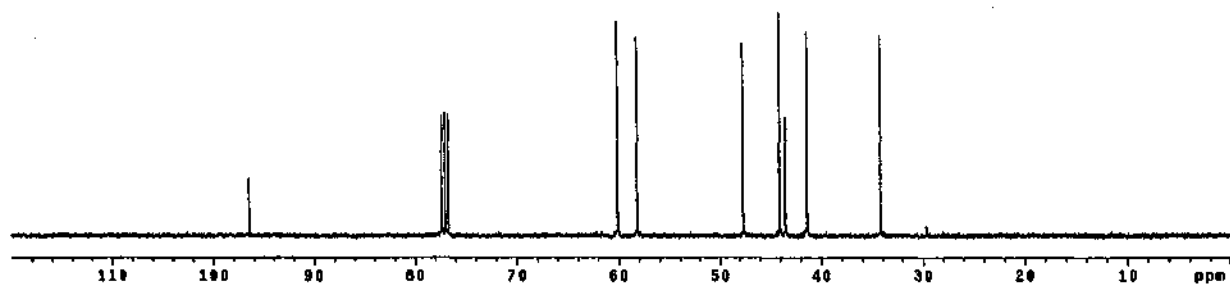
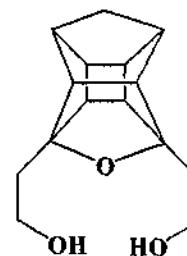
hfil07.d103 in cdcl3
probe=5mmASV
Pulse Sequence: zgpg1



SPECTRUM 8: ^1H NMR spectrum of diol (25) in CDCl_3

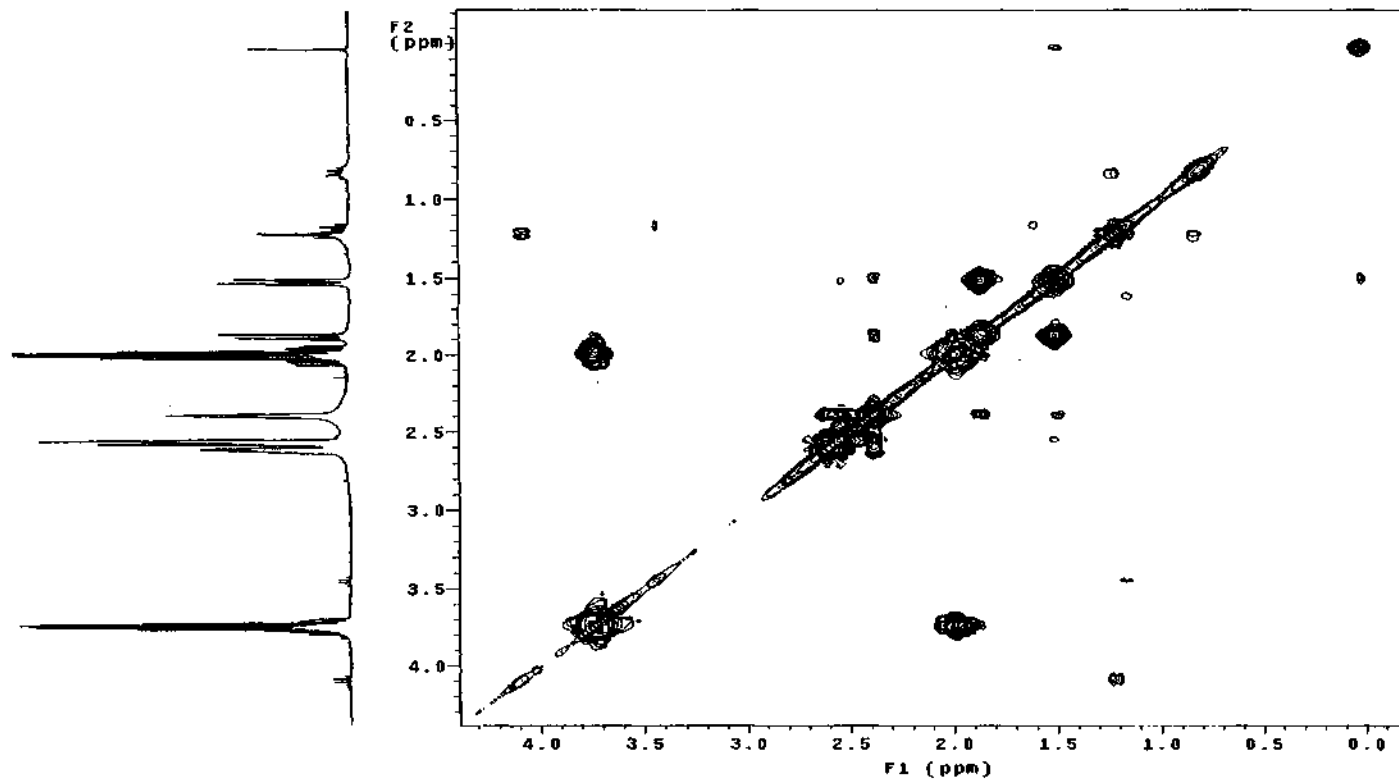
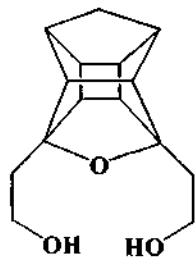
cdcl3.d101 in cdcl3
probe=mm4sv
Pulse Sequence: 42pt1

INDEX	FREQUENCY	PPM	HEIGHT
1	9858.887	96.415	10.9
2	7771.490	77.318	27.1
3	7742.448	77.000	27.7
4	7713.406	76.682	27.2
5	6040.519	60.000	48.0
6	5047.482	48.147	44.5
7	4780.760	47.438	43.2
8	4426.888	44.080	60.8
9	4371.870	43.481	28.8
10	4159.888	41.385	45.8
11	3949.558	38.210	40.8



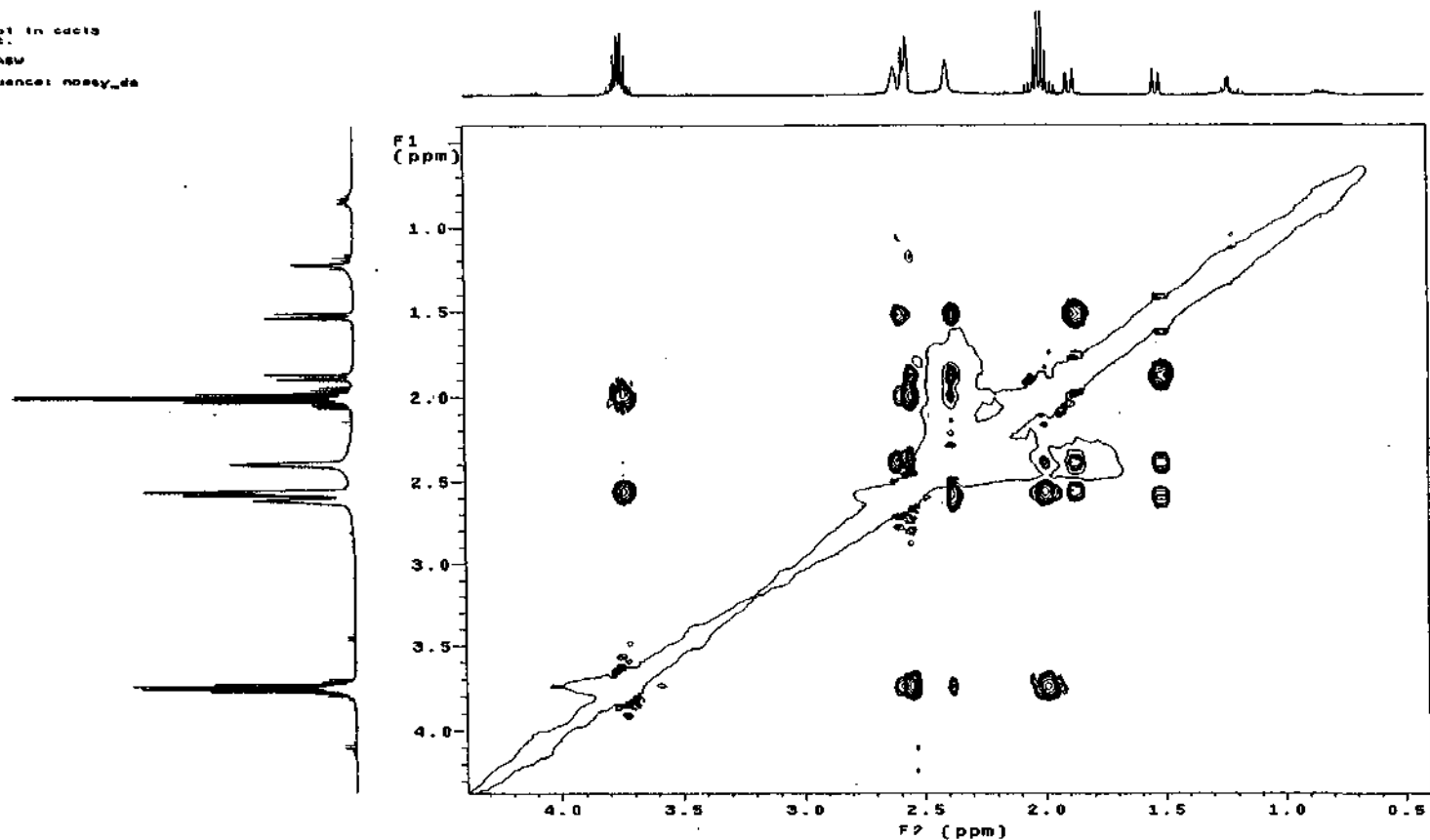
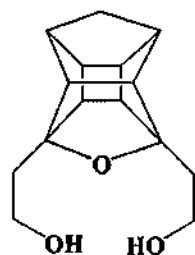
SPECTRUM 9: ¹³C NMR spectrum of diol (25) in CDCl₃

cyd101.d101 in cdcl3
in cosy-90
probe=5mmQNP
Pulse Sequence: relayh



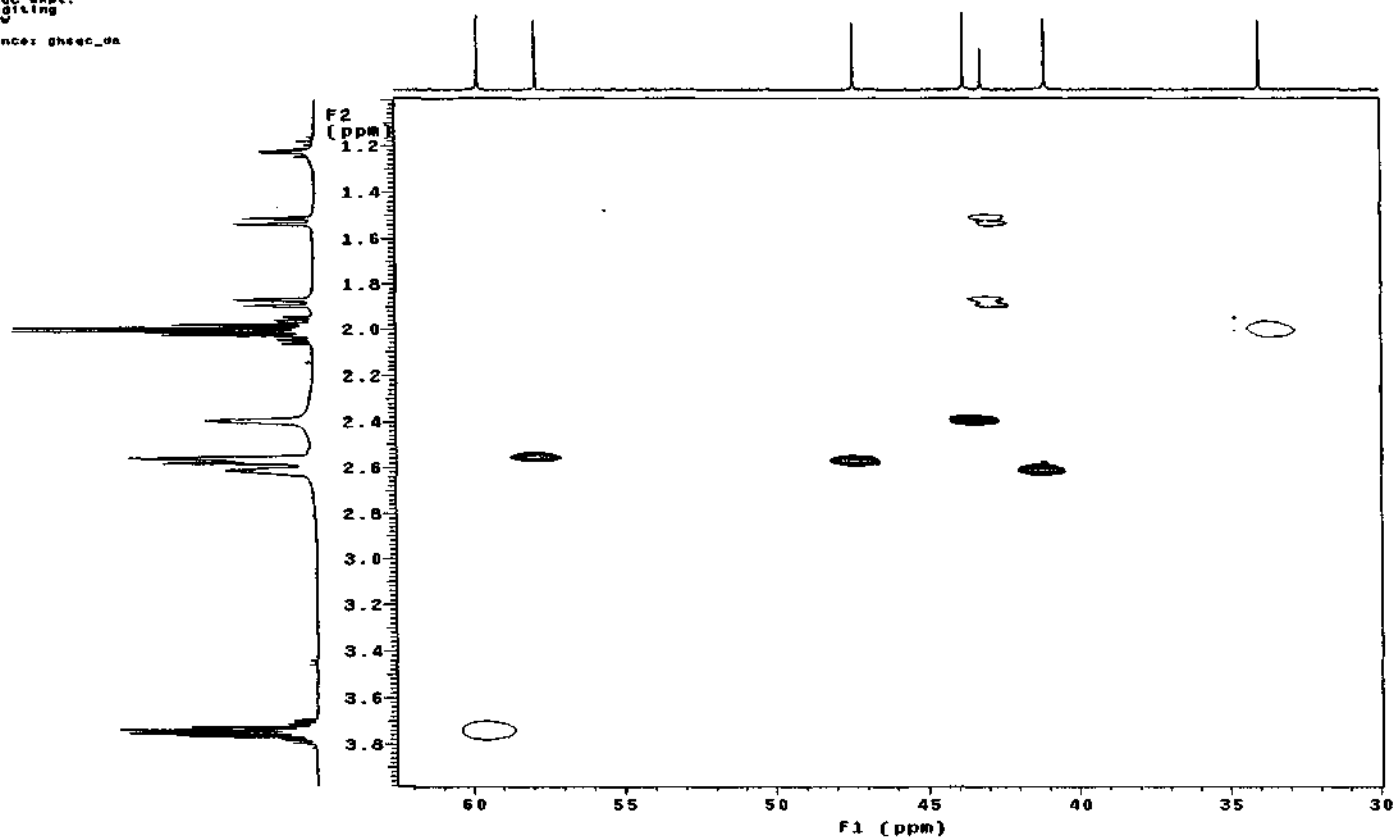
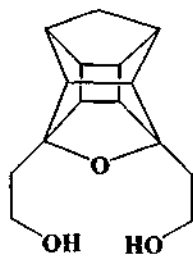
SPECTRUM 10: COSY spectrum of diol (25) in CDCl₃

NOESY.d101 in cdc13
NOESY exp.
mix=188c
probe=5mmAGW
Pulse Sequence: noesy_da



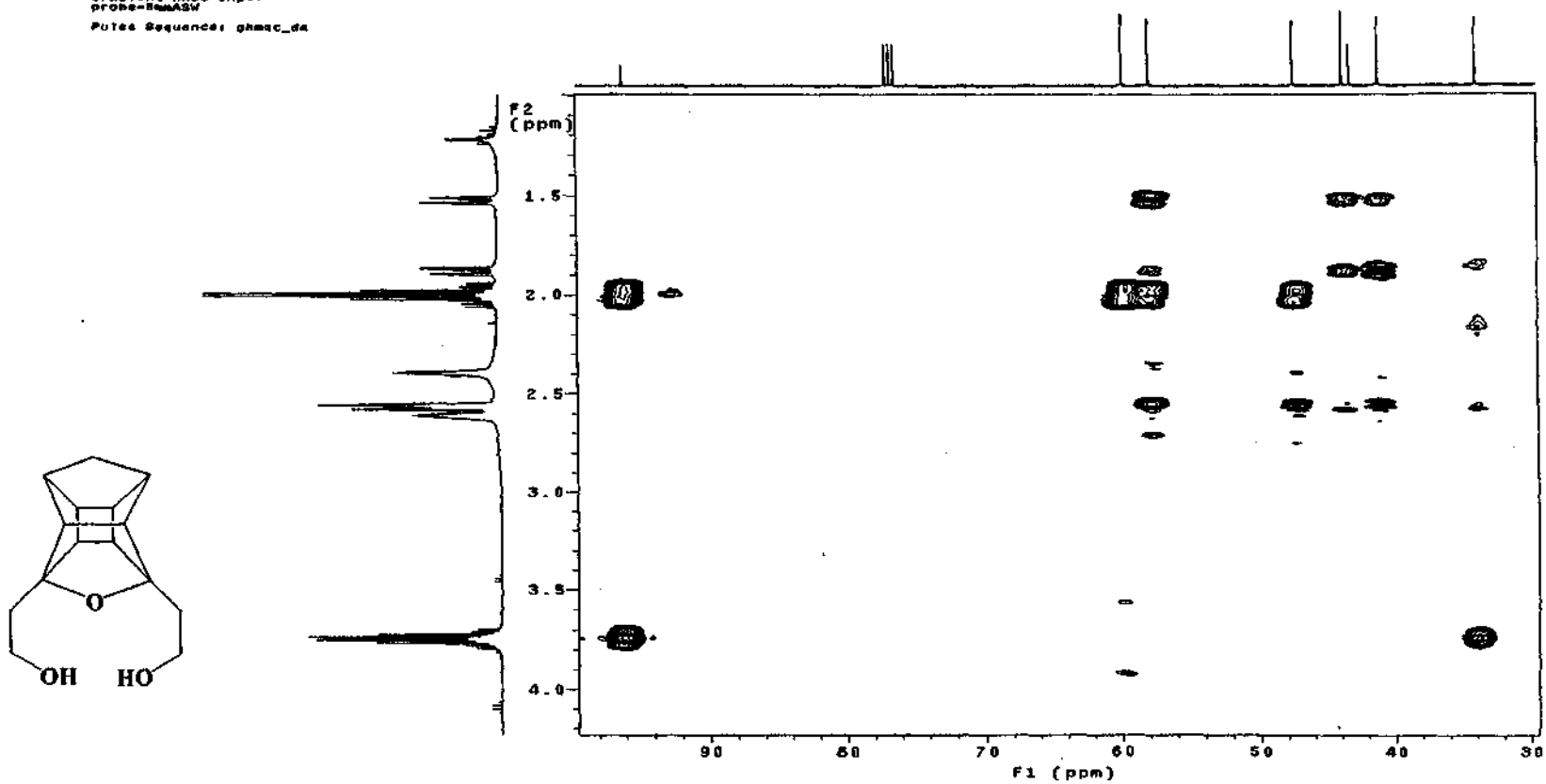
SPECTRUM 11: NOESY spectrum of diol (25) in CDCl₃

HOdiol.d101 in cdcl3
Gradient HSQC expt.
with mult. editing
probe=5mm43v
Pulse Sequence: ghsqc_da

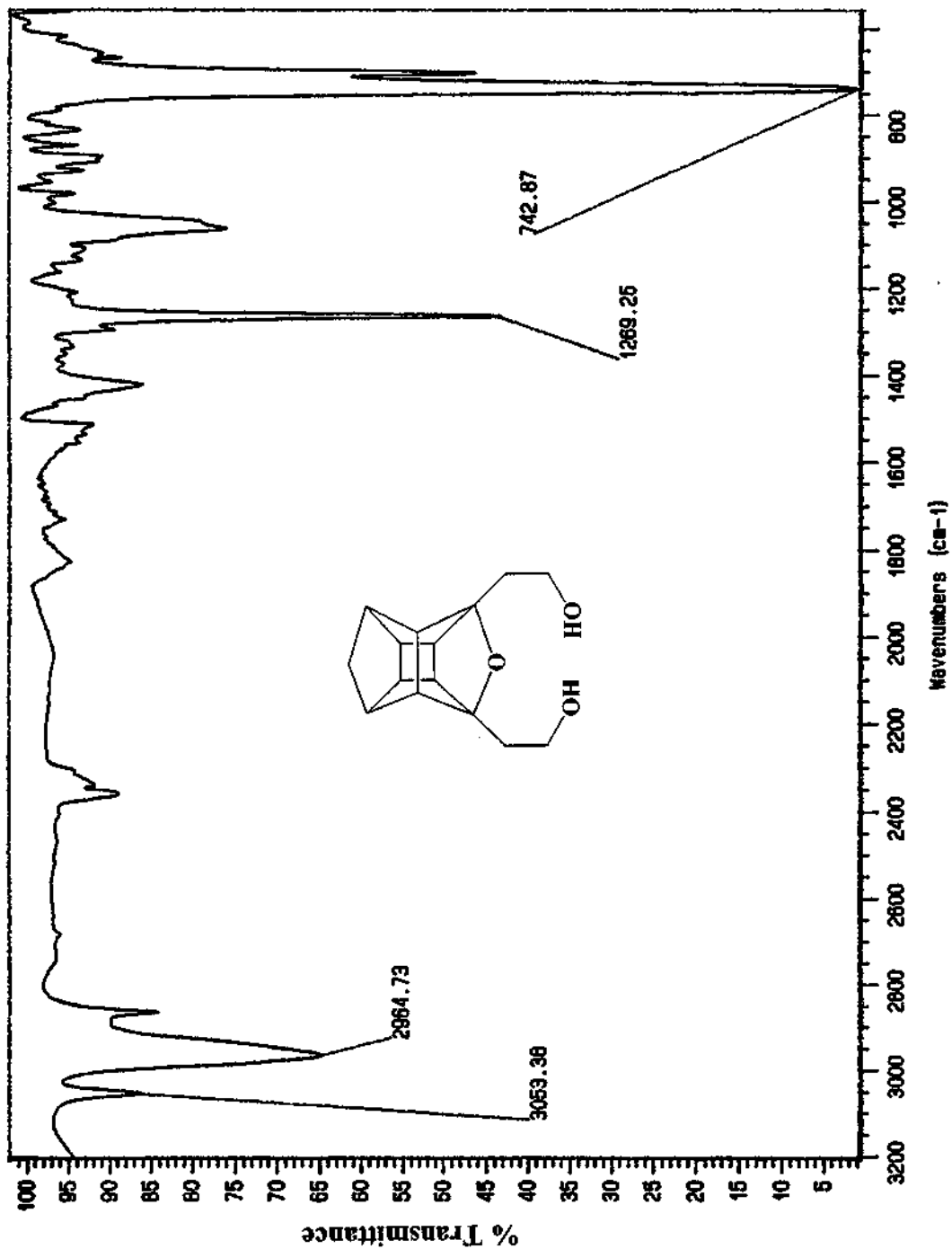


SPECTRUM 12: HSQC spectrum of diol (25) in CDCl_3

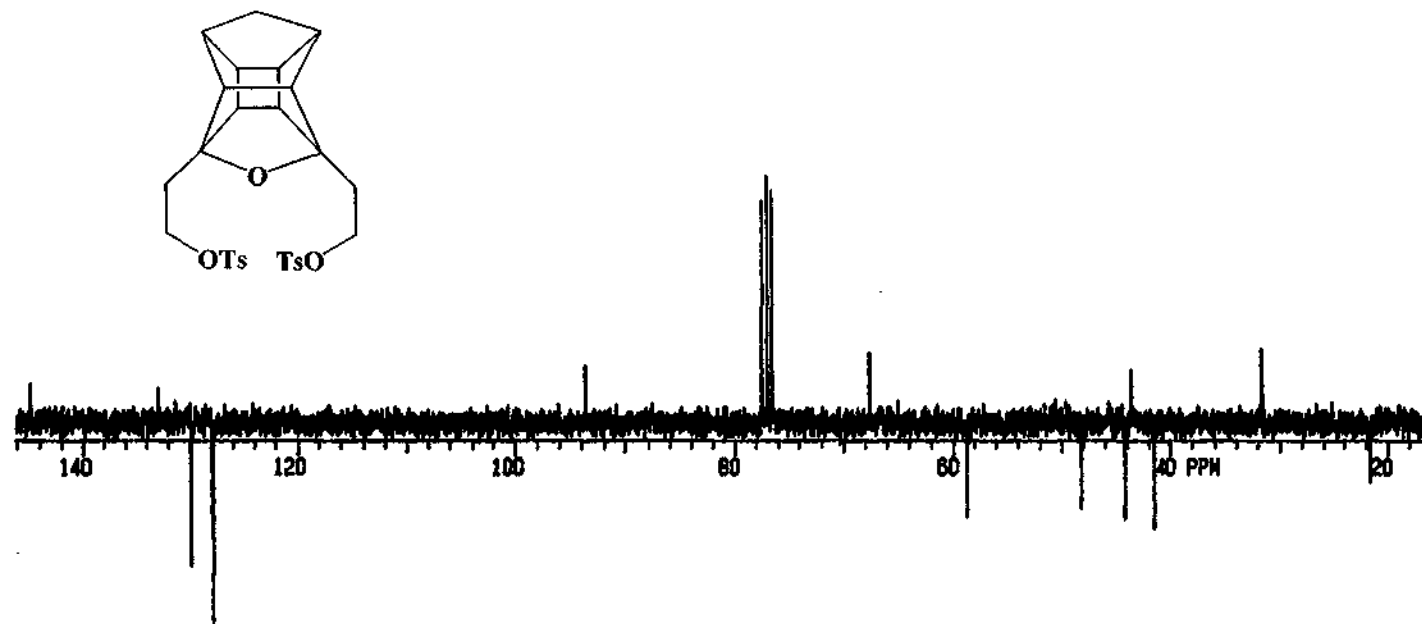
hbdol.d1a1 in cdcl3
Gradient HMQC expt.
probe-BBPA3V
Pulse Sequence: ghmec_da



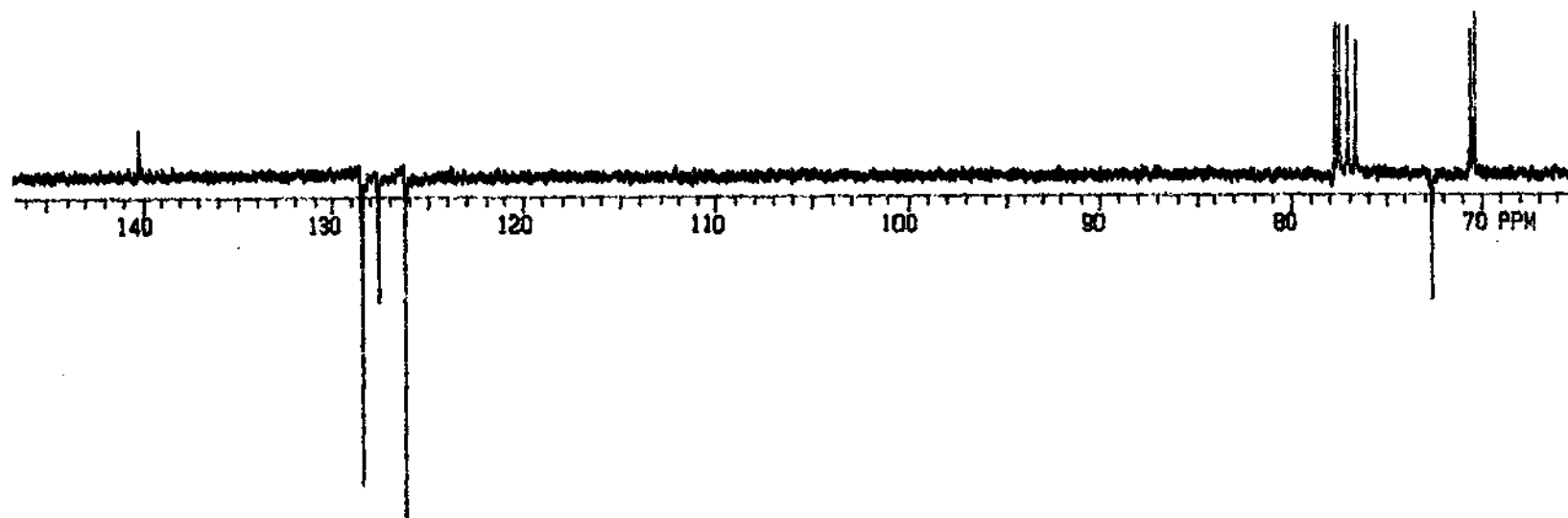
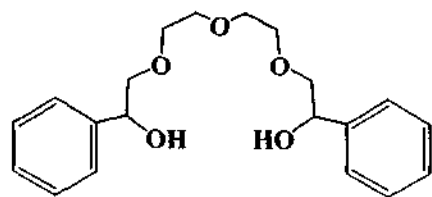
SPECTRUM 13: HMBC spectrum of diol (25) in CDCl₃



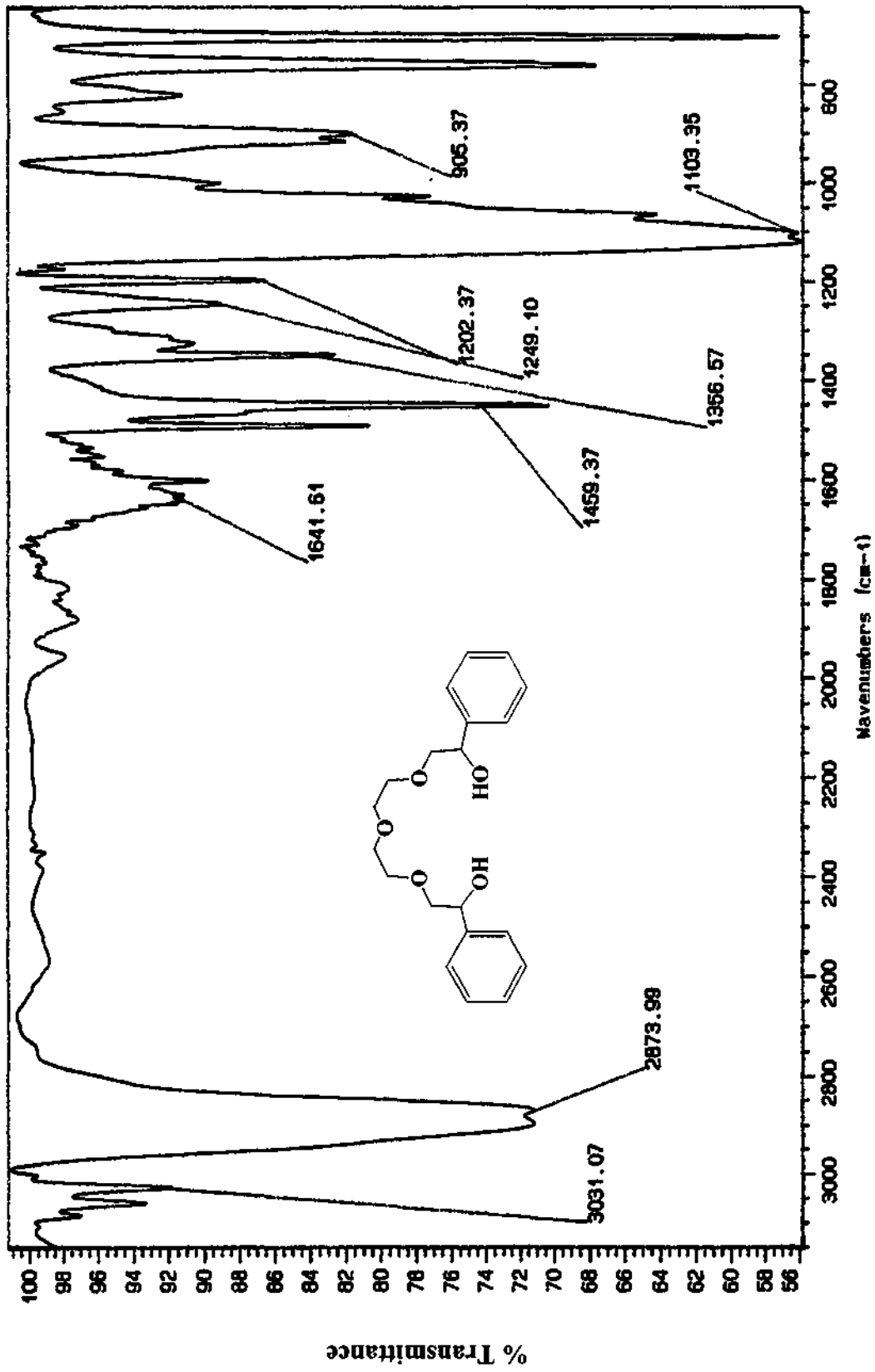
SPECTRUM 14: Infrared spectrum (NaCl) of diol (25)



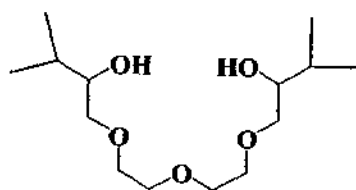
SPECTRUM 15: ^{13}C NMR spectrum of cage ditosylate (54) in CDCl_3



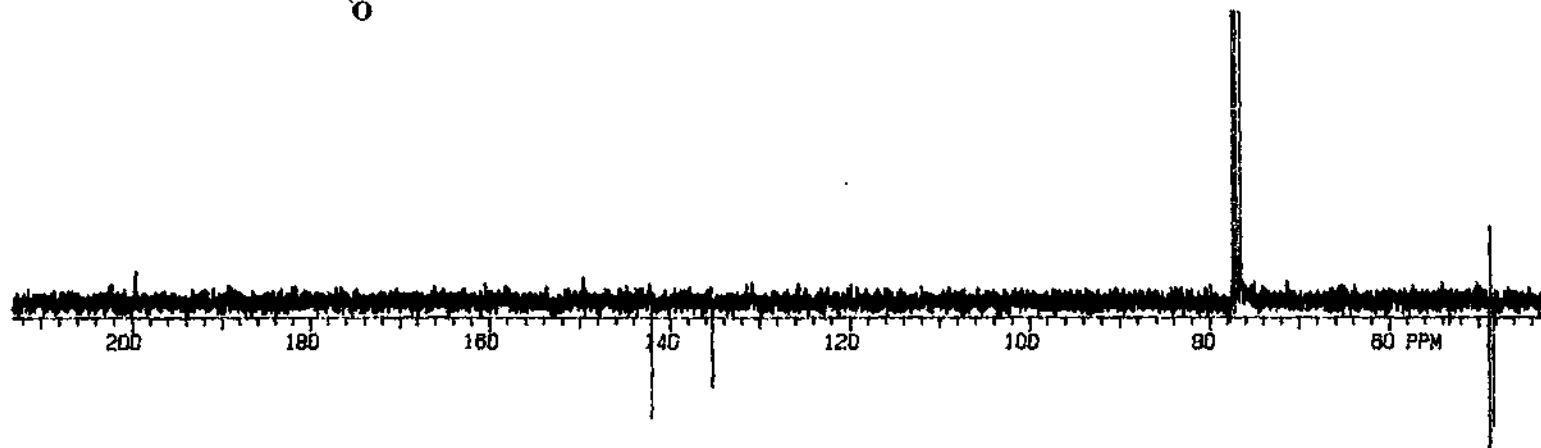
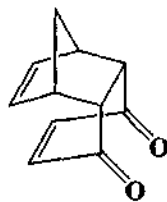
SPECTRUM 16: ^{13}C NMR spectrum of mandelic glycol (55) in CDCl_3



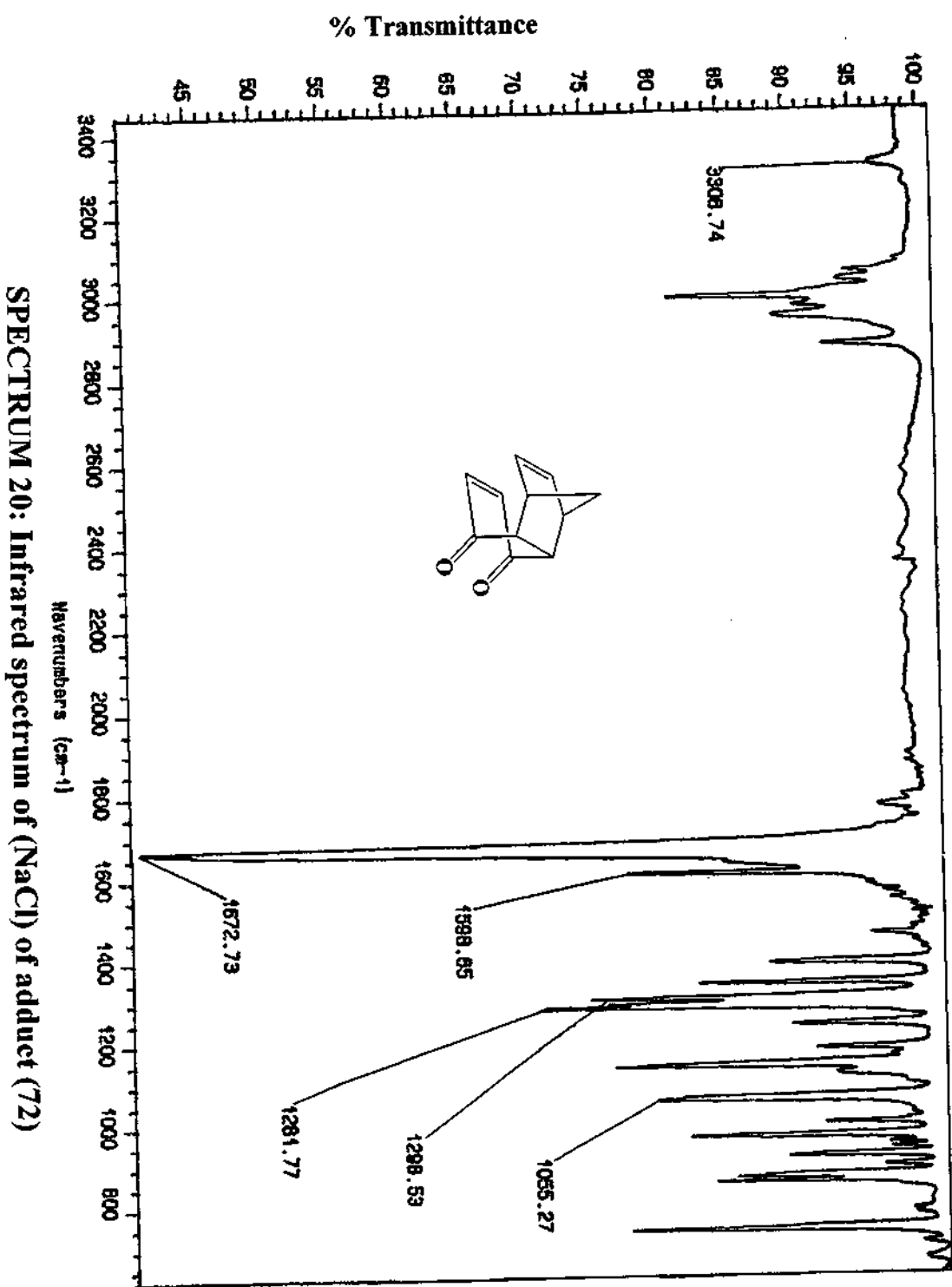
SPECTRUM 17: Infrared spectrum (NaCl) of mandelic glycol (55)



SPECTRUM 18: ¹³C NMR spectrum of isopropyl glycol (56) in CDCl₃

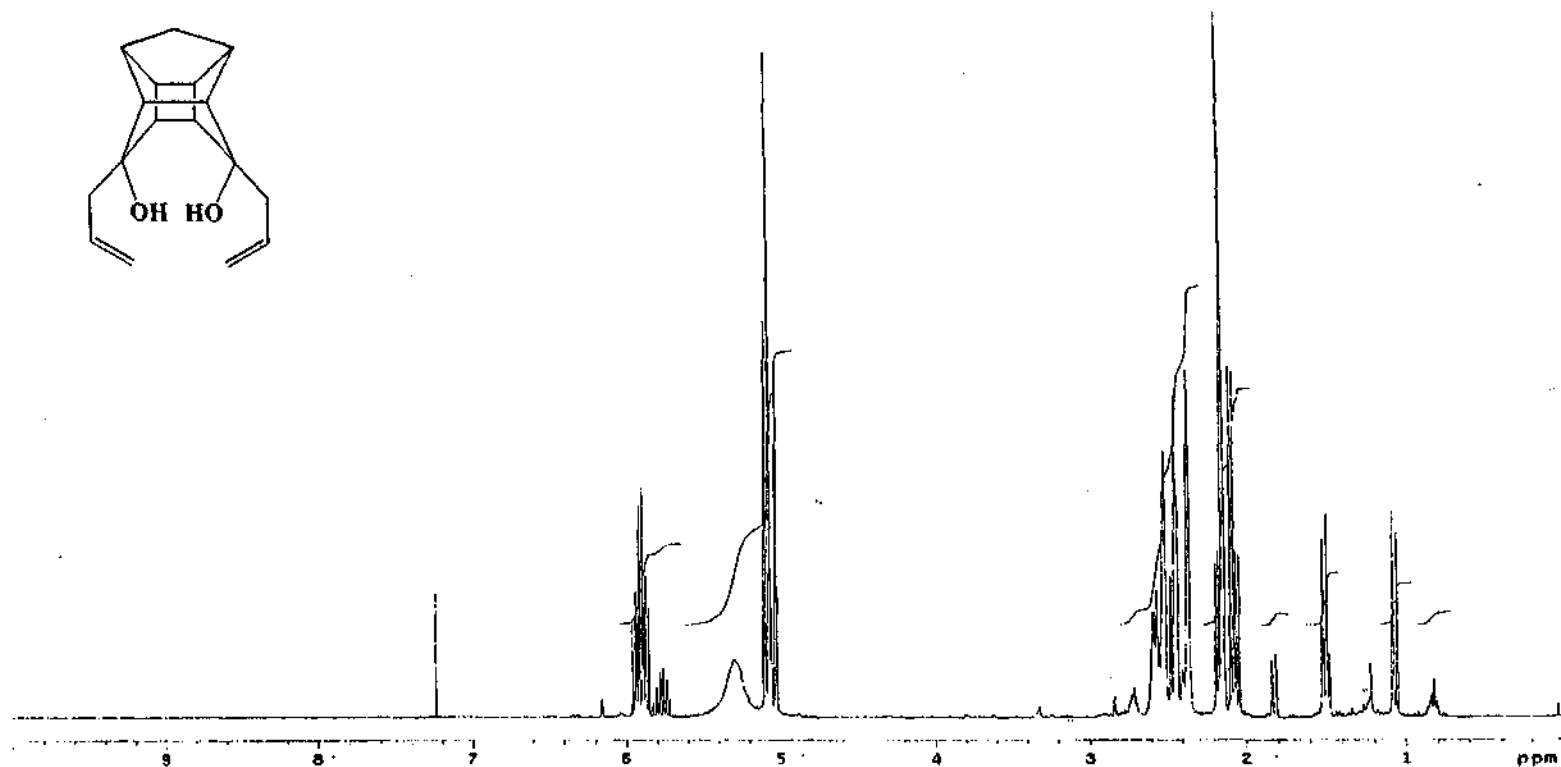
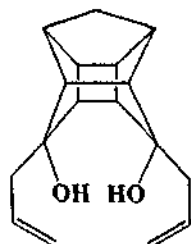


SPECTRUM 19: ^{13}C NMR spectrum of adduct (72) in CDCl_3



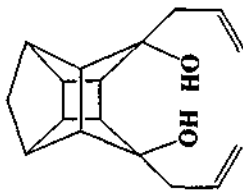
SPECTRUM 20: Infrared spectrum of (NaCl) of adduct (72)

hediol_endo_endo_diol_in_cdc13
probe=5mmASW
Pulse Sequence: zgpg1

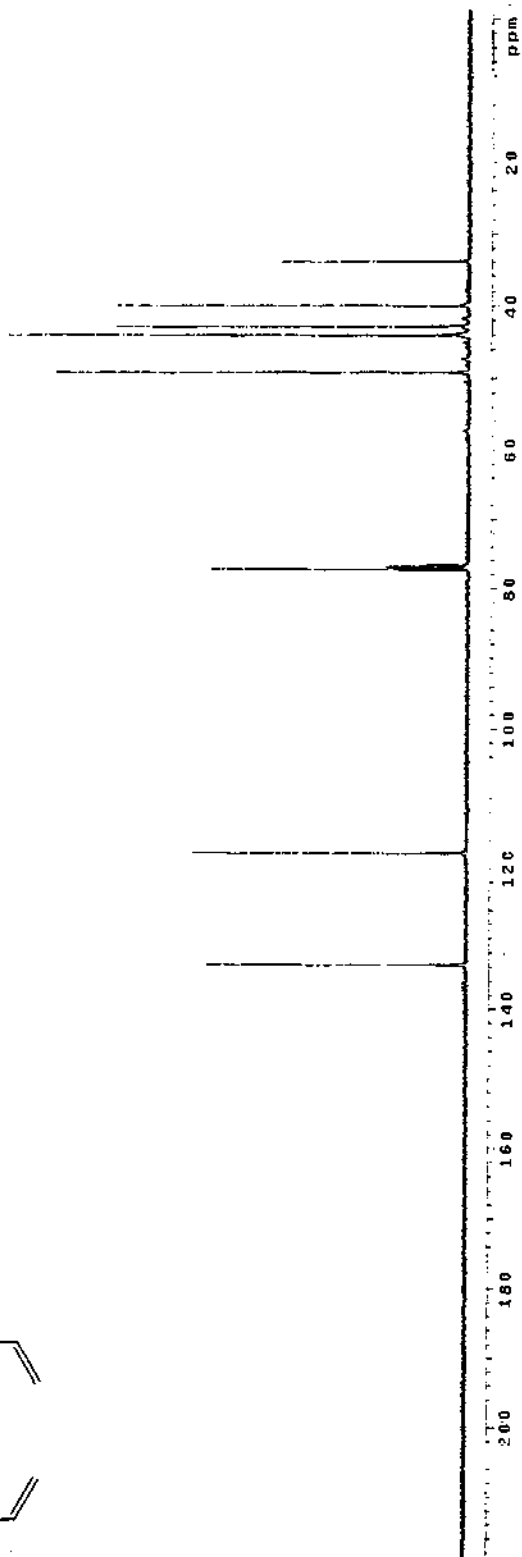


SPECTRUM 21: ¹H NMR spectrum of endo-endo diol (73) in CDCl₃

endo,endo endo diol in cdc13
 Probe=5mmASW
 Pulse Sequence: zgpg30

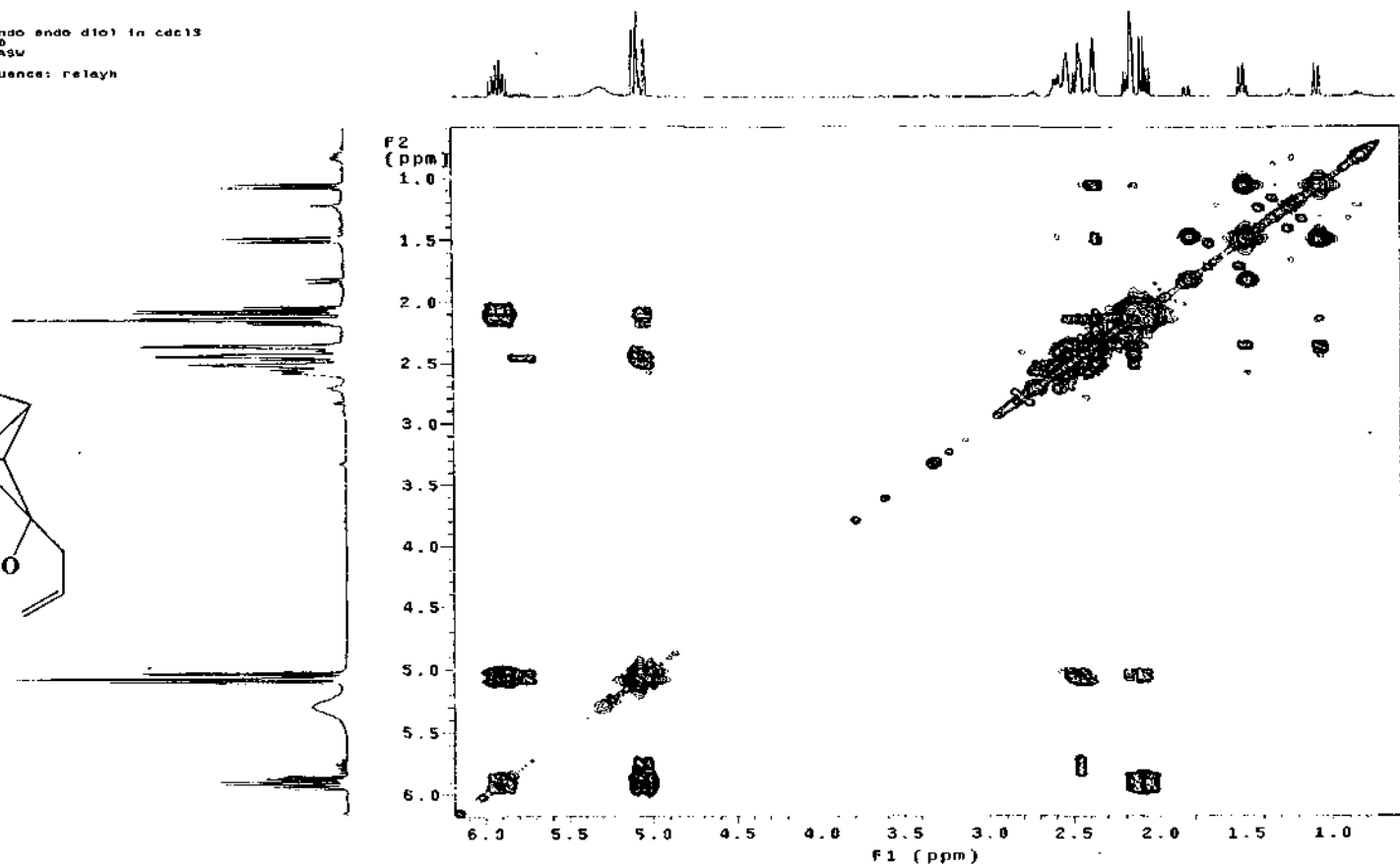
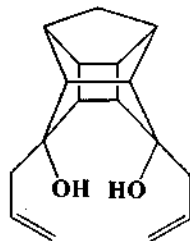


INDEX	FREQUENCY	PPM	HEIGHT
2	18450.467	133.748	58.5
3	13440.488	133.651	58.3
4	11852.000	117.655	58.8
5	11835.978	117.656	4.8
6	7775.990	77.319	15.0
7	7771.875	77.281	55.0
8	7743.488	77.000	17.8
9	7711.401	59.881	17.2
10	3941.826	68.143	84.8
11	4787.128	47.404	11.4
12	4539.809	45.052	11.0
13	4426.647	44.076	100.6
14	4424.558	43.997	98.2
15	4397.091	43.724	10.8
17	4302.484	42.783	75.8
18	4112.284	38.724	13.2
19	4018.284	38.624	38.8
19	3408.281	33.892	38.8



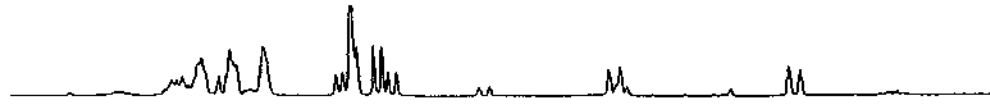
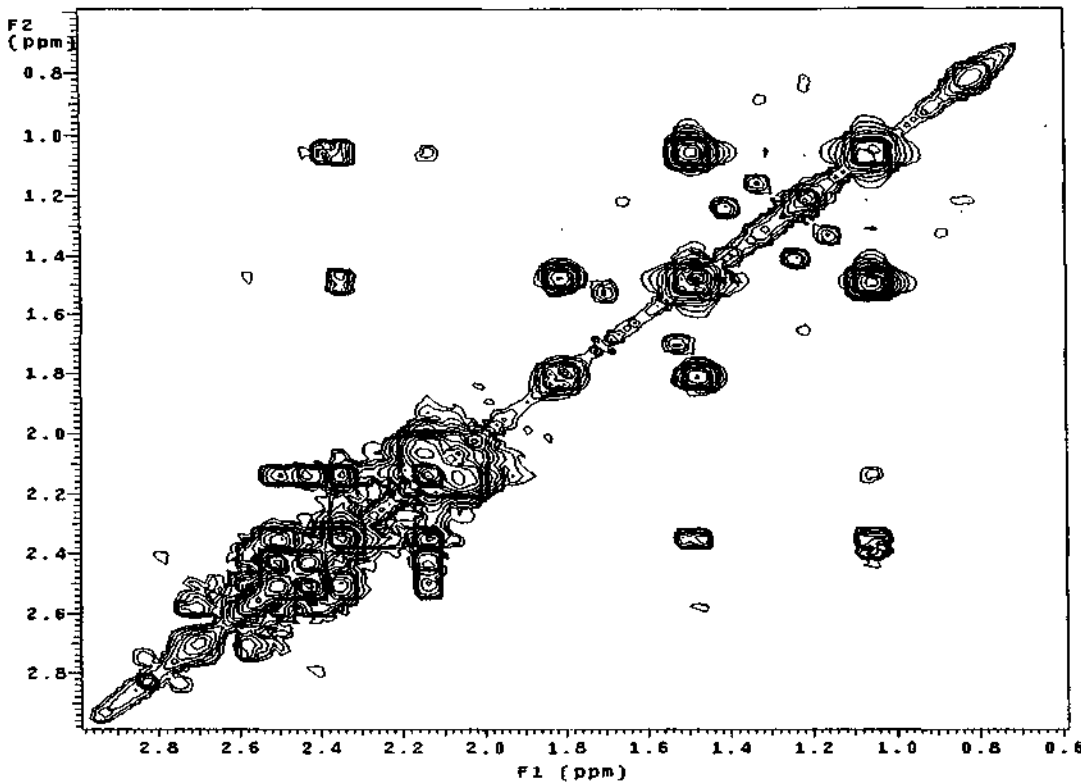
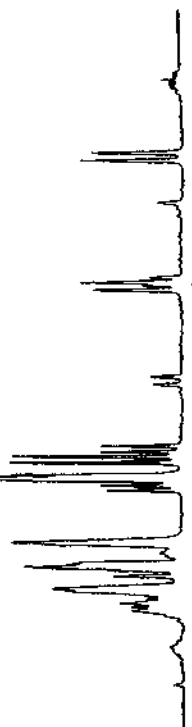
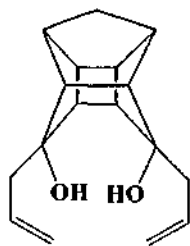
SPECTRUM 22: ¹³C NMR spectrum of endo-endo diol (73) in CDCl₃

cyadiol.endo endo diol in cdcl3
in Casy-80
probe=3mmASW
Pulse Sequence: relayh



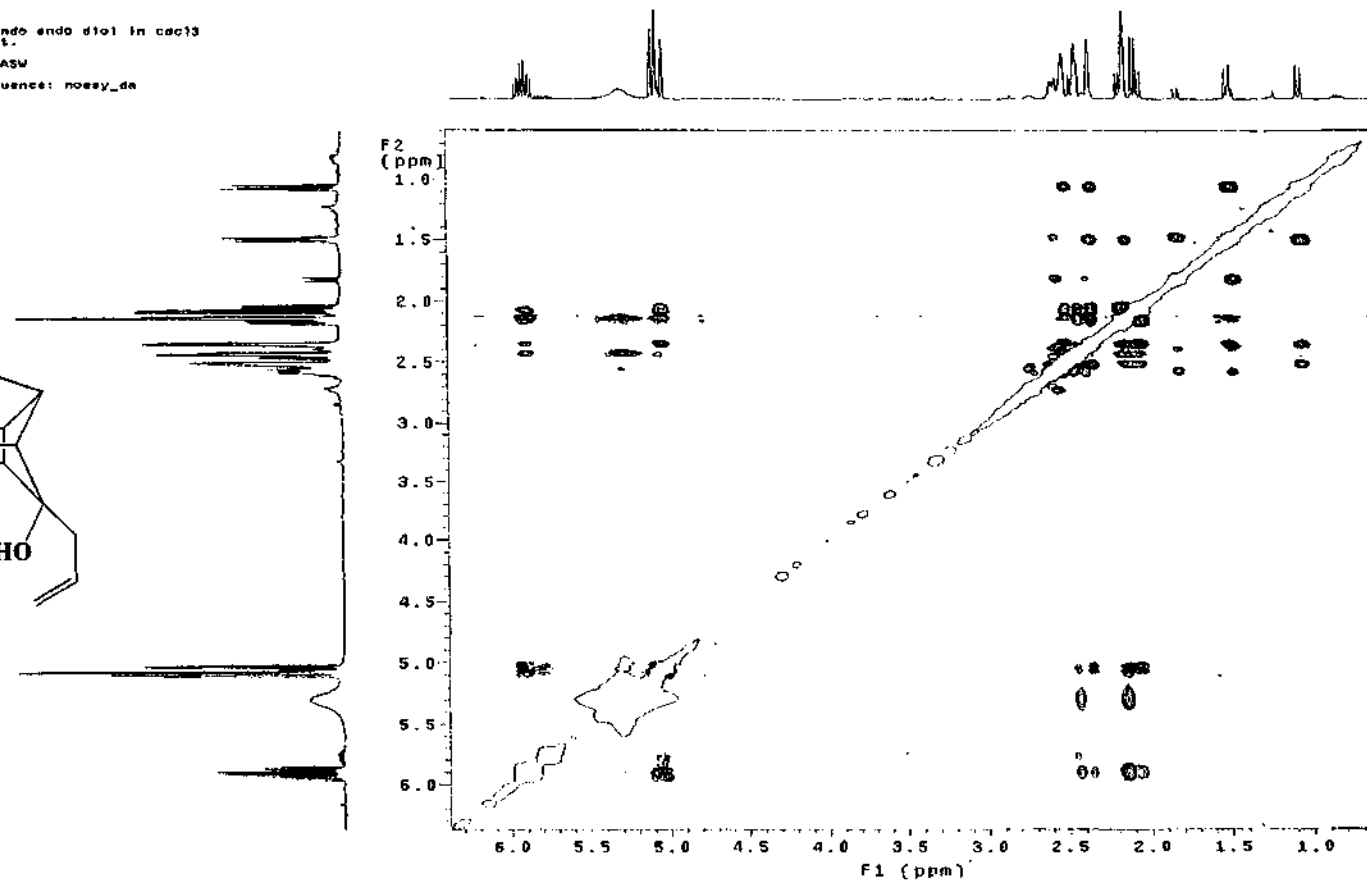
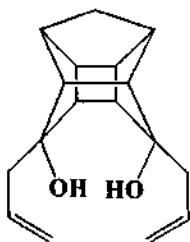
SPECTRUM 23: COSY spectrum 1 of endo-endo diol(73) in CDCl₃

cyed101.endo endo diol in cdcl3
in Cosy-80
probe-5mmASW
Pulse Sequence: relayh



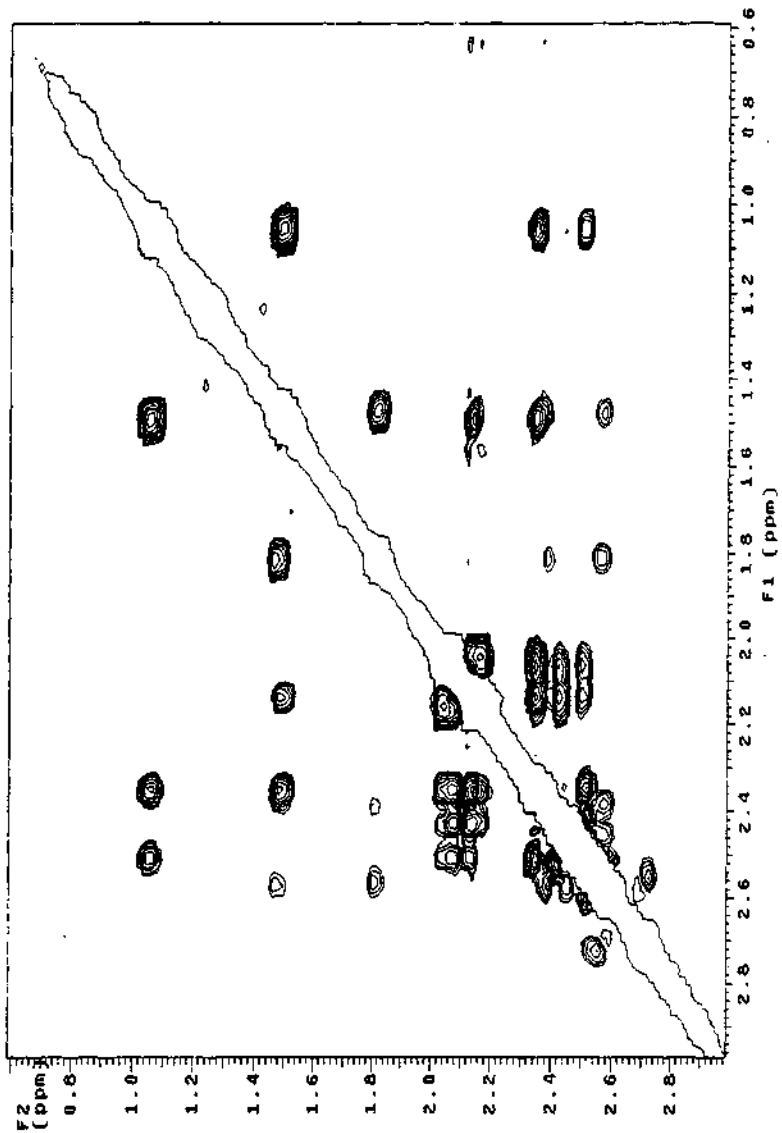
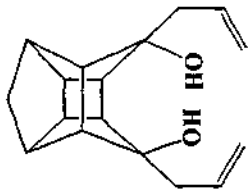
SPECTRUM 24: COSY spectrum 2 of endo-endo diol (73) in CDCl₃

NOed101.endo endo diol in cdc13
NOESY exp1.
mix=1sec
probe=5mmASW
Pulse Sequence: noesy_da



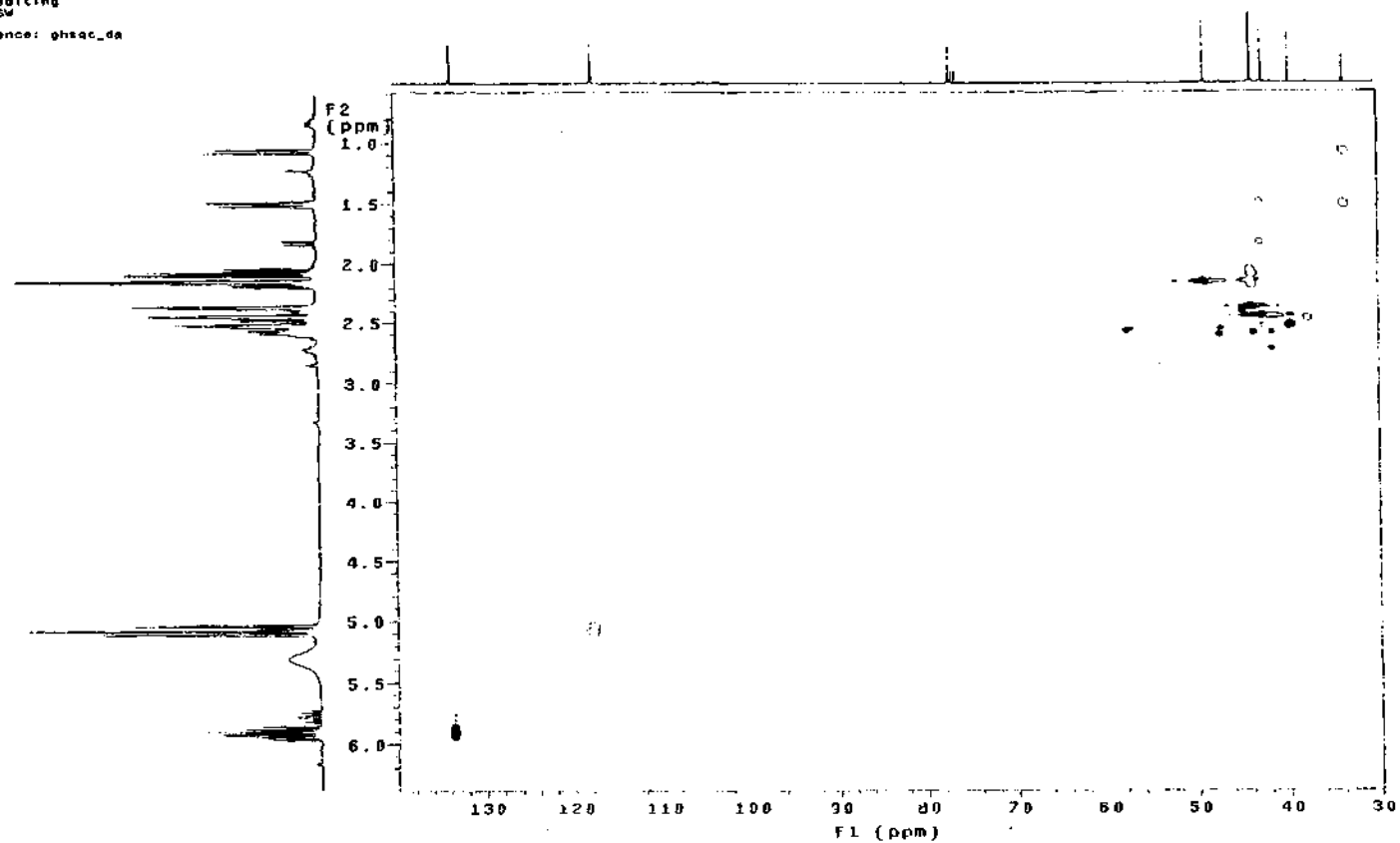
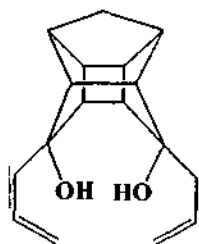
SPECTRUM 25: NOESY spectrum 1 of endo-endo diol (73) in CDCl₃

Molecule: endo endo diol in cdcl3
 Name: nasy_04
 Mixture: no
 Problem: nasy_04
 Pulse Sequence: nasy_04



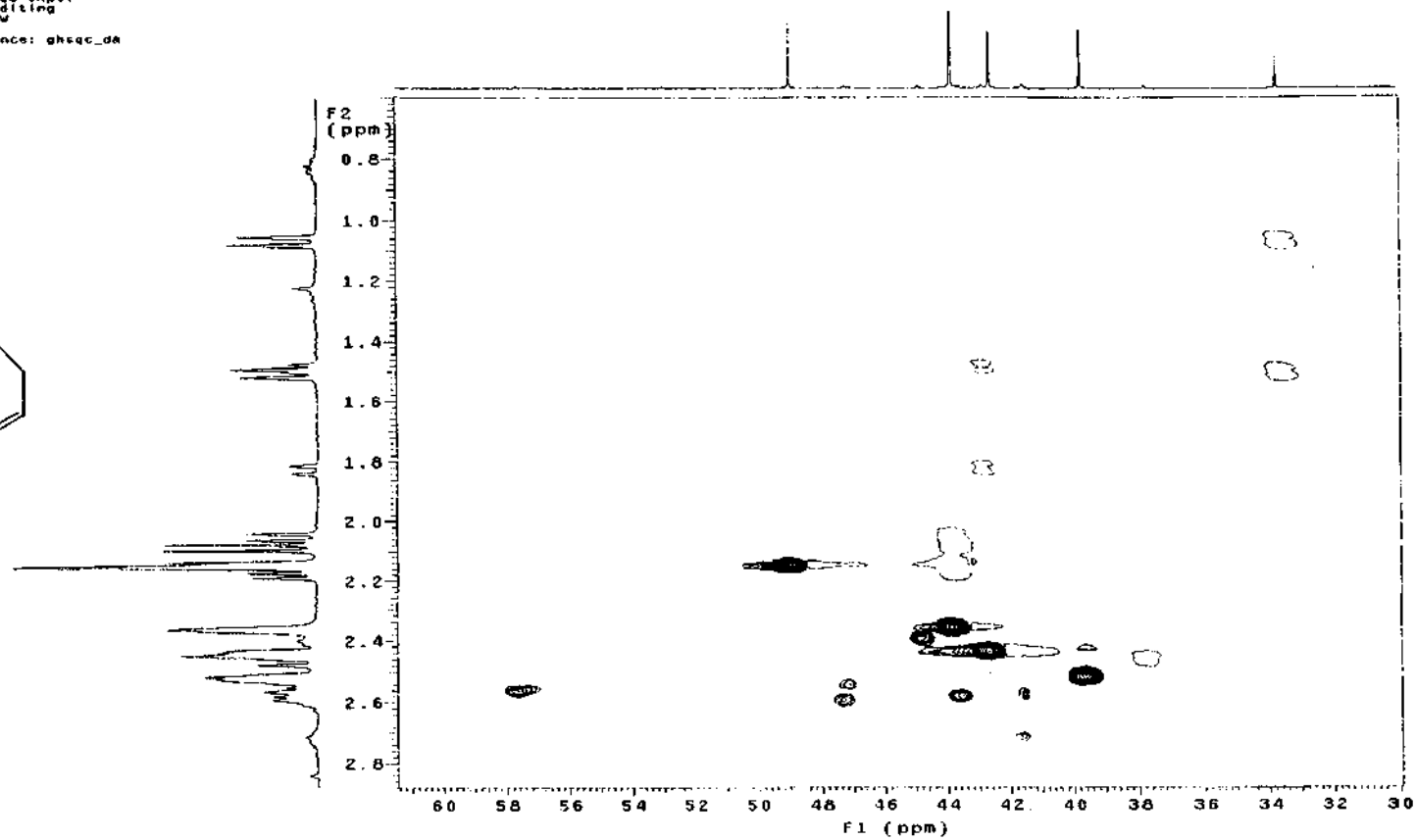
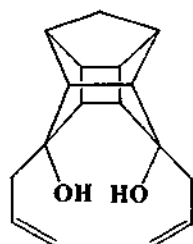
SPECTRUM 26: NOESY spectrum 2 of endo-endodiol (73) in CDCl₃

HOendo1.endo endo diol in cdcl3
Gradient HSQC expt.
with mult. editing
probe=5mmASW
Pulse Sequence: ghsqc_da



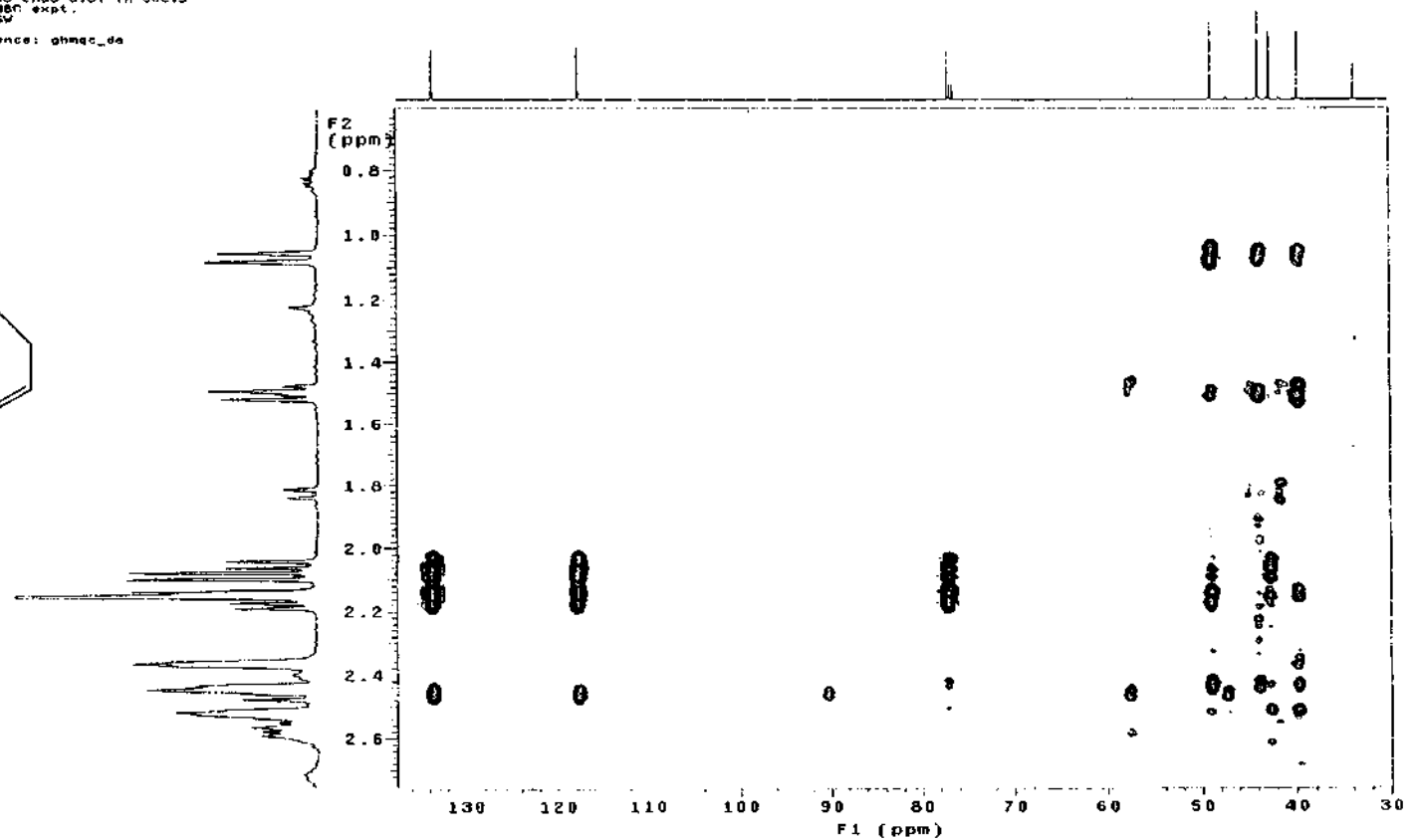
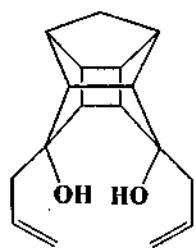
SPECTRUM 27: HSQC spectrum 1 of endo-endo diol (73) in CDCl₃

H0ed1o1.endo endo diol in cdcl3
Gradient HSQC expt.
with mult. editing
probe=5mmASW
Pulse Sequence: ghsqc_da



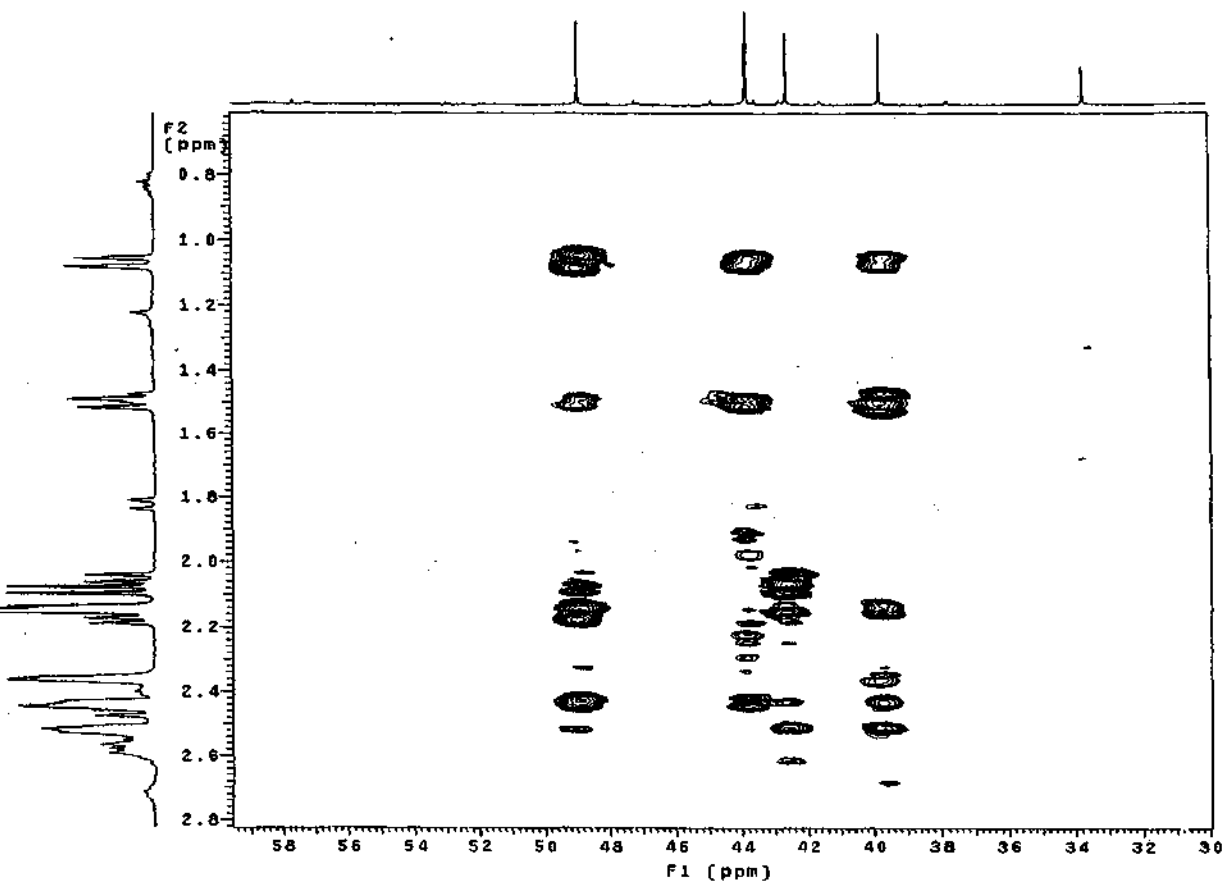
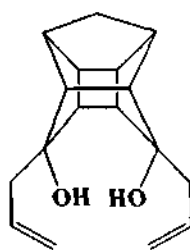
SPECTRUM 28: HSQC spectrum 2 of endo-endo diol (73) in CDCl₃

NSBdiol_endo_endo_diol_in_cdc13
Gradient HMQC expt.
probe=5mmASy
Pulse Sequence: ghmqc_da



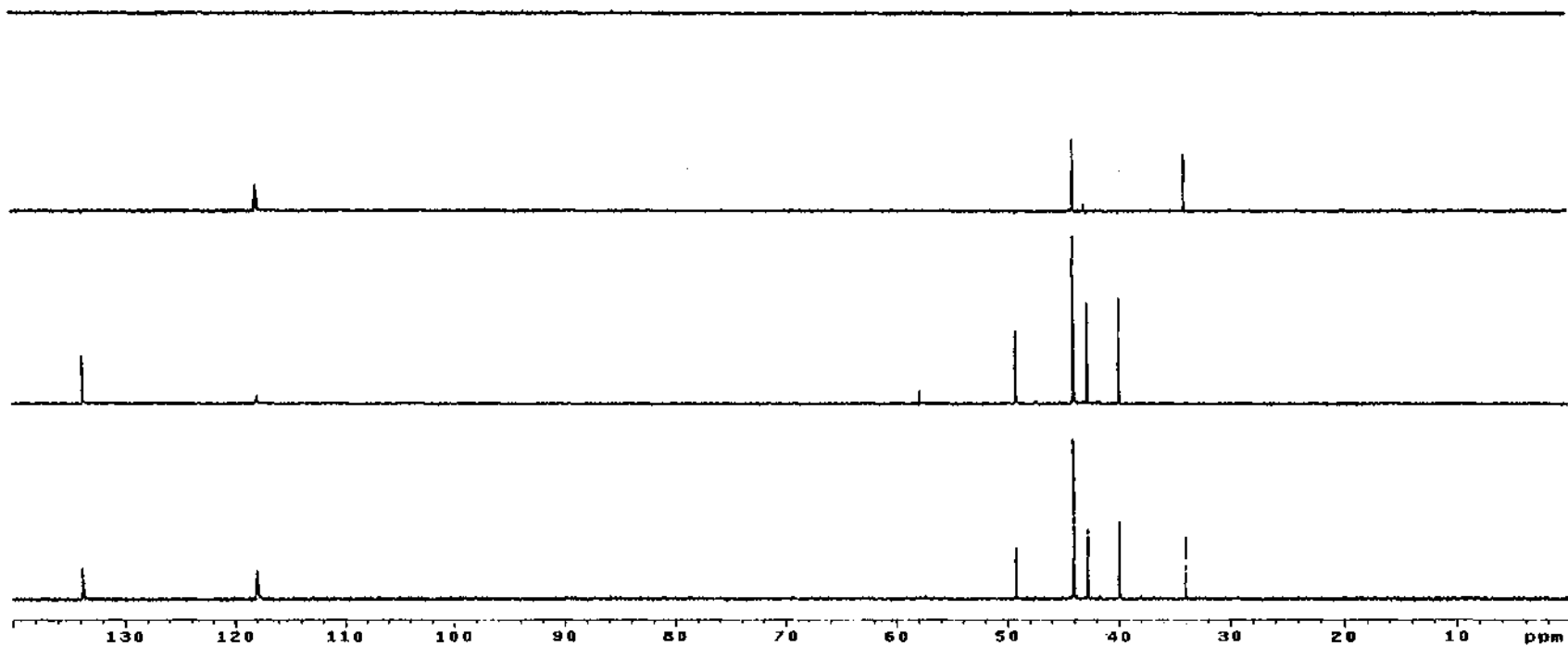
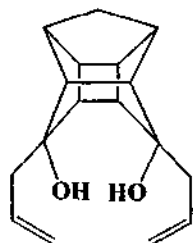
SPECTRUM 29: HMBC spectrum 1 of endo-endo diol (73) in CDCl₃

nmrjol.endo endo diol in cdcl3
Gradient HMBC expt.
Probe-Bmadw
Pulse Sequence: ghmqo_da

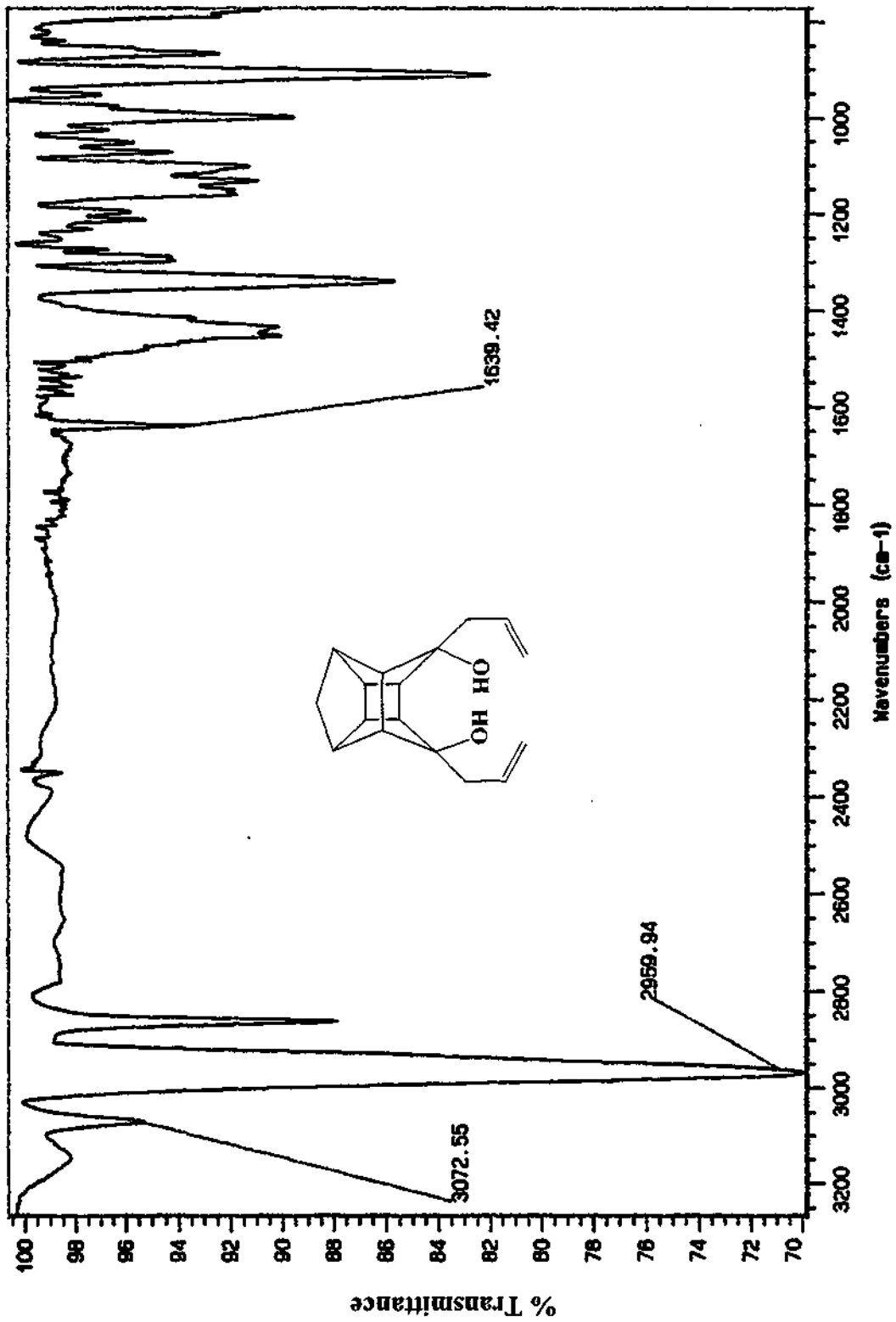


SPECTRUM 30: HMBC spectrum 2 of endo-endo diol (73) in CDCl₃

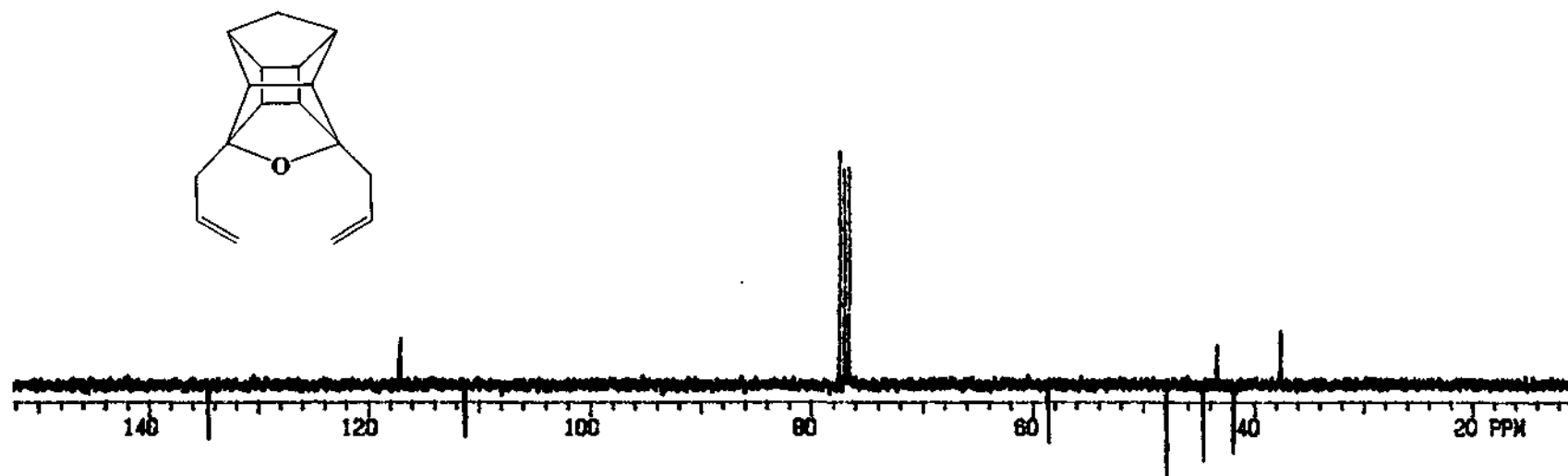
dediol_endo_endo_diol in cdcl3
probe-5mmASW
Pulse Sequence: dept



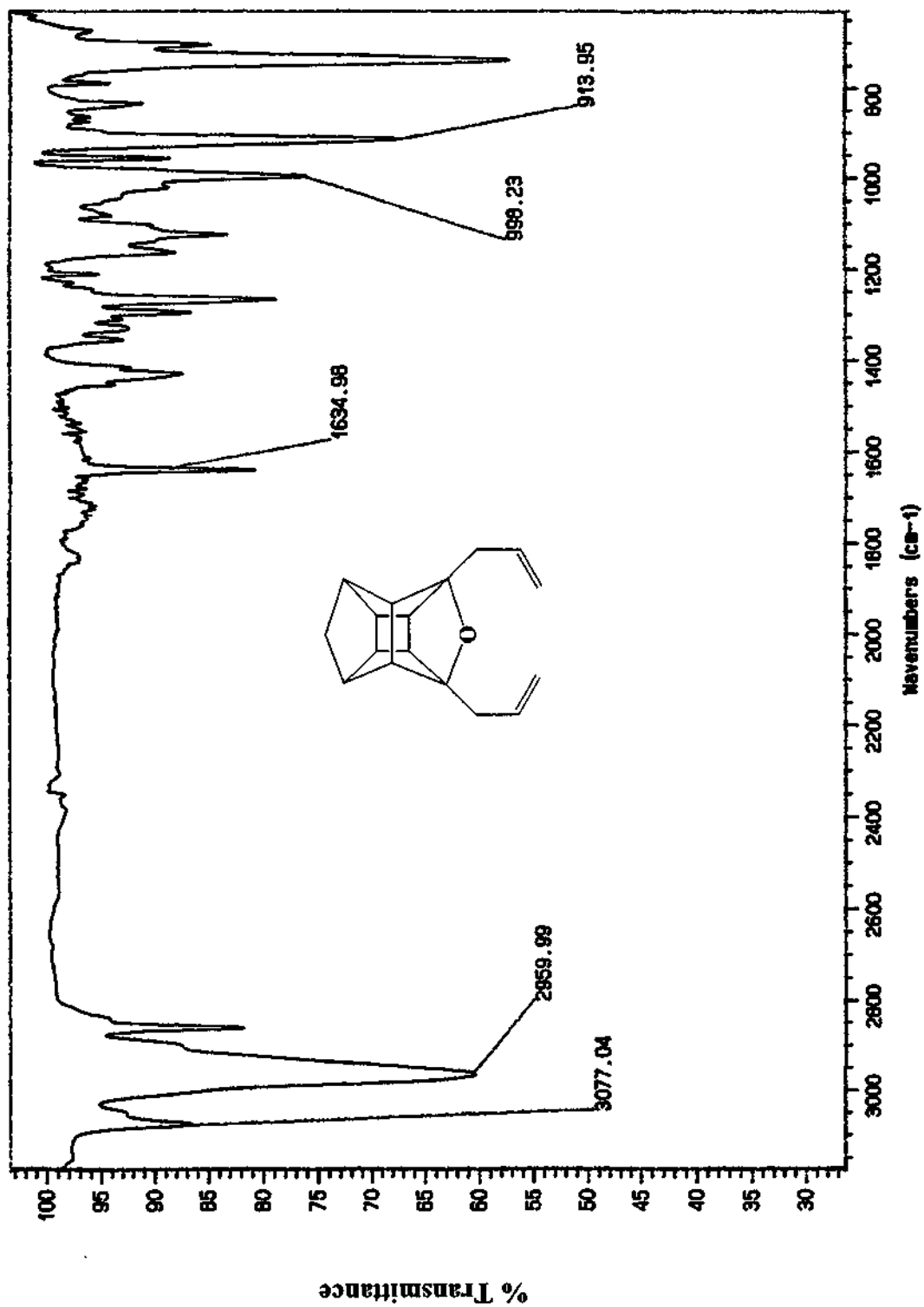
SPECTRUM 31: DEPT spectrum of endo-endo diol (73) in CDCl₃



SPECTRUM 32: Infrared spectrum (NaCl) of endo-endo diol (73)

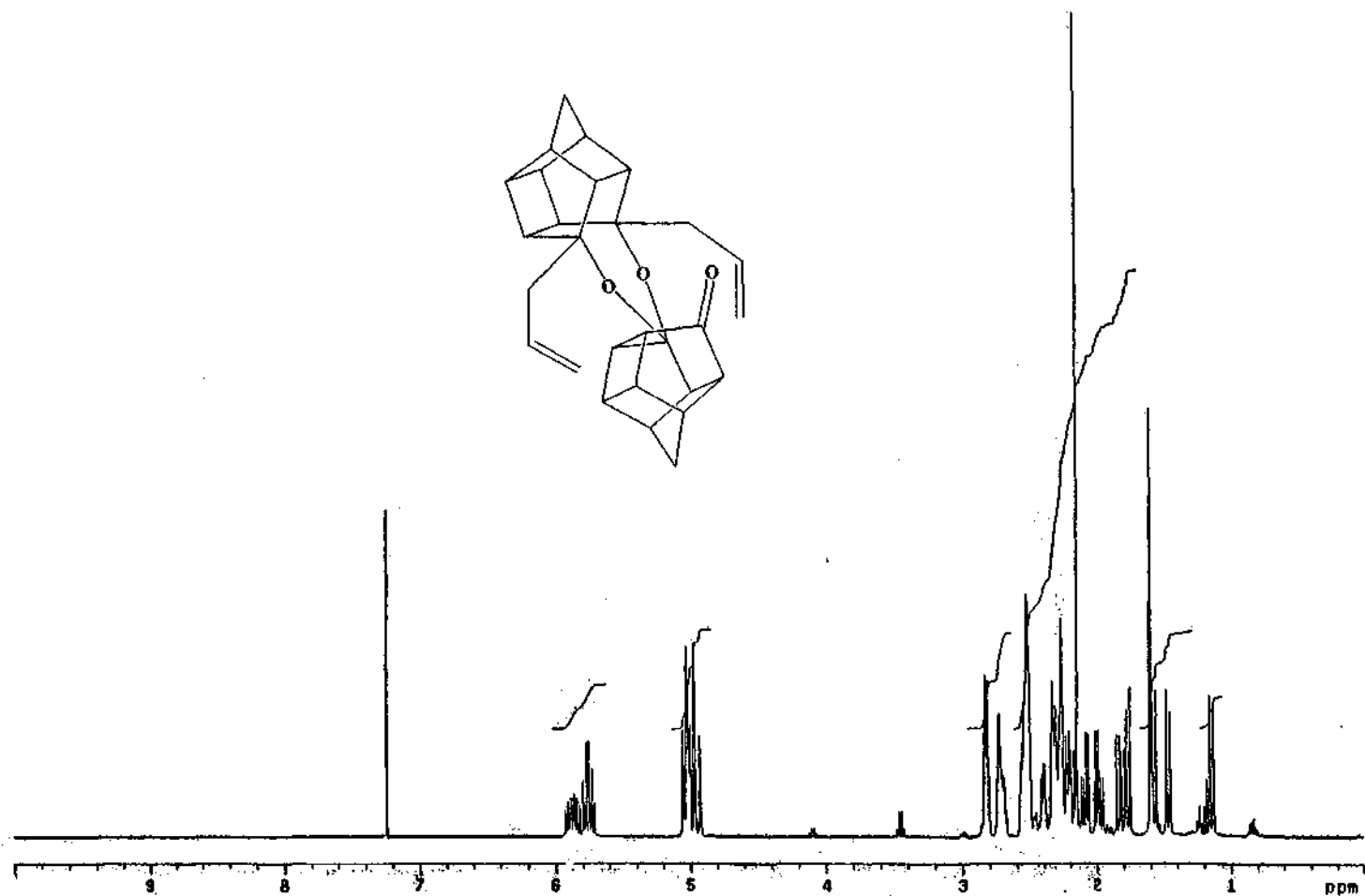


SPECTRUM 33: ^{13}C NMR spectrum of diene (74) in CDCl_3



SPECTRUM 34: Infrared spectrum (NaCl) of diene (74)

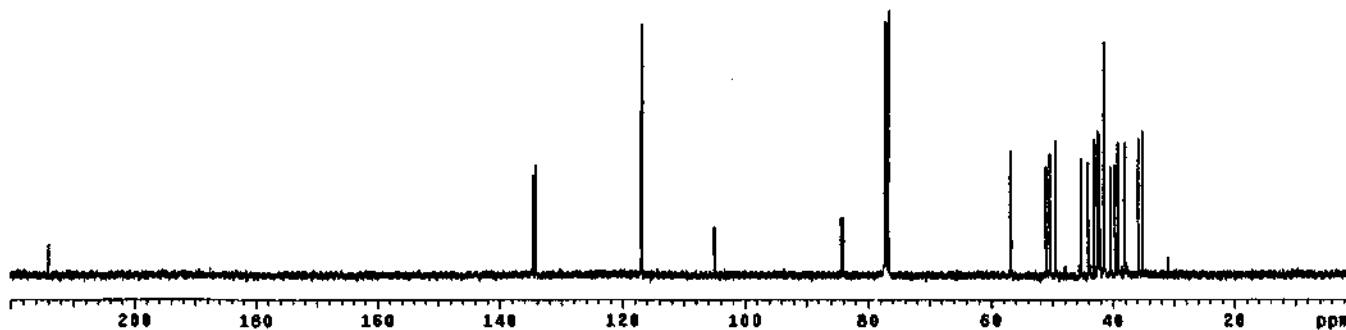
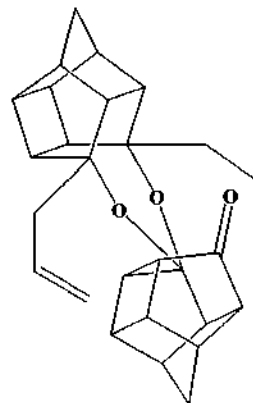
hex.endo_x in cdc13
probe=5mmASW
Pulse Sequence: zgpg30



SPECTRUM 35: ¹H NMR spectrum of Novel dimer (76) in CDCl₃

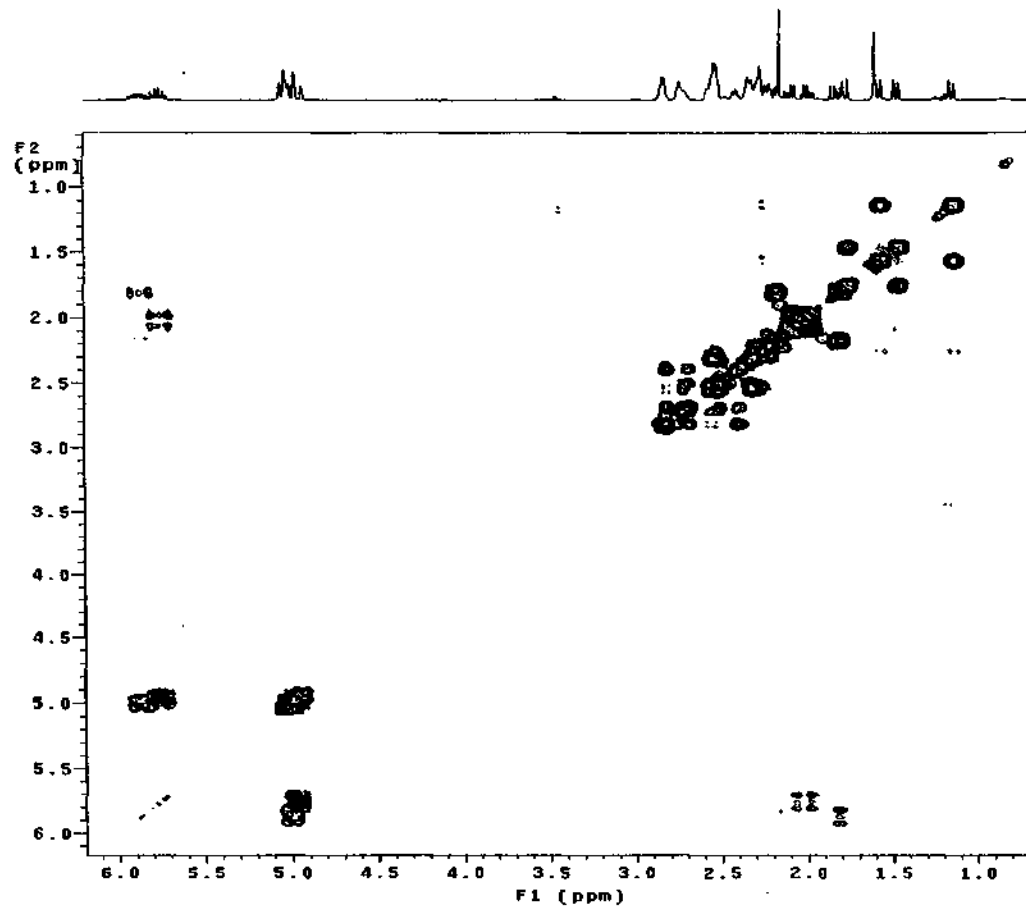
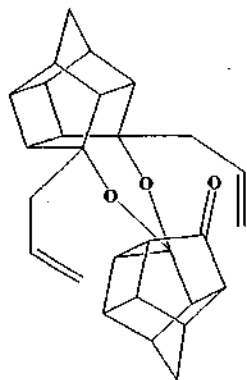
cex.endo_x in cdc13
 probe=5mmASW
 Pulse Sequence: s2pu1

INDEX	FREQUENCY	PPM	HEIGHT
1	21519.072	213.940	5.6
2	13531.430	134.555	10.0
3	13481.083	134.150	20.0
4	11754.817	110.090	47.4
5	10580.132	105.009	9.1
6	8477.811	84.303	10.9
7	8451.543	84.041	11.0
8	7775.040	77.314	47.0
9	7743.730	77.083	47.6
10	7711.001	76.693	50.0
11	5700.306	50.773	23.6
12	5195.810	51.070	24.6
13	5074.639	50.464	23.1
14	4979.252	48.513	25.6
15	4551.691	45.261	22.2
16	4433.771	44.089	21.5
17	4341.484	43.171	25.8
18	4285.453	42.614	24.9
19	4262.157	42.581	27.4
20	4250.261	42.344	24.7
21	4252.493	42.286	22.9
22	4240.725	42.229	26.9
23	4173.990	41.500	44.0
24	4082.975	40.482	20.7
25	3984.898	39.623	21.0
26	3840.201	38.101	25.2
27	3824.043	38.034	25.2
28	3804.037	38.046	26.0
29	3553.150	35.133	27.4



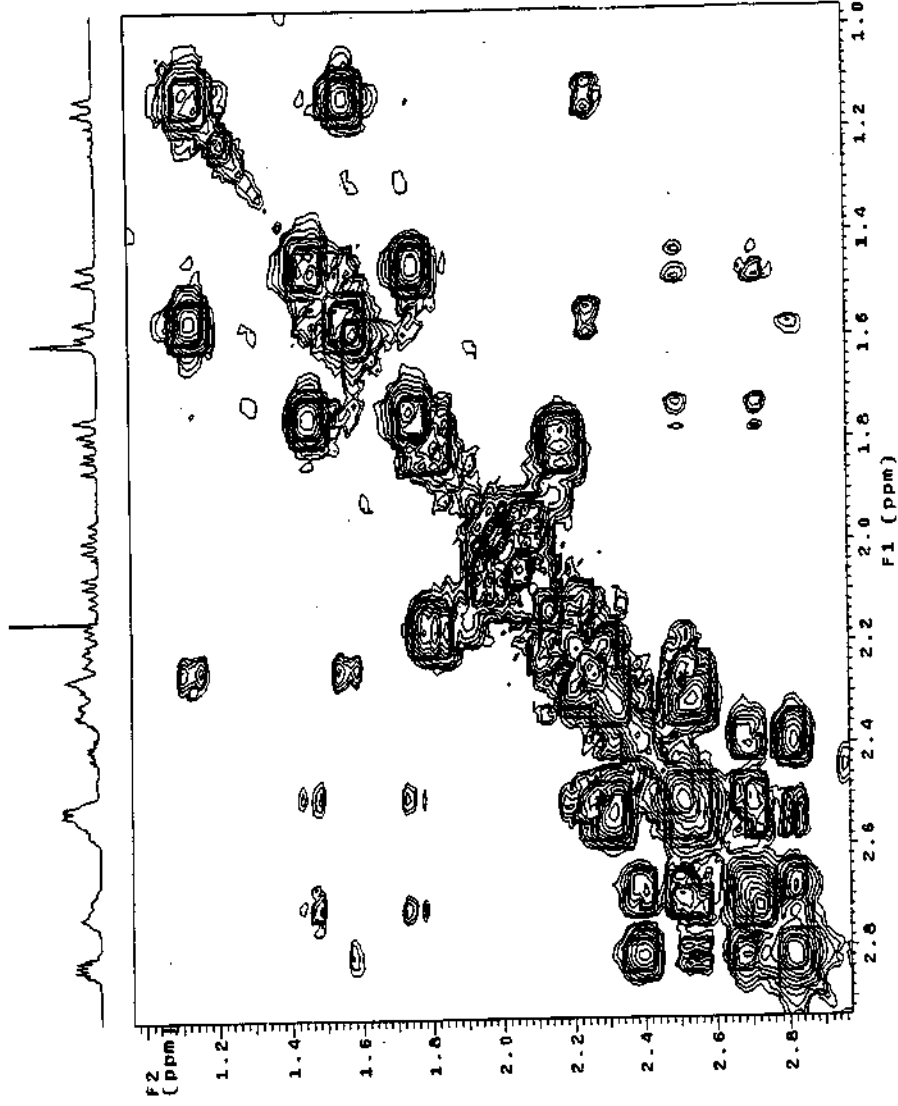
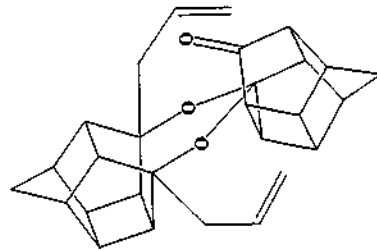
SPECTRUM 36: ^{13}C NMR spectrum of Novel dimer (76) in CDCl_3

cyex.endo_x in cdcl3
in cosy-90
probe=tmaguv
Pulse Sequence: relayh



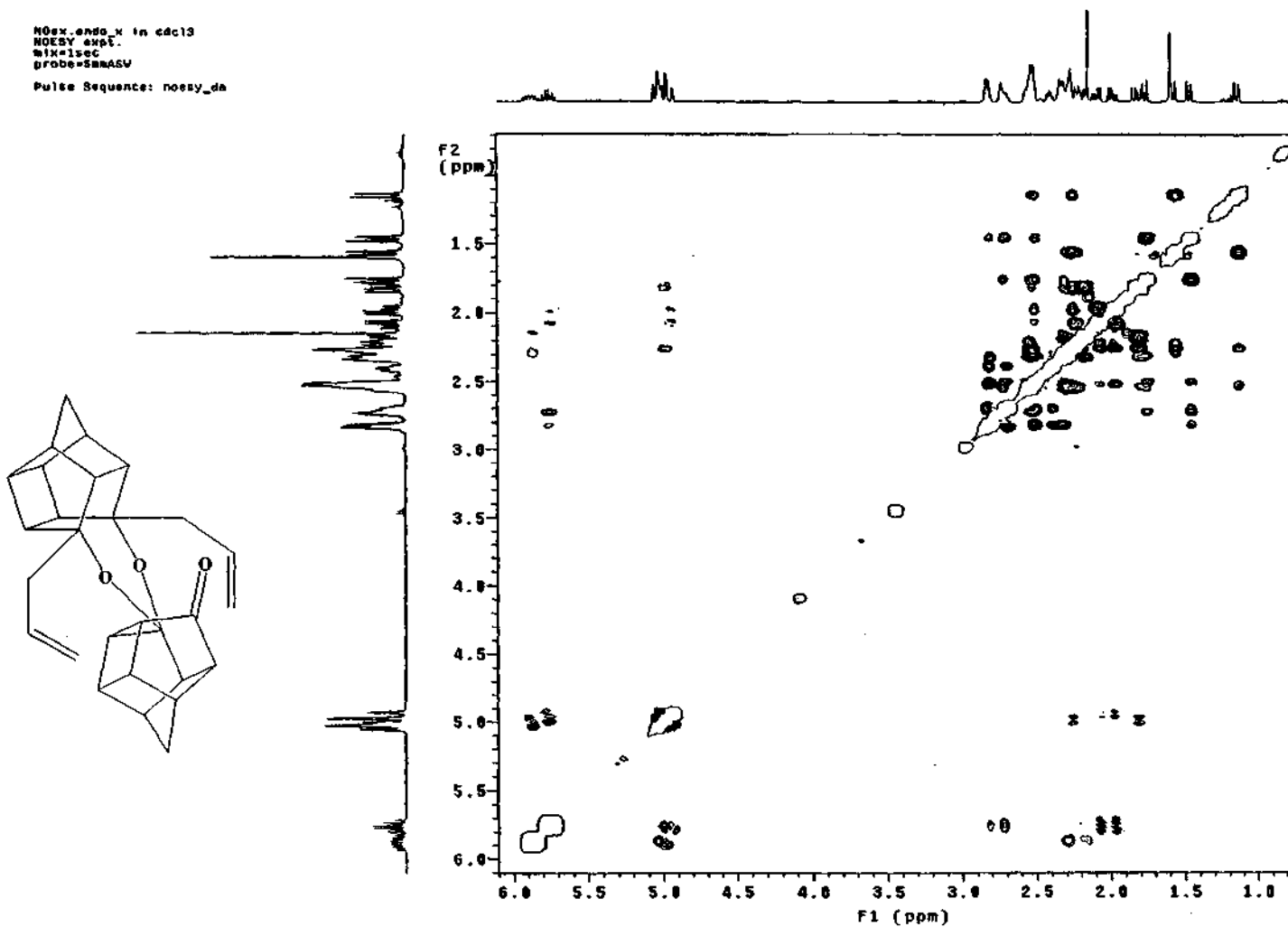
SPECTRUM 37: COSY spectrum 1 of Novel dimer (76) in CDCl₃

nmr data in cdcl3
in cosy
probname: 76
Pulse Sequence: relayh



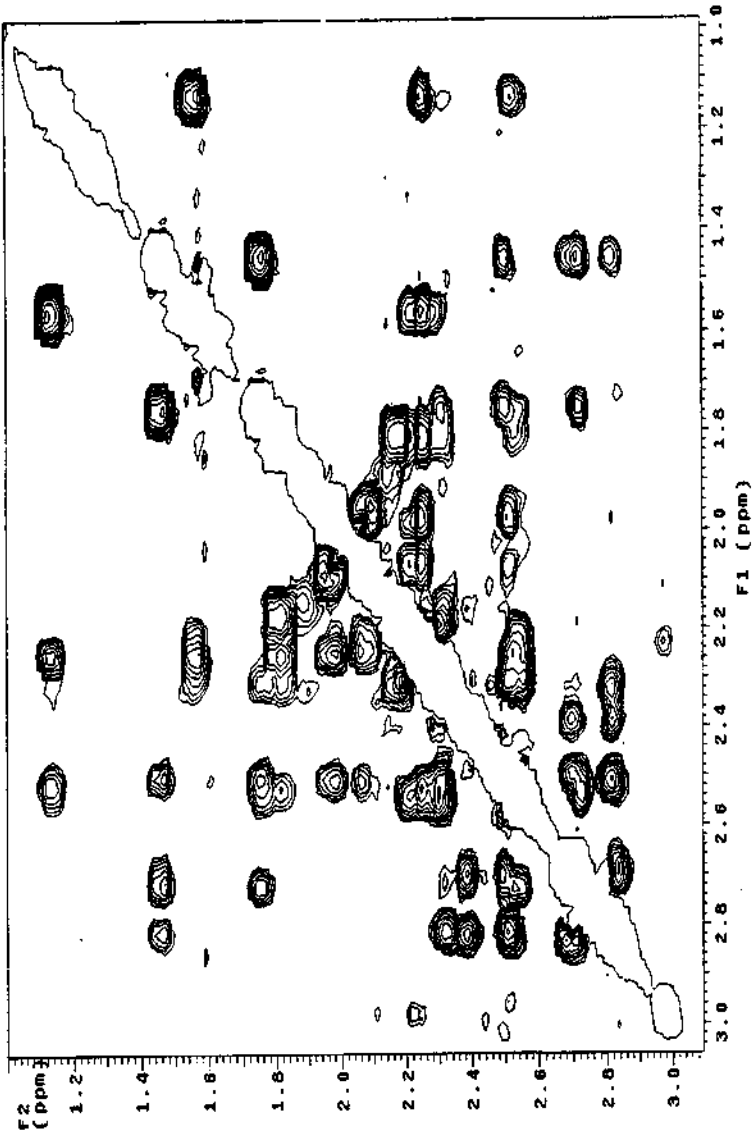
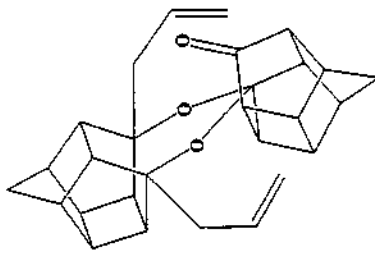
SPECTRUM 38: COSY spectrum 2 of Novel dimer (76) in CDCl₃

NOex_endo_x in cdcl3
NOESY exp1.
mix=1sec
probe=5mmASU
Pulse Sequence: noesy_da



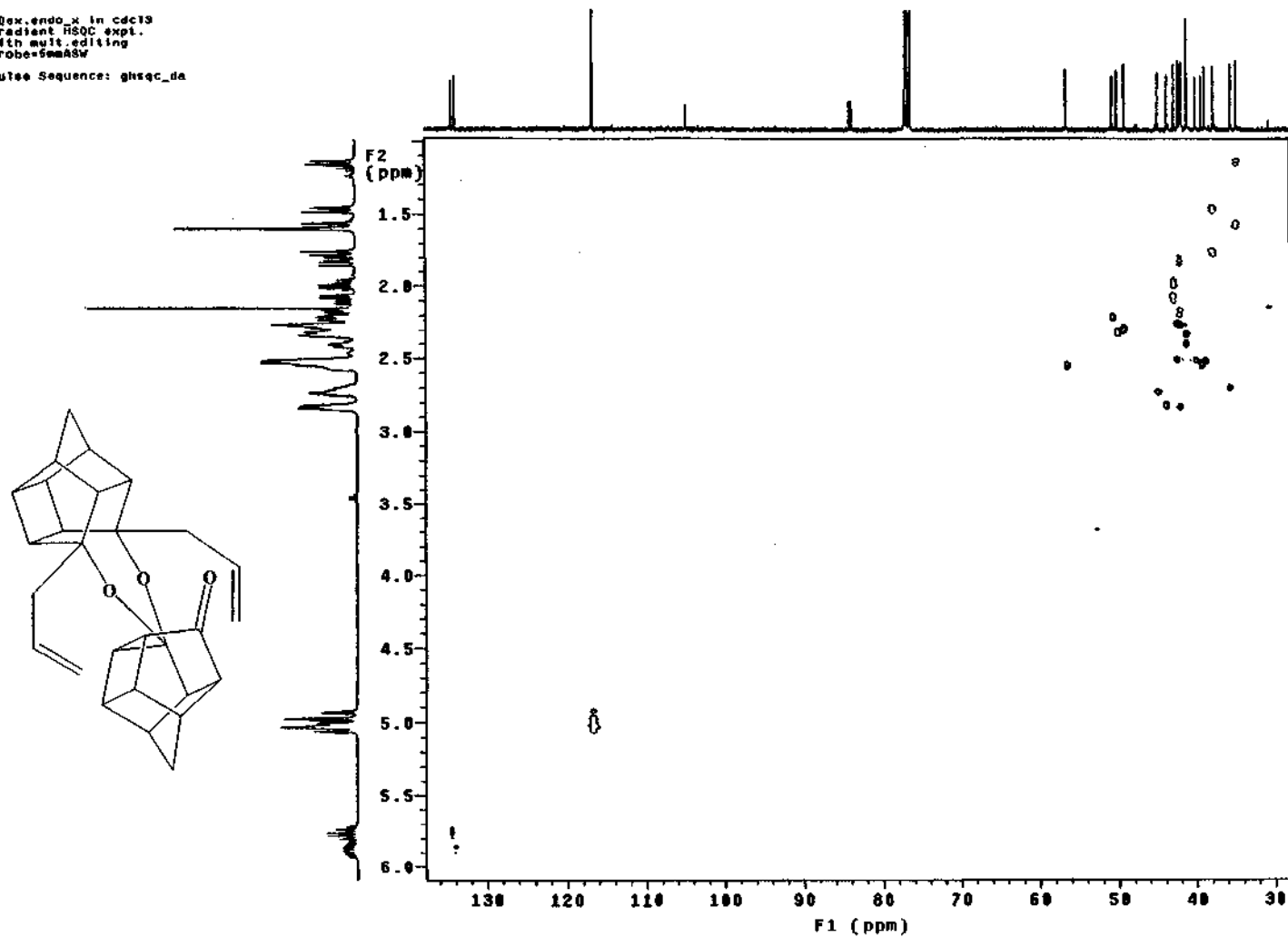
SPECTRUM 39: NOESY spectrum 1 of Novel dimer (76) in CDCl₃

ndex_endo2.in cdcl3
nmr1150pt.
m1150sec
probe-gmasay
Pulse Sequence: noesy_da



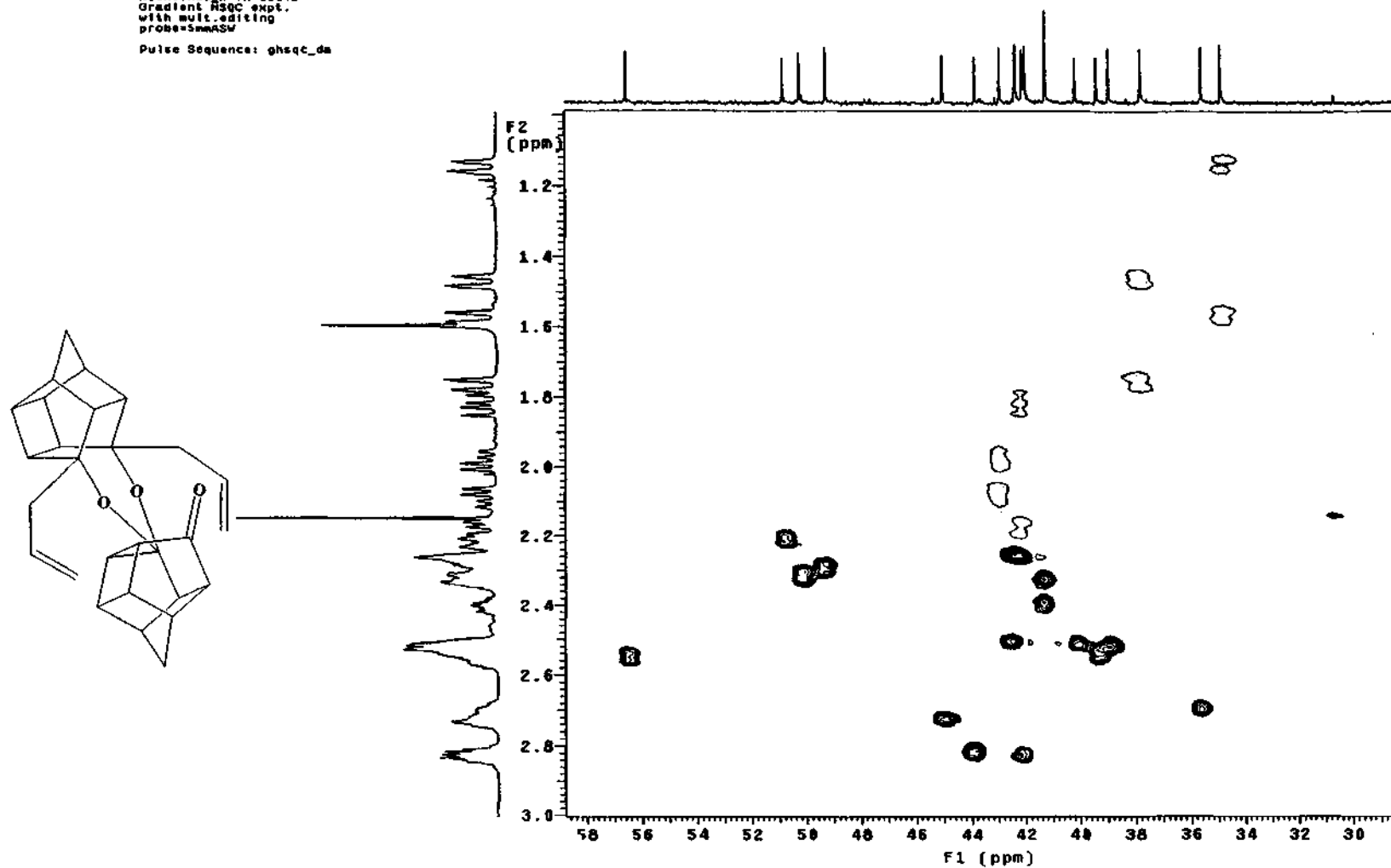
SPECTRUM 40: NOESY spectrum 2 of Novel dimer (76) in CDCl₃

HQex.endo_x in cdcl3
Gradient HSQC expt.
with mult. editing
probe=5mmASV
Pulse Sequence: ghsqc_da



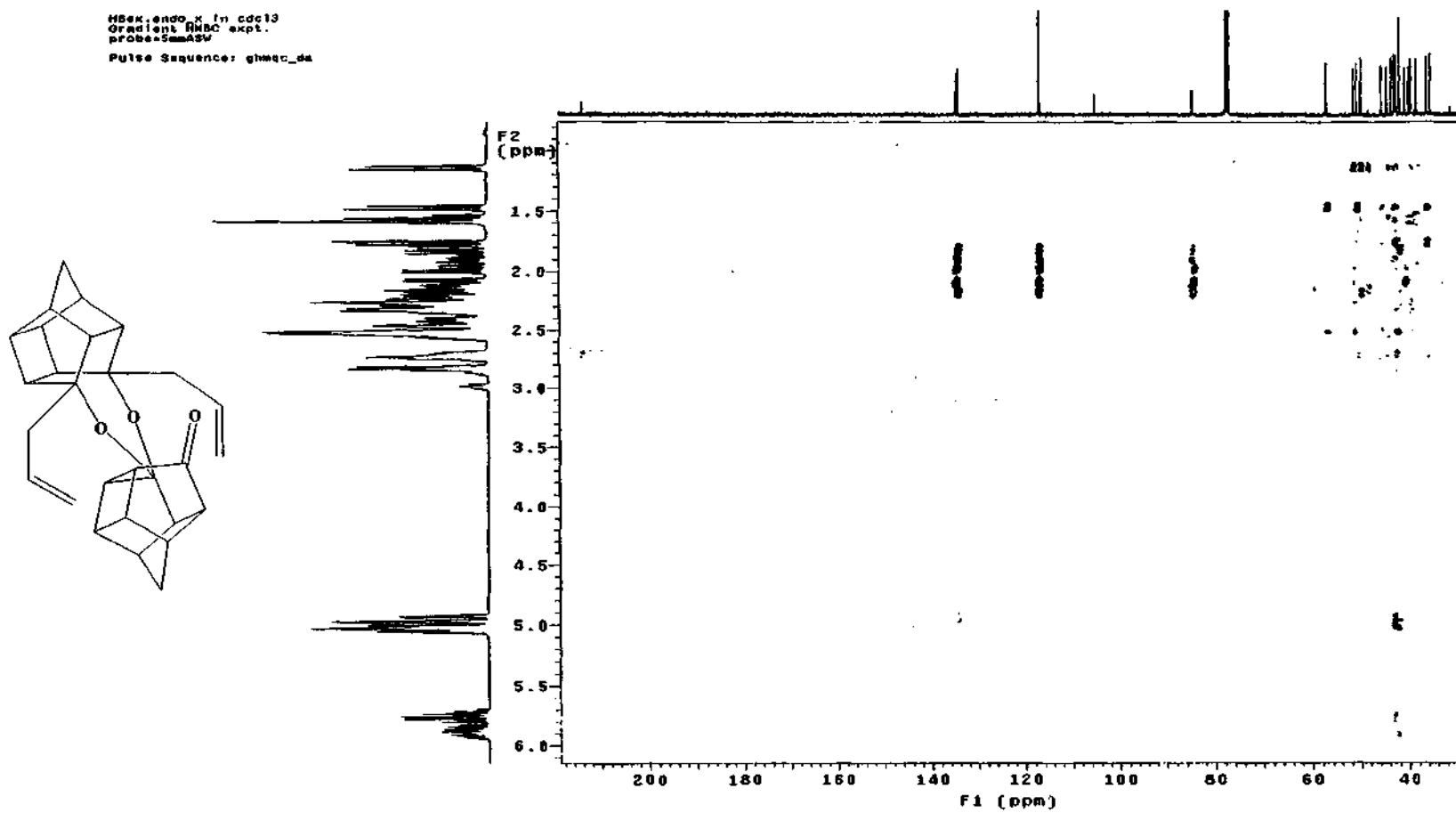
SPECTRUM 41: HSQC spectrum 1 of Novel dimer (76) in CDCl₃

NOex-endo.x in cdc19
Gradient HSQC expt.
with mult.editing
probe=5mmASW
Pulse Sequence: ghsqc_da



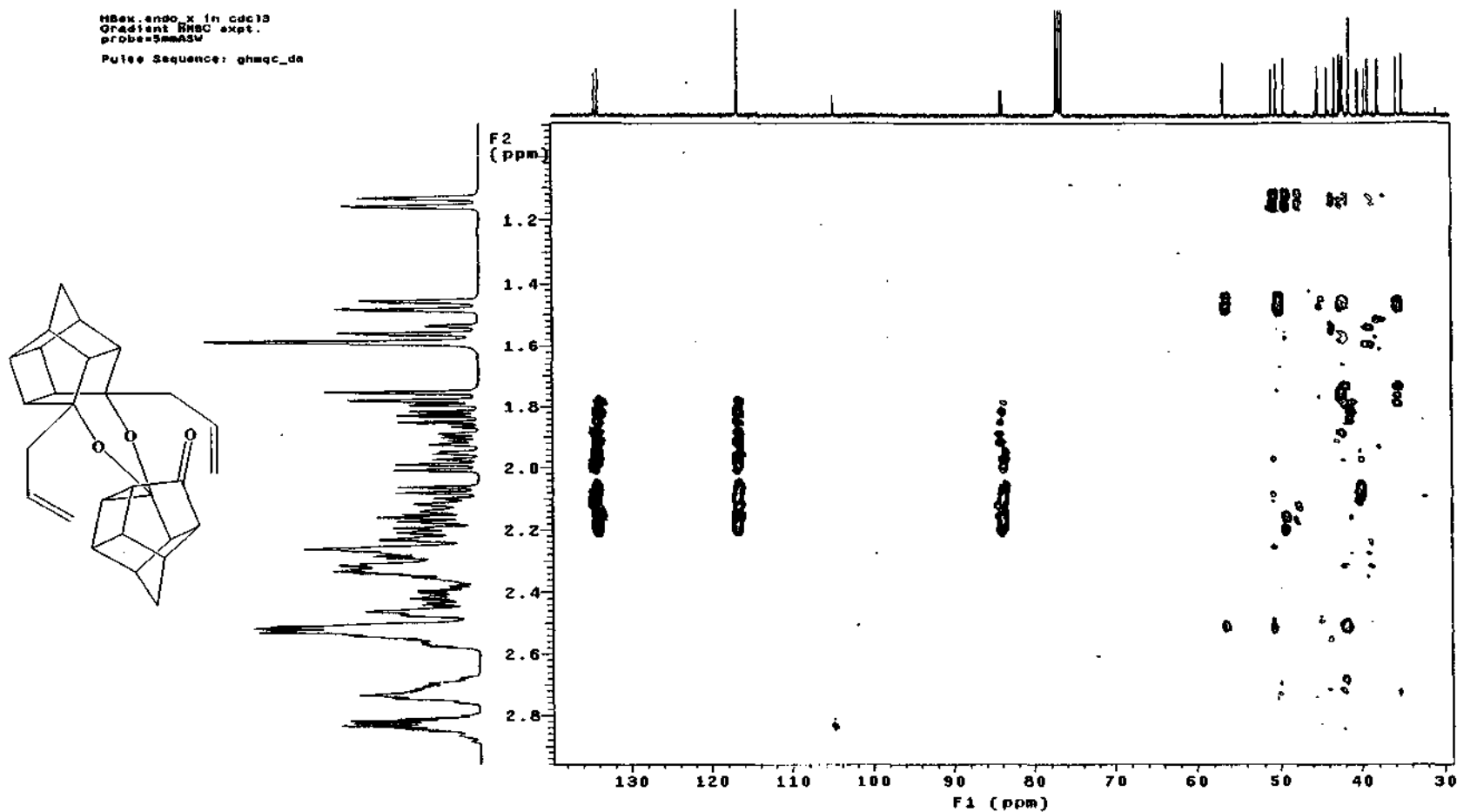
SPECTRUM 42: HSQC spectrum 2 of Novel dimer (76) in CDCl₃

HSQC:endo_1 in cdcl3
Gradient:HMBC expt.
probe:5mmASV
Pulse Sequence: ghmqc_da



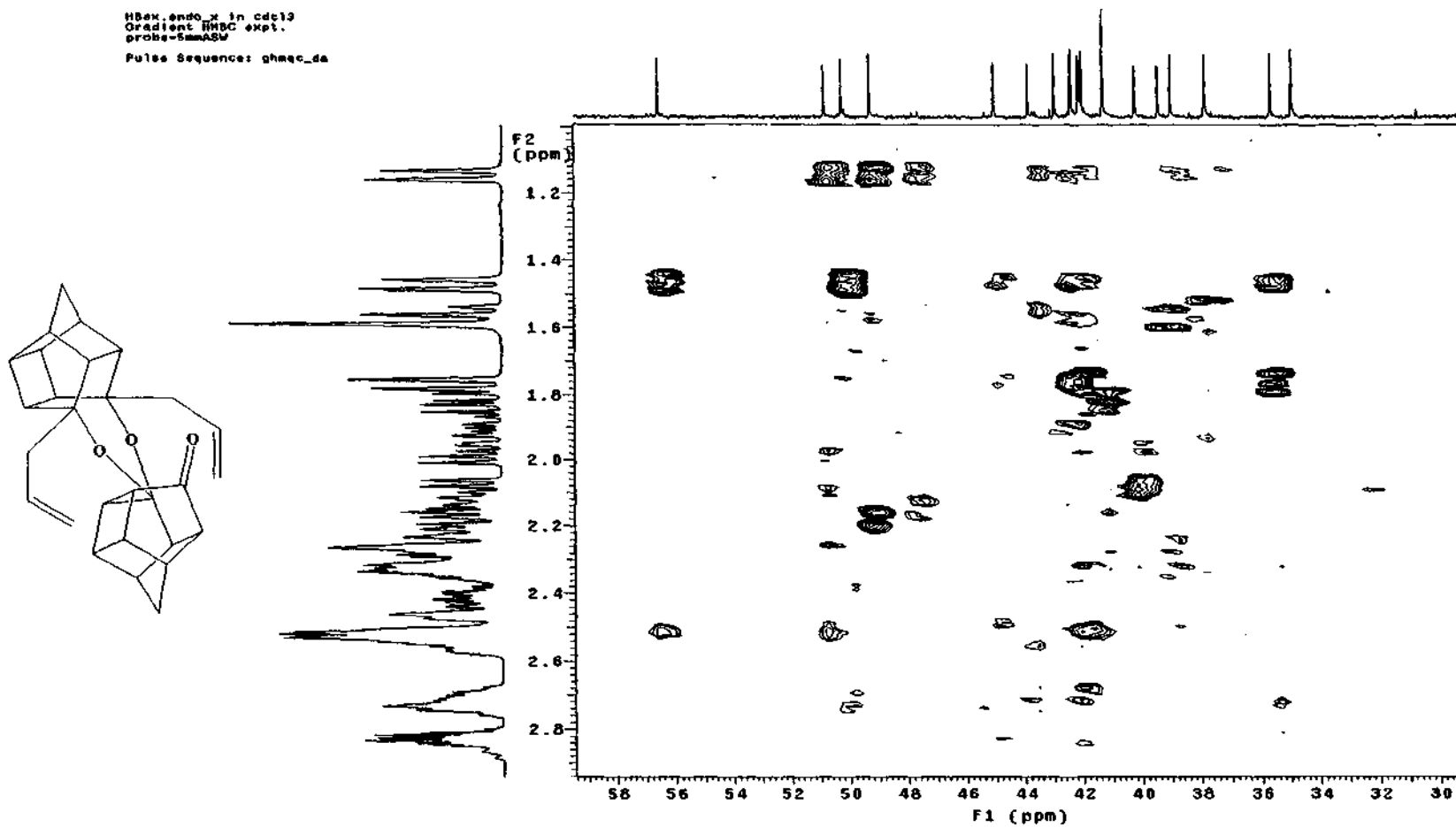
SPECTRUM 43: HMBC spectrum 1 of Novel dimer (76) in CDCl₃

MSKX.ENDO_X IN CDCl3
Gradient HMQC exp.
probe=5mmASX
Pulse Sequence: ghmqc_da

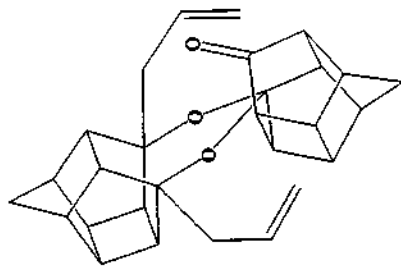


SPECTRUM 44: HMBC spectrum 2 of Novel dimer (76) in CDCl₃

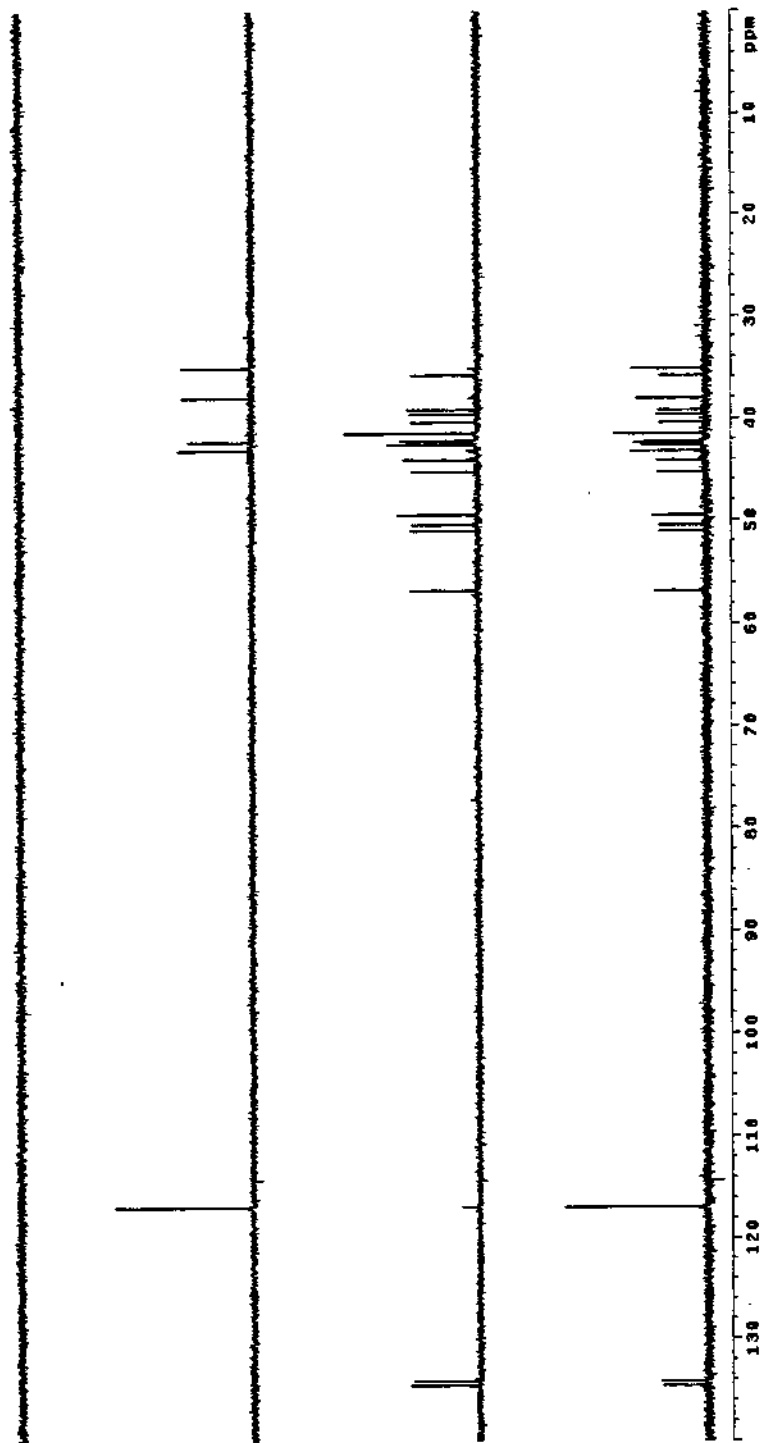
HMBC_endo_x in cdcl3
Gradient HMBC expt.
probe-5mmASW
Pulse Sequence: ghmec_da



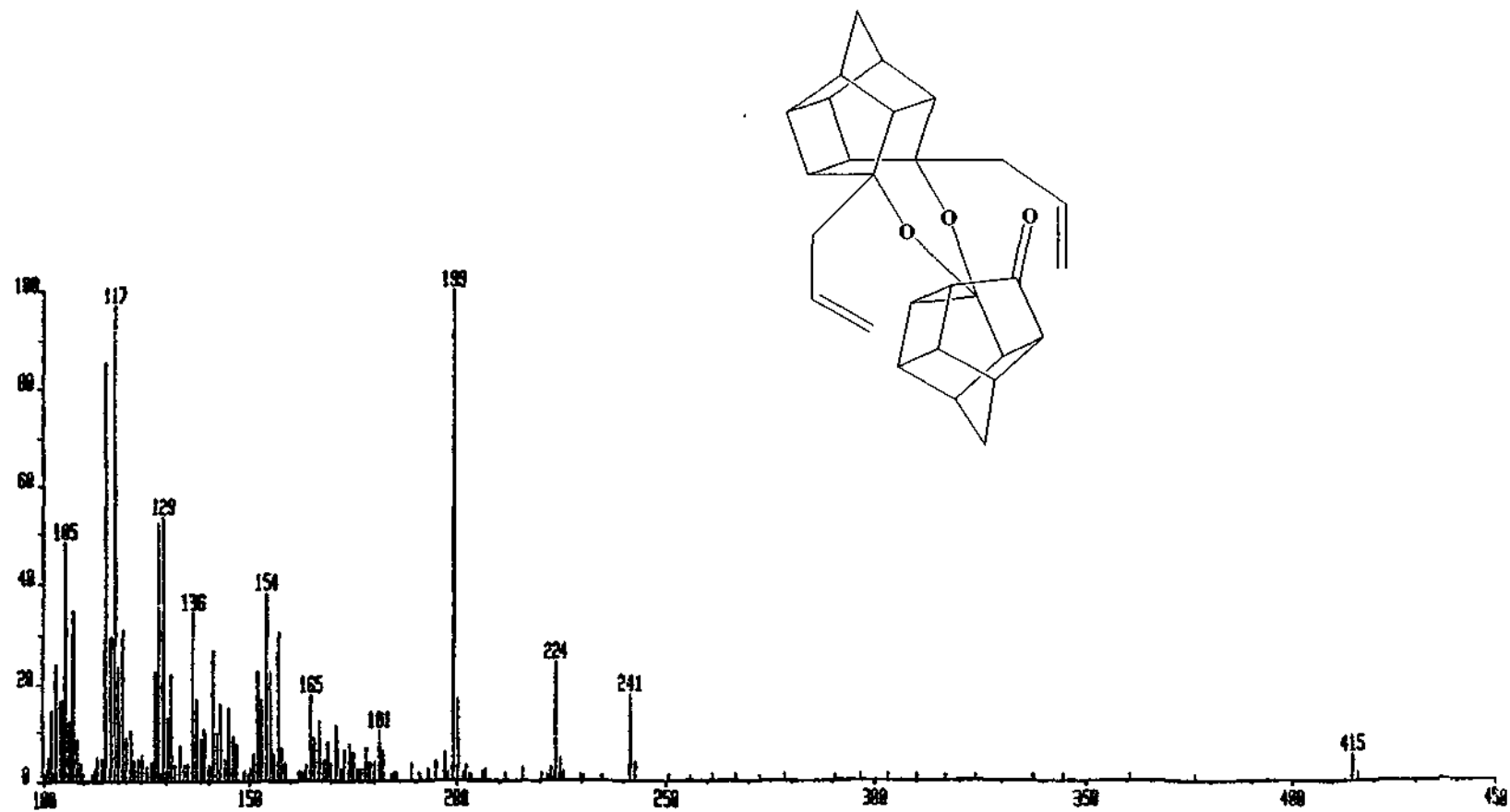
SPECTRUM 45: HMBC spectrum 3 of Novel dimer (76) in CDCl₃



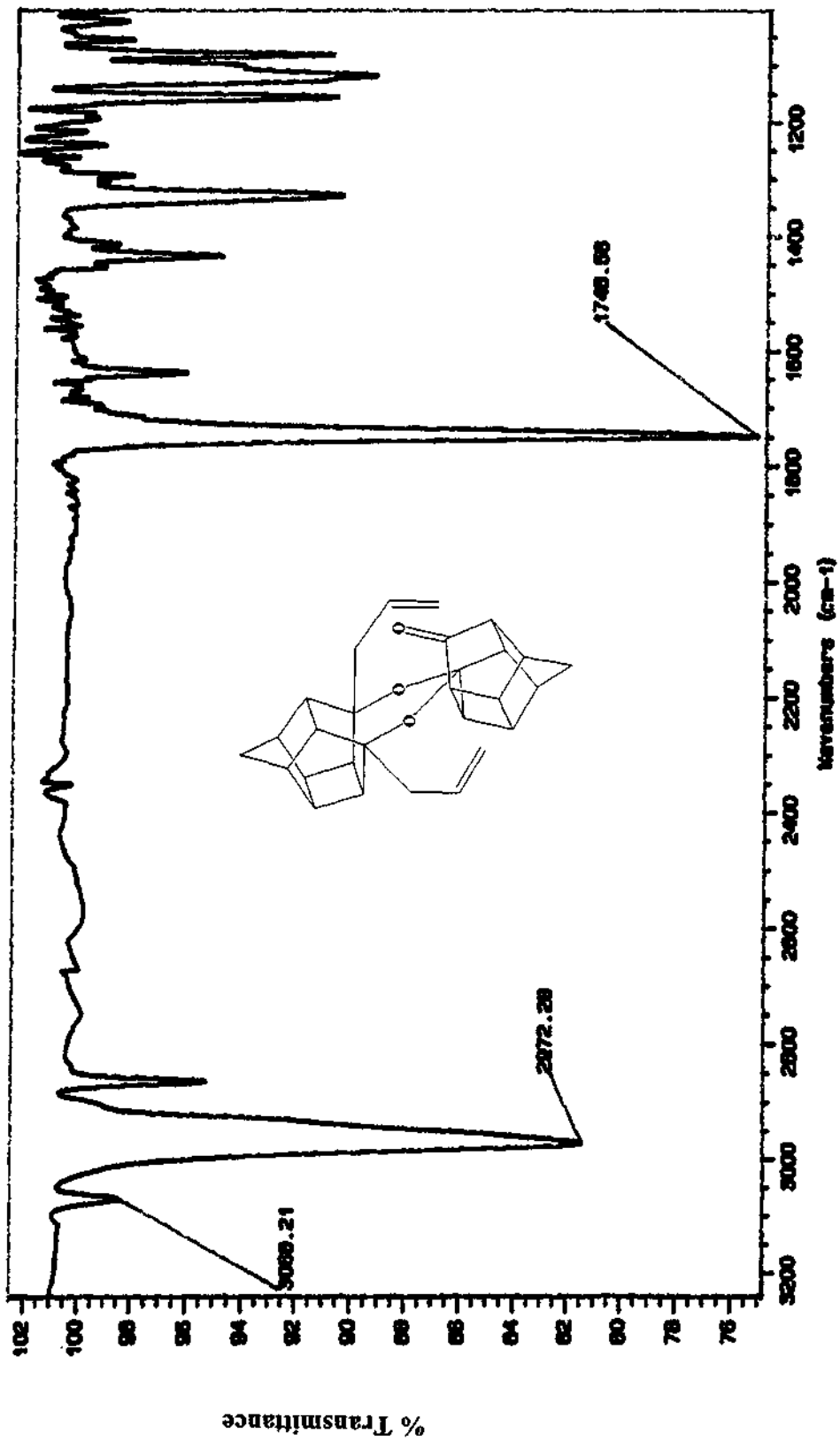
dex.ando.k in cdc13
 probe=sm63v
 Pulse Sequence: dept



SPECTRUM 46: DEPT spectrum of Novel dimer (76) in CDCl₃

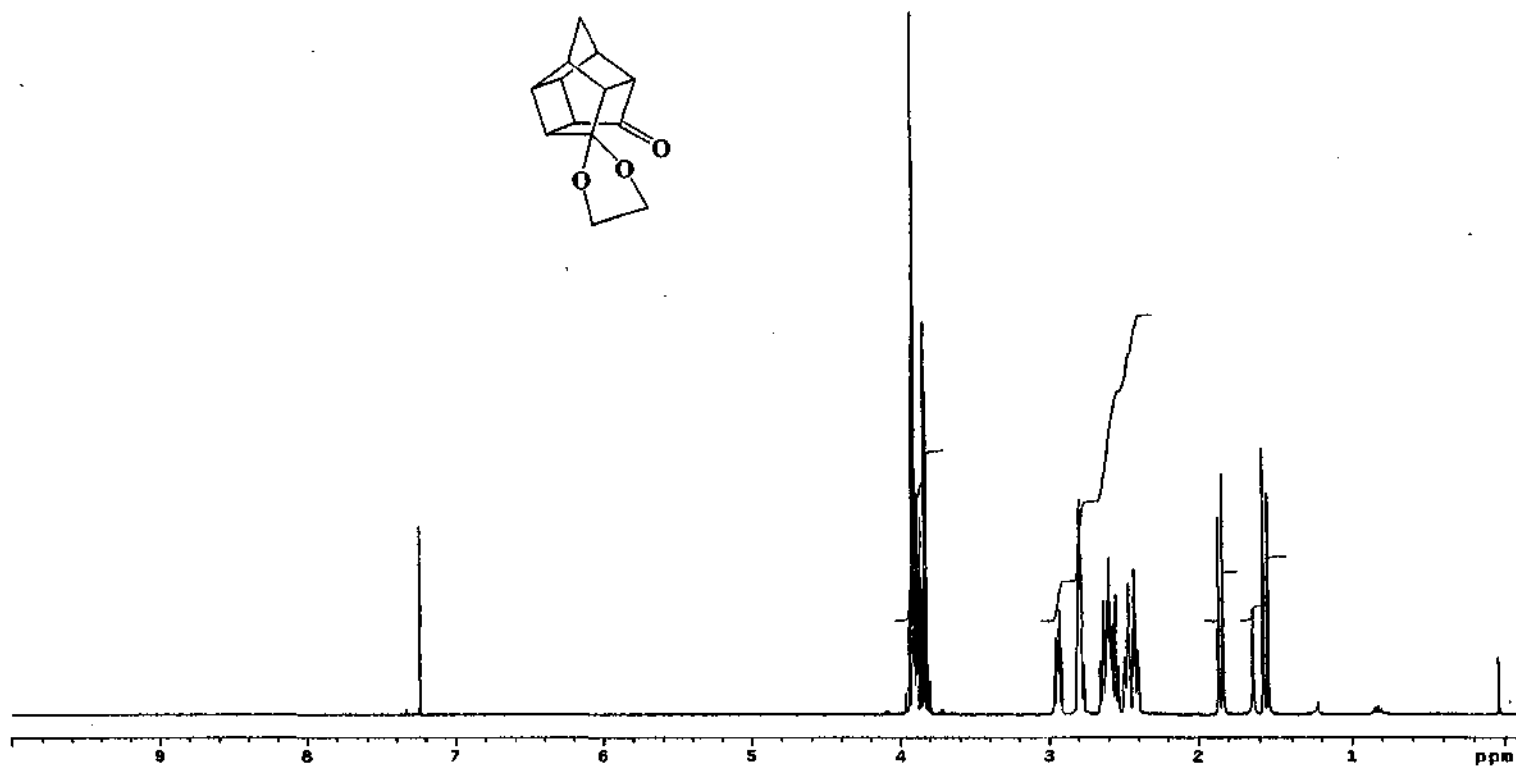
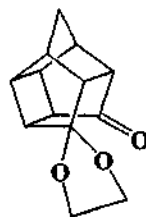


SPECTRUM 47: Mass spectrum (FAB) of Novel compound (76)



SPECTRUM 48: Infrared spectrum (KBr) of Novel compound (76)

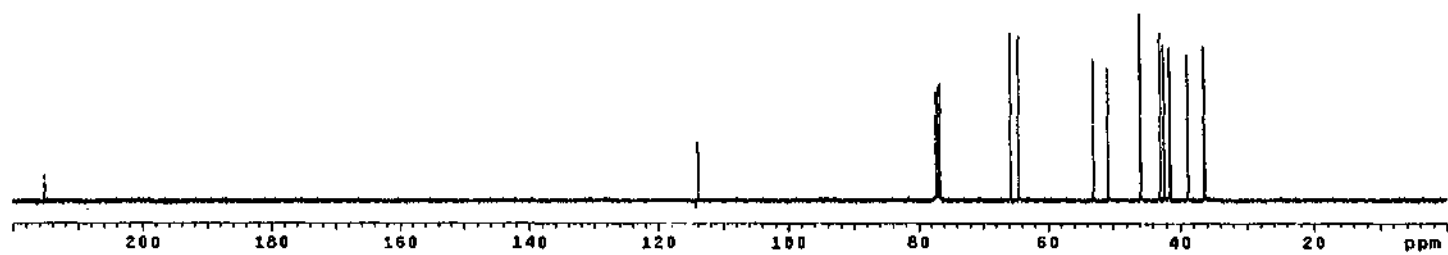
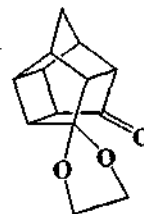
hketal.ketal in cdcl3
probe-gmabov
Pulse Sequence: s2pu1



SPECTRUM 49: ^1H NMR spectrum of ketal (77) in CDCl_3

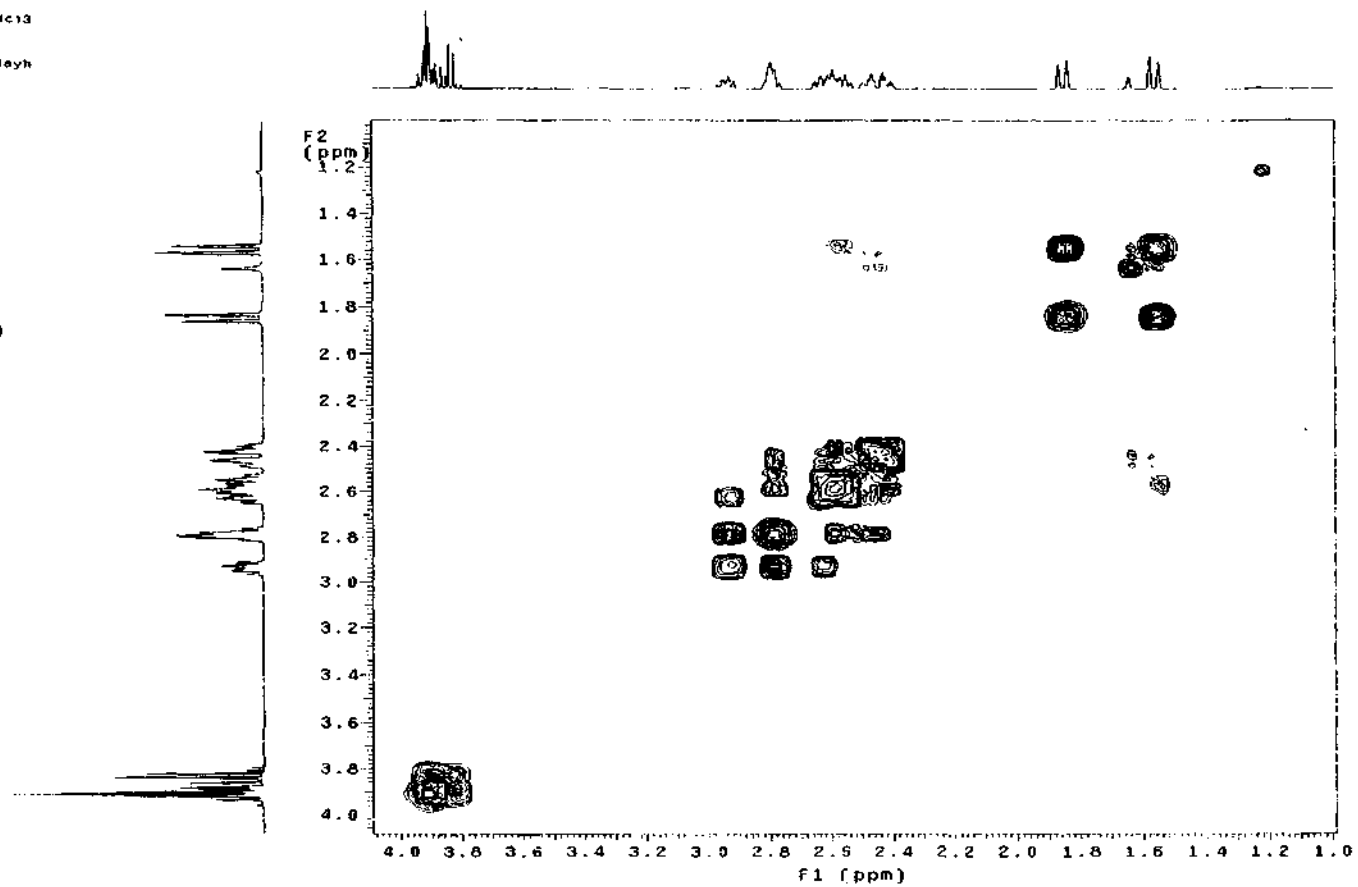
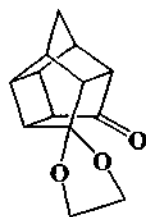
oketal.ketal in cdcl3
PROC=100ASW
Pulse Sequence: g2pu1

INDEX	FREQUENCY	PPM	HEIGHT
1	23044.148	215.227	5.5
2	11486.342	113.991	12.9
3	7774.757	77.211	29.6
4	7743.448	77.000	24.7
5	7711.310	76.880	28.4
6	6607.164	60.701	35.8
7	6486.862	60.905	35.1
8	5331.828	53.017	30.4
9	5101.735	50.731	28.7
10	4608.890	45.631	48.0
11	4306.831	42.887	35.9
12	4263.028	42.282	35.4
13	4188.873	41.456	29.1
14	4156.788	41.325	32.8
15	3883.787	36.718	31.4
16	3863.968	36.335	33.2



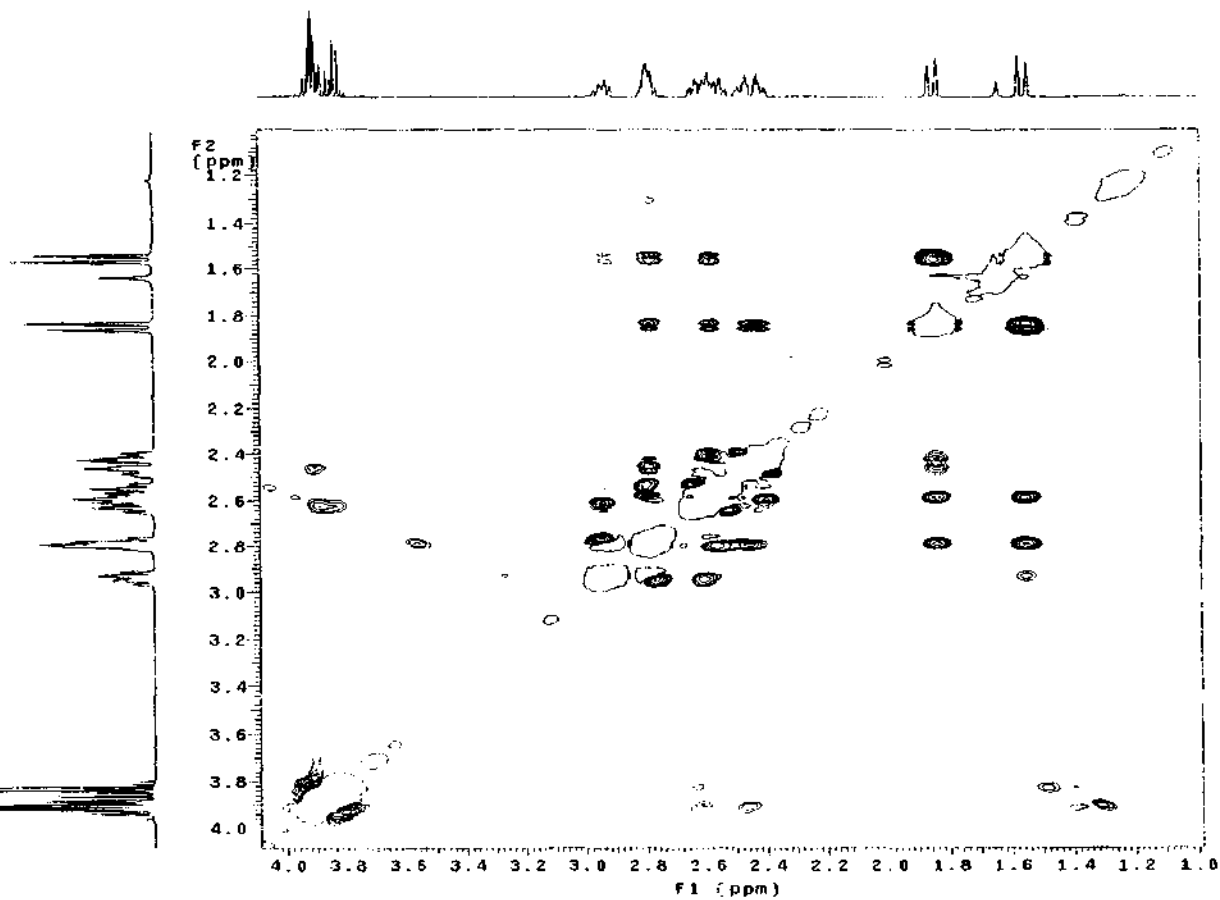
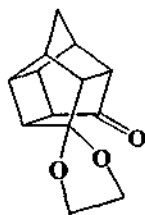
SPECTRUM 50: ¹³C NMR spectrum of ketal (77) in CDCl₃

cyketal.ketal in cdc13
16 Cosy-90
probe=smasw
Pulse Sequence: relayh



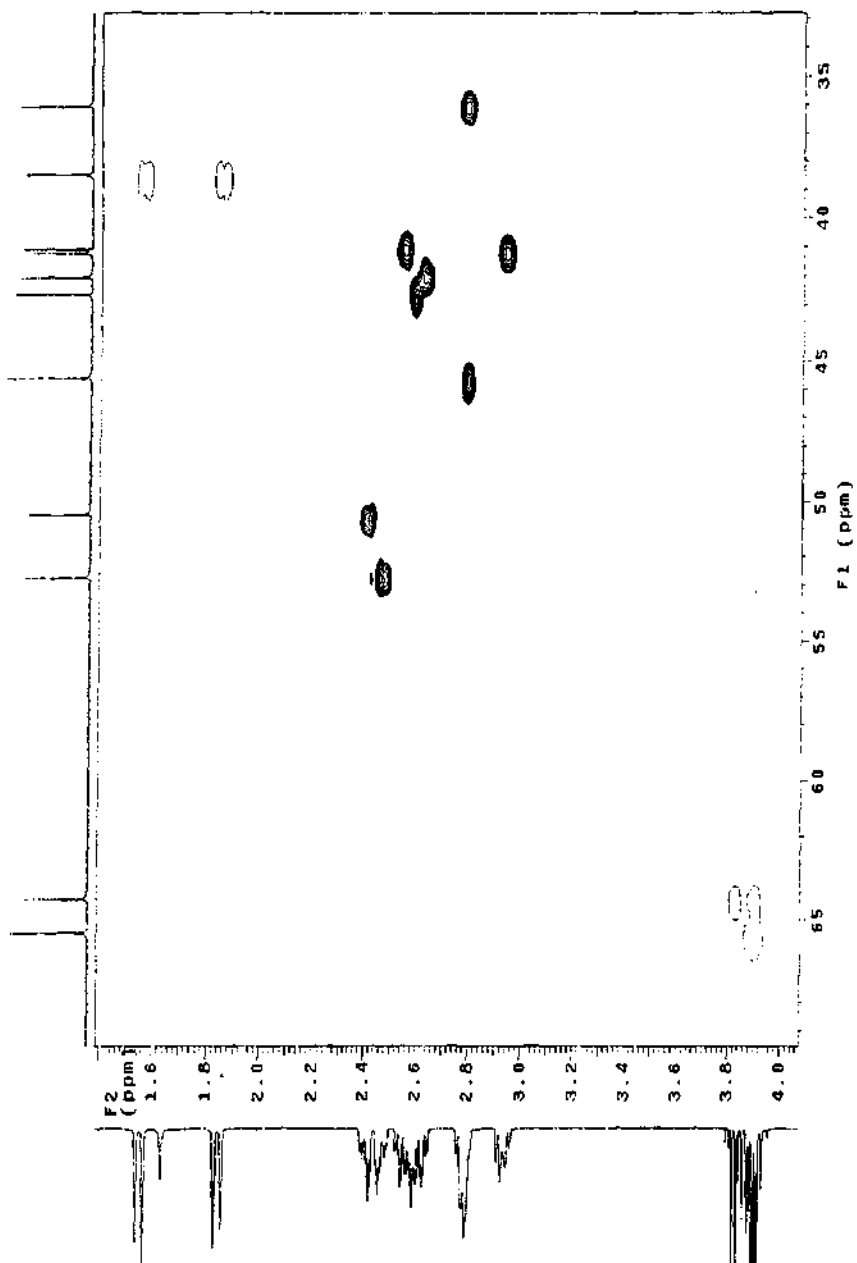
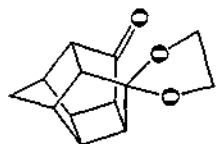
SPECTRUM 51: COSY spectrum of ketal (77) in $CDCl_3$

NOketal.ketal in cdc13
NOESY expt.
mix=1sec
probe=nmrsw
Pulse Sequence: noesy_de



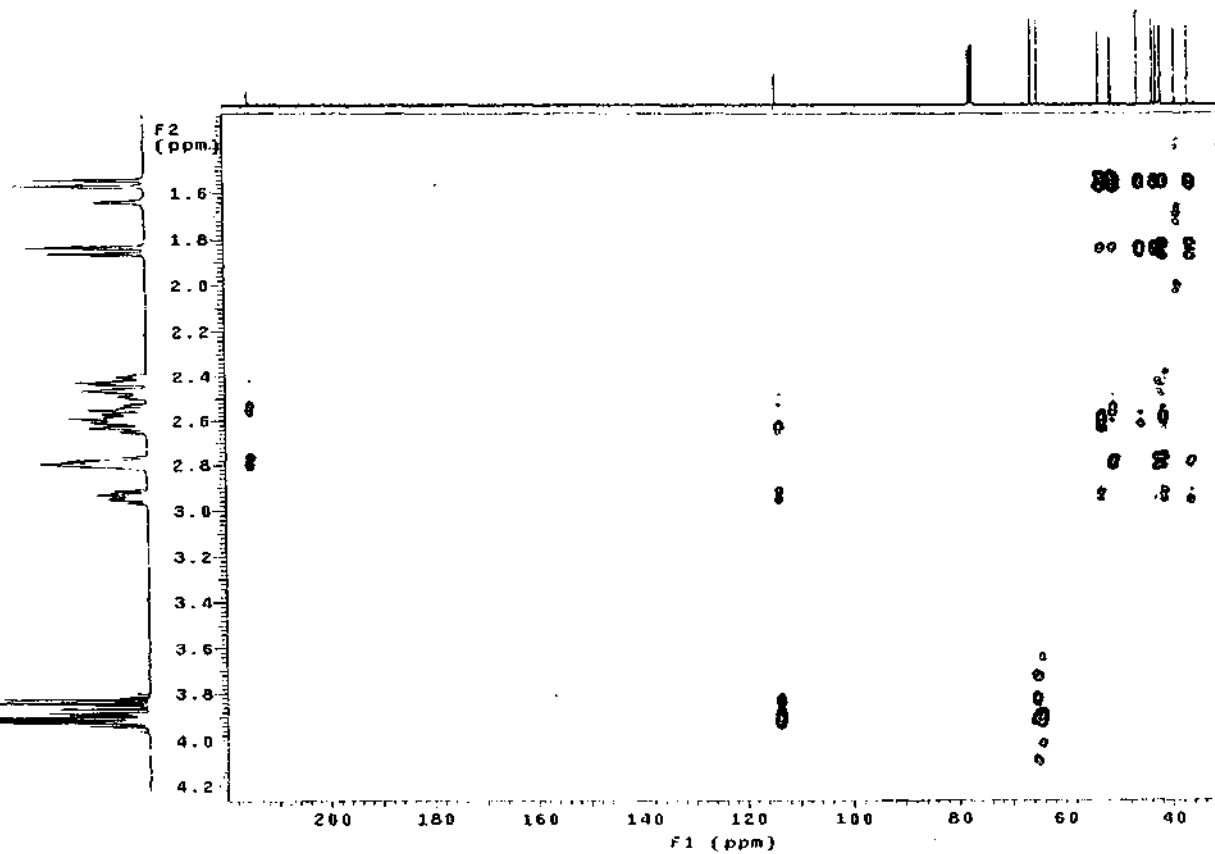
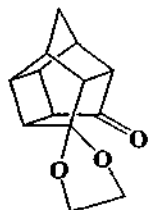
SPECTRUM 52: NOESY spectrum of ketal (77) in CDCl₃

NOxetal_ketal in cdc13
Gradient HSQC xRel.
with multiseptling
PROBHDMSB0
Pulse Sequence: ghsqc_de



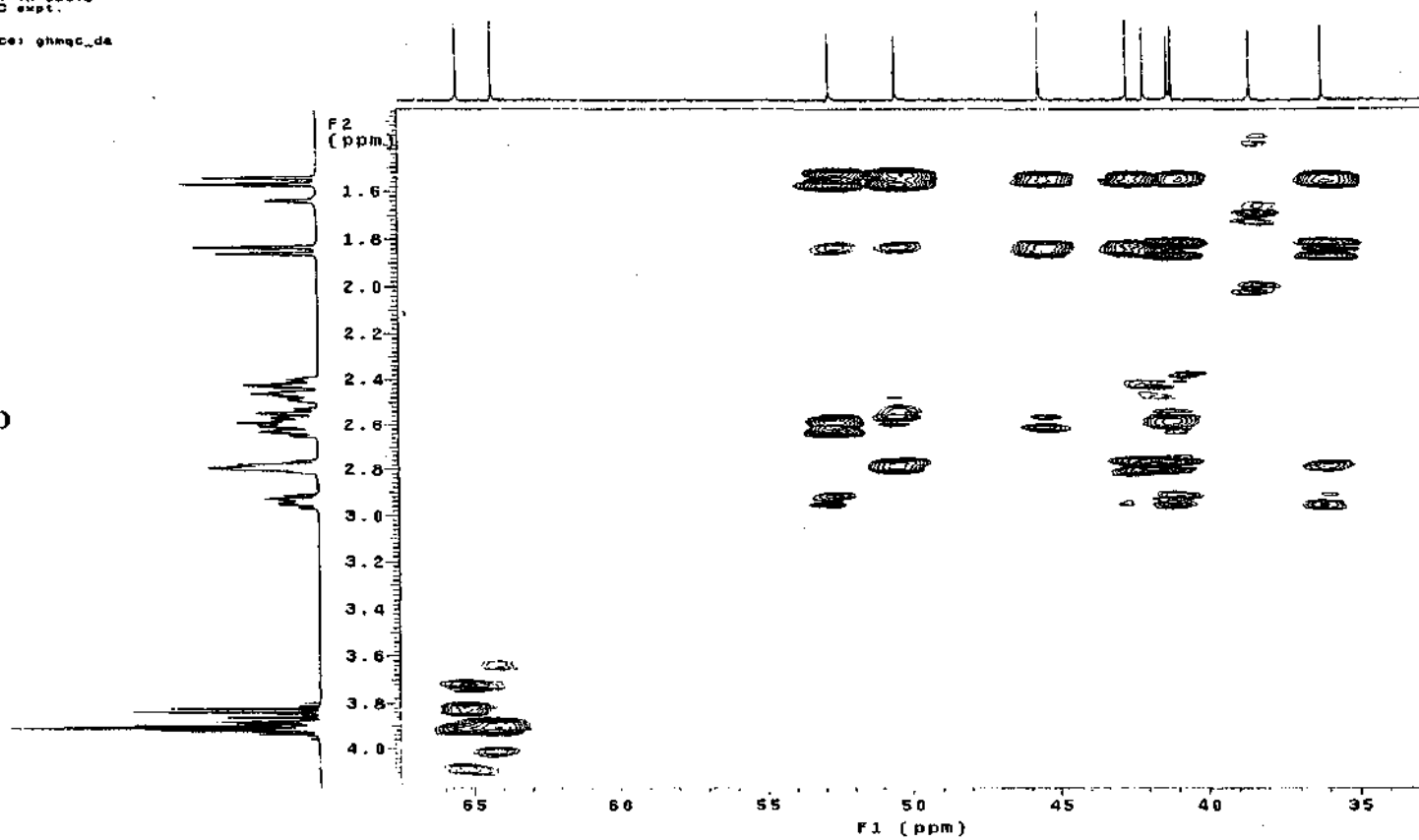
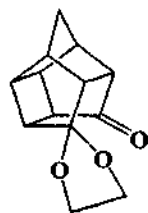
SPECTRUM 53: HSQC spectrum of ketal (77) in CDCl₃

HMketal.ketal in cdcl3
Gradient HMBC expt.
probe=5mmASB
Pulse Sequence: ghmqc_d8



SPECTRUM 54: HMBC spectrum 1 of ketal (77) in CDCl₃

HDketal.ketal in cdcl3
Gradient HMBC expt.
probe=3mmASW
Pulse Sequence: ghmqc_da



SPECTRUM 55: HMBC spectrum 2 of ketal (77) in CDCl₃

APPENDIX TWO
COMPUTATIONAL MODEL

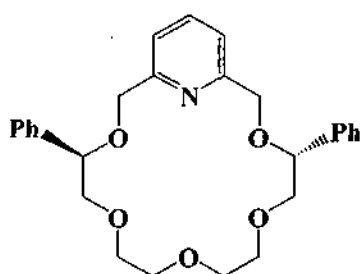
2. DOCKING PROCEDURE

2.1 DETERMINATION OF THE LOWEST ENERGY STRUCTURE OF THE FREE HOST

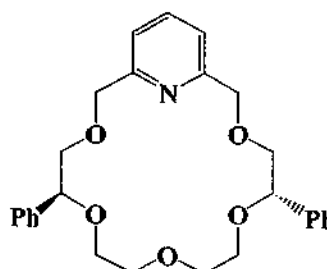
Molecular Mechanics calculations were performed using the MM3 force field and the default parameters presented in Alchemy 2000.¹ The binding energies² for the host-guest complexes are calculated using the following equation:

$$\text{Binding Energy} = E_{\text{complex}} - (E_{\text{host}} + E_{\text{guest}}). \quad \text{Eq 1}$$

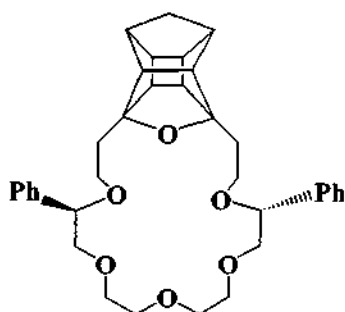
The lowest energy minima structure of the host macrocycles such as (41, 42, 49 and 50) was determined using the following MM3 computational model.



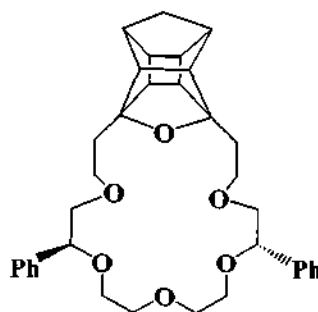
41



42



49



50

¹ Alchemy 2000, Tripos Inc., Copyright 1998, All rights reserved

² Binding Energy = $E_{\text{complex}} - (E_{\text{host}} + E_{\text{guest}})$

- Host macrocycles underwent a Molecular dynamics (MD) calculation at 600 K for 5 ps. This was performed so that rotational barriers could be overcome. A typical plot of the energy vs time during a typical MD calculation is indicated in Figure 2.1 below.

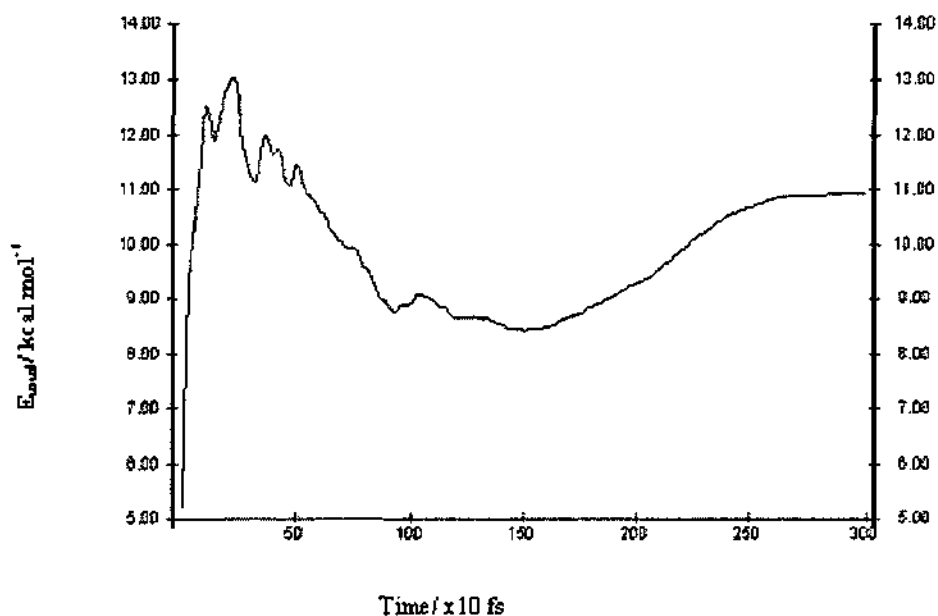


Figure 2.1 Plot of energy vs. time during a typical MD calculation

- The energies of the reaction co-ordinate were plotted and the twenty lowest minima on the graph were manually chosen and optimised with MM3 (see Figure 2.2 below).

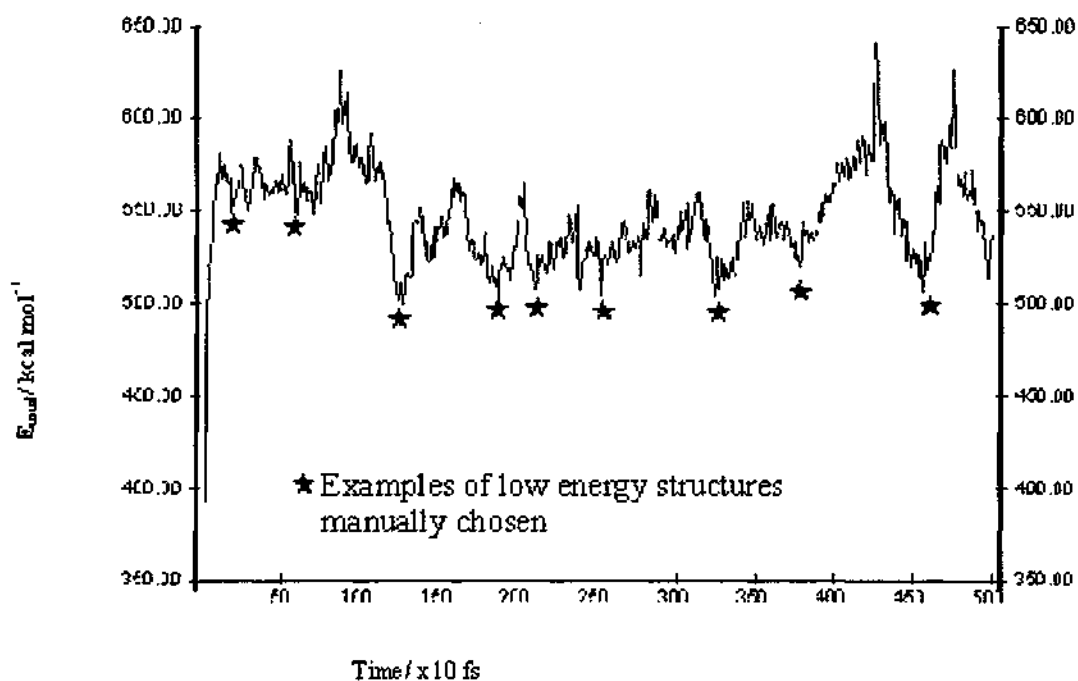


Figure 2 2 A typical Molecular Dynamics plot of Total Energy of the host-guest system vs time

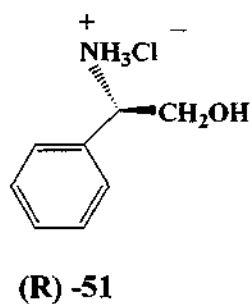
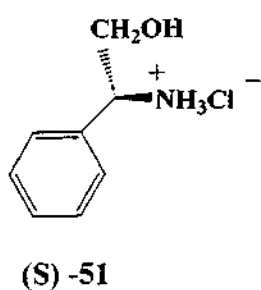
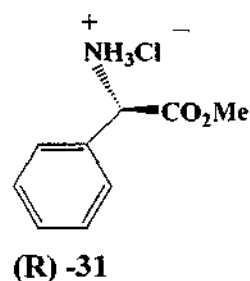
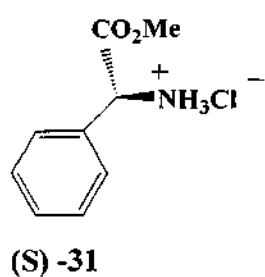
- The structures were then rank ordered and the five lowest structures underwent a MD calculation for 5-10 ps at 600 K to obtain a number of “flat” host structures which then underwent a full matrix minimization.
- The host structures were manually inspected for the degree of flatness, were selected and used to determine the lowest host-guest complex described in §2.4.

The lowest energy minima structures of the guests were determined using the MM3 computational procedure described in §2.2.

2.2 DETERMINATION OF THE LOWEST ENERGY STRUCTURE OF THE FREE GUESTS

A similar procedure was used on the guest molecules (31 and 51).

- MD for 5-10 ps at 600 K was performed on the free guest to obtain a low energy guest structure followed by a normal MM3 full matrix optimisation.
- The same energy E_{guest} is used in equation 1², for the same family of guests. Therefore the same percentage error is involved with respect to the guest.



2.3 DETERMINING THE LOW ENERGY STRUCTURES OF THE HOST-GUEST COMPLEX

The following docking procedure was applied in an attempt to obtain a complex structure in which there is a high degree of interaction between the host and guest. The ammonium moiety of the chiral guest is placed at an approximate distance of 4 Å away from the centre of the host macrocycle (see Figure 2.3). The N-C (nitrogen-carbon) bond is placed perpendicular to the plane of the macrocycle.

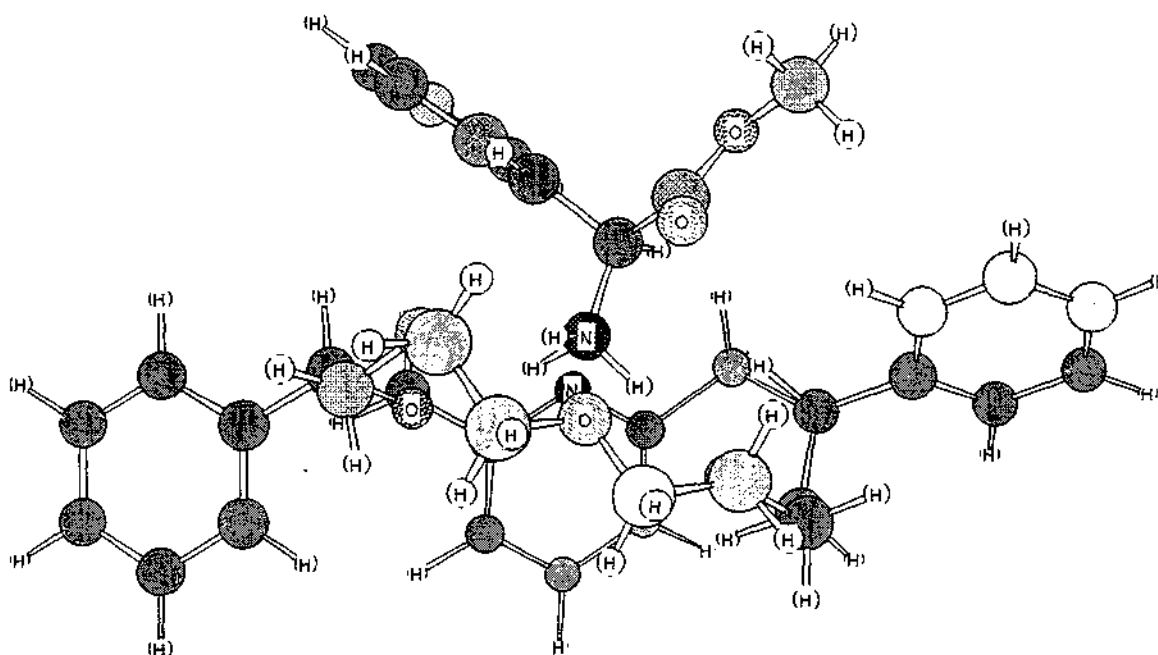


Figure 2.3 Docking procedure used for the host-guest complex

This is done for each of the starting host structures, which are then subjected to a sequence of MM3 molecular dynamics calculations as described below:

- The structure undergoes MD calculations for 5 ps at 1 K.
- The total energy of the system is plotted against time. A typical graph may exhibit an initial maximum followed by one or more minima. The structure, which corresponds to the lowest minimum after the initial maximum, is used in the next MD run for 3 ps at 50 K.

- The procedure as described before is used to find the low energy structure, which undergoes the following MD sequences:

3 ps at 100 K

3 ps at 200 K

5 ps at 300 K and

3 ps at 100 K

- In some cases there are weak interactions between the ammonium ion and the heavy atoms of the macrocycle or unfavourable steric influences resulting in the host-guest complex undergoing dissociation. In these cases the lowest structure at 100 K is optimised with MM3.
- The lowest energy complex conformation obtained from this docking is optimised using the full matrix MM3 minimization to produce a lower energy structure.
- The host-guest structures obtained are rank ordered and the lowest energy complex is used in the conformational search as described in (§2.4)

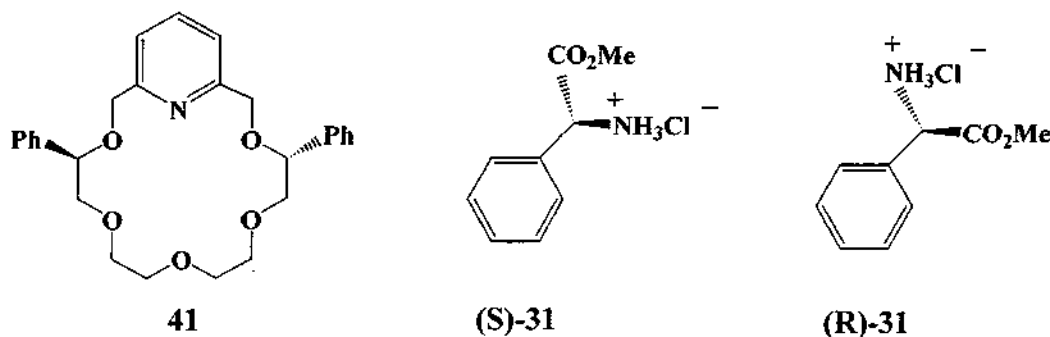
2.4 CONFORMATIONAL SEARCH TO FIND THE LOWEST ENERGY HOST-GUEST COMPLEX

Although the host–guest system undergoes huge movements or rotations during the initial MD procedure it is possible that the energy barriers restrict movement of the guest with regard to the host resulting in the lowest energy complex not being found. In order to ensure that the lowest energy complex is found the following conformational search is performed:

- The lowest energy host-guest complex obtained after MM3 full matrix minimization is taken and rotated by approximately 70° to produce five new starting conformations. Side chains are rotated as well in order to avoid excessive steric hindrances caused by the rotation of the guest.
- The five starting host-guest conformations undergo a sequence of MD calculations 3-5 ps at 1 K and 5 ps at 100 K.
- This is followed by a MM3 optimization of the lowest energy structure.
- After the MM3 optimization, the five structures are rank ordered by energy. The lowest energy E_{complex} is used to determine the approximate binding energy as described by equation 1.²
- For starting structures with a guest of opposite chirality, the chirality of the guest is manually changed. The same MD procedure is followed for the host-guest complexes with guests of opposite chirality. The lowest energy structure for each system is determined and chiral thermodynamic preference is determined in kcal mol⁻¹.

2.5 DETERMINING THE EFFECTS OF SOLVENT ON THE BINDING ENERGY AND ENANTIOSELECTIVITY

The free host (S,S)-**41**, free guest (**31**) and host-guest complexes (S,S)-**41** with (S)-**31** and (S,S)-**41** with (R)-**31** underwent the docking procedure as described above. The lowest optimised free host (S,S)-**41**, free guest (**31**) and host-guest complex (S,S)-**41** with (S)-**31** or (S,S)-**41** with (R)-**31** were selected. Molecular Mechanics calculations were performed using the MM3 force field and the default parameters presented in MacroModel.³



Host-guest complexes (S,S)-**41** with (S)-**31** and (S,S)-**41** with (R)-**31** underwent MM3 optimization in MacroModel. Calculations were performed in:

- No solvent (gas phase)
- Water (solvent phase)
- Chloroform (solvent phase)

The binding energy for the host-guest complexes (S,S)-**41** with (S)-**31** and (S,S)-**41** with (R)-**31** were calculated using the following equation²:

$$\text{Binding Energy} = E_{\text{complex}} - (E_{\text{host}} + E_{\text{guest}}).$$

³ MacroModel is a registered trademark of Schrödinger, LLC, copyright 2004, all rights reserved

APPENDIX THREE
X-RAY CRYSTALLOGRAPHY DATA

CRYSTAL STRUCTURE SOLUTION AND REFINEMENT OF (20), (25), (76) AND (77)

Intensity data were collected on a Bruker SMART 1K CCD area detector diffractometer with graphite monochromated Mo K_{α} radiation (50 kV, 30 mA). The collection method involved ω -scans of width 0.3° . Data reduction was carried out using the program *SAINT+* (Bruker, 1999a).

The crystal structure was solved by direct methods using *SHELXTL* (Bruker, 1999b). Non-hydrogen atoms were first refined isotropically followed by anisotropic refinement by full matrix least-squares calculations based on F^2 using *SHELXTL*. Hydrogen atoms were first located in the difference map then positioned geometrically and allowed to ride on their respective parent atoms. Diagrams and publication material were generated using *SHELXTL* and *PLATON* (Spek, 2003).

REFERENCES

- Bruker (1999). *SAINT+*. Version 6.02 (includes XPREP and SADABS). Bruker AXS Inc., Madison, Wisconsin, USA.
- Bruker (1999). *SHELXTL*. Version 5.1 (includes XS, XL, XP, XSHELL). Bruker AXS Inc., Madison, Wisconsin, USA.
- Spek, A. L., *J. Appl. Cryst.*, **2003**, 36, 7

3.1 DIONE (20)

TABLE 3.1.1. CRYSTAL DATA AND STRUCTURE REFINEMENT FOR (20)

Identification code	5m_gk3_s
Empirical formula	C11 H10 O2
Formula weight	174.19 g/mol
Temperature	173(2) K
Wavelength	0.71073 Å
Crystal system	Trigonal
Space group	P3 ₁
Unit cell dimensions	a = 18.1265(13) Å α = 90°. b = 18.1265(13) Å β = 90°. c = 6.4580(6) Å γ = 120°.
Volume	1837.6(3) Å ³
Z	9
Density (calculated)	1.417 mg/m ³
Absorption coefficient	0.097 mm ⁻¹
F(000)	828
Crystal size	0.38 x 0.36 x 0.33 mm ³
Theta range for data collection	1.30 to 27.99°.
Index ranges	-17 ≤ h ≤ 23, -23 ≤ k ≤ 23, -8 ≤ l ≤ 8
Reflections collected	22385
Independent reflections	2963 [R(int) = 0.0390]
Completeness to theta = 27.99°	100.0 %
Absorption correction	None
Refinement method	Full-matrix least-squares on F ²
Data / restraints / parameters	2963 / 1 / 352
Goodness-of-fit on F ₂	1.038
Final R indices [I > 2σ(I)]	R1 = 0.0345, wR2 = 0.0908
R indices (all data)	R1 = 0.0373, wR2 = 0.0926
Absolute structure parameter	-10(10)

Largest diff. peak and hole

0.247 and -0.266 e.Å⁻³

TABLE 3.1.2. ATOMIC COORDINATES (X 10⁴) AND EQUIVALENT ISOTROPIC DISPLACEMENT PARAMETERS (Å² X 10³) FOR (20).

U(EQ) IS DEFINED AS ONE THIRD OF THE TRACE OF THE ORTHOGONALIZED U_{ij} TENSOR.

	x	y	z	U(eq)
O(1)	6048(1)	7350(1)	5128(3)	37(1)
O(2)	6096(1)	8797(1)	9566(3)	37(1)
C(1)	7099(1)	9469(1)	6706(3)	23(1)
C(2)	8076(1)	9832(1)	6933(3)	24(1)
C(3)	8195(1)	8569(1)	6289(3)	27(1)
C(4)	8789(1)	9080(2)	8065(4)	31(1)
C(5)	8227(1)	9420(1)	8885(3)	27(1)
C(6)	8055(1)	9245(1)	5141(3)	24(1)
C(7)	7080(1)	8874(1)	4881(3)	24(1)
C(8)	6697(1)	7971(1)	5686(3)	23(1)
C(9)	7315(1)	8013(1)	7330(3)	24(1)
C(10)	7339(1)	8613(1)	9166(3)	24(1)
C(11)	6730(1)	8938(1)	8642(3)	23(1)
O(1A)	9396(1)	7250(1)	5647(3)	37(1)
O(2A)	7929(1)	7254(1)	1268(3)	36(1)
C(1A)	7259(1)	6268(1)	4158(3)	22(1)
C(2A)	6863(1)	5282(1)	3960(3)	22(1)
C(3A)	8102(1)	5114(1)	4528(3)	26(1)
C(4A)	7569(1)	4527(1)	2772(4)	32(1)
C(5A)	7245(1)	5110(1)	1974(3)	26(1)
C(6A)	7455(1)	5288(1)	5711(3)	24(1)
C(7A)	7860(1)	6275(1)	5949(3)	22(1)

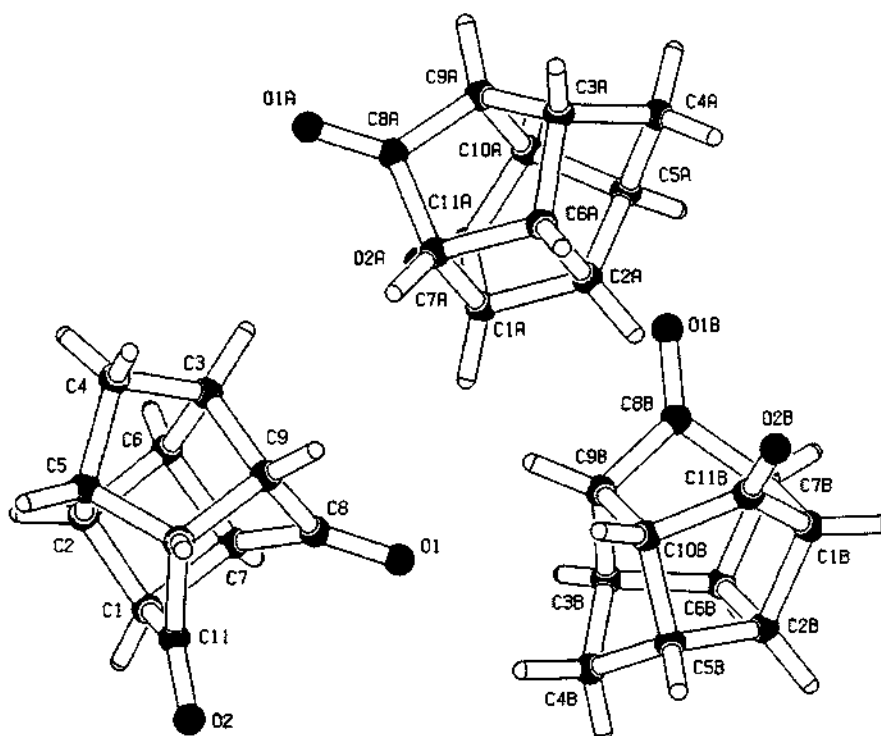
C(8A)	8754(1)	6620(1)	5104(3)	25(1)
C(9A)	8669(1)	5985(1)	3455(3)	23(1)
C(10A)	8065(1)	5981(1)	1656(3)	24(1)
C(11A)	7779(1)	6614(1)	2198(3)	24(1)
O(1B)	6150(1)	5624(1)	-1605(3)	43(1)
O(2B)	4718(1)	4094(1)	2797(3)	37(1)
C(1B)	4044(1)	4434(1)	-38(3)	22(1)
C(2B)	3625(1)	4992(1)	306(3)	23(1)
C(3B)	4825(1)	6426(1)	-246(4)	30(1)
C(4B)	4298(2)	6435(1)	1600(4)	34(1)
C(5B)	4019(1)	5530(1)	2307(3)	28(1)
C(6B)	4180(1)	5606(1)	-1453(3)	26(1)
C(7B)	4610(1)	5060(1)	-1827(3)	25(1)
C(8B)	5510(1)	5615(1)	-1023(3)	28(1)
C(9B)	5432(1)	6144(1)	691(3)	27(1)
C(10B)	4867(1)	5512(1)	2492(3)	26(1)
C(11B)	4582(1)	4597(1)	1881(3)	23(1)

TABLE 3.1.3 BOND LENGTHS [Å] FOR (20)

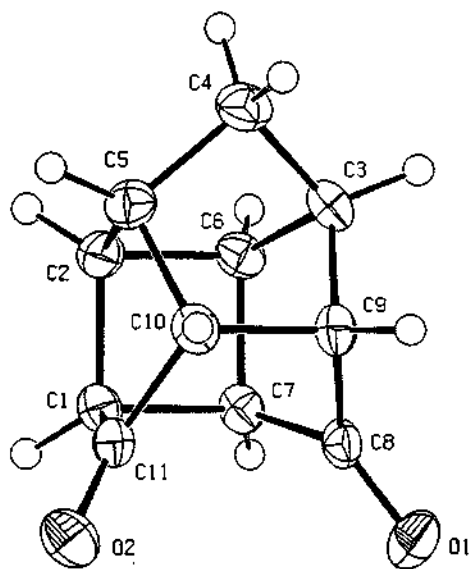
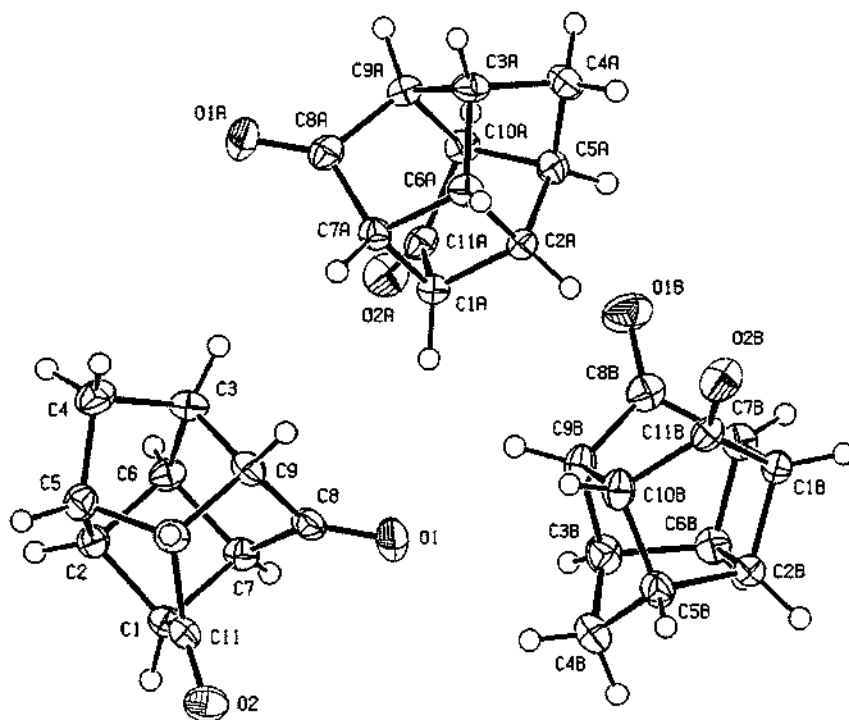
C(1)-C(7)	1.587(3)
C(9)-C(10)	1.595(3)
C(1A)-C(7A)	1.585(3)
C(9A)-C(10A)	1.594(3)
C(1B)-C(7B)	1.585(3)
C(9B)-C(10B)	1.595(3)

Symmetry transformations used to generate equivalent atoms:

DIAGRAMS OF (20)



ORTEP DIAGRAMS OF (20) DRAWN AT THE 50% PROBABILITY LEVEL:



3.2 DIOL (25)

TABLE 3.2.1. CRYSTAL DATA AND STRUCTURE REFINEMENT FOR (25).

Identification code	5m_gk4_s	
Empirical formula	C ₁₅ H ₂₀ O ₃	
Formula weight	248.31 g/mol	
Temperature	173(2) K	
Wavelength	0.71073 Å	
Crystal system	Monoclinic	
Space group	P2 ₁ /c	
Unit cell dimensions	a = 8.8011(2) Å	α = 90°.
	b = 19.8310(4) Å	β = 93.78 (10)°.
	c = 7.00730(10) Å	γ = 90°.
Volume	1220.35(4) Å ³	
Z	4	
Density (calculated)	1.352 mg/m ³	
Absorption coefficient	0.093 mm ⁻¹	
F(000)	536	
Crystal size	0.25 x 0.24 x 0.11 mm ³	
Theta range for data collection	2.05 to 28.00°.	
Index ranges	-11 ≤ h ≤ 11, -26 ≤ k ≤ 26, -9 ≤ l ≤ 9	
Reflections collected	12806	
Independent reflections	2942 [R(int) = 0.0290]	
Completeness to theta = 28.00°	99.5 %	
Absorption correction	None	
Refinement method	Full-matrix least-squares on F ²	
Data / restraints / parameters	2942 / 0 / 159	
Goodness-of-fit on F ²	1.037	
Final R indices [I > 2σ(I)]	R ₁ = 0.0487, wR ₂ = 0.1249	
R indices (all data)	R ₁ = 0.0636, wR ₂ = 0.1354	
Largest diff. peak and hole	0.428 and -0.228 e.Å ⁻³	

TABLE 3.2.2 ATOMIC COORDINATES (X 10⁴) AND EQUIVALENT ISOTROPIC DISPLACEMENT PARAMETERS (Å²X 10³) FOR (25).

U(EQ) IS DEFINED AS ONE THIRD OF THE TRACE OF THE ORTHOGONALIZED U_{IJ} TENSOR.

	x	y	z	U(eq)
C(1)	539(2)	3971(1)	5874(2)	21(1)
C(2)	986(2)	4621(1)	7000(2)	24(1)
C(3)	3730(2)	4480(1)	7476(2)	26(1)
C(4)	3112(2)	4773(1)	9293(2)	31(1)
C(5)	1567(2)	4419(1)	9043(2)	24(1)
C(6)	2483(2)	4664(1)	5911(2)	26(1)
C(7)	2026(2)	4011(1)	4802(2)	23(1)
C(8)	2959(2)	3419(1)	5711(2)	19(1)
C(9)	3486(2)	3713(1)	7688(2)	21(1)
C(10)	1986(2)	3670(1)	8772(2)	20(1)
C(11)	868(2)	3364(1)	7220(2)	18(1)
C(12)	4132(2)	3082(1)	4552(2)	24(1)
C(13)	-494(2)	2980(1)	7844(2)	22(1)
C(14)	5466(2)	3539(1)	4183(2)	30(1)
C(15)	-1448(2)	3402(1)	9111(2)	26(1)
O(1)	1805(1)	2932(1)	6132(1)	20(1)
O(2)	-2841(1)	3060(1)	9384(2)	31(1)
O(3)	6547(1)	3216(1)	3056(2)	36

TABLE 3.2.3 BOND LENGTHS [Å] AND ANGLES [°] FOR (25)

C(1)-C(7)	1.553(2)
C(2)-C(6)	1.567(2)
C(3)-C(4)	1.532(2)
C(4)-C(5)	1.531(2)
C(8)-C(12)	1.510(19)
C(9)-C(10)	1.568(2)
C(11)-C(13)	1.509(19)
C(12)-C(14)	1.519(2)
C(13)-C(15)	1.513(2)
C(8)-C(12)-C(14)	113.02(12)
C(11)-C(13)-C(15)	111.94(12)
O(3)-C(14)-C(12)	112.13(13)
O(2)-C(15)-C(13)	109.36(13)

Symmetry transformations used to generate equivalent atoms:

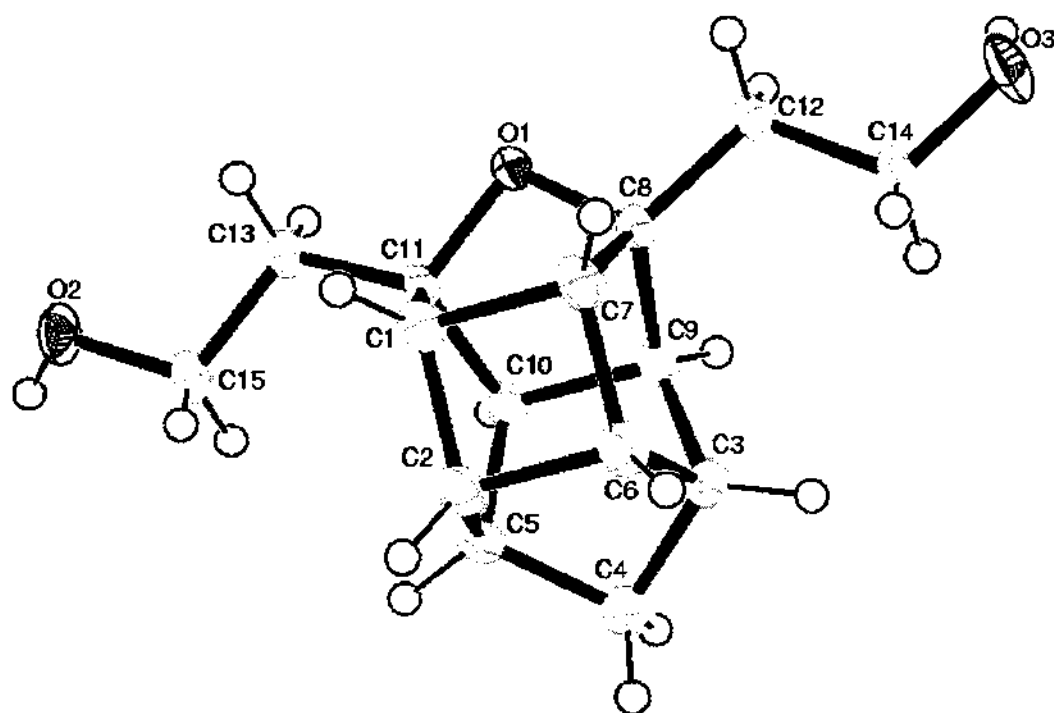
TABLE 3.2.4. HYDROGEN BONDS FOR (25)

D-H...A	d(D-H)/ Å	d(H...A)/ Å	d(D...A)/ Å	(DHA)/ °
O(2)-H(2A)...O(3)#1	0.84	1.85	2.681(16)	171.1
O(3)-H(3A)...O(2)#2	0.84	1.90	2.736(17)	174.3

Symmetry transformations used to generate equivalent atoms:

#1 $x-1, y, z+1$ #2 $x+1, -y+1/2, z-1/2$

ORTEP DIAGRAMS OF (25) DRAWN AT THE 50% PROBABILITY LEVEL



3.3 NOVEL PCU DIMER (76)

TABLE 3.3.1. CRYSTAL DATA AND STRUCTURE REFINEMENT FOR (76)

Identification code	5m_gk1_f	
Empirical formula	C ₂₈ H ₃₀ O ₃	
Formula weight	414.52 g/mol	
Temperature	173(2) K	
Wavelength	0.71073 Å	
Crystal system	Triclinic	
Space group	P $\bar{1}$	
Unit cell dimensions	a = 6.1843(17) Å	α = 86.327(5)°.
	b = 10.963(3) Å	β = 83.046(5)°.
	c = 15.572(4) Å	γ = 80.221(5)°.
Volume	1031.7(5) Å ³	
Z	2	
Density (calculated)	1.334 mg/m ³	
Absorption coefficient	0.085 mm ⁻¹	
F(000)	444	
Crystal size	0.51 x 0.44 x 0.30 mm ³	
Theta range for data collection	1.32 to 28.00°.	
Index ranges	-8 ≤ h ≤ 7, -14 ≤ k ≤ 14, -20 ≤ l ≤ 20	
Reflections collected	10401	
Independent reflections	4949 [R(int) = 0.0156]	
Completeness to theta = 28.00°	99.2 %	
Absorption correction	None	
Refinement method	Full-matrix least-squares on F ²	
Data / restraints / parameters	4949 / 15 / 284	
Goodness-of-fit on F ₂	1.046	
Final R indices [I > 2σ(I)]	R1 = 0.0418, wR2 = 0.1179	
R indices (all data)	R1 = 0.0567, wR2 = 0.1324	
Largest diff. peak and hole	0.375 and -0.201 e.Å ⁻³	

TABLE 3.3.2. ATOMIC COORDINATES (X 10⁴) AND EQUIVALENT ISOTROPIC DISPLACEMENT PARAMETERS (Å²X 10³) FOR (76)

U(EQ) IS DEFINED AS ONE THIRD OF THE TRACE OF THE ORTHOGONALIZED U_{ij} TENSOR.

	x	y	z	U(eq)
C(1)	6368(2)	6727(1)	1361(1)	22(1)
C(2)	5375(2)	5522(1)	1352(1)	23(1)
C(3)	4678(2)	4962(1)	2290(1)	22(1)
C(4)	5130(2)	5739(1)	3016(1)	20(1)
C(5)	7623(2)	5724(1)	2801(1)	21(1)
C(6)	8328(2)	6256(1)	1877(1)	22(1)
C(7)	7403(2)	4563(1)	1025(1)	28(1)
C(8)	6941(2)	3322(1)	1447(1)	31(1)
C(9)	6430(2)	3780(1)	2368(1)	26(1)
C(10)	8473(2)	4374(1)	2493(1)	24(1)
C(11)	9154(2)	4911(1)	1563(1)	25(1)
C(12)	7183(2)	7199(1)	445(1)	31(1)
C(13)	8162(2)	8362(1)	457(1)	35(1)
C(14)	10303(3)	8395(2)	411(1)	42(1)
C(14B)	7222(14)	9473(3)	187(9)	50(1)
C(15)	4714(2)	5134(1)	3927(1)	23(1)
C(16)	2463(2)	4790(1)	4141(1)	26(1)
C(17)	2091(3)	3655(1)	4365(1)	35(1)
C(18)	4282(2)	7953(1)	2574(1)	21(1)
C(19)	2317(2)	9010(1)	2648(1)	25(1)
C(20)	1561(2)	9334(1)	3625(1)	29(1)
C(21)	3045(2)	8566(1)	4233(1)	28(1)
C(22)	5334(2)	8852(1)	3919(1)	26(1)

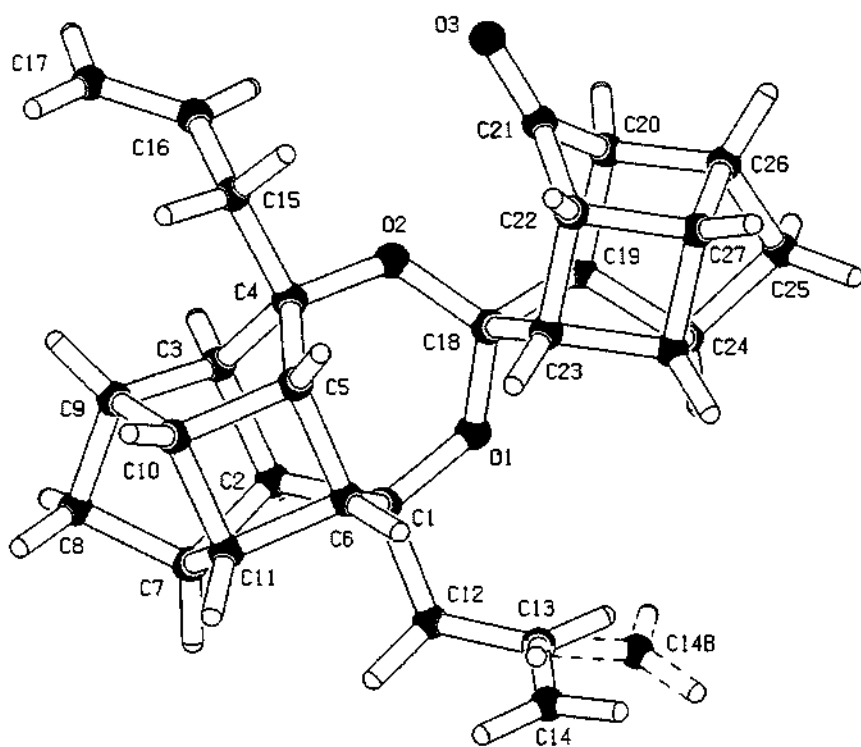
C(23)	6048(2)	8540(1)	2944(1)	23(1)
C(24)	3310(2)	10162(1)	2266(1)	31(1)
C(25)	1950(3)	11237(1)	2775(1)	39(1)
C(26)	2253(2)	10629(1)	3667(1)	34(1)
C(27)	4816(2)	10261(1)	3633(1)	30(1)
C(28)	5532(2)	9940(1)	2664(1)	28(1)
O(1)	4766(1)	7759(1)	1677(1)	24(1)
O(2)	3654(1)	6913(1)	3051(1)	21(1)
O(3)	2482(2)	8020(1)	4905(1)	37(1)

TABLE 3.3.3. BOND LENGTHS [Å] FOR (76)

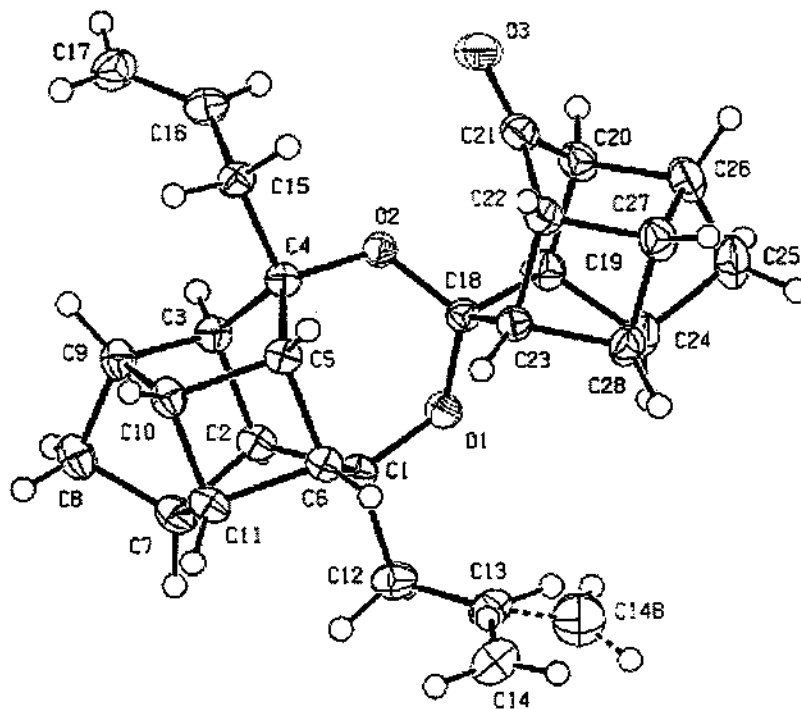
C(2)-C(3)	1.586(17)
C(5)-C(6)	1.557(17)
C(12)-C(13)	1.504(2)
C(13)-C(14)	1.324(2)
C(13)-C(14B)	1.324(3)
C(15)-C(16)	1.496(18)
C(18)-C(19)	1.529(17)
C(18)-C(23)	1.541(17)
C(19)-C(20)	1.580(19)
C(20)-C(21)	1.514(2)
C(21)-C(22)	1.518(18)
C(22)-C(23)	1.571(18)

Symmetry transformations used to generate equivalent atoms:

DIAGRAMS OF (76)



ORTEP DIAGRAMS OF (76) DRAWN AT THE 50% PROBABILITY LEVEL



3.4 KETAL (77)

TABLE 3.4.1. CRYSTAL DATA AND STRUCTURE REFINEMENT FOR (77)

Identification code	5m_gk5_s	
Empirical formula	C ₁₃ H ₁₄ O ₃	
Formula weight	218.24	
Temperature	173(2) K	
Wavelength	0.71073 Å	
Crystal system	Monoclinic	
Space group	C2/c	
Unit cell dimensions	a = 24.7387(10) Å	α = 90°.
	b = 6.6340(3) Å	β = 107.914 (2)°.
	c = 12.7631(5) Å	γ = 90°.
Volume	1993.09(14) Å ³	
Z	8	
Density (calculated)	1.455 mg/m ³	
Absorption coefficient	0.103 mm ⁻¹	
F(000)	928	
Crystal size	0.37 x 0.22 x 0.11 mm ³	
Theta range for data collection	1.73 to 27.99°.	
Index ranges	-32 ≤ h ≤ 32, -8 ≤ k ≤ 8, -16 ≤ l ≤ 11	
Reflections collected	10114	
Independent reflections	2394 [R(int) = 0.0261]	
Completeness to theta = 27.99°	100.0 %	
Absorption correction	None	
Refinement method	Full-matrix least-squares on F ²	
Data / restraints / parameters	2394 / 0 / 145	
Goodness-of-fit on F ²	1.057	
Final R indices [I > 2σ(I)]	R1 = 0.0623, wR2 = 0.1676	
R indices (all data)	R1 = 0.0716, wR2 = 0.1754	
Largest diff. peak and hole	0.584 and -0.263 e.Å ⁻³	

TABLE 3.4.2. ATOMIC COORDINATES (X 10⁴) AND EQUIVALENT ISOTROPIC DISPLACEMENT PARAMETERS (Å²X 10³) FOR (77).

U(EQ) IS DEFINED AS ONE THIRD OF THE TRACE OF THE ORTHOGONALIZED U^{ij} TENSOR.

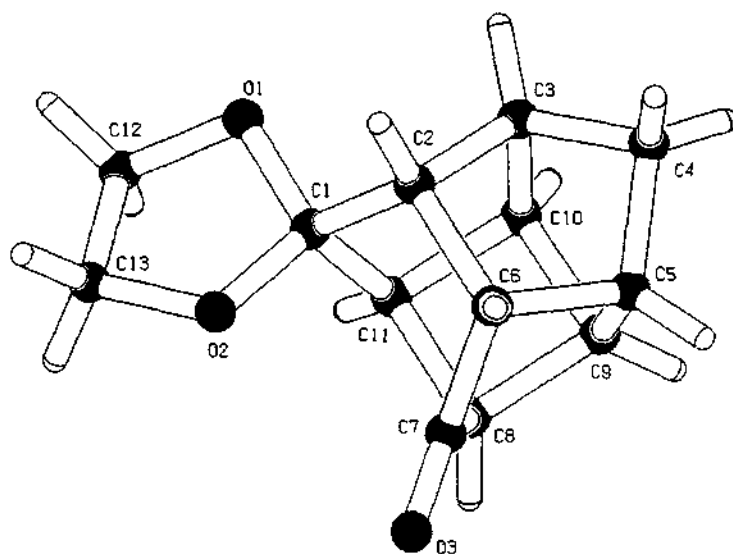
	x	y	z	U(eq)
O(1)	3771(1)	2153(3)	4997(1)	34(1)
O(2)	4259(1)	1357(2)	6759(1)	28(1)
O(3)	4330(1)	3342(3)	9040(1)	35(1)
C(1)	3870(1)	2763(3)	6101(2)	24(1)
C(2)	3315(1)	2870(4)	6361(2)	31(1)
C(3)	3025(1)	4749(4)	5692(2)	33(1)
C(4)	2671(1)	5617(5)	6374(2)	41(1)
C(5)	3157(1)	5697(4)	7447(2)	34(1)
C(6)	3415(1)	3535(4)	7596(2)	31(1)
C(7)	4036(1)	3992(3)	8171(2)	24(1)
C(8)	4182(1)	5648(3)	7494(2)	26(1)
C(9)	3622(1)	6893(3)	7113(2)	30(1)
C(10)	3529(1)	6213(3)	5902(2)	29(1)
C(11)	4083(1)	4950(3)	6275(2)	25(1)
C(12)	4307(1)	1416(4)	4949(2)	34(1)
C(13)	4563(1)	469(3)	6083(2)	28(1)

TABLE 3.4.3. BOND LENGTHS [Å] FOR (77).

C(1)-C(2)	1.510(3)
C(1)-C(11)	1.536(3)
C(2)-C(3)	1.556(3)
C(2)-C(6)	1.581(3)
C(5)-C(6)	1.557(3)
C(5)-C(9)	1.561(3)
C(6)-C(7)	1.514(3)
C(7)-C(8)	1.509(3)
C(8)-C(9)	1.557(3)
C(8)-C(11)	1.569(3)
C(9)-C(10)	1.558(3)
C(12)-C(13)	1.524(3)

Symmetry transformations used to generate equivalent atoms:

DIAGRAMS OF (77):



ORTEP DIAGRAMS OF (77) DRAWN AT THE 50% PROBABILITY LEVEL

